30 October 2009 $10

Science

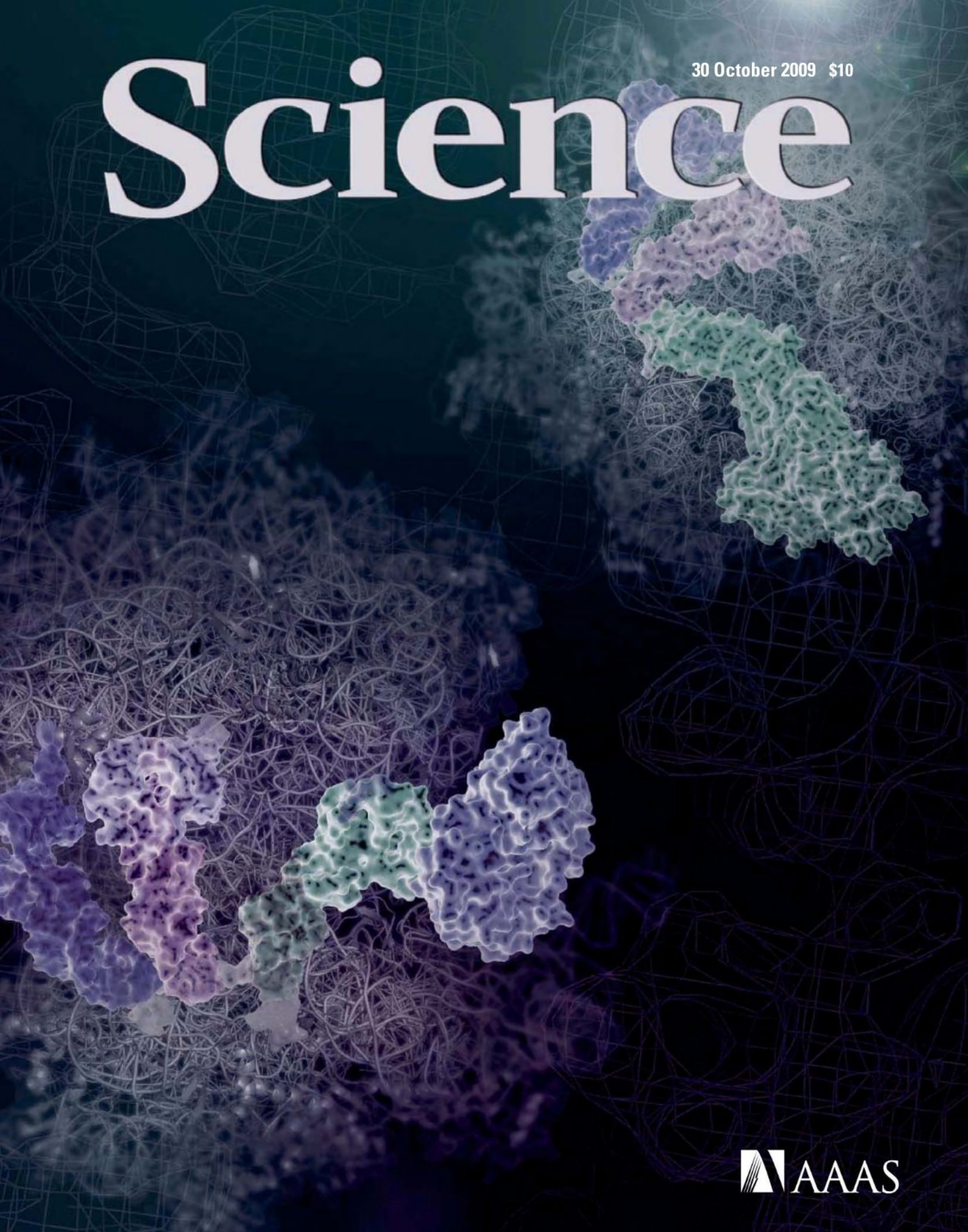

AAAS

Why settle for iffy?

Get the proven value of Illumina® microarrays.

Your research is no place to take unnecessary risks. Not when you can use the proven Illumina microarray platform. Industry-leading call rates and data quality. Flexible options to give you the right array for your study. It's value without compromise.
Only from Illumina.

Find real value at
www.illumina.com/dna

illumina®

GE Healthcare
Life Sciences

Interesting what a little imagination can do

Imagination has always inspired the scientific mind. At GE Healthcare Life Sciences, the same imagination inspires us to provide the most complete range of products and solutions available. Everything from innovative research system platforms, such as ÄKTA™, Biacore™ and IN Cell Analyzer, to everyday lab essentials from our Whatman™ and Amersham™ brands, to a full range of products for bioprocessing. Scientists around the world rely on these brands to deliver reproducible results, with the highest quality, that ultimately helps improve their productivity.

At GE Healthcare Life Sciences, our focus is on helping scientists achieve even more, faster. It's a commitment we have in our genes. And all this is backed by the service, support and investment for the future that being part of GE can bring.

Want to set your imagination free and do more? Why not talk with us today. Visit **www.gelifesciences.com**

I ÄKTA I Amersham I Biacore I IN Cell Analyzer I Whatman I GE Service I

imagination at work

First published September 2009
GE Healthcare Bio-Sciences AB, Björkgatan 30, 751 84 Uppsala, Sweden
GE15-09

EDITORIAL

NEWS OF THE WEEK

NEWS FOCUS

LETTERS

BOOKS *ET AL.*

POLICY FORUM

PERSPECTIVES

BREVIA

CONTENTS continued >>

page 659

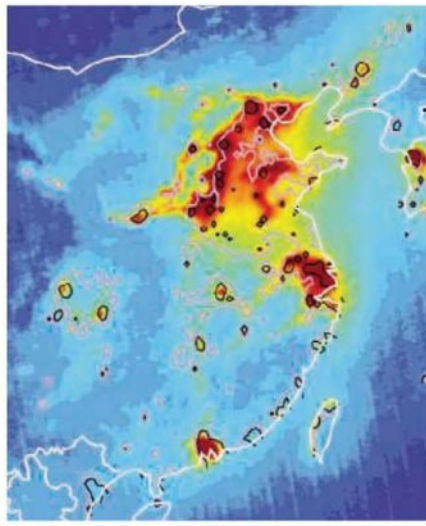

pages 672, 674, & 716

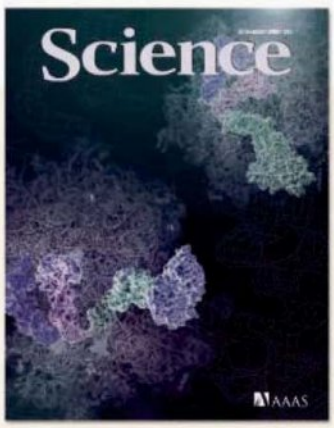

COVER

Crystal structures of the 70S ribosome from the bacterium *Thermus thermophilus* in complex with translation elongation factors Tu (EF-Tu) and G (EF-G). During protein synthesis, EF-Tu (in periwinkle blue, center) delivers an aminoacyl transfer RNA (green) to the ribosome for each amino acid indicated by the messenger RNA. As the polypeptide chain grows, EF-G (in green at top right) helps move the mRNA and tRNAs through the ribosome. See pages 688 and 694.

Images: Larissa Ulisko, Rebecca Voorhees, Martin Schmeing

DEPARTMENTS

Analyzing genetic differences

Genotyping sample and assay technologies by QIAGEN

Rely on trusted automated and manual workflow solutions for:

- **Sample collection and stabilization**
- **Genomic DNA purification, DNA storage, and whole genome amplification**
- **PCR amplification and automated QIAxcel® fragment analysis**
- **HRM® and Pyrosequencing® detection**

Making improvements in life possible — www.qiagen.com

QIAGEN®

Sample & Assay Technologies

RESEARCH ARTICLES

REPORTS

CONTENTS continued >>

pages 678 & 682

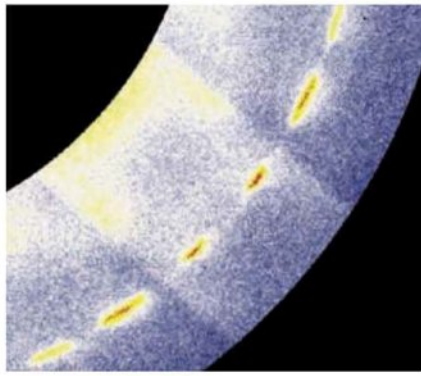

page 708

pages 676, 718, & 722

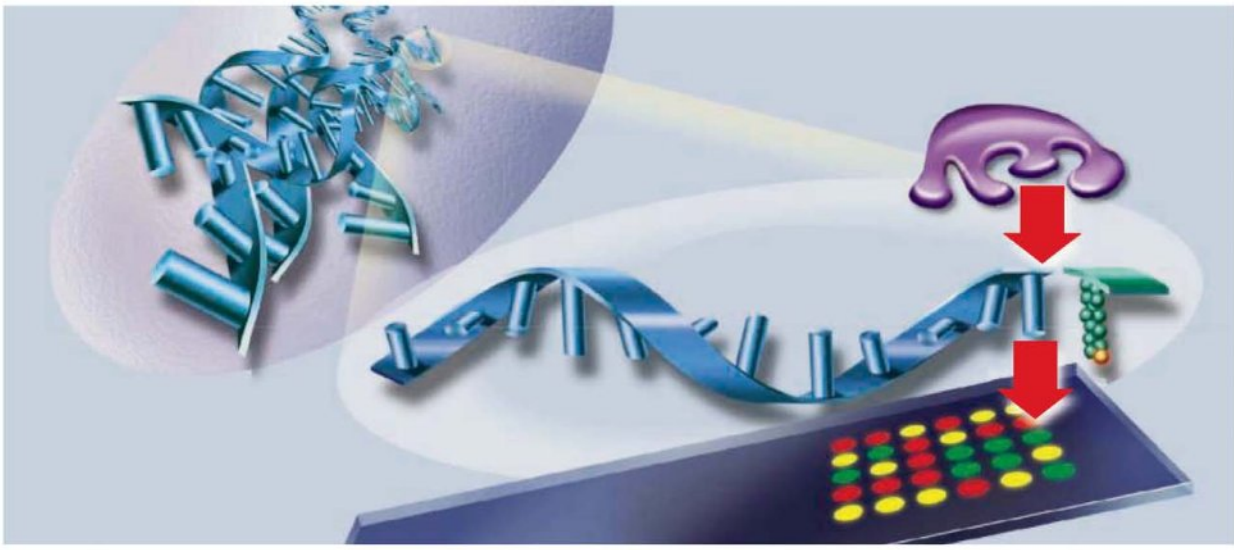

microRNA
RESEARCH DESIGN
Strategies from the Experts
WEBINAR

MicroRNAs, or miRNAs, are increasingly being accepted as playing a crucial regulatory role in normal and dysfunctional cellular processes. They represent a class of small, noncoding RNA molecules, which have been shown to be involved in almost every human pathology currently under study. From tumor progression and virus-host interactions, to immune response and stem cell fate determination, miRNAs are quickly growing in importance as the "master regulators" in cell cycle processes. With a wide variety of research tools and potential work flows available, it can be difficult for scientists to determine the optimal path to a successful miRNA research project. This webinar will bring together three recognized experts in miRNA research and experimental design to share their knowledge and expertise.

Tuesday
November 10, 2009
12 noon Eastern;
9 a.m. Pacific;
5 p.m. GMT

Viewers of the webinar will:

- receive advice on best practices for establishing and running an miRNA research project
- obtain guidance on how to kick-start stalled projects
- hear solutions to common problems encountered in miRNA experiments
- be able to put their specific questions to the panelists live!

Participants:

Neil Kubica, Ph.D.
Harvard Medical School, Boston, MA

Peter T. Nelson, M.D./Ph.D.
University of Kentucky, Lexington, KY

Kai Wang, Ph.D.
Institute for Systems Biology, Seattle, WA

Join our panel of experts in a live discussion. Register to participate.

Questions can be submitted live to the panel during the webinar or in advance via e-mail provided with registration. To register, visit

www.sciencemag.org/webinar

Sponsored by: EXIQON

Science AAAS

Brought to you by the *Science*/AAAS Business Office

SCIENCEONLINE

SCIENCEXPRESS
www.sciencexpress.org

SCIENCENOW
www.sciencenow.org
Highlights From Our Daily News Coverage

SCIENCESIGNALING
www.sciencesignaling.org
The Signal Transduction Knowledge Environment

SCIENCECAREERS
www.sciencecareers.org/career_magazine
Free Career Resources for Scientists

SCIENCETRANSLATIONAL MEDICINE
www.sciencetranslationalmedicine.org
Integrating Medicine and Science

SCIENCEPODCAST
www.sciencemag.org/multimedia/podcast
Free Weekly Show

Download the 30 October *Science* Podcast to hear about pandemic H1N1 and the 2009 Hajj, the contribution of inherited wealth to economic inequality, and more.

ORIGINSBLOG
blogs.sciencemag.org/origins
A History of Beginnings

SCIENCEINSIDER
blogs.sciencemag.org/scienceinsider
Science Policy News and Analysis

SCIENCE (ISSN 0036-8075) is published weekly on Friday, except the last week in December, by the American Association for the Advancement of Science, 1200 New York Avenue, NW, Washington, DC 20005. Periodicals Mail postage (publication No. 484460) paid at Washington, DC, and additional mailing offices.

Domestic individual membership and subscription (51 issues): $146 ($74 allocated to subscription). Domestic institutional subscription (51 issues): $835; Foreign postage extra: Mexico, Caribbean (surface mail) $55; other countries (air assist delivery) $85. First class, airmail, student, and emeritus rates on request. Canadian rates with GST available upon request, GST #1254 88122. Publications Mail Agreement Number 1069624. **Printed in the U.S.A.**

Change of address: Allow 4 weeks, giving old and new addresses and 8-digit account number. **Postmaster:** Send change of address to AAAS, P.O. Box 96178, Washington, DC 20090–6178. **Single-copy sales:** $10.00 current issue, $15.00 back issue prepaid includes surface postage; bulk rates on request.

The identification code for *Science* is 0036-8075. *Science* is indexed in the *Reader's Guide to Periodical Literature* and in several specialized indexes.

AAAS
ADVANCING SCIENCE, SERVING SOCIETY

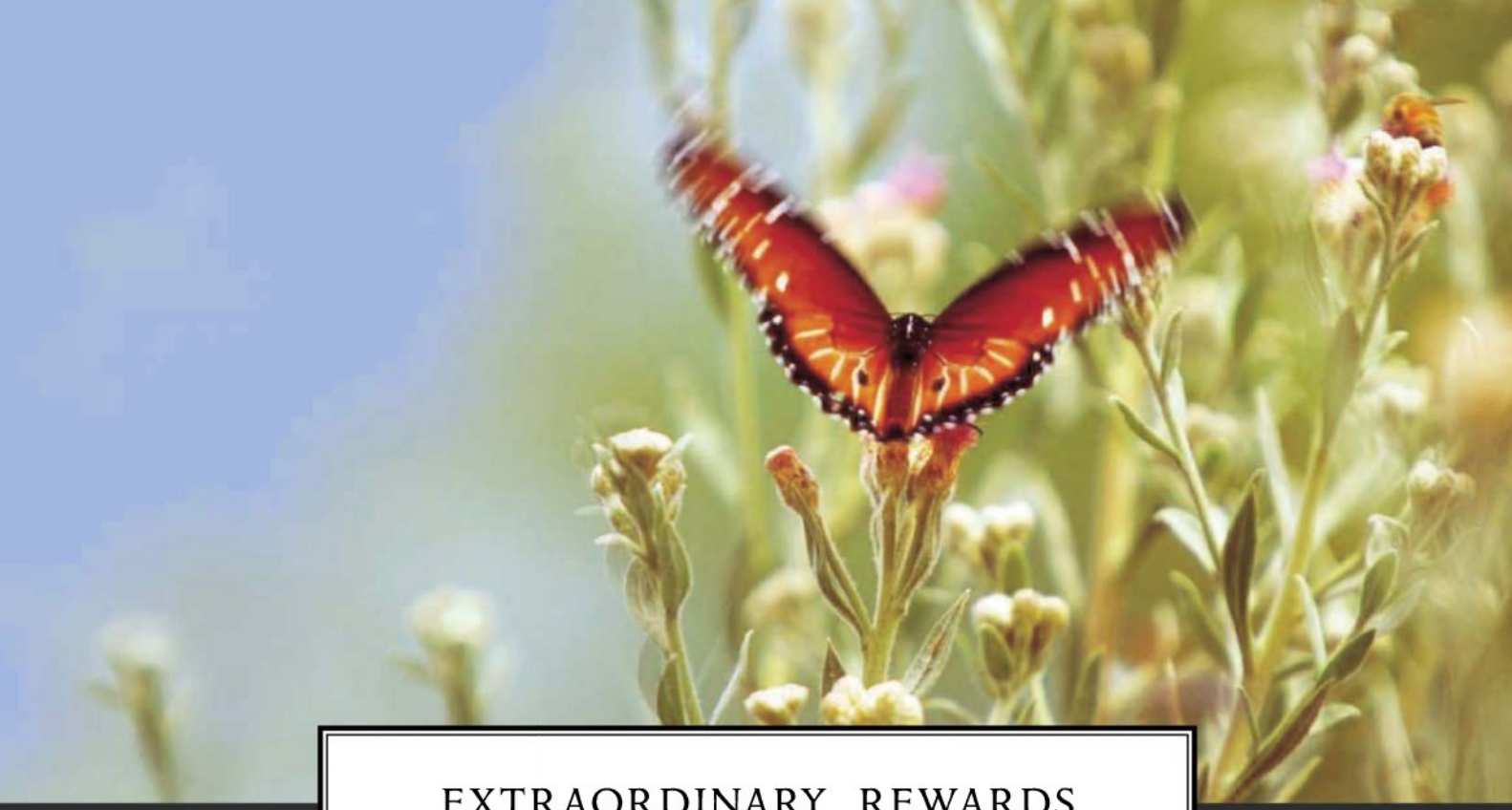

EXTRAORDINARY REWARDS

35th Anniversary Offers

As a trusted resource in the life science community, New England Biolabs would like to thank our customers for 35 years of support. Join us in celebrating our 35th anniversary by visiting www.neb.com to find 12 months of exciting offers, including significant product discounts and giveaways.

Look for the 35th Anniversary Offers icon on our website to learn about our monthly special offer.

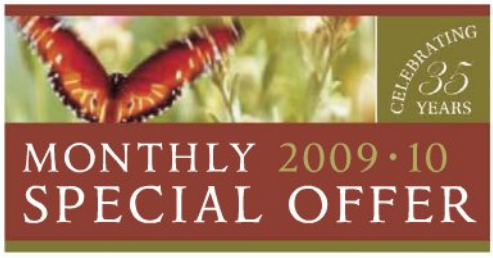

www.neb.com

CELEBRATING 35 YEARS

NEW ENGLAND BioLabs® Inc.
enabling technologies in the life sciences

CLONING & MAPPING	DNA AMPLIFICATION & PCR	RNA ANALYSIS	PROTEIN EXPRESSION & ANALYSIS	GENE EXPRESSION & CELLULAR ANALYSIS

www.neb.com

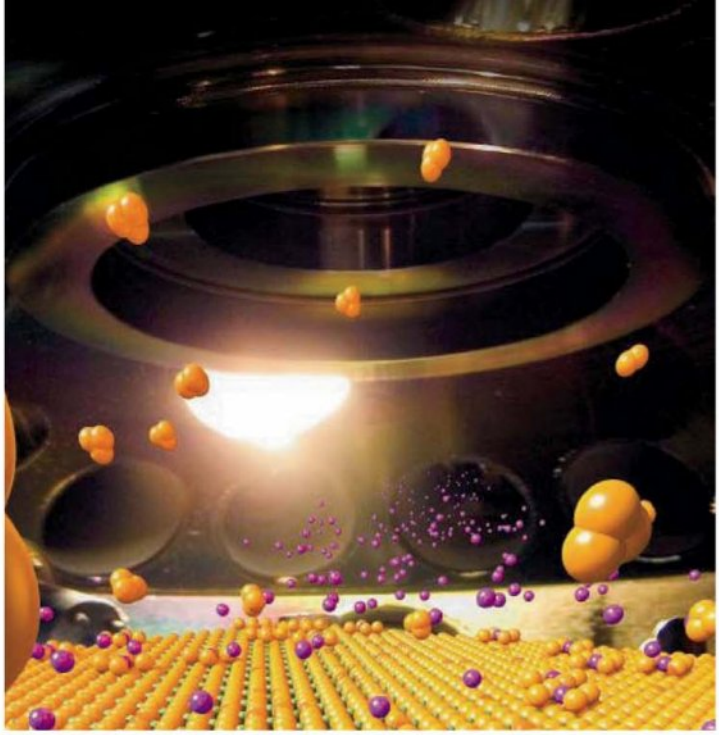

<< Superconductivity Sliced Thin

Since the initial characterization of high-temperature cuprate superconductors, an intriguing challenge has been determining the minimum number of copper oxide planes needed to support the superconducting state. The observation of superconductivity at interfaces of metallic oxides and insulators provides a route to addressing this question. **Logvenov *et al.*** (p. 699) describe a method for layer-by-layer synthesis of alternating oxides of metal and insulators based on La and Cu. Layers three unit cells thick supported superconductivity with a transition temperature of 32 kelvin. When selected layers were then doped with Zn atoms to suppress superconductivity, the interface superconductivity was shown to arise from a single copper-oxide plane.

Origins of Egalitarianism

Wealthy contemporary societies exhibit varying extents of economic inequality, with the Nordic countries being relatively egalitarian, whereas there is a much larger gap between top and bottom in the United States. **Borgerhoff Mulder *et al.*** (p. 682; see the Perspective by **Acemoglu and Robinson**) build a bare-bones model describing the intergenerational transmission of three different types of wealth—based on social networks, land and livestock, and physical and cognitive capacity—in four types of small-scale societies in which livelihoods depended primarily on hunting, herding, farming, or horticulture. Parameter estimates from a large-scale analysis of historical and ethnographic data were added to the model to reveal that the four types of societies display distinctive patterns of wealth transmission and that these patterns are associated with different extents of inequality.

Ribosomes Caught in Translation

To synthesize proteins, the ribosome must select cognate transfer RNAs (tRNAs) based on base-pairing with the messenger RNA (mRNA) template (a process known as decoding), form a peptide bond, and then move the mRNA:tRNA assembly relative to the ribosome (a process known as translocation). Decoding and translocation require protein guanosine triphosphatases (GTPases), and, while high-resolution structures of the ribosome have greatly furthered our understanding of ribosome function, the detailed mechanism of these GTPases during the elongation cycle remains unclear. Two Research Articles now give a clearer view of these steps in bacterial protein synthesis (see the Perspective by **Liljas**). **Schmeing *et al.*** (p. 688, published online 15 October) present the crystal structure of the ribosome bound to Elongation factor-Tu (EF-Tu) and amino-acyl tRNA that gives insight into how EF-Tu contributes to accurate decoding. **Gao *et al.*** (p. 694, published online 15 October) describe the crystal structure of the ribosome bound to Elongation factor-G (EF-G) trapped in a posttranslocation state by the antibiotic fusidic acid that gives insight into how EF-G functions in translocation.

CREDITS (TOP TO BOTTOM): ROBERT J. SUNDLING; PUSCHNIG *ET AL.*

Electron Comings and Goings

Advances in computational chemistry have enabled remarkably detailed calculations of electrons' spatial arrangements in complex molecules. Experimental confirmation of these orbital geometries remains challenging, however, particularly for molecules bound in thin layers to underlying surfaces—a morphology of increasing interest in organic semiconductor development. **Puschnig *et al.*** (p. 702, published online 10 September) mapped the trajectories of photoelectrons emitted from polycyclic aromatic molecules deposited on copper and extracted spatial profiles of the orbitals from which these electrons emerged. The method of analysis takes advantage of the straightforward Fourier relation between position and momentum and complements orbital imaging techniques based on scanning tunneling microscopy.

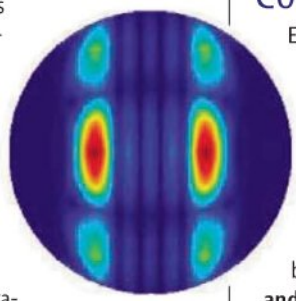

Zinc-Based Bases

Conventional methods of stripping a proton from a hydrocarbon yield an alkali metal-coordinated carbanion as the preliminary product. In certain cases, however, this preliminary product falls apart before it can be used for further constructive synthetic purposes. **Kennedy *et al.*** (p. 706; see the Perspective by **Marek**) show that in such cases, zinc ions can act as potent stabilizers. Specifically, a bimetallic base incorporating both sodium and zinc ions was used to deprotonate the common cyclic ethers tetrahydrofuran and tetrahydropyran. Zinc coordination to the carbanion inhibited an otherwise rapid ring-opening decomposition pathway. Similarly, a zinc-potassium combination facilitated deprotonation of ethylene to a stabilized product.

Converging on Dynamics

Electron diffraction is a versatile technique for discerning atomic-level structure, but the data emerge averaged over the micron–scale area sampled by the electrons, and so blur local distinctions in systems that aren't strictly periodic. A recent approach to minimizing this problem has been to focus the electron beam impinging on the sample. **Yurtsever and Zewail** (p. 708) have now applied convergent focusing to an ultrafast electron diffraction apparatus and were thus able to resolve picosecond structural dynamics in local regions tens of nanometers across. The technique was used to probe heterogeneous temperature changes in laser-heated silicon.

Continued on page 641

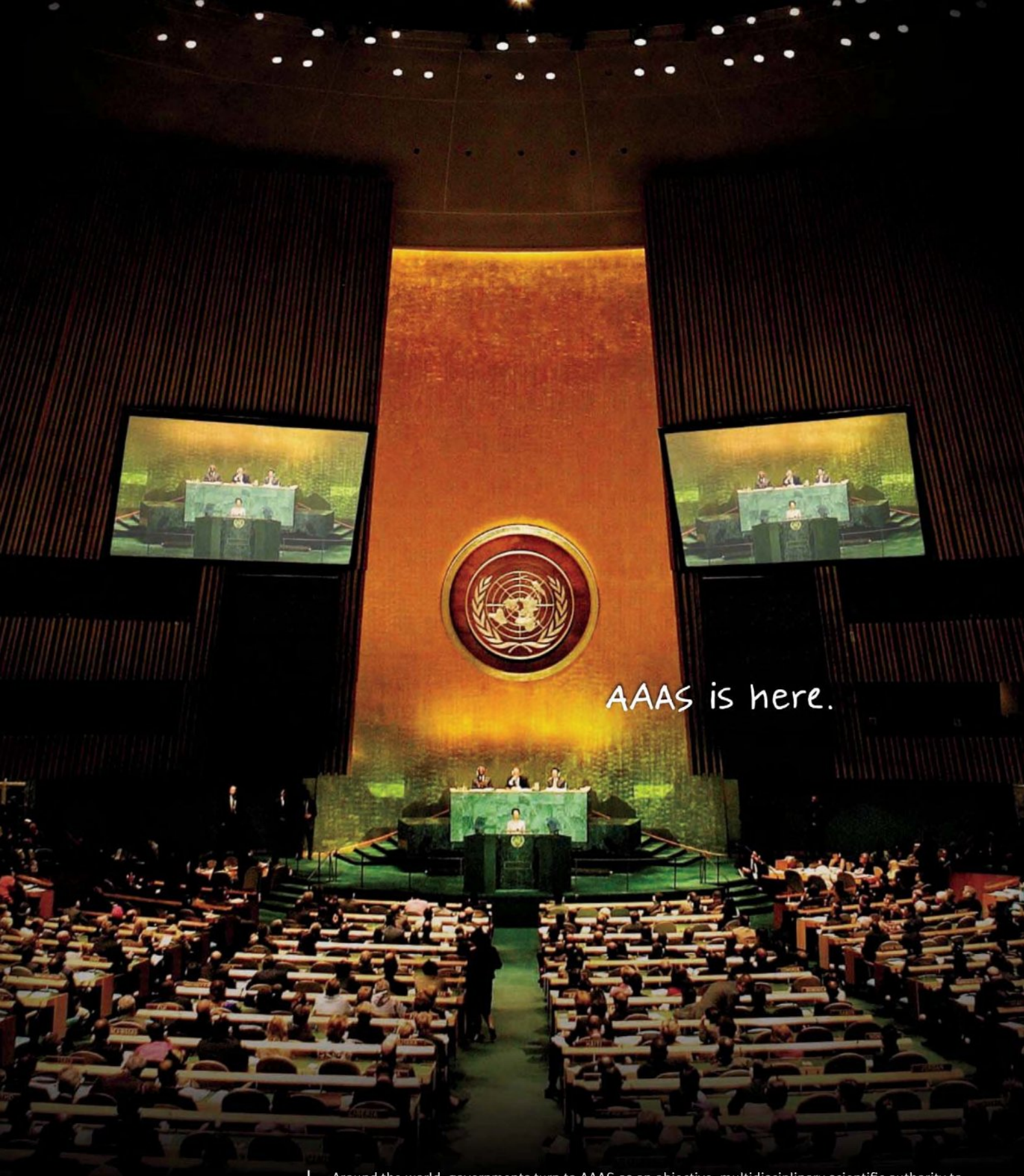

Science funding
Climate regulation
Human rights

Around the world, governments turn to AAAS as an objective, multidisciplinary scientific authority to educate public officials and judicial figures on today's most pressing issues. Our goal is to promote informed policy decisions that benefit society. And this is just one of the ways that AAAS is committed to advancing science to support a healthy and prosperous world.
Join us. Together we can make a difference. **aaas.org/plusyou**

AAAS + U = Δ

Continued from page 639

Of Ancient Iron and Oxygen

Finding clues to understand the early evolution of ocean and atmospheric chemistry and its links to the evolution of life remains a daunting task. Often just a few rock samples provide our only evidence of what conditions on Earth were like long ago. **Reinhard *et al.*** (p. 713) combined iron speciation data from a 2.5-billion-year-old shale from Australia with sulfur isotope data from this and nearby formations to conclude that oxygen chemistry predominanty consisted of an anoxic sulfide–rich water column, instead of iron-rich oceans, as previously speculated. Thus, brief pulses of reduced iron from hydrothermal vents may have been responsible for the formation of nearby banded iron formations and may have provided enough buffering to prolong the appearance of atmospheric oxygen generated by the expansion of newly evolved cyanobacteria.

Flu's Tricky Tricks

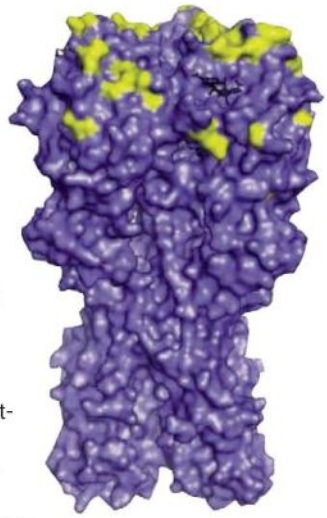

After vaccination against influenza A virus, single-point mutations are selected in hemagglutinin (the virus molecule that binds to sialic acid molecules on the surface of host cells) that escape neutralization by polyclonal antibody responses. **Hensley *et al.*** (p. 734) have discovered that in mice these mutations increased the virus's avidity for sialic acid. Amino acid substitutions that occur during reiterations of immune escape and avidity modulation can thus drive antigenic variation. This constant evolution of influenza viruses requires us to change vaccine components annually, and, for equine influenza, **Park *et al.*** (p. 726) show that as the match between virus and vaccine strains drifts apart with time, the probability of becoming infected and the length of the infectious period increase to the point where outbreaks occur. Nevertheless, even imperfect vaccines may be of benefit to a population because increasing the proportion of vaccinated individuals can supply enough herd immunity to offset a poor antigenic match, especially if used in conjunction with antiviral drugs. For humans, **Yang *et al.*** (p. 729, published online 10 September) estimate that the rate of transmission within U.S. households puts influenza A 2009 H1N1 (the current pandemic "swine flu") in the higher range of transmissibility, compared to past seasonal and pandemic strains. Thus, to achieve mitigation this fall, children should be the first recipients of vaccine, followed by adults—aiming overall for 70% coverage of the population.

All Together Now

Deciding how to change emissions of polluting gases that affect climate through their radiative forcing properties requires that the quantitative impact of these emissions be understood. Most past calculations of this type have considered only the radiative forcing of the specific emission and its atmospheric lifetime. **Shindell *et al.*** (p. 716; see the Perspectives by **Arneth *et al.*** and by **Parrish and Zhu**) use sophisticated atmospheric chemical and climate modeling to determine how gas-aerosol interactions affect the radiative properties of the atmosphere, finding significant departures from the standard method for emissions of methane, carbon monoxide, and nitrogen oxides. These findings should help to optimize strategies for mitigating global warming by reducing anthropogenic emissions.

Iron Sensor

Intracellular iron is an essential cofactor for many proteins, but can also damage macromolecules, so its levels are carefully controlled. Cellular iron homeostasis is mediated by iron regulatory proteins that regulate the expression of genes involved in iron uptake and storage. However, it is not clear how cells sense iron bioavailability (see the Perspective by **Rouault**). Using different approaches, **Salahudeen *et al.*** (p. 722, published online 17 September) and **Vashisht *et al.*** (p. 718, published online 17 September) have identified the F-box protein FBXL5 as a human iron sensor. FBXL5 is part of an E3 ubiquitin ligase complex that regulates the degradation of iron regulatory proteins and thereby cellular iron levels. It contains a hemerythrin domain that binds iron and acts as an iron-dependent regulatory switch, causing the degradation of FBXL5 under low iron conditions. This alternative pathway for the regulation of iron homeostasis has implications for both normal cellular physiology and disease.

CREDIT: HENSLEY *ET AL.*

Dialysis so easy you'll be hooked.

You'll never use anything else again. The new Thermo Scientific Slide-A-Lyzer G2 Dialysis Cassettes enable simple, effective dialysis without the hassle of conventional tubing.

- New top-loading port for pipetting or two side ports for syringe injecting
- Secure – sample stays inside the chamber with unique locking top cap design; built-in buoy means no need for floats
- 95% sample recovery – gives you maximum dialysis of even the smallest samples (0.5 to 70 ml) – available with 2K, 3.5K, 7K, 10K and 20K MWCO membranes
- Stands on lab benchtop for easy viewing and handling

To learn more, visit www.thermo.com/pierce or call +1 815-968-0747 or 800-874-3723. Outside the U.S., contact your local distributor.

New twist-off top and pipetting port.
Pipette directly into the Slide-A-Lyzer G2 Dialysis Cassette or use the side ports for syringe injecting.

Moving science forward

Thermo SCIENTIFIC
Part of Thermo Fisher Scientific

Eric J. Barron is director of the National Center for Atmospheric Research, Boulder, Colorado. E-mail: barron@ucar.edu

Beyond Climate Science

THE UNITED STATES IS MOVING RAPIDLY INTO AN AGE OF CLIMATE-RELATED DECISIONS INVOLVING mitigation and adaptation, following decades of focusing on reducing uncertainties in attribution and prediction. But the nation lacks a deliberate approach to generating the "environmental intelligence" needed to support good decisions.

It is critical to create a single, credible, authoritative source of climate information to support decision-makers. Consider one example: Will U.S. cities or states simply pick one climate model as a basis for decisions? Will the information be defensible as the best available? The level of authority required dictates that a National Climate Service be established. Climate information must also be more accessible. Many decision-makers don't know what is available, where to find it, how to use it, or the limits to appropriate use. A highly developed research-provider–user partnership will be essential to create a useful service. Information from diverse federal agencies should be provided through a single portal. The potential for creating a National Climate Service is high. The U.S. National Oceanic and Atmospheric Administration has a strong foundation, and Congress is actively considering legislation.

The United States also lacks sufficient investment in the sciences required for moving beyond climate science to define impacts and vulnerabilities. In 2001, the United States Global Change Research Program's report "Climate Change Impacts on the United States" described a new vision for climate-impacts research, with integrated regional and sector (e.g., water, health, ecosystems) analysis at its core. However, funding was short-lived. Currently, 40 years of intensive climate model development is being coupled to what amounts to a cottage industry of impact sciences. The result is that our understanding of how ecosystems, water, human health, agriculture, and energy will respond to climate change advances only slowly.

The nation needs a concerted effort to develop predictive models explicitly for adaptation and mitigation. Weather and climate models offer a powerful foundation for expanding the ability to predict a broader range of environmental factors. The potential is enormous. Consider, for example, that infectious diseases have strong relationships to the environment. Imagine the societal benefit of a partnership between the climate and human health communities in developing models to provide advance warning of adverse health outcomes. Although these communities are beginning to interact with positive results, a far more rapid pace is needed to develop predictive capabilities that will adequately serve society.

It is also critical to tackle the issue of spatial and temporal scales. Human vulnerability to climate change largely revolves around how climate change will influence high-impact "weather," such as hurricanes. And regional climate model output with high spatial resolution is a frequently stated need of agencies that manage water, forest, and agricultural resources. Weather and climate prediction must become integrated. Climate information that is useful on a regional scale will only slowly become available without the concerted investments required to enable this new class of models.

Finally, good decisions depend on the ability to create "environmental intelligence" that can be accessed by decision-makers. The strongest intersection between human decision-making and environmental stresses is at a regional or local level. Its five critical elements are integrated regional observations, a comprehensive and accessible regional data and information system, process studies designed to improve regional prediction, a regional climate modeling capability appropriate for society's needs, and efforts to promote the intersection between research, operations, and applications. The uniqueness of this framework stems from the required level of integration, scale of prediction, and promotion of new modes of research.

The deficiencies in the current approach to environmental intelligence are not unique to the United States. The 2009 World Climate Conference has called for a global approach to climate services, although few nations have developed formal plans. This recommendation is a positive development, but it is insufficient. The research strategies and investments needed to define impacts and vulnerabilities and to enable wise decisions are not in place. **– Eric J. Barron**

10.1126/science.1179807

EDITED BY GILBERT CHIN AND JAKE YESTON

BIOMEDICINE

Staying Off the Beating Track

Atrial fibrillation, the most common heart arrhythmia observed in the clinic, occurs when the heart's normal pacemaker activity is disrupted by an aberrant electrical stimulus that in many cases originates in the pulmonary veins. Although individuals with cardiovascular disease are often affected, atrial fibrillation can also arise in healthy folks, and the cellular mechanisms that launch and maintain it are not fully understood. To date, research and treatment efforts have focused on pulmonary vein myocytes as the source of the electrical activity that triggers atrial arrhythmias.

Levin *et al.* describe an unusual cell type whose dysfunction can initiate atrial arrhythmia—at least in mice. These cells, referred to as cardiac melanocytes because they express the melanin synthetic enzyme dopachrome tautomerase (DCT), reside in regions associated with atrial arrhythmia (for instance, in the pulmonary veins and atria) and in culture, display action potentials resembling those of atrial myocytes. Mice lacking cardiac melanocytes are more resistant than wild-type mice to treatments that induce atrial arrhythmias. Furthermore, the enzyme DCT functions as more than a cell marker; mice that lack DCT are more susceptible to atrial arrhythmias, suggesting that this enzyme reduces the likelihood of ectopic electrical activity, possibly via buffering of intracellular calcium and reactive oxygen species. Cardiac melanocytes are also present in relevant areas of the human heart and pulmonary veins, but whether they contribute to atrial fibrillation in humans remains to be determined. — PAK

J. Clin. Invest. **119**, 10.1172/JCI39109 (2009).

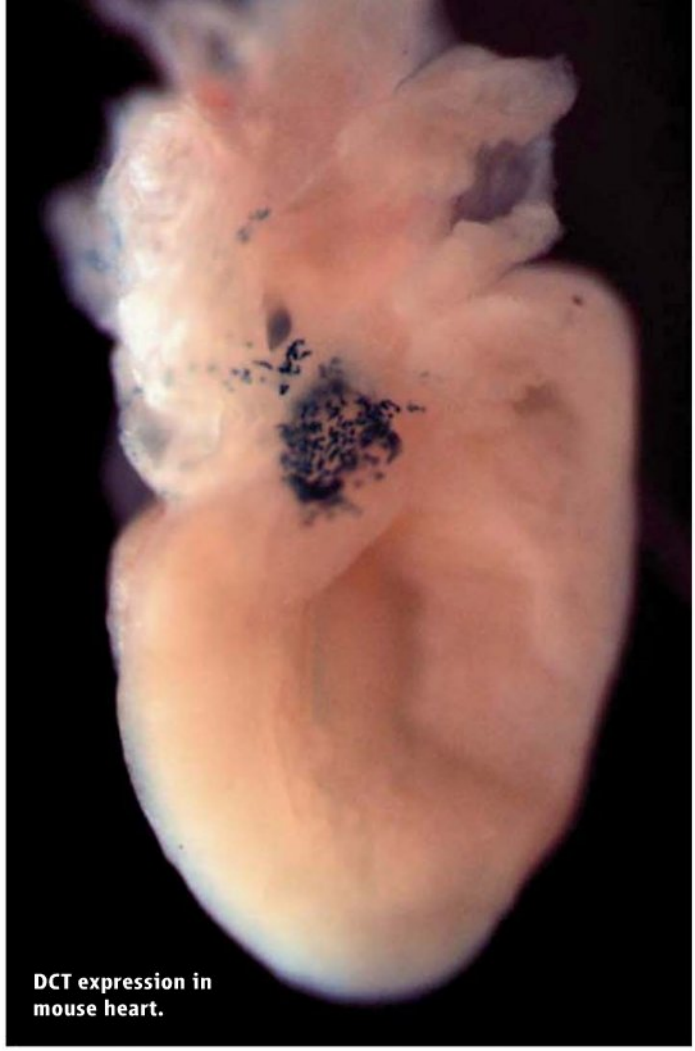

DCT expression in mouse heart.

GEOCHEMISTRY

Fertilizing Fool's Gold

High levels of nitrates released from agricultural fertilizers pose a serious threat to groundwater quality. Ameliorating this problem is not easy, but some help may be available from the natural soil bacterial communities that reduce nitrate into inert N_2 gas. The rate of this denitrification step typically depends on the nature and concentration of the compounds that feed electrons into the process, providing the bacteria with energy. Most often bacteria use abundant organic matter, but in certain environments the iron(II) in minerals such as pyrite (FeS_2) can also be oxidized. By monitoring the groundwater below a stretch of farmland in the Netherlands, Zhang *et al.* found that pyrite-coupled denitrification was the dominant nitrate-consuming reaction. Due at least in part to this reaction, nitrate levels in the groundwater were lower than levels measured 10 years ago; however, groundwater below a nearby unfertilized forest actually became enriched in nitrate over this same period. The transport of nitrate away from the farmland suggests that despite abundant pyrite remaining in the aquifer, complete denitrification occurs more slowly than nitrate's residence time. Complicating matters is the fact that levels of trace elements associated with pyrite (e.g., As, Zn, Ni) increased below the forest as well, signifying that these bacteria may be mobilizing heavy metals in the subsurface despite their benevolence in removing some of the nitrates. — NW

Geochim. Cosmochim. Acta **73**, 6716 (2009).

EVOLUTION

Something from Nothing

Gene duplication is a common means for generating the raw material of new genes, especially because the duplicated coding and regulatory regions provide a ready-made, fully active substrate for evolutionary processes that lead to sub- or neofunctionalization. The de novo origin of genes—which refers to the so-called orphan genes whose ancestry cannot be traced to known genes—is less frequently encountered and thought to occur when transposable elements or genome rearrangements bring together fragments of genetic clay from which a transcribable structure can be built.

Heinen *et al.* identify an orphan gene that has been born directly from a virgin intergenic region in the mouse genome. This gene is limited to the genus *Mus* and appeared roughly 3 million years ago. It is under positive selection, having been subject to a selective sweep in the recent past. Although there are two open reading frames in the transcript, it seems to function as a noncoding RNA that is alternatively spliced and hence named *Polymorphic derived intron-containing* (*Poldi*). *Poldi* is expressed in mouse testis, and knockout of the gene results in reduced testis weight and sperm motility. As differential expression of *Poldi* requires only a simple promoter, and cryptic splicing and polyadenylation signals are already present in intergenic regions, the birth of new genes may be less rare than we thought. — GR

Curr. Biol. **19**, 1527 (2009).

CHEMISTRY

A Stack of Amides

Amides are well arranged to form hydrogen bonds with one another, an interaction that plays a major role in the three-dimensional organization of proteins as well as synthetic supramolecular assemblies. James III *et al.* have discovered that in the case of γ-peptides, a competing and comparably strong organizing force arises from the amide moiety's substantial dipole. Specifically, they probe small test substrates bearing two amide groups using highly sensitive ultraviolet-infrared double resonance spectroscopy in the gas phase. By comparing the data with simulations, they uncover a conformation in which the planar amides at either end of the molecule stack against one another in antiparallel fashion, so their dipoles adopt a mutually attractive orientation. The authors anticipate that the stacking tendency could prove a useful design element in construction of synthetic foldamers. — JSY

J. Am. Chem. Soc. **131**, 14243 (2009).

APPLIED PHYSICS

Quantum Problem Solvers

Quantum computers, when they become available, will harness the power of quantum mechanics to perform calculations and searches, outperforming classical computers at certain tasks. The development of quantum computers is two-pronged: Both hardware and software must be devised. The focus in the software realm is on which problems can be solved and how to do so. Solving a set of linear equations is a generic and important problem in many fields of science, engineering, and mathematics. On a classical computer the computational cost of extracting a solution grows linearly with the size of the system. Harrow *et al.* have developed a quantum algorithm that will solve the problem much more rapidly (scaling as the logarithm of the system size), requiring exponentially less time. Now we wait for the machinery to arrive. — ISO

Phys. Rev. Lett. **103**, 150502 (2009).

IMMUNOLOGY

Sensing Non-Self DNA

One way the immune system recognizes infection is by sensing the presence of foreign nucleic acids in the cytoplasm. Although it had been established that microbial double-stranded DNA (dsDNA) triggered the production of the inflammatory cytokine interferon-β, the identity of the dsDNA sensor remained elusive.

Chiu *et al.* and Ablasser *et al.* suggest that RNA polymerase III (Pol III) is the culprit. Pol III, which transcribes genes encoding several kinds of RNA (such as transfer and ribosomal), has been shown to be present in the cytoplasm, but what it did there was unclear. These authors show that cytoplasmic Pol III transcribes AT-rich microbial dsDNA into 5′-triphosphate–containing RNA that is then detected by the retinoic acid–induced gene I (RIG-I), which proceeds to switch on the production of interferon-β. In the absence of Pol III, infection with *Legionella pneumophila* or Epstein-Barr virus does not induce interferon-β, indicating that Pol III is required for proper immunity both to bacterial and to viral infection. — KLM

Cell **138**, 576 (2009);
Nat. Immunol. **10**, 1065 (2009).

DEVELOPMENT

Leveraging Bank Deposits

Stem cells are essential, yet exceedingly scarce, components of regenerating tissues such as skin and blood. The more broadly useful stem cell—the pluripotent stem cell—can be derived from embryo cells. Remarkably, cells with similar potential can be derived from more specialized cells that have been induced to backtrack under the direction of a suite of four transcription factors. Nevertheless, each of these stem cell sources suffers from distinct problems of availability, utility, and ethics.

Two groups introduce another source of pluripotent stem cells: umbilical cord blood. This blood can be collected fairly easily with little risk to the donor, has suffered less exposure than adult cells to environmental insult, and has found favor in recent years as a source of hematopoietic stem cells. Giorgetti *et al.* show that pluripotency can be induced, even from previously frozen cord blood bank samples, with the use of only two transcription factors. Haase *et al.* describe the derivation of pluripotent cells from the endothelial cells of cord blood and demonstrate the differentiation of these into cells similar to cardiomyocytes (shown above with a cardiac-specific isoform of the muscle protein troponin T in red). — PJH

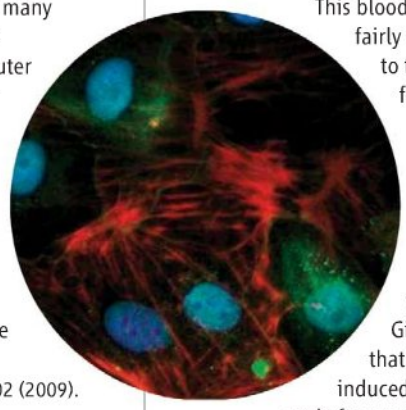

CREDIT: RUTH OLMER

Cell Stem Cell **5**, 353; 434 (2009).

www.sciencemag.org

Science

1200 New York Avenue, NW
Washington, DC 20005
Editorial: 202-326-6550, FAX 202-289-7562
News: 202-326-6581, FAX 202-371-9227
Bateman House, 82-88 Hills Road
Cambridge, UK CB2 1LQ
+44 (0) 1223 326500, FAX +44 (0) 1223 326501

Subscription Services For change of address, missing issues, new orders and renewals, and payment questions: 866-434-AAAS (2227) or 202-326-6417, FAX 202-842-1065. Mailing addresses: AAAS, P.O. Box 96178, Washington, DC 20090-6178 or AAAS Member Services, 1200 New York Avenue, NW, Washington, DC 20005

Institutional Site Licenses please call 202-326-6755 for any questions or information

Reprints: Author Inquiries 800-635-7181
Commercial Inquiries 803-359-4578

Permissions 202-326-7074, FAX 202-682-0816

Member Benefits AAAS/Barnes&Noble.com bookstore www.aaas.org/bn; AAAS Online Store www.apisource.com/aaas/ code MKB6; AAAS Travels: Betchart Expeditions 800-252-4910; Apple Store www.apple.com/eppstore/aaas; Bank of America MasterCard 1-800-833-6262 priority code FAA3YU; Cold Spring Harbor Laboratory Press Publications www.cshlpress.com/affiliates/aaas.htm; GEICO Auto Insurance www.geico.com/landingpage/go51.htm?logo=17624; Hertz 800-654-2200 CDP#343457; Office Depot https://bsd.officedepot.com/portalLogin.do; Seabury & Smith Life Insurance 800-424-9883; Subaru VIP Program 202-326-6417; VIP Moving Services www.vipmayflower.com/domestic/index.html; Other Benefits: AAAS Member Services 202-326-6417 or www.aaasmember.org.

science_editors@aaas.org	(for general editorial queries)
science_letters@aaas.org	(for queries about letters)
science_reviews@aaas.org	(for returning manuscript reviews)
science_bookrevs@aaas.org	(for book review queries)

Published by the American Association for the Advancement of Science (AAAS), *Science* serves its readers as a forum for the presentation and discussion of important issues related to the advancement of science, including the presentation of minority or conflicting points of view, rather than by publishing only material on which a consensus has been reached. Accordingly, all articles published in *Science*—including editorials, news and comment, and book reviews—are signed and reflect the individual views of the authors and not official points of view adopted by AAAS or the institutions with which the authors are affiliated.

AAAS was founded in 1848 and incorporated in 1874. Its mission is to advance science, engineering, and innovation throughout the world for the benefit of all people. The goals of the association are to: enhance communication among scientists, engineers, and the public; promote and defend the integrity of science and its use; strengthen support for the science and technology enterprise; provide a voice for science on societal issues; promote the responsible use of science in public policy; strengthen and diversify the science and technology workforce; foster education in science and technology for everyone; increase public engagement with science and technology; and advance international cooperation in science.

Information for Authors
See pages 807 and 808 of the 6 February 2009 issue or access www.sciencemag.org/about/authors

EDITOR-IN-CHIEF **Bruce Alberts**
EXECUTIVE EDITOR **Monica M. Bradford** NEWS EDITOR **Colin Norman**
MANAGING EDITOR, RESEARCH JOURNALS **Katrina L. Kelner**
DEPUTY EDITORS **R. Brooks Hanson, Barbara R. Jasny, Andrew M. Sugden**

Editorial senior editors/commentary Lisa D. Chong, Brad Wible; **senior editors** Gilbert J. Chin, Pamela J. Hines, Paula A. Kiberstis (Boston), Marc S. Lavine (Toronto), Beverly A. Purnell, L. Bryan Ray, Guy Riddihough, H. Jesse Smith, Phillip D. Szuromi (Tennessee), Valda Vinson, Jake S. Yeston; **associate editors** Kristen L. Mueller, Jelena Stajic, Nicholas S. Wigginton, Laura M. Zahn; **research associate** Alexis Wynne Mogul; **online editor** Stewart Wills; **associate online editors** Robert Frederick, Tara S. Marathe; **web content developer** Martyn Green; **book review editor** Sherman J. Suter; **associate letters editor** Jennifer Sills; **editorial manager** Cara Tate; **senior copy editors** Jeffrey E. Cook, Cynthia Howe, Harry Jach, Barbara P. Ordway, Trista Wagoner; **copy editors** Chris Filiatreau, Lauren Kmec; **editorial coordinators** Carolyn Kyle, Beverly Shields; **publications assistants** Ramatoulaye Diop, Joi S. Granger, Jeffrey Hearn, Lisa Johnson, Scott Miller, Jerry Richardson, Jennifer A. Seibert, Brian White, Anita Wynn; **editorial assistants** Emily Guise, Michael Hicks, Patricia M. Moore; **executive assistant** Sylvia S. Kihara; **administrative support** Maryrose Madrid; **editorial fellow** Melissa R. McCartney

News deputy news editors Robert Coontz, Eliot Marshall, Jeffrey Mervis, Leslie Roberts; **contributing editors** Elizabeth Culotta, Polly Shulman; **news writers** Yudhijit Bhattacharjee, Adrian Cho, Jennifer Couzin, David Grimm, Constance Holden, Jocelyn Kaiser, Sam Kean, Richard A. Kerr, Eli Kintisch, Andrew Lawler (New England), Greg Miller, Elizabeth Pennisi, Robert F. Service (Pacific NW), Erik Stokstad; **intern** Michael Torrice; **contributing correspondents** Dan Charles, Jon Cohen (San Diego, CA), Daniel Ferber, Ann Gibbons, Robert Koenig, Mitch Leslie, Charles C. Mann, Virginia Morell, Evelyn Strauss, Gary Taubes; **copy editors** Linda B. Felaco, Melvin Gatling, Melissa Raimondi; **administrative support** Scherraine Mack, Fannie Groom; **bureaus** New England: 207-549-7755; San Diego, CA: 760-942-3252, FAX 760-942-4979; Pacific Northwest: 503-963-1940

Production director James Landry; **senior manager** Wendy K. Shank; **assistant manager** Rebecca Doshi; **senior specialists** Steve Forrester, Chris Redwood; **specialist** Anthony Rosen; **Preflight director** David M. Tompkins; **manager** Marcus Spiegler; **specialist** Jason Hillman

Art director Yael Kats; **associate art director** Laura Creveling; **senior illustrators** Chris Bickel, Katharine Sutliff; **illustrator** Yana Greenman; **senior art associates** Holly Bishop, Preston Huey, Nayomi Kevitiyagala; **art associates** Jessica Newfield, Matthew Twombly; **photo editor** Leslie Blizard

***Science* International**

Europe (science@science-int.co.uk) **editorial: international managing editor** Andrew M. Sugden; **senior editor/commentary** Julia Fahrenkamp-Uppenbrink; **senior editors** Caroline Ash, Stella M. Hurtley, Ian S. Osborne, Peter Stern; **associate editor** Maria Cruz; **locum editor** Helen Pickersgill; **editorial support** Deborah Dennison, Rachel Roberts, Alice Whaley; **administrative support** John Cannell, Janet Clements, Louise Moore; **news: europe news editor** John Travis; **deputy news editor** Daniel Clery; **contributing correspondents** Michael Balter (Paris), John Bohannon (Vienna), Martin Enserink (Amsterdam and Paris), Gretchen Vogel (Berlin)

Asia Japan Office: Asca Corporation, Tomoko Furusawa, Rustic Bldg. 7F, 77 Tenjin-cho, Shinjuku-ku, Tokyo 162-0808, Japan; +81 3 6802 4616, FAX +81 3 6802 4615, inquiry@sciencemag.jp; **asia news editor** Richard Stone (Beijing: rstone@aaas.org); **contributing correspondents** Dennis Normile [Japan: +81 (0) 3 3391 0630, FAX +81 (0) 3 5936 3531; dnormile@gol.com]; Hao Xin [China: +86 (0) 10 6307 4439 or 6307 3676, FAX +86 (0) 10 6307 4358; cindyhao@gmail.com]; Pallava Bagla [South Asia: +91 (0) 11 2271 2896; pbagla@vsnl.com]

EXECUTIVE PUBLISHER **Alan I. Leshner**
PUBLISHER **Beth Rosner**

Fulfillment Systems and Operations (membership@aaas.org); **director** Waylon Butler; **senior systems analyst** Nomuna Nyamaa; **customer service supervisor** Pat Butler; **specialists** Latoya Casteel, LaVonda Crawford, Vicki Linton, April Marshall; **data entry supervisor** Cynthia Johnson; **specialists** Shirlene Hall, Tarrika Hill, William Jones

Business Operations and Administration director Deborah Rivera-Wienhold; **assistant director, business operations** Randy Yi; **manager, business analysis** Eric Knott; **manager, business operations** Jessica Tierney; **financial analysts** Priti Pamnani, Celeste Troxler; **rights and permissions: administrator** Emilie David; **associate** Elizabeth Sandler; **marketing director** Ian King; **marketing managers** Allison Pritchard, Alison Chandler, Julianne Wielga; **marketing associates** Aimee Aponte, Mary Ellen Crowley, Adrian Parham, Wendy Wise; **marketing executive** Jennifer Reeves; **director, site licensing** Tom Ryan; **director, corporate relations** Eileen Bernadette Moran; **publisher relations, eresources specialist** Kiki Forsythe; **senior publisher relations specialist** Catherine Holland; **publisher relations, east coast** Phillip Smith; **publisher relations, west coast** Philip Tsolakidis; **fulfillment supervisor** Iquo Edim; **fulfillment coordinator** Carrie MacDonald; **marketing manager** Christina Schlecht; **marketing associate** Mary Lagnaoui; **electronic media: manager** Lizabeth Harman; **project manager** Trista Snyder; **assistant manager** Lisa Stanford; **senior production specialists** Christopher Coleman, Walter Jones; **production specialists** Nichele Johnston, Kimberly Oster

Advertising director, worldwide ad sales Bill Moran

Product (science_advertising@aaas.org); **midwest/west coast/w. canada** Rick Bongiovanni: 330-405-7080, FAX 330-405-7081; **east coast/e. canada** Laurie Faraday: 508-747-9395, FAX 617-507-8189; **uk/europe/asia** Roger Goncalves: TEL/FAX +41 43 243 1358; **japan** ASCA Corporation, Nanako Ide +81 (0) 3 6802 4616, FAX +81 (0) 3 6802 4615; ads@sciencemag.jp; **senior traffic associate** Deiandra Simms

Commercial Editor Sean Sanders: 202-326-6430

Project Director, Outreach Brianna Blaser

Classified (advertise@sciencecareers.org); **u.s.: sales manager** Daryl Anderson: 202-326-6543; **midwest** Tina Burks: 202-326-6577; **east coast** Alexis Fleming: 202-326-6578; **west/south central** Nicholas Hintibidze: 202-326-6533; **sales coordinators** Rohan Edmonson, Shirley Young; **international: sales manager** Tracy Holmes: +44 (0) 1223 326525, FAX +44 (0) 1223 326532; **sales** Susanne Kharraz, Dan Pennington, Alex Palmer; **sales assistant** Lisa Patterson; **japan** ASCA Corporation, Jie Chin +81 (0) 3 6802 4616, FAX +81 (0) 3 6802 4615; careerads@sciencemag.jp; **advertising support manager** Karen Foote: 202-326-6740; **advertising production operations manager** Deborah Tompkins; **senior production specialist/graphic designer** Amy Hardcastle; **senior production specialist** Robert Buck; **senior traffic associate** Christine Hall

AAAS Board of Directors retiring president, chair James J. McCarthy; **president** Peter C. Agre; **president-elect** Alice Huang; **treasurer** David E. Shaw; **chief executive officer** Alan I. Leshner; **board** Alice Gast, Linda P. B. Katehi, Nancy Knowlton, Cherry A. Murray, Julia M. Phillips, Thomas D. Pollard, David S. Sabatini, Thomas A. Woolsey

AAAS
ADVANCING SCIENCE, SERVING SOCIETY

Forget DNA purification

Choose Direct PCR

Take the direct route from sample to results

Finnzymes' Direct PCR approach saves you time and cost by allowing amplification of DNA directly from the source material. No DNA purification is needed. Direct PCR is suitable for various kinds of sample materials such as plant and animal tissues, blood, and FFPE tissue samples.

Direct PCR is based on Finnzymes' unique PCR enzymes, Phusion® High-Fidelity and Phire® Hot Start DNA Polymerases. These polymerases are exceptionally tolerant of many PCR inhibitors. To achieve the shortest possible protocols, combine the Direct PCR approach with Finnzymes' Piko® Thermal Cyclers and UTW® reaction vessels.

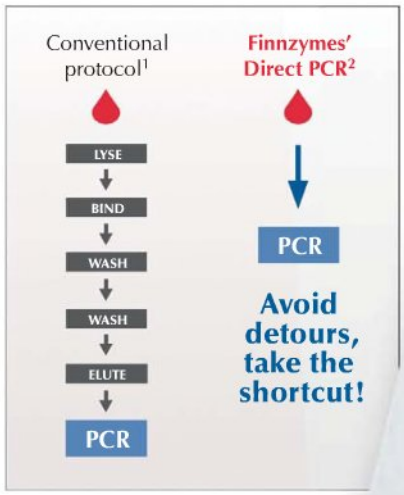

[1] Commercial extraction kit for blood DNA
[2] Phusion® Blood Direct PCR Kit

NEW!

Optimized kits available:

Phire® Plant Direct PCR Kit
for plant material

Phire® Animal Tissue Direct PCR Kit*
for various animal tissues

Phusion® Blood Direct PCR Kit
for blood

Try the Direct PCR Kits now with 30% discount!

1 kit/customer. Please use the code **Science09** when placing an order. Orders in the US can be placed online with New England Biolabs. For other countries, contact your local Finnzymes' distributor. Offer valid through Dec 31, 2009.

*Phire Animal Tissue Direct PCR Kit available in autumn 2009.

See the latest results, application notes and product updates at www.finnzymes.com/directpcr

NEW ENGLAND BioLabs inc.
enabling technologies in the life sciences

Reagents distributed in US and Canada by New England Biolabs.
For other products and countries visit www.finnzymes.com

FINNZYMES
TOOLS FOR MOLECULAR BIOLOGY

Cell as Time Capsule

Biochemist and author Nick Lane, 42, of University College London has won UCL's first £150,000 Provost's Venture Research Prize for researchers "whose ideas challenge the norm and have the potential to substantially change the way we think about an important subject."

Over the next 3 years, Lane proposes to use his prize to tackle a few simple but deep questions, such as: Why have complex cells evolved only once in 4 billion years? "A narrowly genetic perspective suggests that complex life should evolve repeatedly," Lane says. He suspects complexity resulted from a rare merging of two species. Only after our single-celled ancestors engulfed bacteria—which became modern cells' energy-producing mitochondria—did they get enough energy to build and run a complex cell. Once he's put together his theory, Lane says, he plans some experiments with the help of "labs who know what they're doing."

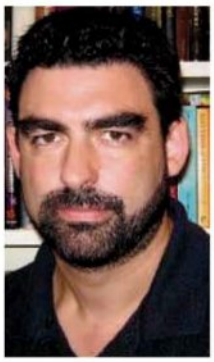

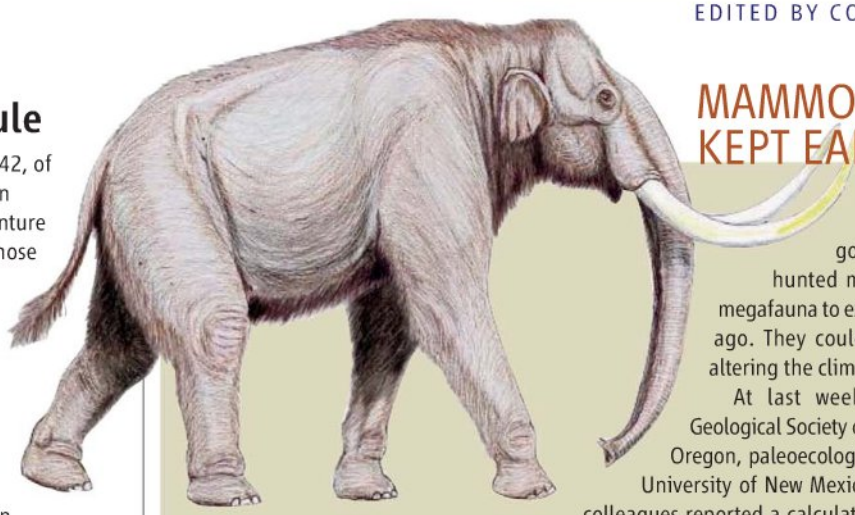

MAMMOTH BURPS KEPT EARTH WARM?

Paleo-Indians were just after a good meal when they hunted mammoths and other megafauna to extinction 13,000 years ago. They couldn't know they were altering the climate too.

At last week's meeting of the Geological Society of America in Portland, Oregon, paleoecologist Felisa Smith of the University of New Mexico, Albuquerque, and colleagues reported a calculation of just how much impact on the climate wiping out the mammoths and 113 other species of large herbivores in the Americas could have had. Such herbivorous mammals, including domestic livestock, belch prodigious amounts of methane, a powerful greenhouse gas, the researchers noted. That's bad for today's climate. But back then, it was on the chilly side anyway. Driving all those large herbivores to extinction robbed the globe of about 10 million tons of methane per year that had been boosting the natural greenhouse effect, the group calculates. Deprived of all those mammoth-size burps, climate would have cooled.

As it happened, the world momentarily staggered back toward the last ice age about then for other reasons. But Smith and colleagues suggest "humans measurably influenced" methane flows, and thus climate, long before agriculture and the trappings of civilization. Paleobiologist Scott Wing of the National Museum of Natural History in Washington, D.C., says, "This is a reminder that there are lots of ways for the climate system and the biota to interact."

Not Out of Java

Most scientists think modern humans evolved only in Africa. But the theory of "multiregionalism" still has its holdouts who think *Homo sapiens* evolved all over the Old World.

Now the biggest study yet of fossil skulls from Australia, Indonesia, Africa, and the Middle East has delivered another blow to that theory. Paleoanthropologist Michael Westaway of the Queensland Museum in Brisbane, Australia, and primatologist Colin Groves of the Australian National University in Canberra compared 26 15,000- to 40,000-year-old skulls from the Willandra Lakes of New South Wales, Australia, with skulls of 19 early modern humans, dated at up to 195,000 years old, and five *H. erectus* skulls from Java (dates uncertain).

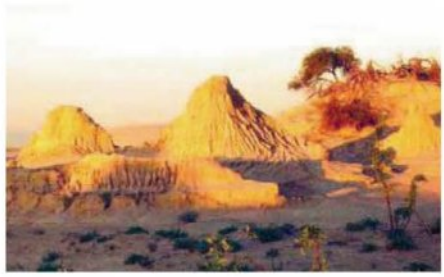

Willandra Lakes region.

Puzzlingly, the Willandra skulls include both light (gracile) and heavy-set (robust) crania. The out-of-Africa camp thinks they all descend from a single population, but some multiregionalists argue that they could have two sets of roots: in robust Indonesian *H. erectus* and gracile people from China. The researchers looked for signs that the robust Willandra individuals inherited some traits, such as a distinctive brow ridge, from the Indonesian hominins. They found none, they reported in the journal *Archaeology in Oceania*. "There were commonalities between the Australian, African, and Middle Eastern people, but the Indonesian specimens stood outside the range," Westaway says.

But paleoanthropologist Fred Smith of Illinois State University in Normal says the jury is still out. He thinks modern humans arose in Africa but later bred with archaic locals around the globe. "I'm still not convinced that it [the study] proves there is no assimilation," he says.

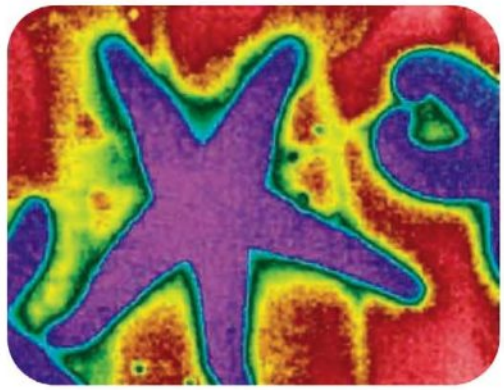

Natural Coolant

This infrared image of a sea star from California's Bodega Bay reveals how it keeps cooler than its surroundings. Marine biologists led by Sylvain Pincebourde of the University of South Carolina, Columbia, put sea stars in aquaria that mimicked changes in heat and water levels in their intertidal habitat. When exposed to warm air at low tide, the researchers found, sea stars wait until high tide and then suck more seawater than usual into a large fluid-filled body cavity. The extra fluid increases the animals' "thermal inertia," buffering them against the next low-tide exposure. The authors report the result in the December issue of *The American Naturalist*.

CREDITS (TOP TO BOTTOM): DMITRY BOGDANOV; ANA HIDALGO; PHOTO BY BRIAN HELMUTH AND SYLVAIN PINCEBOURDE; LYNN SALMON

AIDS vaccines: What next? 652

Hominid find in China 655

SCIENTIFIC MISCONDUCT

Hwang Convicted But Dodges Jail; Stem Cell Research Has Moved On

Disgraced stem cell scientist Woo Suk Hwang was handed a 2-year suspended prison sentence on 26 October for embezzlement and bioethics law violations. And the scientific community seemed to just shrug.

Have South Korean researchers been keenly following the proceedings? Asked before the verdict was announced, Dong-Wook Kim, director of the Korean Stem Cell Research Center in Seoul, replied with a curt "No!" "The scientific community has moved way beyond Hwang and will read about [the verdict] with amusement," agreed George Daley, a stem cell researcher at Children's Hospital Boston.

Suspended sentence. Stem cell scientist Woo Suk Hwang, talking to reporters on 26 October, won't serve jail time.

The nonchalance is quite a change from the anxious attention focused on Hwang in late 2005. Hwang had almost single-handedly brought the goal of therapeutic cloning—generating replacement tissue genetically matched to a patient—within reach. He claimed a first in developing a human embryonic stem (hES) cell line from a cloned blastocyst in 2004 (http://www.sciencemag.org/cgi/content/abstract/1094515) and followed that up with a 2005 paper claiming to have generated 11 patient-specific stem cell lines (http://www.sciencemag.org/cgi/content/abstract/1112286). Hwang became a national hero in Korea, and would-be collaborators and competitors flocked to his Seoul National University (SNU) lab to see how he did it.

But in November 2005, in response to allegations, Hwang admitted that members of his research team had donated oocytes and that other donors had been paid—both ethically questionable practices. Days later, as questions about his work mounted, he informed *Science* that some images in the 2005 paper were duplicated, although he insisted that the results were real. Alan Colman, a stem cell researcher then in Singapore, told *Science* at the time that if Hwang's results did not hold up, many might think the research "too difficult and inefficient to pursue." He and others also worried that ethical lapses would provide ammunition to opponents of hES cell research (*Science*, 16 December 2005, p. 1748).

Hwang's results didn't hold up. On 29 December, an investigative committee at SNU found the 2005 paper fraudulent and on 10 January 2006 concluded that the 2004 paper was bogus as well. (Hwang's one true achievement was cloning a dog, named Snuppy.) The president of SNU called the incident a "blemish on the whole scientific community."

But now, after a criminal trial that lasted 40 months, longer than Hwang's 2 years in the spotlight, the community "feels relieved that we dodged the bullet and that the field has remained vigorous," says Daley.

Several factors blunted the impact of the fraud. The public "soon realized that this is such a bizarre case that it was an aberration," says Insoo Hyun, a bioethicist at Case Western Reserve University in Cleveland, Ohio. More significantly, just 6 months after Hwang's papers were retracted, Kyoto University's Shinya Yamanaka reported that introducing just four genes into mouse skin cells could turn them into something that closely resembles embryonic stem cells. He later showed that this direct reprogramming works with human cells as well, resulting in what are called induced pluripotent stem (iPS) cells.

Since then, several groups have reported creating iPS cell lines from patients with various illnesses. But no one has yet reported success in creating stem cells from a cloned human blastocyst, as Hwang claimed in his 2004 *Science* paper. "I think the game-changing breakthrough of direct reprogramming pushed the nuclear-transfer imperative to the background," Daley says.

TIMELINE OF EVENTS

12 February 2004: "Evidence of a Pluripotent Human Embryonic Stem Cell Line Derived from a Cloned Blastocyst" published in *Science*.

6 May 2004: *Nature* alleges unethical ooctye donation.

19 May 2005: "Patient-Specific Embryonic Stem Cells Derived from Human SCNT Blastocysts," reporting the creation of 11 stem cell lines derived from patients, published in *Science*.

4 August 2005: Hwang's team reports the first cloning of a dog, Snuppy, in *Nature*. ▶

22 November 2005: Korean TV reports evidence of unethical oocyte donation; 2 days later, Hwang admits it's true.

Early December 2005: Anonymous Korean scientists identify duplicated images and questionable DNA fingerprint data in Hwang's papers.

15 December 2005: Hwang and co-author Gerald Schatten ask *Science* to retract their May 2005 paper because of data problems; Hwang continues to defend validity of findings.

29 December 2005: Seoul National University (SNU) investigation reports there is no evidence Hwang's team produced any of the patient-specific stem cells reported in the May 2005 *Science* paper.

10 January 2006: An investigating committee at SNU concludes that both *Science* papers were fraudulent but that Snuppy really is a cloned dog.

20 January 2006: *Science* officially retracts both papers.

20 March 2006: SNU dismisses Hwang.

12 May 2006: Hwang is indicted on charges of fraud, embezzlement, and bioethics violations.

26 October 2009: A Seoul court convicts Hwang of embezzlement and bioethics charges, giving him a 2-year suspended prison sentence.

CREDITS (LEFT TO RIGHT): JO YONG-HAK/REUTERS/LANDOV; YOUNG HO/SIPA/NEWSCOM

Voices of women Nobelists
656

Engineering glaciers
659

Some even see a silver lining in the Hwang affair. "There could be no better case study than Hwang to underline the fact that you have to have ethics and science proceed together," says Hyun. He says the debacle was a catalyst for the International Society for Stem Cell Research to bring together researchers, legal scholars, bioethicists, and policy experts to craft guidelines for hES cell research (*Science*, 2 February 2007, p. 603).

Scientific journals now examine papers more closely. *Science*, for instance, now routinely screens all images in accepted papers, says Katrina Kelner, managing editor of research journals for AAAS, which publishes *Science*. "We did tighten up quite a few policies," including more stringent statements on conflicts of interest and the option to request institutional review board documents. The journal will soon require authors to identify their specific contributions to the research. Mike Rossner, executive director of the Rockefeller University Press in New York City, thinks journals have not gone far enough. "Only a handful do systematic screening of all image data in all papers accepted for publication," he says.

In Korea, researchers are now more committed to proper documentation of lab work and to scrupulous handling of research funds, says Jeong-Sun Seo, a geneticist at SNU College of Medicine. Hyun adds there is a new awareness that "good scientific research is also ethical research." And stem cell research is thriving. "Korea ranked fourth in the world in the number of accumulated publications on human ES cells, according to a report in *Cell Stem Cell* in July 2007," says the Korean Stem Cell Research Center's Kim.

Hwang still has supporters, who turned out in force each time he appeared in court. The Jang Yeong-sil Memorial Foundation, named for a 15th century Korean astronomer, awarded Hwang a medal for scientific excellence earlier this year. Meanwhile, Hwang has returned to veterinary science at the private Sooam Biotech Research Foundation in Gyeonggi Province, where his team has been cloning dogs. The province is also supporting Hwang's efforts to develop pigs for various research purposes. And he is even publishing, but his papers don't attract the attention they once did. **–DENNIS NORMILE**

With reporting by Yvette Wohn.

ENERGY RESEARCH

DOE Gives $151 Million to 'Out-of-Box' Research

Three days after President Barack Obama told a Massachusetts Institute of Technology audience that he would lead the country into a "new frontier" of clean energy research, a fledgling federal agency made a $151 million down payment on that promise.

On Monday, the Advanced Research Projects Agency–Energy (ARPA-E) gave grants to 37 teams at companies, universities, and national labs that are pursuing cutting-edge technologies. "If only one project in a particular area works and produces transformational research, that will be a big success," says Matt Rogers of the Department of Energy (DOE).

Congress created ARPA-E in 2007, but the Bush Administration never liked the idea. Obama's election and the appointment of Steven Chu as energy secretary changed the political dynamic, however, and Congress gave DOE $400 million in this winter's $787 billion stimulus package. Its first solicitation attracted 3700 concept papers (*Science*, 21 August, p. 926), which were whittled down to roughly 300 full proposals.

The awards, averaging $4 million for up to 3 years, are considerably larger than typical DOE grants in basic or applied energy. "The two strategies that the secretary was trying to get away from were either putting all your money into one [idea] or giving a little bit of money to 100 different approaches," said Rogers. The awards have gone to technologies close to commercialization, including wind turbines derived from jet engines, as well as to more fundamental research, such as a type of genetically engineered plant enzyme that could be activated to convert the plant into a biofuel.

Jet set. ARPA-E's first batch of awards includes funding for a novel wind turbine design, shown in this artist's representation.

CREDIT: FLODESIGN WIND TURBINE CORP.

One winner, a joint battery project run by Envia in Hayward, California, and Argonne National Laboratory outside Chicago, Illinois, aims to double storage capacity by using silicon anodes. DOE's vehicle-battery program has focused on developing titanium anodes because they promise longer-lasting batteries. Silicon anodes offer even greater capacity but cause swelling during recharge. A design using nanotubes could lick that problem and make a "huge impact," says Argonne's Khalil Amine. Another grantee, Massachusetts–based start-up 1366 Technologies, has had trouble getting funding to explore cheaper ways to manufacture silicon wafers for photovoltaic cells. So ARPA-E's willingness to take a flyer on such techniques was a godsend, says 1366's Frank van Mierlo.

The agency plans a second solicitation at the end of the year for its remaining $249 million. And some supporters are already worried that Congress might lose patience with the program if, as is expected, many of the projects fall short of producing transformational change.

Representative Bart Gordon (D–TN), chair of the House science committee, confesses that blowback from nonstarters is his "biggest worry." But he thinks "the appropriators will see the value" over time of taking such calculated gambles, offering as proof the agency's 50-year-old counterpart within the Department of Defense. "Look at all the successes out of DARPA," he says.

–ELI KINTISCH

Short supply. Limited blood samples from Thai participants will complicate efforts to find correlates of protection.

HIV/AIDS RESEARCH

Beyond Thailand: Making Sense of a Qualified AIDS Vaccine 'Success'

When researchers announced on 24 September that an AIDS vaccine trial had positive results for the first time in history, many wondered whether they were real. Some prominent skeptics remain, but that debate has largely given way to intense discussions about how to build on this surprising finding. "The results are conceptually a game changer," says AIDS vaccine researcher Gary Nabel, who heads the Vaccine Research Center at the U.S. National Institute of Allergy and Infectious Diseases (NIAID), the main funder of the $105 million study.

Already, researchers have begun discussing the staggering challenge of probing blood samples from the more than 16,000 people in Thailand who participated in the trial to figure out which immune responses led to the modest protection reported. "The scientific community is going to throw everything it can at this," says Nabel. "We can't afford to not pursue every clue we have here."

The key question is whether the study will help reveal the long-sought immune responses that correlate with protection. "There are no guarantees, and it's not going to be easy," Nabel says. Peggy Johnston, who heads HIV/AIDS vaccine research at NIAID, says it's a long shot: "I think it's more likely that we'll be able to *eliminate* a correlate."

But even if these so-called correlates of protection remain elusive, the study is leading researchers to reassess the fundamental differences between preventing and controlling an infection, related findings from recent monkey studies, and the possibility that even a mediocre vaccine can help under some conditions.

The 6-year Thai study, run by the U.S. Military HIV Research Program in collaboration with the Thai Ministry of Public Health, combined two vaccines that each had performed poorly in earlier trials (*Science*, 2 October, p. 26). The study's lead investigators revealed in press conferences in the United States and Thailand last month that HIV infected 51 of nearly 8200 people who received the vaccines versus 74 people of a similar number who received a placebo. Most were heterosexuals who had no high-risk behavior. This translated to 31.2% fewer infections in the vaccinated group, and it just barely met the arbitrary cutoff of statistical significance (see graph). The vaccine unexpectedly had no impact on virus levels in vaccinated people who became infected.

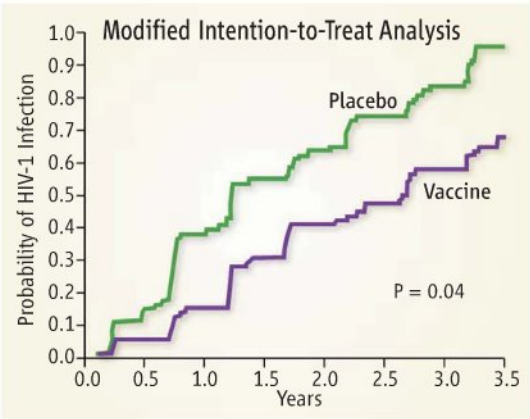

Graphic difference. In this statistically significant analysis, infection rates climb more steeply in the placebo group but then become similar.

Other analyses not initially described to the press but revealed 20 October at an AIDS vaccine meeting in Paris and in a *New England Journal of Medicine* report had slightly lower levels of vaccine efficacy that did not reach statistical significance. "It's definitely not an AIDS vaccine that we would use," says immunologist Bruce Walker of Massachusetts General Hospital in Boston. Still, Walker says the positive "signal" from the trial reveals something about protection. "I think we need to take it seriously," he says.

The U.S. military has enlisted four teams of scientists, including some not affiliated with the study, to decide how best to make sense of this weak signal with the limited plasma and cells collected from individual trial participants. The groups will examine antibody and cellular immunity, whether genetic differences between participants contributed to the protection, and the potential for future animal experiments to shed light on the results.

Sorting out cause and effect will be difficult in part because most people in the study may not have been exposed to HIV. Ideally, researchers would like to compare immune responses in people exposed to the virus during the study who received the vaccine or the placebo. But this trial had a low rate of new infections, 0.19% per year, as most participants reported little or no high-risk behavior such as injecting drugs or commercial sex work. In a subset analysis of HIV-infected people in the highest risk group—which had too few numbers to reach statistical significance—the vaccine did not show any benefit.

The immunologic results reported so far mirror data from earlier studies of these two vaccines that left many researchers unimpressed. The trial designers hoped that the one-two punch of the vaccines used in the Thai study would combine the power of antibodies to prevent infection with what's known as cell-mediated immunity to clear cells that the virus manages to infiltrate. But vaccinated people in the Thai study apparently made only "binding" antibodies, poor cousins to the dreamed-of "broadly neutralizing antibodies" that can stop many strains of the virus in test-tube experiments. Now researchers are wondering whether binding

antibodies offer partial protection. "At least for some populations, it may not be necessary to have broadly neutralizing antibodies," says NIAID's Johnston.

As for cell-mediated immunity, Thai vaccine recipients showed only hints that the vaccines turn on this arm of the immune system—and it could not have been that robust, because the vaccine had no impact on viral levels in people who did become infected.

In addition to comparing infected and uninfected people in the study, researchers will attempt to find correlates of protection by analyzing the viruses that managed to "break through" the vaccine protection. This may reveal immune responses that worked and others that didn't—but may need to be turned up. "That's probably going to be the most informative analysis," says Nabel.

Louis Picker, who does monkey studies of AIDS vaccines at Oregon Health & Science University in Portland, doubts that more will be learned from trial participants' blood samples. "The nonhuman primate model is probably the only way we're going to be able to dissect the Thai results," he says. To Picker and many colleagues, the Thai results suggest that the vaccines protected people against the low doses of virus typically transmitted during sex, and that protection decreased over time because of repeated exposures and waning immunity. His group and others have developed a monkey model that may tease out the mechanism.

Traditionally, researchers vaccinate monkeys and then "challenge" them with high doses of SIV, the simian AIDS virus, given intravenously. Picker, in contrast, challenges vaccinated monkeys with repeated, low doses of SIV given rectally to mimic human sexual transmission across a mucosal surface. "The Thai trial has said that using the low-dose model is probably a good thing to do," says Picker, whose own SIV studies with this approach have linked oft-ignored immune responses to protection.

Another possibility the monkey model can explore is the impact of the canarypox virus, the backbone of one of the vaccines in the Thai study. Koen Van Rompay and Marta Marthas of the University of California, Davis, published a study in 2005 that used an empty canarypox virus as a control in a low-dose challenge experiment with monkeys. The virus itself appears to have protected some animals from SIV, possibly by ramping up the more primitive innate immune system.

The Thai study, for ethical and practical reasons, did not use an empty canarypox virus in the control group. If the canarypox virus by itself did lead to the protection seen in Thailand, van Rompay says, "I don't think they'd be able to figure that out."

Aside from intensifying the hunt for correlates of protection, the Thai results also promise to affect the design of future trials. "Should we be doing efficacy trials in such low-incidence communities that have so few events?" asks Seth Berkley, head of the International AIDS Vaccine Initiative (IAVI). Indeed, some investigators contend that the only way to clarify why the Thai trial had a positive signal is to redo the study in a high-incidence heterosexual population.

Robert Grant, an HIV/AIDS researcher at the University of California, San Francisco, says the Thai study resembles trials of microbicides and behavioral interventions that have had hints of working. "We're going to have to learn to interpret results from prevention trials that show modest effects," says Grant, who is leading a large study of anti-HIV drugs as preventatives. And maybe, he says, researchers will start combining the marginally effective strategies—just as they have done with treatment—to come up with one that has enough power to make a real dent against the spread of HIV.

IAVI's Berkley stresses that the Thai study does at least bring closure to the once thorny question of whether these two vaccines hold promise. They do not. "At the end of the day, the field is going to continue to move forward other products," he says. **–JON COHEN**

With reporting by Martin Enserink.

RATE OF HIV INFECTION AND VACCINE EFFICACY BY RISK GROUP
(Modified Intention-to-Treat Population)

	Vaccine (N = 8197)			Placebo (N = 8198)			Vaccine Efficacy
	Evaluated	Infections	Incidence/Yr.	Evaluated	Infections	Incidence/Yr.	%
Risk Group							
Low	3767	17	0.135	3837	29	0.227	40.4
Medium	2297	12	0.157	2222	22	0.299	47.6
High	1896	22	0.349	1929	23	0.364	3.7

Working hypothesis. People who reported the highest risk behavior did not appear to benefit from the vaccine, but the low and medium risk groups did.

CREDITS (LEF TO RIGHT): ADAPTED FROM S. RERKS-NGARM *ET AL.*, *N. ENGL. J. MED.*, ADVANCED ONLINE EDITION (OCTOBER) © 2009 MASSACHUSETTS MEDICAL SOCIETY; WIKIPEDIA

ScienceNOW.org

From *Science*'s Online Daily News Site

Gene Therapy Helps Blind Children See
A single injection of DNA into the eyes of four children born with a blindness-causing disease has given them enough vision to walk without help. The study confirms that if patients with this disease are given gene therapy early in life, the results can be dramatic. A video accompanying the story shows how one 9-year-old's vision dramatically improved after the procedure. http://bit.ly/4B9vMU

Naked Mole Rat Wins the War on Cancer
With its wrinkled skin and buckteeth, the naked mole rat isn't going to win any beauty contests. But the burrowing desert rodent is exceptional in another way: It doesn't get cancer. The naked mole rat's cells hate to be crowded, it turns out, so they stop growing before they can form tumors. The details could someday lead to a new strategy for treating cancer in people. http://bit.ly/ynJzy

Why Fish and Red Wine Don't Mix
For ages, diners have been told that drinking red wine while eating seafood can produce an unpleasant fishy aftertaste. The rule of thumb has been red wine with meat, white wine with fish. But the rule is not hard and fast. Seafood can taste fine with some reds, whereas some whites can ruin the meal. What's the common factor? http://bit.ly/1EgM7n

Cutting Carbon Emissions, One Home at a Time
You've heard the drill: Drive a fuel-efficient car, insulate your attic, and install energy-saving light bulbs. But what can the average person really do to combat global warming? Quite a bit, according to a new study. By taking a few well-known, readily available measures, researchers argue, Americans could cut their emissions of the greenhouse gas carbon dioxide by as much as 7% over the next decade. http://bit.ly/44qXlQ

Read the full postings, comments, and more on **sciencenow.sciencemag.org**.

U.S. STEM WORK FORCE

Study Finds Science Pipeline Strong, But Losing Top Students

A new study* finds little evidence for leaks in the U.S. pipeline for producing native-born scientists except for a steep drop in the percentage of the highest performing students taking science and engineering jobs. The findings suggest that the United States risks losing its economic competitiveness not because of a work force inadequately trained in science, as conventional wisdom holds, but because of a lack of social and economic incentives to pursue careers in science and technology.

The researchers, led by B. Lindsay Lowell, a demographer at Georgetown University in Washington, D.C., and Harold Salzman, a sociologist at the Urban Institute and Rutgers University, New Brunswick, analyzed data from six longitudinal federal surveys of education and employment trends conducted between 1972 and 2005. The surveys follow students as they graduate from high school and enter college, and again 3 and 10 years after leaving college.

The researchers found that the percentage of high school students who were enrolled in a science, technology, engineering, or mathematics program or had earned a STEM degree 5 years after graduation dipped only slightly between 1972 and 2000, from 9.6% to 8.3%. The percentage of those STEM graduates who were working in STEM occupations 3 years after college increased over the period—from 31.5% for the 1977/'80 cohort to 45% for the 1997/2000 cohort. Similarly, the percentage of STEM graduates who continued to work in STEM occupations 10 years after college rose from 34.8% in the 1977/'87 cohort to 43.7% in the 1993/2003 cohort.

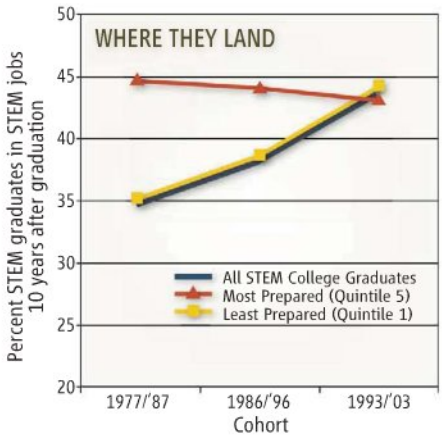

Greener pastures. More recent high-performing STEM graduates than in the past are finding jobs outside the field.

That's not the case for the highest performing students, however, as measured by college entrance test scores and college grades. Although the percentage of those in the top quintile who pursued STEM in college climbed from 21% in the 1972/'77 cohort to 28.7% in 1992/'97, it plunged to 13.8% in 2000/'05. Likewise, the share of the top quintile still holding STEM jobs 10 years out of college dipped from 44.8% in the 1977/'87 cohort to 43.2% in the 1993/2003 cohort (see chart).

The authors say those findings square with anecdotal evidence of STEM graduates being drawn to careers in management and finance starting in the early 1990s. Lowell says employers "seem to be poaching the best and the brightest" of STEM graduates by offering higher salaries for management and other non-STEM positions.

Lisa Frehill, executive director of the Commission on Professionals in Science and Technology, thinks the key to keeping talented STEM majors in science is to emphasize the opportunities that exist to solve society's problems. "Really good people will be less concerned about money if they can do work that is meaningful to them," she says.

–YUDHIJIT BHATTACHARJEE

*"Steady as She Goes? Three Generations of Students through the Science and Engineering Pipeline," www.heldrich.rutgers.edu.

U.S. STEM EDUCATION

Obama's Science Advisers Look at Reform of Schools

Confident that its opinions will be welcomed by the Obama Administration, the President's Council of Advisors on Science and Technology (PCAST) has launched a study of how best to improve U.S. science education. The goal is a quick-turnaround analysis to help guide U.S. policy on ways to raise student test scores and provide higher-octane fuel to run the nation's innovation system.

"Filling the scientific pipeline is a critical issue for this country," says PCAST Co-Chair Eric Lander, who will team up with council member James Gates to lead the study. "Our feeling was that we cannot avoid taking on this challenge."

PCAST will be entering a crowded field. There have been numerous such studies in the past 2 decades, including one by another presidentially appointed body, the National Science Board. Its 2007 report, which called for a national council to coordinate the country's STEM (science, technology, engineering, and mathematics) education system, has been largely ignored. But board chair Steven Beering says that "the problem hasn't changed, and I can't imagine how [PCAST] could come up with a different set of issues to address. The key is to get the White House and Congress to act on them."

Last week, PCAST took its first steps by hearing from two expert panels and Secretary of Education Arne Duncan. The speakers offered suggestions on many topics, including reducing the achievement gap among students, increasing parental involvement, opening up the teacher-certification process, and strengthening the curriculum.

Duncan offered a blunt diagnosis: "Frankly, too often science and math are boring for children … because it's been about memorizing facts, and because students have been taught by teachers who don't know the content themselves." His solution was equally direct: "In the end of the day, it's about how do you get more adults with those skills in front of children."

Several speakers focused on those adults. Cora Marrett, who leads the $1 billion education directorate at the National Science Foundation, homed in on the need to do more research on the undergraduate experience. That's where the nation's teachers are trained, and giving them a stronger foundation in math and science is seen as key to making them better STEM teachers. Carl Wieman, a physics Nobelist, wowed the council with preliminary data on how his research team has begun to transform introductory STEM courses at the University of Colorado, Boulder, by understanding how students learn and then getting faculty to modify their teaching. But Wieman also warned the council not to expect a quick fix. Asked by one member what PCAST could do to implement his work, Wieman answered: "I'm not going to answer that. Despite the long-term nature of education reform, people always want a one-line solution."

Lander said PCAST hopes to deliver its recommendations to the president within 6 months.

–JEFFREY MERVIS

CREDIT: ADAPTED FROM B. LINDSAY LOWELL, H. SALZMAN, H. BERNSTEIN, AND E. HENDERSON

PALEOANTHROPOLOGY

Signs of Early *Homo sapiens* in China?

BEIJING—A fresh find of human fossils claimed to be more than 100,000 years old challenges the prevailing view that our ancestors peopled the world in a migration out of Africa late in the last Ice Age, Chinese scientists say. Other experts, however, argue that it's far too early to make sweeping claims about the significance of the putative *Homo sapiens* fossils: a fragment of a lower jawbone and isolated teeth unearthed in southern China's Guangxi Zhuang Autonomous Region and unveiled there at a press conference earlier this week.

Many experts hold the "Out of Africa" view of modern human origins: We descended from populations of early *H. sapiens* who lived in Africa 100,000 to 200,000 years ago and left Africa perhaps 50,000 years ago. A rival idea with a small band of ardent backers holds that those who left Africa interbred with humans they met on other continents. That's China's take, described as "continuity with hybridization" by Wu Xinzhi of the Institute of Vertebrate Paleontology and Paleoanthropology (IVPP) here. In this view, modern Chinese trace their roots to primitive Asian populations, including "Peking Man" or *H. erectus*, that bred with *H. sapiens* from Africa. "The Guangxi jaw is strong evidence to support this hypothesis," asserts IVPP's Jin Changzhu, who discovered the Guangxi jawbone.

Unearthed. A *Homo* jaw and associated teeth were found in a cave on Mulan Mountain.

Not so, say Out of Africa defenders. "This initial publication makes shaky claims based on preconceptions rather than analytical rigor," says Tim White, a paleoanthropologist at the University of California, Berkeley. The find "is not evidence for 'continuity with hybridization,' " adds paleoanthropologist Hisao Baba of the University of Tokyo. Nevertheless, if the Guangxi dating holds up, it suggests that " 'Out of Africa' by *Homo sapiens* was probably carried out much earlier" than now believed, Baba says. That would mesh with the Liujiang fossils from Guangxi—putative *H. sapiens* remains dated to some 67,000 years ago—and stone tools found in India suggesting to some that *H. sapiens* arrived there at least 75,000 years ago (*Science*, 9 October, p. 224).

Guangxi's jagged karst hills have cast a spell on paleoanthropologists since the late 1950s, as researchers have uncovered fossils of huge extinct apes and some primitive *H. sapiens* teeth there. Those finds prompted Jin in 2007 to systematically excavate six caves in Chongzuo. They hit pay dirt in one—now dubbed *Homo sapiens* cave—at Mulan Mountain.

In 2 years of excavations, the group has unearthed fossils of 55 Ice Age species, including panthers, rhinos, and elephants. The big prize is the *Homo* mandible, whose owner would have had a chin that curved ever-so-slightly outward. *H. erectus* had an inward-sloping chin, whereas modern human chins generally jut out farther than the Guangxi specimen's. Jin's group classifies the fossil as primitive *H. sapiens* and says the intermediate chin suggests interbreeding with *H. erectus*. Uranium isotope dating by R. Lawrence Edwards of the University of Minnesota, Twin Cities, indicates that the fossil-bearing layer is about 110,000 years old, in a paper that will appear in the November issue of *Chinese Science Bulletin*.

Chongzuo is a thought-provoking site, says Richard Potts, director of the Human Origins Program at the Smithsonian Institution in Washington, D.C., who is not ready to assign the jaw to *H. sapiens*. It's "really quite important to continue these studies," he says. Jin is confident that Guangxi's caves hold more secrets. "The jaw is only the beginning," he says. His team resumed excavations at Chongzuo this week.

–RICHARD STONE

CREDITS: JIN CHANGZHU

*Science*Insider

From the *Science* Policy Blog

*Science*Insider broke the story that the Department of Energy may extend by 1 year the operations of **Fermilab's Tevatron** in Batavia, Illinois. That would allow the premier U.S. particle physics lab to have a shot at finding the Higgs boson ahead of its European rival, the Large Hadron Collider, at CERN. http://bit.ly/3ZpVIy

The final report of the blue-ribbon panel on the **future of U.S. human space exploration** suggested, as expected, that NASA should extend shuttle launches into 2011. The panel called for more overall funding, as well as support to operate the space station at least until 2020. http://bit.ly/4dO2Cg

A "perfect storm" of unforeseen problems has delayed delivery of **swine flu vaccine** stocks. The delay means that millions of people could come down with the pandemic disease before the vaccine has had a chance to take effect. http://bit.ly/1hMi1I

Bill McKibben of the climate advocacy group 350.org told *Science*Insider why an **atmospheric carbon dioxide** concentration of 350, lower than the current level of 390, is the right goal for society. http://bit.ly/Soydt

More children than ever are being vaccinated against **deadly diseases**, says the World Health Organization. Some 106 million infants were vaccinated against diseases such as measles and whooping cough in 2008—a record number. http://bit.ly/2NsDFP

Although the United Kingdom has largely resisted the introduction of **genetically modified crops** on its land, a new report by the Royal Society suggests that the plants are needed as part of a multipronged strategy to ensure food security. http://bit.ly/3H6O1h

Harvard University is reassessing options for its $1 billion **Allston science complex**. Construction has begun, but the school is worried that the 27% drop in its endowment could require scaling back plans. http://bit.ly/1h8ywP

For more science policy news, visit **blogs.sciencemag.org/scienceinsider**.

2009 Nobels: Break or Breakthrough for Women?

Until this month, women had never won more than one Nobel science prize in a single year. This year's quartet of laureates talk about what their success might mean for science and society

The first Nobel Prizes were awarded in 1901. But this is the first year that more than one woman has been chosen as a science laureate. Indeed, the four distinguished scientists in the class of 2009—Elizabeth Blackburn and Carol Greider in physiology or medicine, Ada Yonath in chemistry, and Elinor Ostrom in economics—raise the overall tally for women by 31%. But in absolute numbers, these 17 women scientists represent only 2.8% of the membership of this exclusive club.

What will it take to boost those numbers? This year's awardees (*Science*, 9 October, p. 212; 16 October, p. 346) agreed to tackle that question in a telephone roundtable with Jeffrey Mervis of *Science* magazine and Kate Travis of *Science* Careers. Here is an edited version of what they had to say.

Q: Although their presence has grown steadily for the past 3 decades, women hoping for a career in science still face many obstacles. What are the two or three most important steps that need to be taken right now to increase the number of women going into science and to improve conditions for those already in the field?

Elizabeth Blackburn: The big bottleneck in terms of women's advancement—and I'm speaking about biological sciences—is the transition from postdoctoral research to positions in academic or research-intensive institutions. And so the question is, 'How do you give people tools to deal with this?' One very practical thing I've seen at my institution—and I know it's not unique—is having the ability for postdoctoral fellows to attend laboratory leadership courses. They can be as little as 1 week. They don't waste a lot of time, and I've seen them be very effective.

Ada Yonath: Elizabeth talked about a very important stage in the development of a scientist, a man or woman. But I would like to refer to the steps before that. Although girls and young women are taking classes in the life sciences and chemistry, only a few of them make it to the next and the next and the next step. And this is maybe because there is not enough effort made in making them appreciate science and love science and develop their scientific curiosity. I think … maybe it is because we, the established scientists, don't interact with the youth enough. When I talk to them, they say, 'Yeah, I want to study this because I want to be afterwards a lab assistant or a research helper.' Very few say, 'Because I want to solve a problem that interests me.'

Online
sciencemag.org
To hear the complete interview, go to the online version of this article.

Q: Why do you think that is?

A.Y.: I didn't have a mentor, nobody told me to go do a postdoc. I just was very excited and curious about science and solving the problems when they came up instead of thinking from the beginning and then looking at science as a profession. I looked at science as somewhere that I go to satisfy my intellectual needs, and I found ways to bypass the day-to-day problems.

E.B.: Yes, I think that's so important. … I see the difficulty, that they love the science and they feel daunted at the same time. So how does one give them the confidence and the tools to be able to deal with those things that can end up deflecting them from the career that they might have wanted?

Carol Greider: In the past, there hasn't really been leadership courses and those kinds of more formal ways of informing oneself, and so I think that the current mentors don't necessarily know to recommend that [approach] to their younger students. But there is a culture change going on—I certainly have seen it over the last 10 years—of more focus on these kinds of tools to overcome any potential obstacles, to be able to go forward and do what you're excited about.

A.Y.: In Israel, we are doing it. The academicians set up an organization that goes to talk mainly to girls in high schools and in the first college years and try to convey to them the passion, the love, of science. I'm doing it almost four or five times a year, and it works.

Q: What do they ask you?

A.Y.: Well, there are those that talk about the personal aspects, so they ask, 'Why did you do it and how did you do it and how did you solve that or that problem?' And there are some that ask, 'So why was this the problem that interests you?'

CREDITS (LEFT TO RIGHT): JACOB KRIESE/INDIANA UNIVERSITY; BAZ RATNER/REUTERS/LANDOV

Medals of honor. This year's crop of Nobelists includes, from far left, Elinor Ostrom in economics, Ada Yonath in chemistry, and Elizabeth Blackburn and Carol Greider in physiology or medicine.

Q: Do they feel that they can do it, too, or that you are so high up that they could never aspire to the kind of success you have achieved?

A.Y.: First of all, I've been so high up only for a week, and I have been doing it for a few years, so until then I was just another professor. But my life, becoming a scientist, was quite difficult. I was an orphan, we were very poor, and I didn't have any help. Actually, I had to help my family. Let's not talk about it much. But when the girls find out that it could be done, [they think] maybe they can also do it.

Q: Ada, both you and Liz received the UNESCO-L'Oréal Award that honors exceptional women scientists. Do you feel that such gender-based awards are useful?

E.B.: They have a slogan that goes something like, "The world needs science, and science needs women." In any complicated endeavor like science, you need lots of different ways of thinking about things. And women probably do add ways of thinking about things that are scientific, which may be different than men, because of their cultural differences and so forth. Women bring a richness to the research in all fields, not just science.

And so I think this idea that science needs women is really right on target. I like what L'Oréal is doing.

A.Y.: Well, I totally agree. … My little hesitation is, although everything is wonderful and the prize is good and their slogan is good, it's a bit too commercial. If it was less emphasis on L'Oréal, L'Oréal, L'Oréal, I think it would be more efficient. Because women associate L'Oréal with cosmetics, and the fact that it is mentioned so many times, and it's not only the ceremony but before and after for months we have to go and talk about our science but make sure we mention L'Oréal, I don't think it helps.

Q: How is it possible, in today's climate, for the director of the National Institutes of Health, for example, to launch a high-profile competition like the Pioneer Awards and wind up with an inaugural class of grantees that is all men?

Elinor Ostrom: It takes a while for the acceptance of women in multiple disciplines. That's happening more and more, and I think 10 years from now it will be a natural event that the distribution of women and men in their field does not represent the repression that women once faced in going to college or going into graduate school. The problem is the transition. So having it brought to people's attention that, gee, why is it all male repeatedly, is an important thing to do.

Q: Any thoughts on how to get through this transition period?

E.O.: Well, in our program, we have about 50% women applying to go to graduate school. I have a number of [women] colleagues here at Indiana who have full tenure. It's still not quite at the level it should be, but you don't make that [change] overnight.

E.B.: Speaking for the biological sciences, and perhaps to contrast a little bit with what might be the case in the world of economics, the pipeline has been very, very strong for quite a long time for women. They've been populating the Ph.D. and postdoctoral levels at about roughly half men, half women for really quite a long number of years.

Yet there's a very striking discrepancy in the careers after that. So I'm less optimistic that the problem is automatically solving itself. … [This] massive hemorrhaging is nice for other fields but not very nice for the aspirations, perhaps, of the women who put so much of themselves into training for so many years. I think career structure is something we have to look at. For many women, the issue is, 'How am I going to have a family and a life and also tend to a career?'

Q: How did each of you deal with that issue?

E.O.: Well, as a somewhat older participant, I had a clear [choice]. And I made the decision not to have a family because, in earlier times, that would have been a very, very difficult thing to accomplish.

C.G.: I come from the other spectrum in that I was able to see around me a number of women, including Liz, who were able to have children and have a career. So just in the same way that you have to go forward with experiments sometime, not knowing what's going to happen, I just went forward with the experiment of having kids and the career and trying to do both full-time.

Q: To what extent do you have to blend your personal and your professional life to achieve a balance?

A.Y.: In my day-to-day life, I don't sit and think about this, it just comes. This is the way I am and this is the way I run my life, and I don't really sit and organize myself, [saying] tomorrow I have to do this or that. It just happens.

E.B.: Well, yes, I think that the message of balance is somewhat overplayed, because if you're doing something intense like having a family and doing science, they're both intense things. The idea that somehow every day is sort of balanced, I think it's really a bad message to try and send people. … That sounds very boring to me, in this sort of 9-to-5 [world]. Go for these things intensely in the periods when you have to

CREDITS (LEFT TO RIGHT): PAUL SAKUMA/AP PHOTO; JONATHAN ERNST/REUTERS/LANDOV

go for them, and the balance will take care of itself over decades.

C.G.: Many professional women face this kind of issue, and I tell people that it's actually very nice to be in science because what we're judged on in the end is how productive we are and what we get done, and it's not necessarily 9 to 5, and so I feel like I do have a lot of freedom. You know, I'll go out for my son's play at school at two o'clock in the afternoon and then come back again, and that kind of freedom to have a flexible schedule, I think, is not always true in other professions.

Q: Many reports have said that women leave academic science because they are looking for more regular hours and a more predictable schedule.

E.B.: Right. People have been giving them bad information. I think there's a lot of conventional ideas about being a mother and, you know, certain sorts of formulary and stereotypes are there. And I really think that they're not terribly helpful.

Q: Has anything helped you be successful in terms of managing your time?

E.B.: Is it time to tell the Bagel Bites story? … It's about producing beautiful cookies or cupcakes with beautiful icing and you're up till 2 a.m. making them for your children. This is what motherhood is supposed to be like, right? Well, it turns out that if you go to your supermarket, you can buy these little Bagel Bite things, they're called commercially, and you put them in the oven and they have cheese on the top and they bubble and they're lovely and brown and taste wonderful. And you take them to any children's function, and the children swarm over them, they love them, … and it takes 12 minutes in the oven to cook. So my feeling is there's plenty of time … to catch the essence of what it is that people like mothers to do, but you don't have to do it in a very laborious, conventional way.

Q: Now that you have a bully pulpit, are there things that you can do to increase awareness of the importance of attracting women into science?

C.G.: I think just getting out there and talking to people about the opportunities that have come up puts science into the minds of the public. And then by simply being a woman scientist, you have the opportunity to be there and talk about your science.

Q: Will you be disappointed if next year's awards, and those for the following years, do not include women?

E.B.: Oh, we'd like to [achieve] the biological ratio, which is 50–50, so all we're doing this year, I would say, is just approaching a more normal situation.

Q: What about in economics and political science?

E.O.: We wouldn't expect that, every year from now on, we would have one woman and one man receiving the prize in economics. That would be wonderful, but over a period of a decade, beginning to approach 50–50 makes eminent good sense. And if it doesn't, that is something we can be addressing.

Q: How would you address that in the context of the Nobels?

E.O.: Well, it's a delicate problem. But indeed, if 10 years from now the ratio had gone way, way down and someone asked me, I would be very honest and say I was deeply disappointed. Because I know there are very able women out there who aren't being recognized.

Q: Would it say something about the process of recognizing scientific achievement?

E.O.: Well, I think it says something about the processes in academia. As a person who was strongly advised against going to graduate school because I was a woman, I'm at least relieved that that has stopped and that, slowly but surely, we are seeing many more women becoming full professors, being given awards, et cetera. I think we will be seeing a continuation of that, but if we don't, then we better speak up and indicate that something's wrong.

Q: Ada, in chemistry you were the first woman chosen in 45 years. What do you think the prospects are?

A.Y.: It's very nice that women get it, and it's very nice that there is a half-half this year. It was not very nice that the community had to wait 45 years for a woman. But I think the prize should be given for excellence and not pay attention to anything else. And if there is an excellent woman, she should get it. She should not be discriminated against but also not discriminated for. … It's just one prize, and how the [Nobel] committee in Sweden make the decision is above and beyond my understanding. Yet I don't think that gender has to be part of their consideration.

Q: The next time you talk to a 12-year-old girl who shows a passion for science, what would you most want her to know?

C.G.: Well, I was just talking to a group of 9-year-old girls that were interested in science at my daughter's school, actually, and they asked me some of those questions, and what I said was, 'Do what excites you. Follow your passion. Don't necessarily worry about what obstacles might be there, because there are always ways to overcome them. But the most exciting thing is to be able to do what you love, and just don't let anything stand in the way of that.'

E.O.: I think that captured it very well. If you don't choose to do what you're really fascinated by, and then get yourself ready to do it, then your life is not a very worthwhile life.

CREDITS: (TOP) MICHAEL PROBST/AP PHOTO; (BOTTOM, LEFT TO RIGHT) CHRIS MEYER/INDIANA UNIVERSITY; WEIZMANN INSTITUTE OF SCIENCE

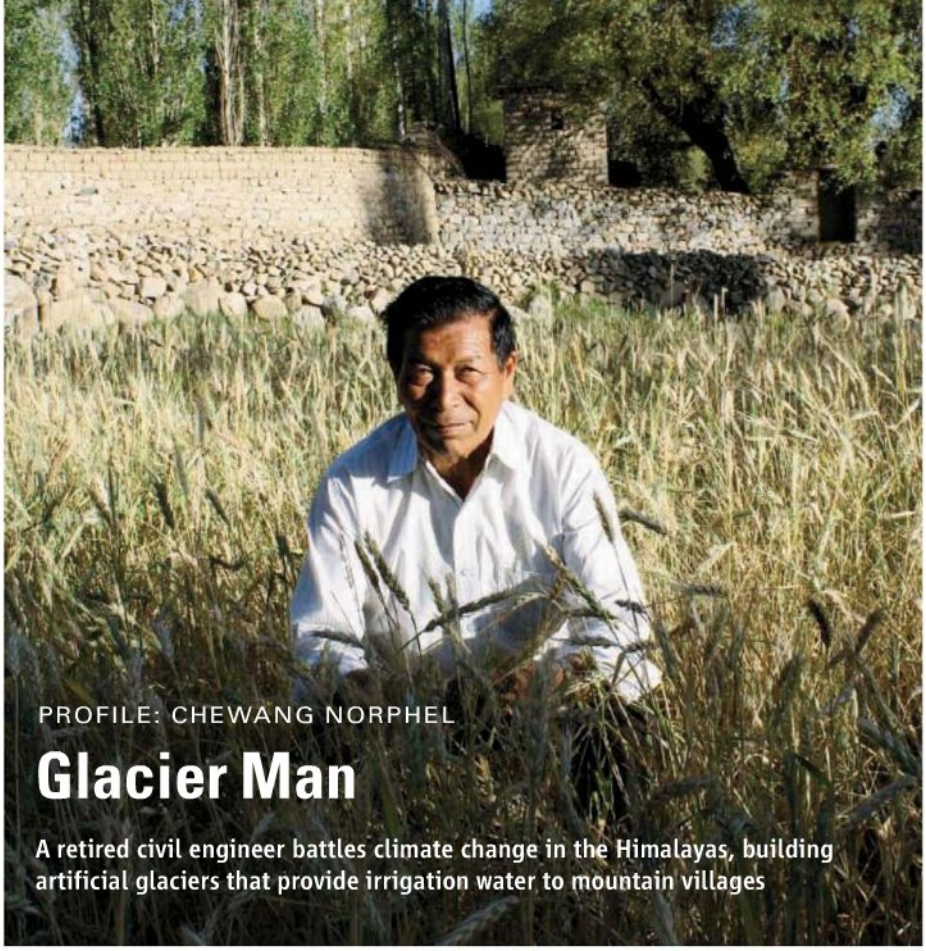

Icy resolve. Despite initial ridicule at his concept, Chewang Norphel has built 10 artificial glaciers

PROFILE: CHEWANG NORPHEL

Glacier Man

A retired civil engineer battles climate change in the Himalayas, building artificial glaciers that provide irrigation water to mountain villages

STAKMO, INDIA—At more than 4000 meters above sea level in the trans-Himalayas, the air is so thin that it can be a struggle simply to breathe. Yet Chewang Norphel is almost jogging across the boulder-strewn landscape, with goatlike agility that belies his 74 years. Tonight, he will sleep in a tent 1000 meters higher up, at temperatures that dip 10°C below freezing, so as to continue his work in the morning. And what unusual work it is: Norphel makes glaciers. He takes a barren, high-altitude desert and turns it into a field of ice that supplies perfectly timed irrigation water to some of the world's poorest farmers.

So far, Norphel has built 10 artificial glaciers, which sustain crops that feed some 10,000 people. It's become his obsession. "When it is very cold and very difficult work, I have to remain focused. All I can think about is making the most successful glacier," he says.

Legend has it that villagers in nearby Pakistan once grew glaciers to block Genghis Khan and his Mongol warriors from advancing through mountain passes, but until Norphel came along there was little evidence that man could reliably duplicate this geological trick. Thanks to his talent, Norphel is now known as "Glacier Man" among the locals in these mountains. Wearing a beige sweater, gray pants, and a pair of leather lace-up shoes, he looks more schoolteacher than superhero, but Norphel has arguably pulled off something miraculous, doubling agriculture yields in one of the most climate-change ravaged regions in the world.

Part engineer, hydrologist, and glaciologist, Norphel has had to create his own field of expertise. "What he has achieved in such circumstances, in remote parts of this mountainous desert, is remarkable," says Pankaj Chandon, coordinator of the WWF-India's High Altitude Wetlands Conservation Programme in the Himalayas, based in Leh, who has followed Norphel's progress over the past decade. "It is testament to his sheer force of character. But also, he has come up with a unique, innovative idea that provides water when it is needed. It is a fantastic adaptation technology for the climate changes that we are experiencing in this region."

From runaway to road builder

Leh, where Norphel was born into a farming family, is the principal town of the ancient kingdom of Ladakh. Wedged between Pakistan, Afghanistan, and China, the territory consists entirely of mountains. It's the highest inhabited region on Earth, originally settled by pilgrims and traders traveling on the Silk Road between Tibet and India or Iran. It's now home to an 80% Tantric Buddhist population.

In the 1940s, when Norphel was growing up, there was just one school in Leh, a primary school, and the young boy had to beg his father to attend it. "He agreed as long as I also kept up my faming duties. So I would rise at 4 a.m. and take the cows and goats for grazing before school. After school, I would rush home to help in the fields," Norphel recalls. Even there, however, he thought of school, scratching times tables and equations into the dirt with a stick as he minded the herds.

The youngest of three brothers in a poor family, Norphel expected that he would be sent to live in a Buddhist monastery after primary school, as tradition dictates. So, at 10 years old, he simply ran away to attend the nearest secondary school, in Srinagar more than 400 kilometers away. He paid for lessons by cooking and cleaning for his teachers.

As his education progressed, Norphel realized two things: He loved mathematics and science, and he wanted to help the farmers he'd seen struggling so hard during his early childhood. One of his heroes was his father's cousin, who had been to London, returned to Leh as Ladakh's first engineer, and built the town's airport and the road from Leh to Srinigar.

There was no university in the state at that time, so Norphel traveled south to Lucknow to earn a civil engineering degree. He loved the rigor of the subject and the practical application of physics and materials science. "You can really make a difference with engineering. You can solve people's problems quickly and in a way that they can see," he says.

Norphel ultimately returned to Leh as a governmental civil engineer. There was hardly a road or bridge in the region when he started in 1960, and everything had to be built by hand. Over the next 35 years, the enthusiastic, raven-haired engineer became a familiar site to the locals, who grew to trust him. "There is scarcely a village in Ladakh where I have not made a road, a culvert, a bridge, a school building, an irrigation system, or a zing [a small water-storage tank fed by glacial meltwater]," he says.

More than 90% of those he helped were subsistence farmers, living and working in tightly knit communities. There was no money around—when Norphel needed labor for his projects, people willingly came forward. His designs had to be sustainable, using locally available materials. For example, he built a number of canals in which instead of using an expensive cement lining that would crack during winter, he allowed

CREDITS: N. PATTINSON

weeds to grow and thicken, their roots naturally plugging the gaps.

Vanishing ice and a gush of inspiration

By the time Norphel retired in 1995, priorities among Ladakhis were shifting from road-building to a far more serious problem: water scarcity. "Glaciers were vanishing and streams were disappearing," Norphel says. "People would beg me to bring them water. Their irrigation systems were drying up and their harvests were failing. The government was starting to bring in grain rations."

In the so-called rain shadow of the Himalayas, Ladakh receives just 5 centimeters of rainwater a year—about the same as the Sahara desert. The population is entirely dependent on the melting of glaciers and snow. But global warming has hit this region particularly hard. The tree line has risen more than 150 meters during Norphel's lifetime, and glaciers have retreated by as much as 10 kilometers.

Above the small village of Stakmo, Norphel points up at the dark rock slopes rising from the valley. "There were two large glaciers here and here," he says, "and many smaller ones that only persisted during wintertime." The glaciers that remain are now far from the villages and at high altitudes where they don't produce significant meltwater until May or June.

That's too late to help local farmers. Because they experience such a brief summer, villagers must plant their one annual crop of barley, peas, or wheat by late March; otherwise it won't mature before winter arrives in September, after which the temperature drops below –30°C.

By the mid-'90s, Norphel was living in the small village of Skarra, a few kilometers outside of Leh, with his wife and a daughter they adopted from one of his brothers. Determined to address the irrigation problem, Norphel came upon inspiration within 100 meters of his house, one bitingly cold winter morning. "I saw water gushing from a pipe and was thinking what a shame it is that so much abundant water is wasted during wintertime—the taps are left open to stop the water freezing in the pipes and bursting them," he says. "Then I noticed that on its route to the stream, the water crossed a small wooded field, where it was collecting in pools. Where the trees provided shade, it was freezing into ice patches. By early March, the ice patches melted."

Norphel realized that if he could somehow copy this on a much larger scale, he would have a way of storing up this winter water in an artificial glacier that would melt at just the right time for crop sowing and irrigation.

Scorn, then gratitude

It was a beautifully simple concept, but the initial reception to it was rough. "People laughed when I first presented the idea," Norphel says. "Officials and villagers were skeptical. 'What crazy man are you? How can anyone make a glacier?' I was told."

Norphel's idea was to divert the lost winter water from its course down the mountain, along regularly placed stone embankments that would slow it down and allow it to spread and trickle across a large, shaded surface depression a few hundred meters from the village. Here, the slowed water would freeze and pack into a glacier that would begin melting when the sun rose high enough in spring to expose the thick ice sheet—just in time for the sowing season.

But Norphel had no equipment and, even after some relentless lobbying, just a little seed money from the national Desert Development Programme. That was a problem given the societal change in the region that had occurred over the past decade. As water scarcity increased and the roads brought in trucks with government-subsidized grains, many villagers had left their fields to find paying jobs. "The attitude completely changed: If I wanted any of the villagers to repair a canal or help build a new glacier, I had to pay them," Norphel says.

He thus built his first artificial glacier with very little help, above the village of Phuktse. It was an immediate success, supplying water to irrigation channels from late March to late April, after which meltwater from the natural glacier higher up took over. "When people saw the benefits of the artificial glacier, they started helping me and we stretched the length of the glacier to 2 kilometers," Norphel says.

Giving thanks. Norphel (*left*) with a local farmer—some call him a "miracle worker."

The glacier supplies water for crops sustaining more than 1500 people in four villages. It's so precious that during the irrigation season, a man sleeps by the sluice gate to guard against water theft. "It was like a miracle, people quickly started to cultivate more land and started planting willow and poplar trees between their fields," says Phuktse

CREDITS: N. PATTINSON

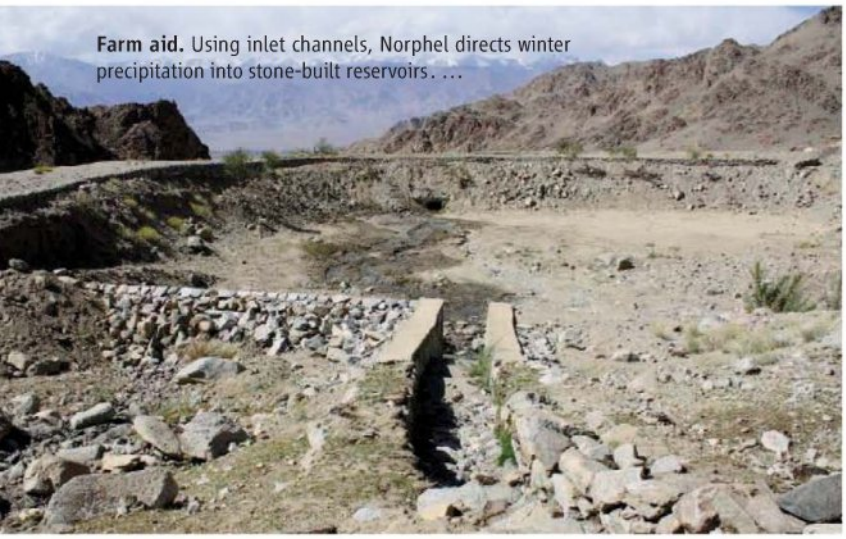

Farm aid. Using inlet channels, Norphel directs winter precipitation into stone-built reservoirs. ...

The stored water freezes into an artificial glacier and in the spring, outlets direct meltwater into irrigation. ...

farmer Skarma Dawa. "This technology is very good because it works and it is simple and there's very little maintenance required."

Norphel has built nine glaciers since that first one, which he began in the late 1980s and worked on until 1994. They average 250 meters long by 100 meters wide; the Phuktse glacier remains the largest. Norphel estimates that each one provides some 6 million gallons (23,000 meters^3) of water, although there has been no accurate analysis to date, and the undulating ground makes it difficult to guess the volume of ice in each glacier.

Each artificial glacier is built using local labor and materials for about 3 to 10 lakh Indian rupees (US$6000 to $20,000), depending on the size and site, compared with about US$34,000 for a cement water reservoir, Norphel says. "And the technique also helps recharge groundwater and nearby springs," he points out.

"Before the artificial glacier, we really struggled to get any barley," says Tashi Tundop, a 76-year-old farmer from Stakmo village. "But now we can grow many crops, even potatoes, which need to be planted earlier in the spring, but sell for much more money. I get three times more income than I used to."

A new climate threat

Norphel's glaciers are site specific—they require a certain altitude, water flow, and surface area temperature, so they are not suitable for every location, notes Andreas Schild, head of the International Centre for Integrated Mountain Development in Kathmandu. "Nevertheless, we are going to have to do some serious out-of-the-box thinking when it comes to sustainable water storage and investigate the efficiency of artificial-glacier technology," Schild says.

Norphel notes that he has already had interest in his glaciers from nongovernmental organizations working in Afghanistan and Turkmenistan. "In some areas, reservoirs are a much more practical solution," he says. "But in terms of water storage and release at the irrigation season, you can't beat artificial glaciers."

Despite his success, there has been little attention from the academic world. "I could do with some scientific help from specialists," Norphel says. "I am trying to collect data on how and where the glacier forms best, and which parts precipitate first and why, so that I can improve on them and people can use the technique elsewhere.

This September day, Norphel and his glaciers receive their first scientific visitor. Adina Racoviteanu, a geography graduate student at the Institute of Arctic and Alpine Research and the National Snow and Ice Data Center at the University of Colorado, Boulder, is passing through Stakmo en route to her glacier field stations farther east. When she offers to make Norphel a topographic map of the artificial glacier site using her hand-held GPS monitor, a $3000 device, his eyes light up. The pair spend the next several hours taking readings across the site, achieving what would take Norphel weeks to do with his tape measure and plumb line.

Later that day, as Norphel leaps nimbly across the boulders above Stakmo village, he points out his latest design tweaks. In 2006, when it rained for a week and the Zanskar River, which freezes over each winter, melted ahead of time, flash floods and landslides devastated his glacier here. "Blocking walls and canals were damaged by floods," recalls Norphel. "I'm still at the experimental stage, but I've been able to completely redesign this glacier site to make it withstand floods better.

The Stakmo site will soon have three artificial glaciers at increasing altitudes, so by the time the lowest one is spent, the one above it will have begun melting, and then the highest before the natural one at the top starts to liquidize. Norphel points out his latest seepage-avoidance technology: a 200-meter cement chamber that will be connected to the artificial glacier with 2- to 3-meter-long pipe. This will help distribute and freeze sheets of water evenly in the artificial glacier as well as providing a water reservoir for later in the year. "Creating the first such chamber is difficult in terms of design and funding," he says. "The rest will still be expensive but easy to replicate."

Money remains a huge problem. Norphel says that 75 other nearby villages are in suitable locations for his artificial-glacier technique, but he lacks funds, and what funds are promised do not typically arrive in full. The watershed development program allots $50,000 per project per village, but so far, only $12,000 has been released in two installments over the past 6 years.

And there's another problem: continued climate change. There is less and less snowfall during wintertime, when it is needed to contribute to Norphel's artificial glaciers. Instead, rain is arriving in September, ruining the harvests. It's a worrying trend. "These glaciers are not magic formations. They need that water over winter," says Norphel.

As the "retired" engineer makes his way up the mountain to his glacial work site, singing drifts up the valley from the villagers in the fields below, who are harvesting the last of this year's barley with simple scythes. It's a scene that must have played out for centuries. Without the Glacier Man, this village might well have fallen silent a decade ago.

–GAIA VINCE

Gaia Vince is freelance writer following climate change around the world at wanderinggaia.com.

CREDITS: N. PATTINSON

The strategy has helped farming villages such as Stakmo maintain productive harvests.

Vegging out. In arid northwest Bangladesh, gardens are catching on as a simple way to compensate for declining rice yields.

CLIMATE CHANGE

Hot, Flat, Crowded—And Preparing for the Worst

In a clarion call to other developing nations, Bangladesh is girding itself against the hazards of a warmer world

RAJSHAHI, BANGLADESH—Pale-green sprouts of summer rice are just poking up from water the color of milky tea pooled behind low earthen banks. These terraced rice paddies are a traditional farming method for coping with monsoon downpours. Another age-old adaptation of this community in northwest Bangladesh is *deowal bari*: thick mud walls that keep homes cool even as temperatures outside soar above 40°C.

But a changing climate is forcing locals to further improvise—and fast. This region of Bangladesh in recent years has received only about half the winter rainfall it averaged over the past half-century. Farmers here are often unable to sow winter crops. Compounding these woes, monsoon rains came nearly a month late in 2009, cutting short the main growing season. "Between May and December, we used to plant two rice crops," says Alfaz Hossain, a local farmer. Now, he says, they plant only one. That has forced villagers to largely rely on a single harvest of *aman*, or "summer rice," all year long.

Conditions are expected to deteriorate. The first high-resolution model of South Asia predicts that if average temperatures rise about 3°C by 2100, monsoons will rev up 2 weeks later than they do now, and rain will come in less frequent but more intense bursts, climatologist Noah Diffenbaugh of Purdue University in West Lafayette, Indiana, and colleagues reported in the 3 January issue of *Geophysical Research Letters*. That's bad news for a country that gets hammered regularly by floods, cyclones, and droughts. Bangladesh is "nature's laboratory for natural disasters," says Ainun Nishat, senior adviser at the International Union for Conservation of Nature's Dhaka office.

Now Bangladesh is striving to become a global showcase for climate change adaptation. Earlier this month, its government approved a wide-ranging strategy for dealing with climate change that includes ramping up civil engineering projects to control flooding and protect farmland from rising sea levels. Researchers here are also testing crops that better tolerate floods and drought.

Realizing that time-honored approaches to living off the land no longer suffice, Bangladesh has implemented more community-level projects than any other country to gird people for climate shifts. With support from Livelihood Adaptation to Climate Change, a program run by the United Nations (U.N.) Food and Agriculture Organization and Bangladesh's Department of Agriculture Extension, farmers in Basuldanga, in the northwest, have been testing new ways to eke out a living. With program-supplied seeds and pointers from agricultural field officers, once-bare patches between houses are brimming with vegetables such as spinach and gourds watered from newly dug ponds that collect rainwater. There are now so many gardens, agricultural officers refer to Basuldanga as *subzee gram*, or "vegetable village." "Vegetable cultivation can't replace the loss of paddy [rice], but it provides a little bit of help," says local farmer Mohammed Mostafa.

Given the uncertainties of climate modeling, "improving overall resilience is the way to go," says Neil Adger, head of adaptation research at the Tyndall Centre for Climate Change Research in Norwich, U.K. He and others are calling for adaptation measures in Bangladesh and elsewhere that help people regardless of how the climate changes. There's little time to spare. "We are running, but the climate is running faster," says Habib Mohammad Naser, a soil scientist at the Bangladesh Agricultural Research Institute in Dhaka.

Averting hunger

The U.N. has so far amassed about $350 million in four funds to help high-risk locales adapt to climate change, including pilot efforts to fight malaria in Colombia and to strengthen shorelines on Kiribati, a Pacific island nation. But this funding is a thimbleful of what's needed: The World Bank estimates that as much as $100 billion a year is required to prepare people in vulnerable areas for climate change. That's assuming the world gets its act together to rein in greenhouse gas emissions. If not, says disaster

CREDITS: MASON INMAN

Old and new. Thick mud walls of homes are a time-honored adaptation to scorching heat, while newly dug ponds collect rainwater for irrigation.

expert Ian Burton of the University of Toronto in Canada, "then the cost of adaptation is going to be enormous."

Although Bangladesh had been working on adaptation plans for several years, 2007 was a wake-up call. That year, after two severe floods and a cyclone, rice production overall fell 10% short of need; in some districts half or more of the crop was wiped out. Bangladeshis waited in long lines for government handouts, and food riots broke out.

Climate change presents many challenges for South Asia, but in Bangladesh, not surprisingly, "agriculture will be the hardest-hit sector," predicts Sheikh Ghulam Hussain, an agricultural scientist with the Bangladesh Agricultural Research Council. Although the country's rice production nearly tripled with Green Revolution techniques—improved seeds, more irrigation, and more fertilizer—progress here, as across much of Asia, has stalled. Bangladesh must ratchet up yields by at least 40% by midcentury to keep its population fed, says Hussain.

For more than a decade, Hussain has been modeling the effect of hotter weather and higher carbon dioxide levels on crops. An average annual temperature rise of up to 2°C above present day will have a negligible effect on rice in Bangladesh, his models predict. "But if it goes beyond that, to three or four degrees, then it will be a problem" for rice, says Hussain, who forecasts roughly a 25% decrease in rice production.

Raising production in a warmer climate will be a huge challenge, Hussain says, "but there are many options," including improved crop varieties, shifts to new crops such as maize, and more efficient fertilizer use.

One promising development is rice that can withstand being underwater for days on end (*Science*, 18 July 2008, p. 330). Since severe floods often swamp Bangladesh, plant physiologist Jiban Krishna Biswas of the Bangladesh Rice Research Institute (BRRI) in Dhaka and colleagues are testing how rice responds to floods simulated in swimming pool–sized concrete tanks. Varieties with the gene *sub1* can survive 2 weeks underwater—more than twice as long as ordinary rice. The gene slows the plant's growth to conserve energy and preserve chlorophyll, allowing it to spring back once floodwaters subside. One variety, Swarna *sub1*, could be ready for farmers in 2 or 3 years, says Biswas. "It would be a breakthrough," he says, because Swarna *sub1* could be suitable for up to 1 million hectares, or one-sixth of Bangladesh's summer rice.

BRRI researchers have also developed a rice variety called BRRI Dhan 47 that can withstand high salt levels, and they are experimenting with aerobic rice, in which no standing water remains on a field, cutting water use in half. But scientists are making fewer inroads into traits such as tolerance to drought and heat. Therefore, Hussain argues, the main threat to rice from a warming world is sterility: When rice plants flower in summer, temperatures above 35°C for more than 8 hours straight often sterilize the plant's spikelets, preventing these from developing into rice grains. "Once this threshold is crossed, we will be in trouble," Hussain says. Developing varieties that flower earlier in the morning could help avoid this problem, but the genes controlling flowering time haven't been identified.

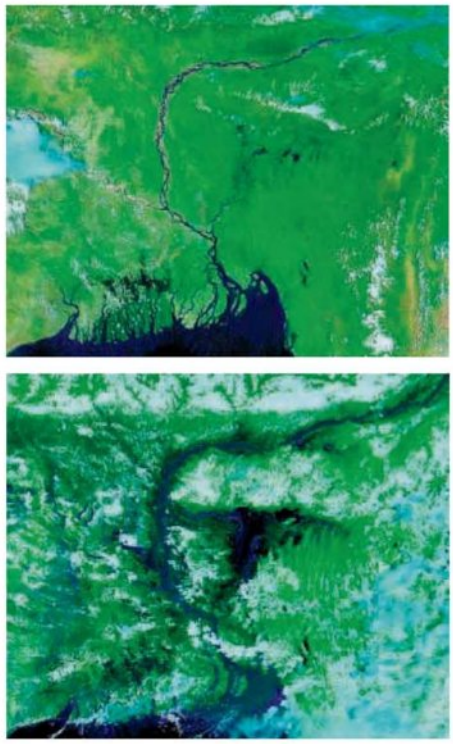

Inundated. Much of Bangladesh's cropland (*top*) was deeply flooded after intense monsoon rains in July 2007 (*bottom*).

CREDITS: MODIS RAPID RESPONSE TEAM AT NASA GSFC

Turning back the tide

The need for hardier rice, particularly salt-tolerant varieties, will only grow. As climate changes, a broad swath of Bangladesh is expected to grow saltier, and some areas could even disappear under the waves. Nearly a fifth of Bangladesh sits less than a meter above sea level; recent estimates forecast sea level rises of up to 2 meters by 2100 (*Science*, 5 September 2008, p. 1340). In Bangladesh, "river waters will be more saline, and the people will find that their lands are no longer suitable for agriculture. They will lose their livelihoods," predicts S. M. Mahbubur Rahman of the Institute of Water Modeling in Dhaka. Bangladesh's climate change strategy warns that "sea-level rise could result in the displacement of millions of people."

To blunt the ill effects, Bangladesh's adaptation strategy calls for a Dutch-style overhaul of coastal polders: pockets of land enclosed by several-meter-tall earthen embankments that protect against high tides and moderate storm surges when cyclones tear through. Engineers have already built an extensive network of such embankments. Bangladesh's plans call for extending, strengthening, and building them higher.

The integrity of inland embankments is also a major worry. Although torrential downpours fill rice paddies—an essential part of the agricultural cycle—too much rain can lead to flooding that wipes out crops. In 1998, the worst year on record, about two-thirds of Bangladesh was deep underwater, some places for as long as 2 months.

Seasonal flooding seems to have worsened in recent years, says climate scientist M. Monirul Mirza of Environment Canada in Toronto. Severe floods, in which more than a third of the country is inundated, hit five times between 1987 and 2007, compared with just twice in the previous 2 decades, he says. With a 2°C average global temperature rise, one of Mirza's studies predicts, more intense monsoon rainfall would increase the area in Bangladesh hit by severe floods by at least 25%. Sea-level rise would compound the problem by slowing river flow, resulting in deeper and longer-lasting floods.

Bangladesh's climate change strategy estimates that strengthening embankments and other adaptation projects would cost about $5 billion over the first 5 years. So far, the government has contributed $70 million to a trust fund to pay for the work, says S. M. Munjurul Hannan Khan, deputy secretary of the Ministry of Environment and Forests, and other countries have pledged contributions, including $30 million from the United Kingdom.

Grassroots efforts are critical. "It's necessary for officials to learn from farmers and pass information up to research scientists and planners," says U.K. soil scientist Hugh Brammer, who for more than 40 years has helped Bangladesh shape its strategy for agriculture and flood control. If Bangladesh's recipe for adaptation works, it may end up being emulated as other countries brace for the consequences of a warmer world.

–MASON INMAN

Mason Inman is a writer in Karachi, Pakistan.

Meet the cell 668

Electronic waste 670

LETTERS | BOOKS | POLICY FORUM | EDUCATION FORUM | PERSPECTIVES

LETTERS

edited by Jennifer Sills

Too Sanitary for Vultures

THE CURRENT CRISIS OF BIODIVERSITY HAS HIT OLD-WORLD VULTURES ESPECIALLY HARD; populations that flourished in the mid-20th century over much of Asia and Africa are in some cases close to extinction (*1*). In Europe, however, vultures have been spared, and today the Mediterranean basin is home to the largest populations of the Western Palearctic (*2*). The availability of carcasses around stock farms became a decisive factor in the survival and expansion of vulture populations in southern Europe (*3*).

The outbreak of bovine spongiform encephalopathy (BSE) in 2001 led to the passing of sanitary legislation (Regulation CE 1774/2002) that greatly restricted the use of animal byproducts not intended for human consumption. All carcasses of domestic animals had to be collected from farms and transformed or destroyed in authorized plants, contradicting member states' obligations and efforts to conserve scavenger species (*4*). The effects of this policy include a halt in population growth, a decrease in breeding success, and an apparent increase in mortality of young age classes (*2*).

Conservation concerns determined the appearance of a number of European dispositions (2003/322/CE 2005/830/CE) regulating the use of animal byproducts as food for necrophagous birds. Although the aim of these dispositions is to guarantee food supplies, in practice the spatial distribution of feeding stations has become almost totally predictable and habitat quality has been modified artificially as a result. The repercussions of these changes on individuals, populations, and communities of avian scavengers are undoubtedly significant (*2*, *5*–*7*).

Bearded vulture

Griffon vulture

CREDITS: (TOP) ANTONI MARGALIDA; (BOTTOM) JORDI BAS

Partial solutions to this problem are being found, albeit slowly. In 2009, the European Union began discussing a Spanish proposal for a revised regulation of the use of animal byproducts not intended for human consumption. In April 2009, amendments were approved by the European Parliament obliging the European Commission to regulate exceptions that will guarantee the supply of carcasses and thus satisfy the requirements of avian scavenger populations. It is hoped that the definitive legislation will be in place by 2010 to 2011. The philosophy of this new policy should allow member states a greater flexibility in carrion provisioning. Taking into account sanitary guarantees, it seems clear that encouraging fallen stock to be left in situ is the most ecologically harmonious, inexpensive, and efficient management method for the conservation of scavengers. Fortunately, current knowledge of scavenger ecology is increasing rapidly and so, more than ever, collaboration between ecologists, veterinarians, farmers, and legislators is both possible and desirable.

JOSÉ A. DONÁZAR,[1] ANTONI MARGALIDA,[2]* MARTINA CARRETE,[1] JOSÉ A. SÁNCHEZ-ZAPATA[3]

[1]Department of Conservation Biology, Estación Biológica de Doñana, CSIC, 41092 Sevilla, Spain. [2] Bearded Vulture Study and Protection Group, El Pont de Suert, 25520 Lleida, Spain. [3]Department of Applied Biology, University Miguel Hernández, 33012 Orihuela, Alicante, Spain.

*To whom correspondence should be addressed. E-mail: margalida@inf.entorno.es

References

1. R. Koenig, *Science* **312**, 1591 (2006).
2. J. A. Donázar, A. Margalida, D. Campión, Eds., *Vultures, Feeding Stations and Sanitary Legislation: A Conflict and Its Consequences from the Perspective of Conservation Biology* [Munibe 29 (suppl.), Sociedad de Ciencias Aranzadi, Donostia, Spain, 2009].
3. J. A. Donázar, C. Fernández, *Biol. Conserv.* **53**, 83 (1990).
4. J. L. Tella, *Nature* **410**, 408 (2001).
5. M. Carrete *et al.*, *Ecol. Appl.* **16**, 1674 (2006).
6. M. Carrete *et al.*, *Biol. Lett.* **2**, 624 (2006).
7. G. N. Robb *et al.*, *Front. Ecol. Environ.* **6**, 476 (2008).

Underestimating Energy

IN THE NEWS FOCUS STORY "LEAPING THE efficiency gap" (D. Charles, 14 August, p. 804), Stephen Selkowitz states that "[n]o one measures building performance," which is true of most building designers and owners. Even when someone does take these measurements, they reveal a systematic bias—much lower energy use is predicted than is actually found. For example, the Swedish city of Malmö opened a small community in 2001 as a model of sustainability (*1*). The design objective for the project was 105 kWh/m^2 per year. Estimates of energy use for 20 buildings were in the range from 32 to 107 kWh/m^2 per year. Although seven buildings had measured performance that met the design objective, each of the buildings used more energy than estimated, with a range for the group of 74 to 356 kWh/m^2 per year. Careful investigation showed a lower electrical load than expected, but actual heat use significantly higher than expected. Another example is the highly publicized Lewis Center at Oberlin College (*2*), which similarly measured energy use in the range of 120 to 200 kWh/year after a design team estimated that it would be only about 64 kWh/year. Furthermore, in its first year, the Energy and Environment building at Stanford was pre-

Pollution and climate change
672

Inheritability of wealth
678

dicted to use 198 kWh/m^2 per year, but actual energy use is 380 kWh/m^2 per year (*3*). More and better performance data, improved analytical methods to predict performance, and improved construction methods will all be required to improve estimation accuracy.

JOHN KUNZ,[1]* TOBIAS MAILE,[1] VLADIMIR BAZJANAC[2]

[1]Center for Integrated Facility Engineering, Stanford University, Stanford, CA 94305, USA. [2]Environmental Energy Technologies Division, Lawrence Berkeley National Lab, Berkeley, CA 94720, USA.

*To whom correspondence should be addressed. E-mail: kunz@stanford.edu

References

1. B. Persson, *Sustainable City of Tomorrow: B01—Experiences of a Swedish Housing Exposition* (Swedish Research Council, distributed by Coronet Books Inc., Stockholm, 2005), pp. 108–109.
2. J. H. Scofield, *ASHRAE Trans.* **108**, 1214 (2002).
3. J. Kunz, T. Maile, V. Bazjanac, "Summary of the energy analysis of the first year of the Stanford Y2E2 building" (CIFE Tech. Rep. no. TR183, version 2, 2009); http://cife.stanford.edu/online.publications/TR183.pdf.

Nutrient Imbalances: Follow the Waste

IN THEIR POLICY FORUM ("NUTRIENT IMBALances in agricultural development," 19 June, p. 1519), P. M. Vitousek and colleagues appropriately addressed the consequences of both overextraction and excess application of nutrients in low-input, rotation, and high-input corn production systems in Kenya, the United States, and China, respectively. The authors provided several on-farm mitigating approaches to these imbalances and called for a more sustainable approach to nutrient management in both developed and developing nations. Unfortunately, the human waste stream and the resulting nutrient redistribution went unmentioned.

Over the past 200 years, global populations have become increasingly urban, shifting from 97% rural in 1800 to about 50% in 2007 (75% in developed countries) (*1*). Nutrients in plant and animal products collected broadly across rural landscapes are increasingly concentrated in urban environs where waste removal efforts result in transformation of nutrients into gases, dilution into rivers and marine bodies, and deposition in pits and landfills. Only a fraction of these assets (nutrients and carbon) are ever returned to rural lands. As a result, soils are slowly being drained of trace elements, soil carbon reserves are being depleted, and it is necessary to mine nutrients and chemically produce N fertilizer to satisfy crop demands. Global N fertilizer use (*2*) currently outpaces global human N demand (*1*, *3*) by a factor of 7 at an annual energy expense equivalent to 1.1 billion barrels of oil. Conversely, N in human excreta in urban centers is nearly equivalent to the total global anhydrous NH_3-N production and represents sufficient N to fertilize 100 million hectares of cropland at 150 kg N ha^{-1} year^{-1}. Sustainable agriculture cannot be achieved until we learn to efficiently and safely redistribute the nutrients in agricultural byproducts and human excreta to the soils of rural landscapes.

THOMAS H. DELUCA

SENRGy, Bangor University, Bangor, Gwynedd LL57 2UW, UK. E-mail: t.h.deluca@bangor.ac.uk

References

1. United Nations, "World urbanization prospects: The 2007 revision—Highlights" (United Nations, Tech. Rep. no. E.04.XIII.6, 2008).
2. J. N. Galloway *et al.*, *Science* **320**, 889 (2008).
3. D. H. Calloway, S. Margen, *J. Nutr.* **101**, 205 (1971).

Nutrient Imbalances: Pollution Remains

IN THEIR POLICY FORUM ("NUTRIENT IMBALances in agricultural development," 19 June, p. 1519), P. M. Vitousek *et al.* propose a promising idea: Compare solutions to nutrient challenges among countries and regions. However, policies to control nonpoint pollution are not so easy to design. The United States and the European Union are mentioned as examples of places that have reduced nutrient imbalances, yet pollution remains very high in their water.

European regulations include the 1991 Urban Wastewater Directive, with investments above 100 billion euros. The huge investments of the Wastewater Directive should have reduced pollution, but the European data (*1*) for the past 15 years on nitrate concentration indicate only a slight reduction in rivers and a 50% increase in pollutant levels in aquifers. The data from the Organisation for Economic Cooperation and Development (*2*) also found that most major European rivers show no abatement of nitrates and some have even grown worse.

The Nitrates Directive of 1991 also sought to reduce pollution. The Nitrates Directive only applies to cultivation over aquifers declared officially polluted, not to cultivation over whole basins or very polluting crops that do not receive subsidies (such as greenhouses). The achievements of this Directive are questionable (*3*).

Nonpoint pollution is a common pool "resource" (or public bad) where economic instruments such as taxes and subsidies fail (*3*). Policy-makers must recognize that pollution abatement is impossible without farmers' voluntary cooperation and active support. This is also the message of this year's Nobel prize in economics.

JOSE ALBIAC

Department of Agricultural Economics, CITA-DGA, 50059 Saragossa, Spain. E-mail: maella@unizar.es

References

1. European Environment Agency (EEA), *Core Set of Indicators N° 020, Nutrients in Freshwater* (EEA, Copenhagen, 2009).
2. Organisation for Economic Co-operation and Development, *OECD Environmental Data Compendium 2006* (OECD, Paris, 2007).
3. J. Albiac *et al.*, in *The Management of Water Quality and Irrigation Technologies*, J. Albiac, A. Dinar, Eds. (Earthscan, London, 2009), pp. 61–81.

Response

AS DELUCA SUGGESTS, APPLICATIONS OF N fertilizer worldwide exceed human consumption of that N in the form of protein by several-fold. Our Policy Forum focused in part on the more than 80% of fertilizer N (and P) that does not make it into our diet—the fertilizer that could in some sense be considered "wasted." DeLuca is correct in pointing out that closing nutrient cycles by returning agriculturally derived nutrients to crops would make an additional contribution to the sustainability of intensive agriculture. A parallel problem exists for nutrients in animal waste, due to the adop-

Letters to the Editor

Letters (~300 words) discuss material published in *Science* in the previous 3 months or issues of general interest. They can be submitted through the Web (www.submit2science.org) or by regular mail (1200 New York Ave., NW, Washington, DC 20005, USA). Letters are not acknowledged upon receipt, nor are authors generally consulted before publication. Whether published in full or in part, letters are subject to editing for clarity and space.

tion of confined animal feeding operations (CAFO), which use feed derived from fertilized crops in distant areas (*1*, *2*). In either case, the result is too much N and P in waste near the city or CAFO, and not enough where food or feed is grown.

Albiac points out, and our Policy Forum noted, that the reduction in excess nutrient applications in the midwestern United States and Northern Europe has not ended serious nutrient pollution of surface or groundwater (or the atmosphere) in those regions. Part of the problem may be the decades-long residence time (from application to appearance in surface water) of added nutrients in many systems (*3*); part no doubt reflects inadequacies of the policy instruments designed to reduce water (and air) pollution by excess agricultural nutrients. The European Union in particular has put substantial resources into efforts to reduce this pollution, as Albiac describes, and the relatively small successes to date are disappointing. Albiac points to restricted spatial coverage and inadequate engagement of stakeholders as reasons for failed nutrient policies. Equally important, efforts to date have not been sufficiently systematic; they have not considered the full mass balance of excess nutrients and their multiple possible fates. Excess nutrients cannot be controlled piecemeal (for example, by considering only nitrate rather than total N or by considering effects on aquatic systems in isolation from effects on the atmosphere). Successful policies must address the problem of excessive nutrient applications at their source. Maintaining the high levels of production that we require to meet aggregate cereal and meat demand while reducing losses of nutrients to the environment represents a very difficult challenge. Meeting that challenge will require careful, well-monitored, long-term experiments with policy instruments as well as with agricultural nutrients themselves.

P. M. VITOUSEK,[1]* R. NAYLOR,[2] T. CREWS,[3] M. B. DAVID,[4] L. E. DRINKWATER,[5] E. HOLLAND,[6] P. J. JOHNES,[7] J. KATZENBERGER,[8] L. A. MARTINELLI,[9] P. A. MATSON,[10] G. NZIGUHEBA,[11] D. OJIMA,[12] C. A. PALM,[11] G. P. ROBERTSON,[13] P. A. SANCHEZ,[11] A. R. TOWNSEND,[14] F. S. ZHANG[15]

[1]Department of Biology, Stanford University, Stanford, CA 94305, USA. [2]Woods Institute for the Environment and Freeman Spogli Institute for International Studies, Stanford University, Stanford, CA 94305, USA. [3]Environmental Studies, Prescott College, Prescott, AZ 86301, USA. [4]Department of Natural Resources and Environmental Sciences, University of Illinois, Urbana, IL 61801, USA. [5]Department of Horticulture, Cornell University, Ithaca, NY 14853, USA. [6]National Center for Atmospheric Research, Boulder, CO 80307, USA. [7]Aquatic Environments Research Centre, School for Human and Environmental Sciences, University of Reading, Whiteknights, Reading RG6 6AB, UK. [8]Aspen Global Change Institute, Aspen, CO 81611, USA. [9]Centro de Energia Nuclear na Agricultura–Universidade São Paulo (CENA-USP), Avenida Centenario 303, 13416-000, Piracicaba, SP, Brazil. [10]School of Earth Sciences, Stanford University, Stanford, CA 94305, USA. [11]The Earth Institute, Columbia University–Lamont Campus, Palisades, NY 10027, USA. [12]The Heinz Center for Science, Economics, and the Environment, Washington, DC 20009, USA. [13]Department of Crop and Soil Sciences, Michigan State University, Hickory Corners, MI 49060, USA. [14]Department of Ecology and Evolutionary Biology and INSTAAR, University of Colorado, Boulder, CO 80309, USA. [15]College of Resources and Environmental Science, China Agricultural University, Beijing 100094, China.

*To whom correspondence should be addressed. E-mail: vitousek@stanford.edu

References

1. R. Naylor *et al.*, *Science* **310**, 1621 (2005).
2. G. P. Robertson, P. M. Vitousek, *Ann. Rev. Environ. Res.* **34**, 97 (2009).
3. V. Escaravage, P. M. J. Herman, C. H. R. Heip, *J. Integr. Environ. Sci.* **3**, 97 (2006).

CELL BIOLOGY

The Unit of Life

A well-known biologist and co-author of one of the most popular cell biology textbooks (not *Science*'s editor-in-chief) recently told me that he thought we need more decent books about biology written for people outside the field. Science is about the pursuit of knowledge, but once that knowledge is gained we scientists tend to inadvertently keep it to ourselves. We should take responsibility for sharing it more widely, because it has consequences for the whole of society and society funds the majority of our research. While I was slowly digesting this idea and considering the possibility of attempting to write such a book myself, I received developmental biologist Lewis Wolpert's *How We Live and Why We Die*, which essentially tackles this issue. "The secret lives of cells" shouldn't be kept secret, and Wolpert makes a good start at breaking the silence.

How We Live and Why We Die
The Secret Lives of Cells
by Lewis Wolpert
Norton, New York, 2009. 252 pp. $24.95. ISBN 9780393072211.
Faber and Faber, London. £14.99. ISBN 9780571239115.

And so, indeed, where to start? The workings of a cell are mind-numbingly complex: from DNA to genes to proteins to processes. Wolpert engages the reader at a level everyone can relate to, by following the course of cellular life and thus in a sense the life of a human. He leads us on a journey through cell and human development and from function to malfunction. Within that framework, Wolpert first explains the fundamentals, such as the nature of DNA and proteins. He then proceeds from basic cellular processes to the unique characteristics of different cell types. Maintaining interest while conveying these preparatory details using words alone can be difficult. Biologists have historically used Latin for naming purposes, a practice that now necessitates detailed descriptions of pretty much everything. The short glossary at the book's end is very useful in this regard, but the complexity of the topic requires the unseasoned reader to devote full attention throughout the text.

To aid readers through this bombardment of facts, Wolpert often invokes engaging visual analogies. Some—such as describing the mitochondrion as a "sausage"—I found slightly odd. But likening the cell cycle to a washing machine program is elegantly simple and, I am sure, will enlighten those encountering it for the first time. There was a surprising amount of humor within the text. For example, Wolpert describes sperm as swimmers with flippers and lipid molecules in solution as "tiny animals that hate water" (because they keep their heads firmly protected, reluctantly allowing only their tails to get wet). His characterization of signal transduction (translating an extracellular signal into an intracellular response) as being "apparently eccentric" has my full support.

Although the analogies offer a welcome respite from the more routine descriptions, a few illustrations would have been useful—particularly given the short text. Nonetheless, by only naming a handful of genes and smartly choosing ones with the more critical functions or memorable names, Wolpert keeps his account fairly manageable. And once you've made it through the basics without losing the plot, the text easily flows into descriptions of diseases and functions of the human body. These are perhaps the more intriguing aspects for the lay reader and are certainly far easier to grasp.

Wolpert occasionally brings in his own personal experience of events, offering both researchers and the public some unusual insights. He reveals his personal hero (Sydney Brenner) and details some circumstances surrounding several ground-breaking discoveries, making them more vivid. In the context of cell migration and the development of the face, we even learn of his "large nose" (which does have a photographic illustration on the dust jacket).

Wolpert's account is impressively up to date, although the speed at which some fields are currently forging ahead inevitably means certain details have already been supplanted. The recent revolution in genomics has accelerated the pace of biological discoveries, and some researchers predict that neurobiology will soon reveal substantial insights into the workings of the brain, exposing what really makes us human. A similar book written only five years from now will likely look vastly different—and will certainly need to be a lot longer. The author does not specifically mention current gaps in our knowledge, but throughout the text it is possible to notice where they lie.

Perhaps unexpectedly, Wolpert doesn't devote much space to controversial issues relevant to society. He does, however, refer to some of the better-known topics, particularly those surrounding the study and use of human stem cells. I would have preferred more focus on these issues, as they would have worked well in the book's educational context and are of considerable interest to all readers.

Nonetheless, on reaching the end of the book, which doesn't take very long, you can appreciate just how much ground Wolpert

Human cells.

CREDIT: SEBASTIAN KAULITZKI/ALAMY

manages to cover. To get through it all, he mostly sticks to the point, which renders some parts a bit disjointed. Also, his rapid progress generally leaves no room to give the unknowing reader a sense of the years of study that led to the eventual identification and characterization of the basic cellular processes. In a few cases, most notably the development of cell theory, the author does elaborate on the historical context. Whereas the concept of the cell makes perfect sense to us with the benefit of hindsight, the original construction of the concept required the development of new technologies and lots of unconventional thinking.

The last chapter, subtitled "the mystery of the first cell," is actually about the very beginning. It tempts with the promise of explaining all, but Wolpert waits a few pages before going into some of the current theories for the origin of life, which are at present fairly unsatisfying. Cells are keeping some of their secrets, and understanding the origin of the cell remains a notable challenge. So, in the end there is no end. *How We Live and Why We Die* comes full circle from the cell's beginning to the beginning of the cell. But Wolpert manages to pack a great deal of cell biology into the book's couple hundred pages.

–Helen Pickersgill

10.1126/science.1181549

MATHEMATICS

Correspondence in Flux

Brie Finegold

Thinking about "the calculus of friendship" is not as cold an exercise as it might first seem. We depend on a continuity in our friendships, ignoring lapses in communication and momentary mean streaks. Mathematics is no different: As Steven Strogatz notes, "Experience teaches us that change can be sudden, discontinuous, and wrenching. Calculus draws its power by refusing to see that."

The Calculus of Friendship
What a Teacher and a Student Learned About Life While Corresponding About Math

by Steven Strogatz

Princeton University Press, Princeton, NJ, 2009. 180 pp. $19.95. ISBN 9780691134932.

The spring of his freshman year in college, Strogatz (now an applied mathematician at Cornell University) began to exchange letters with his high school calculus teacher, Don Joffray. At some point, their amiable correspondence about math problems led to a true friendship. In *The Calculus of Friendship*, Strogatz weaves their letters into reflections on the philosophical similarities between calculus and human relationships and portrays a friendship firmly founded on a love of dreaming up and solving calculus problems. Student and teacher switched roles as their correspondence ebbed and flowed over the course of 30 years. Their excitement in sharing mathematical jewels and tidbits leaves us as anxious to read the next letter as its recipient must have been.

Strogatz recalls how his teacher's storytelling abilities quickly instilled listeners with a sense of respect for those who solve mathematical puzzles. While teaching, Joffray did not strive to impress the class with his own quickness. Rather "in a hushed tone, he'd tell us about the time that Jamie Williams wrote down a formula for the nth term of the Fibonacci sequence." The Fibonacci sequence (0, 1, 1, 2, 3, 5, 8, 13, 21, …) is a sequence of integers in which every term after the initial pair is the sum of the previous two terms. Of course, now we are goaded into wondering how to figure out a formula for the sequence's nth term that depends only on n. And readers who ruminate over the problem to no avail will find the answer later in the book.

Becoming invested in answering mathematical questions is a major benefit of reading the book. Have you ever been dissatisfied with the standard proof that the square root of two is irrational? (The square root of two is the length of the hypotenuse of a triangle whose legs are of length one. And a number is irrational if it is not the ratio of two integers.) Writing from his college dorm, Strogatz describes to his former teacher a geometric proof of this fact. It is easy to follow yet avoids the tone (too frequently found in textbooks) of "okay, dummy, so this is step one." The respect and admiration the two men held for each other and for the inner workings of mathematics are palpable in their writing. And although some solutions are explicitly worked through, the problems presented in the book are tantalizing on their own. They would be well worth some scribbles on a napkin during lunch.

One can also feel the personality and humor of these pen pals emerging through their symbol-sprinkled sentences. In a letter concerning Fourier series, Joffray gives the name "camel hump theorem" to the fact that no matter what natural number k one picks, $\int_{-\pi}^{\pi} \sin^2 kx\, dx = \pi$. He writes, "Geometrically I saw this as a squeezing of a camel's humps as k escalates through the natural numbers." Joff, as Strogatz begins to call him, ends the next paragraph with "Humph!" A sketch of a camel with humps (for the case $k = 3$) follows.

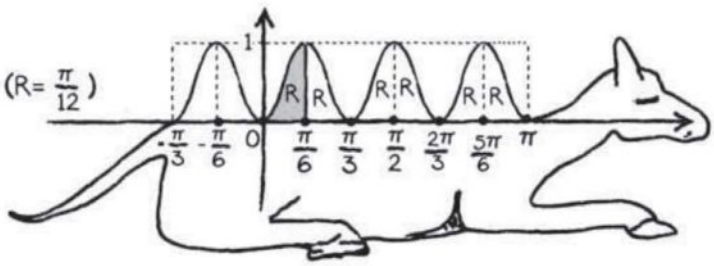

The camel's humps for $k = 3$.

CREDIT: DON JOFFRAY/FROM *THE CALCULUS OF FRIENDSHIP*

Key ideas that are used by scientists of all types float to the surface again and again via specific problems. We learn of young Strogatz's frustration when he devises a problem whose solution cannot be expressed in terms of the familiar elementary functions. We share in his use of computer approximations and dimensional analysis as tools for gaining intuition about a problem. We notice that there is merit to finding multiple proofs to one theorem.

Most important, we share in the joy of doing mathematics, not just the results. Were it true that phrases like "And that's the beauty of this!" appeared in technical papers as often as they do in *The Calculus of Friendship*, more people might be drawn to reading modern research papers.

10.1126/science.1181148

The reviewer is at the Department of Mathematics, University of California, Santa Barbara, CA 93106, USA. E-mail: briefly@math.ucsb.edu

SCIENCE AND REGULATION

The Electronics Revolution: From E-Wonderland to E-Wasteland

Discarded electronics present serious threats to health and ecosystems, making e-waste regulations a policy priority.

Oladele A. Ogunseitan,[1*] Julie M. Schoenung,[2] Jean-Daniel M. Saphores,[3] Andrew A. Shapiro[4]

Since the mid-1990s, electronic waste (e-waste) has been recognized as the fastest-growing component of the solid-waste stream, as small consumer electronic products, such as cellular phones, have become ubiquitous in developed and developing countries (*1*). In the absence of adequate recycling policies, the small size, short useful life-span, and high costs of recycling these products mean they are routinely discarded without much concern for their adverse impacts on the environment and public health. These impacts occur throughout the product life cycle, from acquisition of raw materials (*2*) to manufacturing to disposal at the end of products' useful life.

This creates considerable toxicity risks worldwide (*3*, *4*). For example, the mean concentration of lead in the blood of children living in Guiyu, China, a notorious destination for improper e-waste recycling (*5*), is 15.3 μg/dl. There is no known safe level of exposure to lead; remedial action is recommended for children with levels above 10 μg/dl (*6*). Polybrominated diphenyl ethers used as flame-retardants in electronics have been detected in alarming quantities (up to 4.1 ppm lipid weight) in California's peregrine falcon eggs, raising the specter of species endangerment (*7*, *8*).

We recently estimated that each U.S. household has at least four small (≤4.5 kg) and between two and three large (>4.5 kg) e-waste items in storage (*9*); this represents 747 million e-waste items, weighing over 1.36 million metric tons. Moreover, most people (67%) in the United States are not aware of e-waste disposal restrictions or policies (*9*). The United States, one the largest generators of e-waste in the world (*4*), does not have legally enforceable federal policies that require comprehensive recycling of e-waste or elimination of hazardous substances from electronic products. Without a coherent U.S. policy, informed by challenges faced by similar efforts around the world, it will be difficult to reach a global consensus.

Patchwork of E-Waste Standards

The European Union (EU) adopted two comprehensive directives for managing e-waste: the Restriction on the Use of Hazardous Substances (RoHS), and the Waste Electrical and Electronic Equipment (WEEE) (*10*). China's own WEEE regulations will take effect in 2011. The Basel Convention (*11*), which regulates movement of hazardous wastes across international borders (and includes a technical working group on e-waste), has been ratified by 169 of the 192 United Nations (UN) member countries. Unfortunately, the United States is the only member country of the Organisation for Economic Co-operation and Development that has not ratified the convention. Within the United States, only 19 states have e-waste laws (14 others pending), although most do not provide sufficient infrastructure or dedicated revenue streams to enforce compliance and to promote public participation (*9*, *12*, *13*). This uneven patchwork of policies has created "risk holes." Poor communities and developing countries are disproportionately affected. Consequences are particularly troubling in Africa, China, and India (*4*, *14*, *15*). Markets for second-hand electronics thrive in such places, along with improper recycling of domestic and illegally imported e-waste to recover valuable materials.

Potential Action in U.S. Congress

The U.S. Senate is considering the Electronic Device Recycling Research and Development Act (S. 1397, a version of bill H.R. 1580 passed by the House of Representatives) (*16*–*18*). If made law, the act could fund e-waste engineering research, development, and demonstration projects; engineering curriculum development; and research into nontoxic, environmentally responsible alternative products. The bill would also call for the U.S. National Academy of Sciences to investigate barriers and opportunities for reducing e-waste, decreasing the use of hazardous materials in electronic products, and enabling product design for efficient reuse and recycling. The act addresses an especially overdue need: It asks the National Institute of Standards and Technology to establish a database of physical properties of "green" alternative materials for use in electronic products. Yet it is unclear which properties will be available in this database, or whether human and ecological toxicity data, energy demand, and other socioeconomic indicators will be included.

While developing and implementing national policy in the United States, lessons could be learned from challenges faced by similar programs already under way. The European Commission in 2007 began phasing the REACH program (Registration, Evaluation, Authorization, and Restriction of Chemical Substances) into enforceable law. REACH addresses manufacturers' responsibilities to manage risks from chemicals in

[1]Program in Public Health and School of Social Ecology, University of California, Irvine, CA 92697, USA. [2]Department of Chemical Engineering and Materials Science, University of California, Davis, CA 95616, USA. [3]Department of Civil and Environmental Engineering and Department of Economics, University of California, Irvine, CA 92697, USA. [4]Department of Electrical Engineering and Computer Science, University of California, Irvine, CA 92697, USA.

*Author for correspondence. E-mail: Oladele.Ogunseitan@uci.edu

their products. There has been some confusion about the overlap of REACH and RoHS. They have different approaches to risk characterization and management, and they specify different processes by which they can be implemented by different EU members (*19*).

Also informative, from a major U.S. state-level effort, is the contentious intersection of California's RoHS-like Electronic Waste Recycling Act (EWRA), and the broader, REACH-like, California Green Chemistry Initiative (CGCI). EWRA focuses on very specific chemicals, but the same consumer electronics are covered by the CGCI, which focuses on more comprehensive assessment of toxic chemicals in consumer products and comparative assessment of alternative chemicals through the kind of database outlined in S. 1397. Had it been signed into law, California Assembly Bill 147 would have required manufacturers to declare hazardous materials content in consumer electronics, a specification that was not part of the original EWRA, but that is essential for the CGCI (*20*).

Research Needs

Technology is available to recover precious materials from e-waste, but the bottleneck is consumer participation, collection, dismantling, and sorting to separate the material components (e.g., plastics, different types of metals, and glass). So, to make a difference in confronting the global e-waste challenge, S. 1397 must call for policy research to characterize the factors that motivate consumers to recycle. For example, Californians are willing to pay extra for "green" electronics products (e.g., containing fewer toxic substances, capable of being economically recycled) and to drive up to 8 miles to drop-off products for environmentally sensitive recycling (*21*, *22*). In addition, political mandates and economic incentives are key tools for engaging manufacturers, who will need to assume greater responsibility for designing electronic products that contain safer materials and are easily managed after consumers no longer want them (*23*, *24*). Research to advance recycling technology, such as through improved sorting and labeling, and logistics of product take-back, are necessary to make e-waste recycling economically viable (*25*).

To have a larger impact, research must go beyond management. Solutions to the e-waste problem should not be developed as "end-of-the-pipeline" treatments of hazardous waste; the entire life cycle must be included in the solution. There is a promising collaboration between the UN Environment Programme (UNEP) and the Society for Environmental Toxicology and Chemistry to produce guidelines for product social life-cycle assessment. Integrating the guidelines with human disease end points or ecotoxicological assessments remains problematic (*26*).

Research to identify alternatives to toxic materials and investments in smelter facilities to safely recycle e-waste sorely lag behind the pace at which new electronic devices are invented, which in turn supports consumers' habits of buying replacements for electronic products that are still functioning perfectly (*4*, *25*, *27*, *28*). Improved standards for materials testing could eliminate the need for exemptions to toxic-substance policies for sensitive industries (e.g., medical, military, and aerospace technologies) (*29*). Improved testing of materials and a robust toxics database may encourage manufacturers to consider toxicity early during product design rather than in retrospect, only after performance standards and economic considerations have first been satisfied.

Education

S. 1397 calls for e-waste education programs, but hurdles remain (*30*). The bill targets only undergraduate engineering students and industry professionals, but investigators in other disciplines, such as toxicology, need to be engaged. Efforts should include graduate programs, where opportunities for cross-disciplinary work are increased (*31*).

Conclusion

Bart Gordon, Chairman of the U.S. House Committee on Science and Technology, said that "we need our future engineers to understand that whatever they put together will eventually have to be taken apart (*32*)." They must also understand social, ecological, and public health consequences of their inventions. Manufacturers must adopt a cradle-to-cradle stewardship model for their products (*33*). S. 1397 will be most effective if its expected outcomes in research products, inventions, and workforce and public education are linked to regulatory policies that provide uniform guidance for nationwide e-waste management and "green" electronic product design in light of international, interdisciplinary dimensions of the problem.

References and Notes

1. R. Widmer *et al.*, *Environ. Impact Assess. Rev.* **25**, 436 (2005).
2. K. Hayes, R. Burge, *Coltan Mining in the Democratic Republic of Congo: How Tantalum-Using Industries Can Commit to the Reconstruction of the DRC* (Fauna & Flora International, Cambridge, 2003).
3. J. D. Lincoln, O. A. Ogunseitan, J.-D. Saphores, A. A. Shapiro, *Environ. Sci. Technol.* **41**, 2572 (2007).
4. UNEP, *E-Waste, the Hidden Side of IT Equipment's Manufacturing and Use. Environ. Alert Bull.* **5**, 1 (2005); www.grid.unep.ch/product/publication/download/ew_ewaste.en.pdf.
5. R. Stone, *Science* **325**, 1055 (2009).
6. X. Huo *et al.*, *Environ. Health Perspect.* **115**, 1113 (2007).
7. M. Petreas, D. Oros, *Chemosphere* **74**, 996 (2009).
8. A. Holden *et al.*, *Environ. Toxicol. Chem.* **28**, 1906 (2009).
9. J.-D. Saphores, H. Nixon, O. A. Ogunseitan, A. A. Shapiro, *J. Environ. Manage.* **90**, 3322 (2009).
10. J. M. Schoenung, O. A. Ogunseitan, J.-D. Saphores, A. A. Shapiro, *J. Ind. Ecol.* **8**, 59 (2004).
11. The Basel Convention on the Control of Transboundary Movements of Hazardous Wastes and their Disposal, *Nairobi Declaration on the Environmentally Sound Management of Electrical and Electronic Wastes and Decision VIII/2*; www.basel.int/meetings/cop/cop9/docs/09e.doc.
12. National Electronics Recycling Infrastructure Clearinghouse, www.ecyclingresource.org/ContentPage.aspx?Pageid=28&ParentID=0.
13. Electronics Take Back Coalition, *State Legislation*, www.electronicstakeback.com/legislation/state_legislation.htm.
14. H.-G. Ni, E. Y. Zeng, *Environ. Sci. Technol.* **43**, 3991 (2009).
15. A. Bandyopadhyay, *Environ. Eng. Sci.* **25**, 1507 (2008).
16. Electronic Device Recycling and Development Act (S. 1397), introduced in the Senate 6 July 2009; http://thomas.loc.gov/cgi-bin/bdquery/z?d111:SN01397:l/bss/111search.html.
17. U.S. House of Representatives Committee on Science and Technology, Electronics Waste Research and Development Act (H.R. 1580); http://science.house.gov/legislation/leg_highlights_detail.aspx?NewsID=2403.
18. For the current status of H.R. 1580, see www.opencongress.org/bill/111-h1580/actions_votes.
19. F. Abrams, "Dealing with the devil: Could REACH be better than ROHS?" *Electronics Design, Strategy, News*, 5 February 2008; www.edn.com/article/CA6528666.html.
20. California Assembly Bill 147: Hazardous Waste: Electronic Waste, www.leginfo.ca.gov/cgi-bin/postquery?bill_number=ab_147&sess=CUR&house=B&author=saldana. Vetoed by California Governor Schwarzenegger on 11 October 2009.
21. J.-D. Saphores, H. Nixon, O. A. Ogunseitan, A. A. Shapiro, *J. Environ. Plann. Manage.* **50**, 113 (2007).
22. J.-D. Saphores, H. Nixon, O. A. Ogunseitan, A. A. Shapiro, *Environ. Behav.* **38**, 183 (2006).
23. D. S. Khetriwal, P. Kraeuchi, R. Widmer, *J. Environ. Manage.* **90**, 153 (2009).
24. H.-Y. Kang, O. A. Ogunseitan, A. A. Shapiro, J. M. Schoenung, *Environ. Sci. Technol.* **41**, 373 (2007).
25. H.-Y. Kang, J. M. Schoenung, *Resour. Conserv. Recycling* **45**, 368 (2005).
26. UNEP and Society for Environmental Toxicology and Chemistry, *Guidelines for Social Life Cycle Assessment of Products: Social and Socio-economic LCA Guidelines Complementing Environmental LCA and Life Cycle Costing, Contributing to the Full Assessment of Goods and Services Within the Context of Sustainable Development* (UNEP, Paris, 2009), 104 pp.
27. J. D. Lincoln, A. A. Shapiro, J. Earthman, J.-D. Saphores, O. A. Ogunseitan, *IEEE Trans. Electron. Packag. Manuf.* **31**, 211 (2008).
28. O. A. Ogunseitan, *JOM J. Miner. Met. Mater. Soc.* **59**, 12 (2007).
29. A. A. Shapiro, J. Bonner, O. A. Ogunseitan, J.-D. Saphores, J. M. Schoenung, *IEEE Trans. Compon. Packag. Tech.* **29**, 60 (2006).
30. J. B. Zimmerman, P. T. Anastas, *ACS Symp. Ser.* **1011**, 137 (2009).
31. J. M. Schoenung, O. A. Ogunseitan, D. Eastmond, in *Proceedings of the IEEE International Symposium on Sustainable Systems and Technology (ISSST)*, Tempe, AZ, 18 to 20 May 2009; 10.1109/ISSST.2009.5156760.
32. B. Gordon, floor speech on H.R. 1580, http://science.house.gov/press/PRArticle.aspx?NewsID=2435.
33. W. McDonough, M. Braungart, *Cradle To Cradle: Remaking the Way We Make Things* (North Point Press, New York, 2002), 208 pp.

34. Funded in part by NSF (CMS-0524903) and the University of California Toxic Substances Research and Teaching Program (UC-44157).

10.1126/science.1176929

ATMOSPHERIC SCIENCE

Clean the Air, Heat the Planet?

Measures to control emissions of air pollutants may have unintended climatic consequences.

Almut Arneth,[1,2]* Nadine Unger,[3] Markku Kulmala,[2] Meinrat O. Andreae[4]

The push toward cleaner air in Beijing before the 2008 Olympic Games was a vivid reminder of the need to control air pollution, not only in Asia but in many regions of the world (*1*). There is mounting evidence for particle- and ozone-related health effects (*2*, *3*). Furthermore, ozone and aerosol particles affect Earth's radiation balance (*4*, *5*): Many aerosols cool the atmosphere (a negative forcing), whereas ozone and black carbon aerosol have a warming effect (a positive forcing). There is thus a strong motivation for treating air pollution control and climate change in common policy frameworks (*5*, *6*). However, recent model studies (*7*–*9*) have shown that changes in pollutant and precursor emissions, atmospheric burden, and radiative forcing are not necessarily proportional. Furthermore, as Shindell *et al*. report on page 716 of this issue, current models do not capture many of the complex atmospheric processes involving aerosols and reactive trace gases (*10*).

The idea that air pollution control could help to mitigate climate change, buying time until greenhouse gas reductions take effect, seems attractive, because air pollutants are short-lived in the atmosphere compared with CO_2 and other greenhouse gases. The radiative forcing of these short-lived species is uncertain but may be large. The contribution of anthropogenic ozone to global warming may be twice the mean Intergovernmental Panel on Climate Change (IPCC) value of +0.35 W m^{-2} (*4*). Ramanathan and Carmichael have inferred a forcing of +0.9 W m^{-2} for current black carbon levels (*11*)—more than half the value of the current CO_2 forcing. Assuming a climate sensitivity of 2° to 4°C for a doubling of CO_2, elimination of black carbon emissions could decrease global surface temperature by 0.5° to 1°C (*11*).

Alternatively, pollution control could accelerate climate change if reduction of short-lived pollutants with negative forcing—especially sulfate aerosols—outweighs reduction of those with positive forcing (*12*). Climate sensitivity analysis suggests temperature increases well above IPCC estimates for all but the lowest estimates of net aerosol forcing (*12*). Changes in the atmospheric aerosol load may thus lead to a strong greenhouse gas warming response. In support of this argument, Shindell and Faluvegi have suggested that decreasing sulfate aerosol concentrations and increasing black carbon concentrations have contributed notably to the rapid Arctic warming in recent decades (*13*).


How will air pollution measures affect global climate?

The distribution of short-lived species is inherently uneven, and a small global mean radiative forcing may hide substantial variation arising from localized emissions and specific oxidation and deposition pathways. Moreover, major source areas are likely to spread or migrate from the mid-latitudes to the subtropics or tropics, which have economies with different emission spectra (*14*) and are warmer, moister, and more photochemically active. As Shindell *et al*. show, reaction pathways of a given compound can affect the concentrations of several others (*10*). Accounting for the complex nonlinear interactions of aerosol and gas-phase chemistry, the authors obtain global warming potentials (*15*) that are higher for methane or CO, but lower for nitrogen oxides, than previous estimates that largely ignored these effects. Projections of climate effects due to air pollution control clearly must account for a very complex set of interactions.

How will the geographically inhomogeneous changes in emissions translate into the metric that dominates the political debate—the global and local surface temperature? Model studies have recently begun to address this question (*7*–*9*). The decadal climate impact of the future evolution of short-lived species was compared in three different transient chemistry-climate simulations (*8*) for a rapid economic growth scenario using both fossil fuel and renewable energies. The three models applied different emissions projections, especially for black carbon. By 2050, two models showed 20 to 40% of additional global warming from short-lived species compared with greenhouse gases alone; the third model showed virtually no global mean effect from short-lived species.

In a related study, Kloster *et al*. assumed full implementation of state-of-the art technologies for aerosol control. In this case, the combined effects from aerosol reductions and greenhouse gas increases led to a projected increase in global mean temperature of 2.2 K at 2030 relative to today, nearly doubling the effect of greenhouse gases alone (*9*). Maximum abatement in the industry and power sectors (dominated by sulfate aerosol) yielded a somewhat lower response of 1.9 K; maximum abatement in the domestic and transport sectors (dominated by black carbon) still caused an increase of 1.4 K. Reductions of short-lived species are clearly no panacea for our climate change problems.

Direct and indirect interactions between climate change, land ecosystems, and chemistry can amplify or dampen the climate effects of air pollutants, but are poorly represented in models. The climate effects of reduced sulfate could be offset by possibly enhanced production of secondary organic aerosol if their biogenic precursor emissions are stimulated by warmer temperatures (*16*, *17*). However, such climate feedbacks may be diminished if secondary aerosol precursor emissions are inhibited by rising CO_2 (*18*). Furthermore, land use and land cover change may alter biogenic and pyrogenic

[1]Department of Physical Geography and Ecosystem Analysis, Lund University, 22362 Lund, Sweden. [2]Department of Physics, University of Helsinki, 00014 Helsinki, Finland. [3]NASA Goddard Institute for Space Studies, Center for Climate Systems Research, Columbia University, New York, NY 10025, USA. [4]Max Planck Institute for Chemistry, Biogeochemistry Department, 55020 Mainz, Germany.

*To whom correspondence should be addressed. E-mail: almut.arneth@nateko.lu.se

emissions of short-lived species as strongly as, if not more than, climate change. These interactions are increasingly being studied (*18*) but are not yet well understood.

Like many others in the climate debate, we have focused on surface temperature, but other aspects of climate change—especially the amount, distribution, and intensity of rainfall—are at least as important to human well-being. Changing aerosol burdens may alter local and regional cloud cover and precipitation, change the intensity or timing of the monsoon circulation, and even shift precipitation across national borders (*19*, *20*). Changes in cloud cover and precipitation will also feed back on the photochemistry and rainout of short-lived species (*9*). These issues must be considered if aerosol emissions are to become part of climate policy.

Given the toxicity of pollutants, the question is not whether ever stricter air pollution controls will be implemented, but when and where (*1*). The jury is out on whether air pollution control will accelerate or mitigate climate change. Still, the studies available to date (*7*–*9*, *13*) mostly suggest that air pollution control will accelerate warming in the coming decades. Climate change policies may have to include a "pollution safety margin" in greenhouse gas reduction targets. CO_2, indeed, is not the only gas (*21*).

References and Notes

1. D. D. Parrish, T. Zhu, *Science* **326**, 674 (2009).
2. J. J. West, A. M. Fiore, L. W. Horowitz, D. L. Mauzerall, *Proc. Natl. Acad. Sci. U.S.A.* **103**, 3988 (2006).
3. J. Kaiser, *Science* **307**, 1858 (2005).
4. P. Forster *et al.*, in *Climate Change 2007: The Physical Science Basis. Contribution of Working Group I to the Fourth Assessment Report of the Intergovernmental Panel on Climate Change*, S. Solomon *et al.*, Eds. (Cambridge Univ. Press, Cambridge/New York, 2007).
5. J. Hansen, M. Sato, R. Ruedy, A. Lacis, V. Oinas, *Proc. Natl. Acad. Sci. U.S.A.* **97**, 9875 (2000).
6. T. C. Bond, *Environ. Res. Lett.* **2**, 045030 (2007).
7. H. Levy, M. D. Schwarzkopf, L. Horowitz, V. Ramaswamy, K. L. Findell, *J. Geophys. Res.* **113**, D06102 (2008).
8. D. T. Shindell *et al.*, *J. Geophys. Res.* **113**, D11109 (2008).
9. S. Kloster *et al.*, *Clim. Dyn.*, 10.1007/s00382-009-0573-0 (2009).
10. D. T. Shindell *et al.*, *Science* **326**, 716 (2009).
11. V. Ramanathan, G. Carmichael, *Nat. Geosci.* **1**, 221 (2008).
12. M. O. Andreae, C. D. Jones, P. M. Cox, *Nature* **435**, 1187 (2005).
13. D. Shindell, G. Faluvegi, *Nat. Geosci.* **2**, 294 (2009).
14. N. Unger, D. T. Shindell, D. M. Koch, D. G. Streets, *J. Geophys. Res.* **113**, D02306 (2008).
15. Global warming potential, a metric often used in climate policies such as the Kyoto Protocol, is the calculated cumulative radiative forcing of a gas over a specified time period (e.g., 100 years) in response to an emissions pulse, relative to a reference gas (normally CO_2).
16. M. Hallquist *et al.*, *Atmos. Chem. Phys.* **9**, 5155 (2009).
17. M. Kulmala *et al.*, *Atmos. Chem. Phys.* **4**, 557 (2004).
18. A. Arneth *et al.*, *Biogeosci. Disc.* **6**, 7717 (2009).
19. D. Rosenfeld *et al.*, *Science* **321**, 1309 (2008).
20. M. O. Andreae *et al.*, *Science* **303**, 1337 (2004).
21. K. P. Shine, W. T. Sturges, *Science* **315**, 1804 (2007).

22. The authors acknowledge support from the Academy of Finland (M.K., A.A.), the Swedish research councils VR and Formas (A.A.), and the NASA Atmospheric Chemistry Modeling and Analysis Program (N.U.).

10.1126/science.1181568

CHEMISTRY

The Basics of Zinc Activation

The stubborn carbon-hydrogen bonds of an organic compound can be replaced by more reactive carbon-zinc bonds.

Ilan Marek

The least reactive bonds of organic molecules, single carbon-hydrogen (C–H) bonds, are often the sites where we want to perform a chemical reaction. Metals such as magnesium and lithium can be used to "activate" these bonds by creating organometallic compounds that have more reactive metal-carbon (M–C) bonds (*1*). If these goals are to be achieved with metalating reagents, which replace a C–H bond with a M–C bond, then these reagents must maximize reactivity, selectivity, and stability—seemingly incompatible goals. Although many useful reactions of this type are well known for basic organometallic species formed from lithium, the activation can sometimes be "too good" and lead to a cascade of unwanted side products. Greater control might result if metals such as Zn, which would form less polar bonds, could be used, but the kinetics for this less reactive metal might be expected to be slow for the task (*2*–*4*). However, on page 706 of this issue, Kennedy *et al.* (*5*) report the preparation of a well-defined bimetallic zinc compound that, with help from alkali metals, selectively reacts with C–H bonds.

Schulich Faculty of Chemistry, Technion-Israel Institute of Technology, Haifa 32000, Israel. E-mail: chilanm@tx.technion.ac.il

The hydrogen atoms on certain molecules are only minimally acidic; there is a high energy barrier for activating the C–H bond (i.e., removing a proton and leaving behind the organic anion, or carbanion). Thus, strong bases, such as alkyllithiums, are generally required to overcome the weak acidity of the proton on hydrocarbons so that they will undergo permutational exchange, that is, exchange a hydrogen atom for a more reactive organometallic group.

A potential additional problem is selectivity; many different hydrogen atoms are present in most organic molecules, and subtle differences in their environment must be exploited to discriminate between them chemically. However, the carbanions formed often undergo unwanted rearrangements, and therefore the third obstacle is balancing the high reactivity of such reagents with product stability, which is needed for practical applications as well as characterization studies.

Pioneering work of Schlenk led to development of basic organolithium species that were used for decades to perform metalations. However, these bases are prone to undesirable side reactions as a result of their high reactivity and their strong nucleophilicity (their ability to donate electrons). Furthermore, the inherent stability of the newly formed carbanion can also

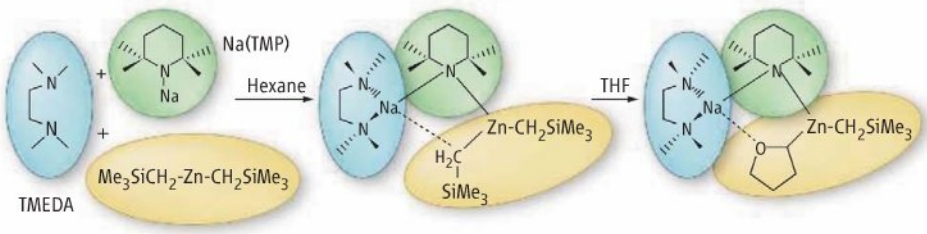

Holding reactive molecules in rings. Many organometallic reagents, such as alkyllithium compounds, can displace a carbon-hydrogen bond with a carbon-metal bond, but the species formed can be unstable. Kennedy *et al.* created a reagent that avoids such dissociation by complexing three compounds such as Na(TMP) (where TMP is 2,2,6,6-tetramethylpiperidide), bis(trimethylsilylmethyl)zinc, and TMEDA (*N*,*N*,*N*′,*N*′-tetramethylethylenediamine) in hexane solution. Reaction with tetrahydrofuran (THF) creates a stable Zn–C bond through the stabilizing effect of a five-membered ring, O–Na–N–Zn–C.

be troublesome. A typical example is the easy metalation adjacent to oxygen of cyclic ether tetrahydrofuran (THF) that invariably leads to unwanted ring-opening fragmentation (*6*):

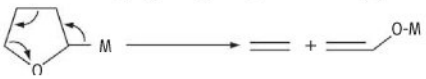

To avoid side reactions, more elaborate reagents were introduced that combined two or more distinct components, usually a combination of organic anions and cations. Although synthetically extremely useful, their exact structures remain elusive, which made their improvement a somewhat empirical effort (*7*). The strategy of Kennedy *et al.* led to the design of a bimetallic dicationic-dianionic reagent with outstanding synthetic applications, such as the formation of an unexpectedly stable zinc-substituted THF, or THF-heterozincate, at ambient temperature that avoids ring opening or cleavage.

This transformation is quite unexpected, given previous attempts to make such compounds. Kennedy *et al.* designed a new alkali-metal–mediated zinc cationic species that forms through the co-complexation of three species (see the figure), NaTMP, bis(trimethylsilylmethyl)zinc, and TMEDA in hexane solution (*8*); TMP and TMEDA are organic compounds that contain nitrogen atoms that form bonds to the metals. The reagent that forms can directly metalate THF because it traps the fragment that would otherwise undergo deprotonation. It does so by creating a fused ring, O–Na–N–Zn–C, that increases the overall stability of the complex (see the figure). The carbon atom in the ring formed by metalation of cyclic ethers has also become a stereogenic center.

A preliminary reactivity study shows that the trapping reaction of zinc-activated THF with benzoyl chloride leads to the desired coupled product in an isolated 70% yield. This reaction also works with the larger homolog of THF, tetrahydropyran. The metalation of ethylene at 50°C with the potassium analog of the sodium-zinc reagent created a vinyl anion trapped by chelation to two metals. Zinc forms a single σ bond to the deprotonated carbon atom, and potassium interacts with the π orbital of the unsaturated ethylene unit.

This remarkable preparation of stable zinc derivatives of cyclic ethers opens new horizons in organometallic chemistry and raises many questions. One immediate question concerns the effect of the Na-O chelation in the stability of the product. Does it really stabilize the species toward elimination reactions (and, in such case, why is the five-element ring so effective), or is it only needed for the permutational exchange processes? In other words, will monometallic zincated THF, if it can be prepared, be stable toward fragmentation?

The past decade has witnessed a remarkable reassessment of metalation chemistry. The work of Kennedy *et al.* changes the perceived wisdom that low polarity metals were too slow to react. It also pinpoints a specific combination of bimetallic ligands that execute zinc metalation that is facilitated by entrapping fragments before they undergo unwanted reactions. The presence of a stereogenic center in the reagents formed could be exploited by using an enantiomerically pure base. Numerous applications could then be envisioned in the field of natural product chemistry, such as the synthesis of polyketides.

References

1. F. Leroux, M. Schlosser, E. Zohar, I. Marek, in *The Chemistry of Organolithium Compounds*, Z. Rappoport, I. Marek, Eds. (Wiley, Chichester, 2004), pp. 435–493.
2. Y. Kondo *et al.*, *J. Am. Chem. Soc.* **121**, 3539 (1999).
3. S. H. Wunderlich, P. Knochel, *Angew. Chem. Int. Ed.* **46**, 7685 (2007).
4. M. Mosrin, P. Knochel, *Org. Lett.* **11**, 1837 (2009).
5. A. R. Kennedy, J. Klett, R. E. Mulvey, D. S. Wright, *Science* **326**, 706 (2009).
6. A. Maercker, *Angew. Chem. Int. Ed. Engl.* **26**, 972 (1987).
7. M. Schlosser, *Mod. Synth. Meth* **6**, 277 (1992).
8. R. E. Mulvey, *Acc. Chem. Res.* **42**, 743 (2009).

10.1126/science.1181863

CLIMATE CHANGE

Clean Air for Megacities

Air pollution in megacities has severe health impacts, but its control could provide opportunities for climate change mitigation.

David D. Parrish[1] and Tong Zhu[2]

As of 2008, over half of humanity lives in cities. The number of megacities (with populations over 10 million) grew from 3 in 1975 to 19 in 2007, and is projected to increase to 27 in 2025 (*1*). These megacities are the engines of growing economies, but are also very large sources of air pollutants and climate-forcing agents. The growth of megacities greatly aggravates the health impacts of polluted air, yet it may also provide an opportunity to mitigate climate change, if implemented air quality policies are designed to also reduce global warming.

Exposure to airborne particles and ozone raises mortality and hospital admissions due to respiratory and cardiovascular disease (*2*, *3*). These health impacts increase very rapidly with the population size of a city [(*4*, *5*) and see the figure, panel A]. All the world's megacities exceed the World Health Organization (WHO) guideline for particulate matter (see the figure, panel B).

Yet, greater population density could act to mitigate climate change because it might allow for more efficient energy use (*4*, *6*), and hence lower per capita CO_2 emission. Further, air quality control strategies that reduce total energy use—such as fast and convenient public transport, improved vehicle mileage standards, and more energy-efficient buildings—also reduce CO_2 emissions. Many such strategies are more effectively implemented as urban populations grow (*7*).

Furthermore, given that megacities are economic engines, they are better able to generate the wealth needed to address air quality and climate change issues, and to build the infrastructure required for more efficient energy use. Efforts to optimize the co-benefits of air quality and climate change policies will pay dividends for all countries. An important example is the reduction of ozone formation and soot emissions; these species have pronounced health effects (*8*, *9*), are key climate-forcing agents (*10*–*12*), and—given their short atmospheric lifetimes—allow a rapid climate response to emission reductions.

The scientific and engineering knowledge accumulated as earlier developing megacities dealt with air quality problems is a crucial resource for developing megacities. The pronounced air pollutant levels that accompanied past development can perhaps be avoided. For example, ozone reached very high concentrations in Los Angeles (*13*) before responding to control strategies over the past three decades (see the figure, panel C). In Mexico City (*14*, *15*), high ozone concentrations appeared later, peaked in the early 1990s, apparently

[1]Chemical Sciences Division, Earth System Research Laboratory, National Oceanic and Atmospheric Administration, Boulder, CO 80305, USA. E-mail: david.d.parrish@noaa.gov [2]State Key Lab for Environment Simulation and Pollution Control, College of Environmental Sciences and Engineering, Peking University, Beijing 100871, China. E-mail: tzhu@pku.edu.cn

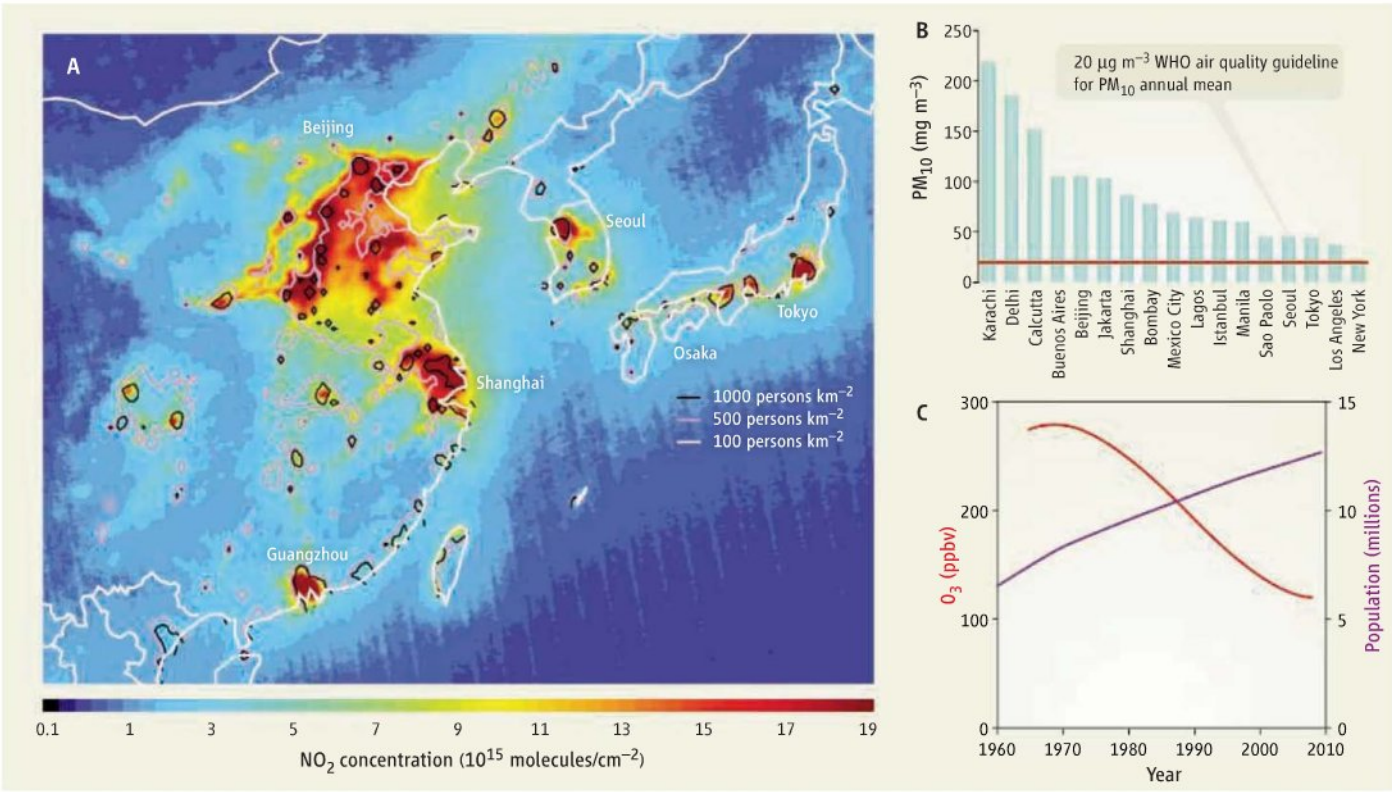

Centers of pollution. (**A**) Satellite image (*22*) of NO_2 concentrations over Asia. NO_2 is a short-lived pollutant released from combustion processes and is a precursor to ozone pollution. NO_2 concentrations are elevated in urban areas. (**B**) Annual mean concentrations of particles with diameters of less than 10 μm (PM_{10}) in the world's megacities (*23*). (**C**) Population and evolution of maximum ozone concentration in Los Angeles. Red line, polynomial fit to observed annual maximum ozone concentrations (*13*). Purple line, population of Los Angeles from (*24*). ppbv, parts per billion by volume.

never reaching the peak Los Angeles concentrations, and have since declined more rapidly there than in Los Angeles. The limited research data sets available from Beijing (*16*) suggest that ozone concentrations, although low in the 1980s, are increasing rapidly there, with concentrations measured during preparations for the 2008 Olympics Games (*17*) comparable to those in Los Angeles and Mexico City. However, Beijing has already implemented aggressive emission controls on automobiles and limits heavy truck traffic in the city to nighttime to mitigate traffic congestion (*18*). Motorized vehicles are the main emitters of ozone precursors in these three (and likely all) megacities, because growing vehicle fleets generally accompany megacity development. Past experience suggests that it is efficient and ultimately cost-effective for megacities to introduce vehicular emission controls before the expensive and lengthy development of locally tailored control programs (*19*).

Major scientific challenges lie in understanding the dual role of particulate matter as the air pollutant with the greatest health impacts, and as both a cooling and a warming agent for climate (*20*, *21*). On balance, particulate matter in the atmosphere is believed to presently compensate for a large fraction of the warming effects of greenhouse gases, but there is large uncertainty in our understanding of its net climate effects and on the different time and space scales on which particulate matter affects climate. Whereas CO_2 is mixed nearly uniformly throughout the globe, the shorter-lived particulate matter has strong regional differences in its effect on temperature and precipitation patterns (*21*).

References and Notes

1. United Nations, *World Urbanization Prospects: The 2007 Revision Highlights* (United Nations, New York, 2008).
2. B. Brunekreef, S. T. Holgate, *Lancet* **360**, 1233 (2002).
3. C. A. Pope, III, M. Ezzati, D. W. Dockery, *N. Engl. J. Med.* **360**, 376 (2009).
4. L. M. A. Bettencourt, J. Lobo, D. Helbing, C. Kühnert, G. B. West, *Proc. Natl. Acad. Sci. U.S.A.* **104**, 7301 (2007).
5. Primary pollutant concentrations grow as a power-law function of population (*4*); that is, they increase as N^{β}, where N is the population size and the exponent β is between 0 and 1. Thus, the concentrations of pollutants such as NO_2 are greater, and impact larger areas, over the more populated cities. Because each person is exposed to the pollutant concentration, the population-integrated exposure increases roughly as $N^{1+\beta}$. Air pollution thus becomes a rapidly increasing health problem as cities grow.
6. N. B. Grimm *et al.*, *Science* **319**, 756 (2008).
7. J. D. Marshall, *Environ. Sci. Technol.* **42**, 3133 (2008).
8. M. Jerrett *et al.*, *N. Engl. J. Med.* **360**, 1085 (2009).
9. T. Stoeger *et al.*, *Environ. Health Perspect.* **114**, 328 (2006).
10. D. S. Stevenson *et al.*, *Geophys. Res. Lett.* **25**, 3819 (1998).
11. M. Z. Jacobson, *Nature* **409**, 695 (2001).
12. V. Ramanathan, G. Carmichael, *Nat. Geosci* **1**, 221 (2008).
13. The ozone data are running 3-year averages of the fourth-highest maximum 8-hour average from the Air Quality Data Statistics Web site of the California Air Resources Board (www.arb.ca.gov/adam/welcome.html).
14. H. A. Bravo, R. J. Torres, *Atmos. Environ.* **34**, 499 (2000).
15. M. J. Molina, L. T. Molina, *J. Air Waste Manage. Assoc.* **54**, 644 (2004).
16. M. Shao, X. Y. Tang, Y. H. Zhang, W. J. Li, *Front. Ecol. Environ* **4**, 353 (2006).
17. See http://ceh.pku.edu.cn/carebjindex.html.
18. The communiqué on the Environmental Status of Beijing, 1999–2008 (Beijing Municipal Environmental Protection Bureau, www.bjepb.gov.cn/bjhb/publish/portal0/tab375/).
19. D. D. Parrish *et al.*, *Atmos. Environ.* (2009).
20. D. T. Shindell *et al.*, *Science* **326**, 716 (2009).
21. A. Arneth *et al.*, *Science* **326**, 672 (2009).
22. Image prepared by L. Lamsal and R. Martin (Dalhousie University) from tropospheric NO_2 column data for 2005 to 2007 retrieved by KNMI (Royal Netherlands Meteorological Institute); 2005 population density data from http://sedac.ciesin.columbia.edu/gpw/.
23. K. D. Pandey *et al.*, *Ambient Particulate Matter Concentrations in Residential and Pollution Hotspot areas of World Cities: New Estimates Based on the Global Model of Ambient Particulates (GMAPS)*, The World Bank Development Economics Research Group and the Environment Department Working Paper (World Bank, Washington, DC, 2006).
24. United Nations Population Division, *World Urbanization Prospects: The 2007 Revision Population Database* (http://esa.un.org/unup/).

10.1126/science.1176064

CELL BIOLOGY

An Ancient Gauge for Iron

A protein with a domain that binds to oxygen and iron acts as a sensor to control iron metabolism in human cells.

Tracey A. Rouault

Mammalian cells must manage the import, export, and sequestration of iron to achieve the cytosolic concentrations needed to support the synthesis of iron-binding proteins and prevent unfavorable iron-dependent oxidation events. Key to this maintenance are the iron regulatory proteins IRP1 and IRP2, which respond to the cytosolic iron pool by binding to target mRNA and regulating the synthesis of iron metabolism proteins (*1*–*3*). On pages 718 and 722 of this issue, Vashisht *et al*. and Salahudeen *et al*. (*4*, *5*) report that human cells gauge cellular iron and concomitantly alter the activity of IRPs through a mechanism that depends on the protein FBXL5. FBXL5 senses iron through an evolutionarily conserved hemerythrin domain that is related to a family of iron- and oxygen-binding proteins in bacteria and invertebrates.

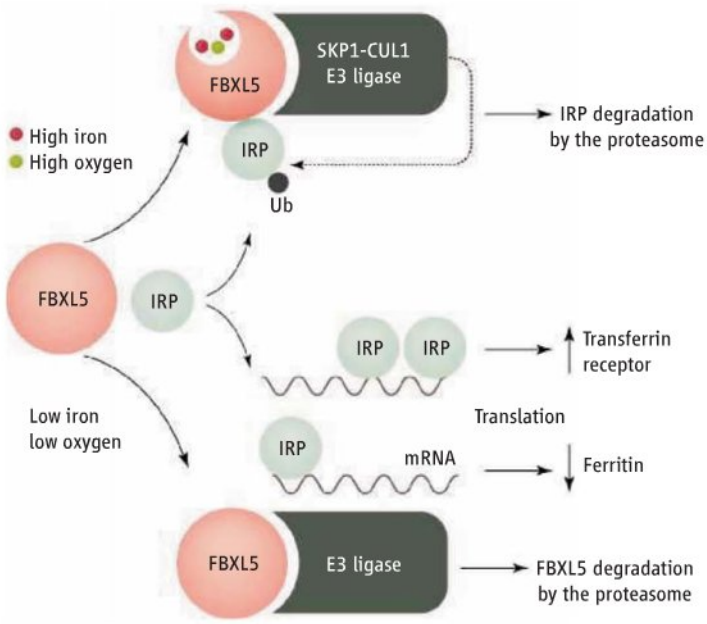

Regulation of iron homeostasis. The concentrations of iron and oxygen in mammalian cells determine the stability of FBXL5, which consequently determines whether IRPs are degraded by the ubiquitin (Ub)-proteasome system or kept available to control the expression of target mRNAs. These mRNAs encode proteins important in cellular iron homeostasis, including ferritin (an iron sequestration protein) and the transferrin receptor (an iron uptake protein). FBXL5 likely contains an oxygen-bridged di-iron binding site within a conserved hemerythrin domain. IRPs bear motifs that are targets for FBXL5, but the accessibility of these motifs may determine the efficiency of FBXL5-mediated degradation.

The role of FBXL5 in iron sensing was discovered through two approaches. Vashisht *et al*. focused on identifying new roles for mammalian F-box proteins. The F-box is a 42– to 48–amino acid motif composed of three α helices that form a pyramidal shape. The human genome includes more than 20 proteins that contain both an F-box (*6*) and a domain of leucine-rich repeats (FBXL) that provides the architecture for protein-protein interactions (*7*). An F-box protein tethers a target protein to an E3 ligase complex that tags the target with ubiquitin molecules, thereby marking it for degradation by the proteasome (*8*). To identify new targets of FBXL5, its F-box was deleted and the resulting protein (which could avoid degradation) was expressed in cultured human cells. IRP1 and IRP2 were identified (by mass spectrometry) as FBXL5 binding proteins.

In a different approach, Salahudeen *et al*. used RNA interference to decrease the expression of E3 ligase components in cultured human cells. When cells were treated with iron, IRP2 degradation was observed. However, IRP2 was spared from degradation in cells that lost expression of FBXL5 or any of the components of the SCF class of multimeric E3 ligases (which contain the proteins Skp1, Cullin 1, and RBX1) (*8*).

Unexpectedly, both groups identified a conserved hemerythrin domain at the N terminus of FBXL5. Previously, hemerythrins were recognized as oxygen-carrying proteins in invertebrates and as potential oxygen sensors in bacteria, but were not known to exist in higher life forms (*9*). Hemerythrin consists of a four–α helix barrel structure in which an active site is formed by two iron atoms ligated to residues from all four helices, and bridged by one oxygen atom from the solvent (see the figure). Molecular oxygen binds to one of the iron atoms; upon binding, each iron atom donates an electron to the oxygen molecule to form a hydroperoxide, which is stabilized by the surrounding protein sheath (*9*, *10*). Thus, dioxygen binding and the concomitant oxidation of the two bound iron atoms increases the iron-binding affinity and stability of the hemerythrin domain.

Both groups report that the binding of iron and oxygen to the hemerythrin domain stabilizes FBXL5, whereas a lack of iron (or lack of oxygen in the presence of sufficient iron) results in degradation. Deletional analyses of FBXL5 established that the N-terminal 161 amino acids were required for iron-dependent degradation (*5*). In addition, the C-terminal region of FBXL5, which contains the leucine-rich repeats, binds to IRPs (*4*, *5*). Because iron and oxygen stabilize FBXL5, targeting of IRPs for degradation occurs in cells that are iron-replete. Thermal denaturation experiments of the N-terminal 161–amino acid fragment suggest that removal of iron leads to unfolding of the hemerythrin domain (*5*), which likely exposes FBXL5 to attack by yet another specific E3 ligase (*4*, *5*). These discoveries reveal that FBXL5 directly interacts with iron, enabling it to sample iron levels in real time, and that iron stabilizes FBXL5, allowing it to target IRPs for degradation.

Although both IRP1 and IRP2 are targets for FBXL5, there is another layer of regulation for IRP1 that protects it from iron-dependent degradation. In cells that are rich in iron, IRP1 ligates an iron-sulfur cluster and functions as an aconitase, interconverting citrate and isocitrate (*1*). The presence of the iron-sulfur cluster likely drives a conformational change in IRP1 (*11*) that limits accessibility of the "degron," the sequence(s) on target proteins to which FBXL5 binds. When cells are low in iron, IRP1 loses its iron-sulfur cluster and undergoes a conformational change that enables it to bind to sequences in mRNA known as iron-responsive elements (IREs) (*1*–*3*). Similarly, in iron-depleted cells, IRP2 also binds to IREs.

The IRE-binding activity of IRP1 and IRP2 differentially controls the transla-

Molecular Medicine Program, National Institute of Child Health and Human Development, Bethesda, MD 20892, USA. E-mail: trou@helix.nih.gov

CREDIT: N. KEVITIYAGALA/SCIENCE

tion of mRNAs. For example, when iron is low, IRPs inhibits the translation of mRNA encoding the cytosolic iron-binding protein ferritin. This reduces iron sequestration, making it available for cellular processes. IRP binding also protects mRNA encoding the transferrin receptor (which transports iron into cells) from degradation, and consequently boosts its expression when the concentration of cytosolic iron is low. As expected, manipulations of FBXL5 activity affected the amounts of ferritin (*4*) and transferrin receptor mRNA in cells (*5*). Thus, the activity of the IRE-IRP regulatory system is controlled by FBXL5, which directly reflects cellular iron status through the iron binding of its conserved hemerythrin domain (*10*).

In the parsimonious evolutionary process, hemerythrin was surpassed by heme as the oxygen carrier of choice (*12*). However, it seems that in higher life forms, the hemerythrin domain was successfully repurposed as an iron sensor to function in cellular iron homeostasis.

References and Notes

1. T. A. Rouault, *Nat. Chem. Biol.* **2**, 406 (2006).
2. M. L. Wallander, E. A. Leibold, R. S. Eisenstein, *Biochim. Biophys. Acta* **1763**, 668 (2006).
3. M. U. Muckenthaler, B. Galy, M. W. Hentze, *Annu. Rev. Nutr.* **28**, 197 (2008).
4. A. A. Vashisht *et al.*, *Science* **326**, 718 (2009); published online 17 September 2009 (10.1126/science.1176333).
5. A. A. Salahudeen *et al.*, *Science* **326**, 722 (2009); published online 17 September 2009 (10.1126/science.1176326).
6. J. R. Skaar, V. D'Angiolella, J. K. Pagan, M. Pagano, *Cell* (2009).
7. J. Bella, K. L. Hindle, P. A. McEwan, S. C. Lovell, *Cell. Mol. Life Sci.* **65**, 2307 (2008).
8. T. Cardozo, M. Pagano, *Nat. Rev. Mol. Cell Biol.* **5**, 739 (2004).
9. R. E. Stenkamp, *Chem. Rev.* **94**, 715 (1994).
10. A. L. Feig, S. J. Lippard, *Chem. Rev.* **94**, 759 (1994).
11. W. E. Walden *et al.*, *Science* **314**, 1903 (2006).
12. D. M. J. Kurtz, *Essays Biochem.* **34**, 85 (1999).

13. Supported by the Intramural Program of the National Institute of Child Health and Human Development.

10.1126/science.1181938

BIOCHEMISTRY

Leaps in Translational Elongation

Electron microscopic and crystallographic studies shed light on key steps in the protein synthesis process in ribosomes.

Anders Liljas

Ribosomes are the sites of protein synthesis in all cells. They are complexes of one or two small and two large RNA molecules and a multitude of proteins and are divided into a small and a large subunit. This complex system, with its many functional steps, cannot be described in a cartoon fashion. Each year, further details of the complexity of protein synthesis emerge. Two Research Articles in this week's issue (*1*, *2*) and two other recent studies (*3*, *4*) shed light on the mechanisms, dynamics, and functions of key elements in the protein synthesis process.

To synthesize new proteins, the ribosome translates the information encoded in messnger RNA (mRNA) into a chain of amino acids. New amino acids are delivered by a transfer RNA (tRNA) called aminoacyl-tRNA to the A site (see the figure, panel A). In the decoding center, the ribosome ensures that the codon (a sequence of three nucleotides that specifies an amino acid) of the mRNA matches the anticodon of the tRNA and that the correct amino acid is thus inserted. Next, the peptidyl-tRNA in the P site donates its growing polypeptide to the amino acid on the tRNA in the A site. The newly formed peptidyl-tRNA is then translocated from the A to the P site. Simultaneously, the empty tRNA in the P site is moved into the exit or E site.

This protein synthesis process would be very inefficient without the catalytic participation of translation factors and without the small molecule guanosine 5′-triphosphate (GTP). Some translation factors are enzymes of the family guanine triphosphatases (GTPases), which bind and hydrolyze GTP to guanosine diphosphate (GDP). The elongation factor Tu (EF-Tu), in complex with GTP and an aminoacyl-tRNA, delivers the tRNA into the A site of the ribosome. Translocation of the newly formed peptidyl-tRNA is catalyzed by elongation factor G (EF-G) in complex with GTP.

During the polypeptide chain elongation cycle, the ribosomal subunits rotate with respect to each other to assist the movement of the tRNAs. This "ratcheting" process (*5*) has so far been studied mainly by single-particle reconstruction with low-temperature electron microscopy (cryo-EM). Cate and co-workers (*3*) recently described the crystallographic details of ratcheting, including intermediate stages. They identified four ribosomal conformations, corresponding to different stages in the translation process. In addition to the rotation of the subunits, the head domain of the small subunit swivels in a coordinated fashion. The contacts between the subunits undergo strain or change during ratcheting.

It has not been possible to study the ribosomal binding of translational GTPases by crystallography, because their binding site was occupied by the L9 protein of a neighboring ribosome in the crystals. Good structural information about ribosome-bound GTPases is available from cryo-EM (*6*–*8*), but the higher

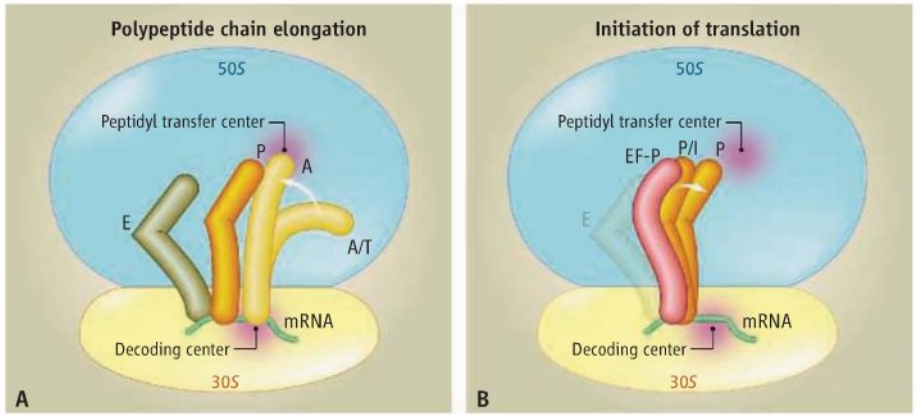

Essential steps in translation. (**A**) The two ribosomal subunits 30S (yellow) and 50S (blue), with the decoding center and the peptidyl transfer center. The mRNA (green) binds to the 30S subunit. Four different positions for tRNA molecules are indicated: The A site binds aminoacyl-tRNA, the P site binds peptidyl-tRNA, and the E site binds exiting tRNA. Schmeing *et al.* (*1*) show that the bent tRNA in the A/T site is bound together with EF-Tu. A movie showing an animation of decoding by the ribosome and EF-Tu is available in Schmeing *et al.* (movie S1) at www.sciencemag.org/cgi/content/full/1179700/DC1. (**B**) The initiator tRNA first binds to the P/I site. Binding of EF-P on the E-site side of the tRNA moves the tRNA to the P site (*4*).

CREDIT: P. HUEY/SCIENCE

Molecular Biophysics, Lund University, Se 79333 Leksand, Sweden. E-mail: anders.liljas@mbfys.lu.se

resolution offered by crystallography has been lacking, hampering efforts to elucidate how GTP hydrolysis is induced. Ramakrishnan and coauthors now report crystallographic studies of EF-Tu (*1*) and EF-G (*2*) bound to the ribosome. These studies became possible only after growing a new form of crystals, in which part of protein L9 was removed.

When the GTPases hydrolyze their bound GTP molecules on the ribosome, they lose their binding conformation. Fortunately, antibiotics can be used to lock the factors into the ribosome-binding conformation. The authors used kirromycin for EF-Tu and fusidic acid for EF-G.

EF-Tu delivers the aminoacyl-tRNA to the ribosome by binding to the binding site for translational GTPases. The new work (*1*) shows that as long as EF-Tu is bound to the ribosome and the tRNA, it bends the tRNA into the A/T site (see the figure, panel A). This is done smoothly, in contrast to earlier models suggesting a kink (*9*). Upon GTP hydrolysis, EF-Tu is released, and the tRNA springs into the A site and places the amino acid in the peptidyl transfer center (see the figure, panel A) (*1*). What induces the GTP hydrolysis remains unclear. The sarcin-ricin loop of the ribosomal 23*S* RNA could be involved, because it is close to the factor-bound GTP and to an EF-Tu residue that is essential for hydrolysis. Ribosomal protein L11 is also at the binding site. The flexible protein L12 has also been implicated but is not seen in this structure.

When EF-G binds to the ribosome (*2*), it pushes the peptidyl-tRNA from the A site into the P site. The conformation of EF-G on the ribosome is different from conformations in crystals of EF-G alone. EF-G is a six-domain protein, with the domains II, III, IV, V, G, and G′. The new work (*2*) shows that domain IV interacts with the anticodon part of the peptidyl-tRNA, rather than with the codon of the A site. The antibiotic fusidic acid is located between the G domain and domain III. The ribosomal components best placed to induce GTP hydrolysis are the sarcin-ricin loop, the L12 stalk (including parts of the 23*S* RNA), and the ribosomal proteins L11 and L10 (the latter with three dimers of L12). The L12 stalk is bent toward EF-G. In addition, one carboxyl-terminal domain of L12 interacts with the G′ domain; a similar interaction has been observed before (*10*).

Like EF-Tu and EF-G, most translation factors interact with the tRNAs on the ribosome. The elongation factor P [EF-P, also called initiation factor 5A (eIF5A) or eIF4D in eukaryotes] is conserved but essentially ignored by the field. Aoki *et al.* have suggested that it stimulates the accommodation of initiator tRNA into the P site and the formation of the first peptide bond (*11*). Steitz and co-workers recently determined the structure of EF-P bound to the ribosome (*4*). In the absence of EF-P, the initiator tRNA binds to a preliminary site, P/I, on the ribosome (*12*) (see the figure, panel B). This site provides the correct interaction with the initiation codon in the P site, but the amino acid of the initiator tRNA is not in the peptidyl transfer site. This may be because there is no tRNA in the E site, nor does a growing polypeptide lock the initiator into the P site. The L-shaped EF-P, mimicking a tRNA (*13*), binds to the E-site side of the initiator tRNA and moves it into the P site (see the figure, panel B) (*4*). Thus, EF-P places the initiator tRNA in the P site to be engaged in the formation of the first peptide bond, as suggested by Aoki *et al.* (*11*).

The two papers from Ramakrishnan and co-workers (*1*, *2*) open the way for crystallographic studies of the range of translational GTPases. Cate and co-workers (*3*) provide better-resolved pictures of the dynamics in the interaction between the subunits and within the small subunit, and Steitz and co-workers (*4*) illuminate the essential functions of a poorly understood translation factor in a step between initiation and elongation. Together, these papers are true milestones in research on translation.

References and Notes

1. T. M. Schmeing *et al.*, *Science* **326**, 688 (2009); published online 15 October 2009 (10.1126/science.1179700).
2. Y. G. Gao *et al.*, *Science* **326**, 694 (2009); published online 15 October 2009 (10.1126/science.1179709).
3. W. Zhang, J. A. Dunkle, J. H. D. Cate, *Science* **325**, 1014 (2009).
4. G. Blaha, R. E. Stanley, T. A. Steitz, *Science* **325**, 966 (2009).
5. J. Frank, R. K. Agrawal, *Nature* **406**, 318 (2000).
6. J. C. Schuette *et al.*, *EMBO J.* **28**, 755 (2009).
7. E. Villa *et al.*, *Proc. Natl. Acad. Sci. U.S.A.* **106**, 1063 (2009).
8. S. R. Connell *et al.*, *Mol. Cell* **25**, 751 (2007).
9. M. Valle *et al.*, *EMBO J.* **21**, 3557 (2002).
10. J. M. Harms *et al.*, *Mol. Cell* **30**, 26 (2008).
11. H. Aoki *et al.*, *FEBS J.* **275**, 671 (2008).
12. G. S. Allen, A. Zavialov, R. Gursky, M. Ehrenberg, J. Frank, *Cell* **121**, 703 (2005).
13. K. Hanawa-Suetsugu *et al.*, *Proc. Natl. Acad. Sci. U.S.A.* **101**, 9595 (2004).

Published online 15 October 2009;
10.1126/science.1181511
Include this information when citing this paper

ECONOMICS

Foundations of Societal Inequality

Daron Acemoglu[1] and James Robinson[2]

The degree to which economic success is passed through generations and the ability of societies to generate wealth depend on their institutions and social arrangements.

Economic and social outcomes, including incomes, poverty, life expectancy, and infant mortality, differ widely between societies. Such inequalities within countries also vary to a great degree. Despite the importance and ubiquity of these differences, their sources are poorly understood and hotly debated. Although we know how the broad patterns of inequality between countries have evolved over the past two centuries (*1*, *2*), most of what we know about within-country inequality comes from contemporary data. On page 682 in this issue, Borgerhoff Mulder *et al.* (*3*) show that wealth inequality in 21 historical and contemporary "small-scale societies" is determined by the intergenerational transmission of different types of assets. What makes the findings important for social science is the link between inequality and institutions that regulate the inheritability of assets.

Wealth inequality in any society reflects not only the differential earnings of the current generation, but also what they have inherited from their parents. The greater the amount of wealth that can be inherited across generations, the greater we expect wealth inequality to be (*4*). The inheritance of wealth is in turn determined by a society's institutions and the nature of its assets. In most modern societies, material assets, such as land or capital, can be passed from parent to offspring with a minimal inheritance tax. But there is considerable variation among societies with similar types of assets and economic systems. Polities from contemporary communist North Korea to the Ottoman Empire limited the inheritability of wealth for most of their citizens. European nations, throughout much of their histories, allowed inheritance only for certain assets and for certain segments of society; for example, serfs in England did not even con-

[1]Department of Economics, Massachusetts Institute of Technology, Cambrige, MA 02142–1347, USA. E-mail: daron@mit.edu [2]Government Department, Harvard University, Boston, MA 02138, USA. E-mail: jrobinson@gov.harvard.edu

trol their human assets and much of the land was under common ownership until the 19th century. In the New World, the economic and social rights of slaves and many indigenous populations were severely restricted. These institutional choices of societies have major consequences both for wealth inequality and economic growth.

Borgerhoff Mulder *et al*. show that in agrarian societies, where institutions enable the intergenerational transmission of material assets such as land and livestock, there is greater inheritability of wealth between generations than in hunter-gatherer societies. They also document interesting patterns in the inheritability of human assets, including human capital (skills) embodied in individuals and social "relational capital" embodied in the network of relationships among the members of the society. Their core finding, concerning the relationship between institutions regulating the inheritability of assets and inequality, is central to understanding the differences in economic and social outcomes across societies. But it also raises several questions: What determines the institutional differences between these societies? Could these differences be due to the underlying nature of assets and the technology of production?

One answer comes from the dominant paradigm on the emergence of agriculture and complex societies—that the Neolithic revolution was a technological breakthrough, resulting from a unique coincidence of environmental conditions that made domestication of plants and animals both feasible and desirable (*5*). This agricultural revolution allowed division of labor both in production and in the social sphere, and led to the emergence of complex societies, other technological breakthroughs, and institutions that protect asset ownership. In this light, differences in institutions (construed broadly as those concerning asset inheritability) between agricultural and hunter-gatherer societies are largely a reflection of their different technologies of production.

An alternative way of interpreting the patterns presented by Borgerhoff Mulder *et al*. is that institutional innovations preceded technological innovations and paved the way for the emergence of agriculture and subsequently of complex societies. In this view, institutions are a powerful and autonomous force, not simply an adaptation to preexisting (or autonomously evolved) technological conditions. They shape—as much as they are shaped by—the technological trajectory of societies. These technologies are key for the generation and distribution of wealth, but they are situated in a context defined by a society's institutions. Institutional factors—in particular, those related to security of property rights and constraints on political power—play a powerful role in shaping technological developments and economic growth (*6*), and account for the ability and willingness of different nations to adopt and develop new technologies and create entrepreneurial dynamism. Such a role explains the strikingly divergent trajectories of modern nations in an age where technology is largely global and is available for those who wish to adopt it. It also explains how income and wealth inequality is so different in the United States, continental Europe, and Latin America.

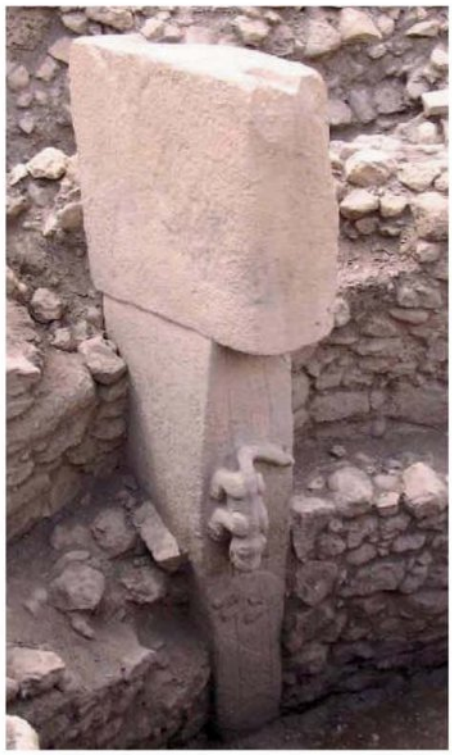

CREDIT: WIKIMEDIA

Institutional innovation. Sites such as Göbekli Tepe, Turkey, suggest that hunter-gatherer societies had evolved institutions to support major public works projects and monumental constructions, and thus had a complex social hierarchy prior to their adoption of farming.

The recognition that institutions play an autonomous role in creating economic inequalities is consistent with evidence that they have also shaped the origins of modern societies. Archaeological studies suggest that rather than being a consequence of the transition from foraging to farming, sedentary life was more likely a prerequisite for it (*7*). For example, in Abu Hureyra in northern Syria on the Euphrates River, Natufian hunter-gatherers formed a sedentary village of around 100 to 300 people at least 500 years before taking up farming around 11,000 years ago (*8*). Perhaps transition to sedentism (and therefore the subsequent transition to farming) was the consequence of institutional innovations. Evidence from sites such as Göbekli Tepe in eastern Turkey (see the figure) suggests that certain hunter-gatherer societies achieved great social complexity and acted collectively to build religious and public works. Such public works likely required a social hierarchy and the ability to mobilize resources—"complex institutions" typically associated with agricultural societies. This conjecture is consistent with extensive evidence of institutional change prior to farming. In Natufian settlements, there was trade for dentalium shells and obsidian, and there were chiefs, political hierarchy, and most likely, considerable inequality—all of this prior to farming (*9*). It is in fact hard to see how such societies could have farmed without preexisting notions of property rights and some hierarchy of authority. It is thus quite possible that societies first underwent major institutional innovations and then subsequently transitioned to agriculture. That institutional variation is not a simple consequence of technology and the nature of assets is also consistent with the results of Borgerhoff Mulder *et al*., which show substantial differences in inheritability of assets and inequality not only between, but also within hunter-gather, horticultural, pastoral, and agricultural societies.

Institutional structures, technologies, and economic outcomes across several societies should be compared, and existing archaeological and anthropological evidence reinterpreted, in light of alternative theoretical frameworks. Such research will further characterize the interplay between institutions, technology, and economic and social outcomes, and the role of institutional innovations in facilitating or laying the foundations of the process that led to agriculture and ultimately to our modern society.

References

1. A. Maddison, *The World Economy: A Millennial Perspective* (Organisation for Economic Cooperation and Development, Paris, 2001).
2. D. Acemoglu, S. Johnson, J. A. Robinson, *Q. J. Econ.* **117**, 1231 (2002).
3. M. Borgerhoff Mulder *et al*., *Science* **326**, 682 (2009).
4. G. S. Becker, N. Tomes, *J. Polit. Econ.* **87**, 1153 (1979).
5. J. Diamond, *Guns, Germs and Steel: The Fate of Human Societies* (Norton, New York, 1997).
6. D. Acemoglu, S. Johnson, J. A. Robinson, in *Handbook of Economic Growth*, P. Aghion, S. Durlauf, Eds. (North-Holland, Amsterdam, 2005), vol. 1A, pp. 386–472.
7. B. D. Smith, *The Emergence of Agriculture* (Scientific American Library, New York, 1998).
8. G. C. Hillman, A. J. Legge, A. M. T. Moore, *Village of the Euphrates: From Foraging to Farming at Abu Hureyra* (Oxford Univ. Press, Oxford, 2000).
9. B. Bender, *World Archaeol.* **10**, 204 (1978).

10.1126/science.1181939

BARNARD LECTURE

As Climate Change Intensifies, McCarthy Urges Adaptation Focus

Scientific assessments of climate change have evolved dramatically over the past three decades, amassing evidence to persuade the world that warming is real and that humans are the primary cause. But greenhouse gas concentrations have continued to soar, and influential climate expert James J. McCarthy says future assessments must focus on how humanity can best adapt.

James J. McCarthy

At the 10th AAAS Robert C. Barnard Environmental Lecture, McCarthy said climate change is already fueling drought and other extreme events that are most keenly felt on a regional scale. The longer emissions remain unchecked, he warned, "the harder adaptation will be, particularly for those parts of the world that are unprepared" for these extreme events.

Strategies such as switching to crops better suited to warmer growing conditions and relocating businesses from areas vulnerable to sea-level rise should be considered immediately, according to a June report by the United States Global Change Research Program. McCarthy, chairman of the AAAS Board, was a member of the report's 31-author team.

"We may reach a point," McCarthy said, "where we're going to be so desperate that we will need to look critically at various geoengineering approaches" such as burying CO_2 in abandoned oil fields and seeding the atmosphere with fine particles to reflect some sunlight back to space.

The annual Barnard Lecture is endowed by the international law firm of Cleary, Gottlieb, Steen & Hamilton to honor Barnard, the late counsel to the firm, for his contributions to environmental and public health law.

McCarthy is the Alexander Agassiz Professor of Biological Oceanography at Harvard University. He has served on several global and regional assessment panels, and he used his talk to trace the evolution of assessments from the 1970s to the upcoming climate summit in Copenhagen. Thousands of scientists worldwide, working under the Intergovernmental Panel on Climate Change (IPCC), issued critical reports in 1990, 1995, 2001, and 2007 that helped move governments to action on climate change, said McCarthy, who was co-chair of a working group for the 2001 report.

But because past goals for greenhouse gas stabilization established by United Nations treaties in Rio de Janeiro and Kyoto have not blunted emissions, "we are headed to dangerous territory at breakneck speed," he warned.

Climate change has been established as unequivocal, McCarthy said, but the next report must assess more directly the regional impacts of climate change and how to cope with them. The most recent IPCC report identified such impacts on every continent. "In every nation," he cautioned, "there will be people who will be vulnerable."

Along with his work on the June report "Global Climate Impacts in the United States," McCarthy was a lead author on the Arctic Climate Impact Assessment in 2004–2005. These regional snapshots, he said, may help politicians and their constituents to grasp the immediate stakes of climate change.

"In different regions they make projections, so that people who have been wondering what's happening with their water or what's happening with their winters or their summers can see that they are consistent with the projections that come from our climate models," he explained.

The U.S. report also underscores the importance of reducing greenhouse emissions and producing and using energy more efficiently. Nations could begin serious mitigation today without further research, McCarthy said. "What is lacking is resolve."

—Earl Lane and Becky Ham

Extreme threat. Researchers say continuing climate change could make severe events such as the August 2009 Station Fire in Southern California more prevalent.

CREDIT: (BOTTOM) COURTESY OF BRENT BUFFINGTON, JPL

ANNUAL MEETING

AAAS Council Reminder

The next meeting of the AAAS Council will take place during the AAAS Annual Meeting and will begin at 9 a.m. on 21 February 2010, in San Diego, California, in the Marina E&F Ballrooms of the San Diego Marriott.

Individuals or organizations wishing to present proposals or resolutions for possible consideration by the council should submit them in written form to AAAS Chief Executive Officer Alan I. Leshner by 27 November 2009. This will allow time for them to be considered by the Committee on Council Affairs at its winter meeting.

Items should be consistent with AAAS's objectives and be appropriate for consideration by the council. Resolutions should be in the traditional format, beginning with "Whereas" statements and ending with "Therefore be it resolved."

Late proposals or resolutions delivered to the AAAS Chief Executive Officer in advance of the February 2010 open hearing of the Committee on Council Affairs will be considered, provided that they deal with urgent matters and are accompanied by a written explanation of why they were not submitted by the November deadline. The Committee on Council Affairs will hold its open hearing at 2:30 p.m. on 20 February 2010 in the Coronado Room of the San Diego Marriott. Summaries of the council meeting agenda will be available during the Annual Meeting at the AAAS information desk and in the AAAS headquarters office in the San Diego Convention Center. A copy of the full agenda will be available for inspection in the headquarters office.

10-GHz Self-Referenced Optical Frequency Comb

Albrecht Bartels,[1]* Dirk Heinecke,[1,2] Scott A. Diddams[2]*

A mode-locked femtosecond laser emits an evenly spaced grid of frequencies that can be phase-coherently linked to a primary frequency standard, that is, to a cesium atomic clock. Such frequency combs can cover the entire visible and near-infrared spectral regions and have become invaluable as precise frequency rulers for modern optical frequency metrology (*1*). However, the teeth of the combs have been too densely spaced (0.1 to 1 GHz) to be spectrally resolved in a straightforward manner and are thus not accessible for individual use. Combs with large mode spacings (i.e., greater than 10 GHz) have required compromises both in terms of bandwidth and average power, resulting in pulses that are too weak and too long in duration for efficient nonlinear spectral broadening. By taking advantage of a combination of laser and fiber optic technology, we overcame these limitations of power and bandwidth to directly make a 10-GHz frequency comb. The result is more than 50,000 modes spanning a wavelength range from 470 to 1130 nm that can be directly resolved with a diffraction grating, a result that should accelerate progress in diverse applications including precision spectroscopy with individual comb teeth (*2*); calibration of high-resolution astronomical spectrographs (*3*, *4*); and synthesis of optical, terahertz, and microwave waveforms via line-by-line pulse shaping (*5*).

Our frequency comb is based on a Ti:sapphire laser with a 30-mm-long ring cavity (Fig. 1) (*6*, *7*). The roundtrip period is only 100 ps, resulting in a repetition rate and thus a frequency comb spacing of $f_R = 10$ GHz. For a femtosecond laser, the 1.2-W average output power is relatively high; however, this translates to a pulse energy of merely 120 pJ at the output and only ~6 nJ circulating inside the cavity. At such low pulse energies, care must be taken to maintain a high peak intensity in the Ti:sapphire crystal in order to support stable pulsed operation via Kerr-lens-mode-locking. We account for this requirement by using tight focusing into the gain crystal and appropriately balancing the intracavity dispersion to support pulses with a duration below 40 fs. The direct output spectrum of the laser (Fig. 1) shows that, for the ~1200 modes within the full width at half maximum, 0.5 mW per individual 10 GHz mode is exceeded, an impressive combination of power and bandwidth among existing frequency comb sources.

Absolute frequency stabilization of the comb requires measurement and control of both the repetition rate (f_R) and the comb's offset frequency (f_0). f_R is easily measured with a fast photodiode, whereas f_0 is measured with a nonlinear f-2f interferometer after spectral broadening of the laser output to more than an octave (*1*). In our case, spectral broadening is achieved in a microstructured fiber with a 1.5-μm core and negative group velocity dispersion at the wavelength of the laser (*7*). A key feature of the fiber is its sealed input, which allows us to achieve coupling efficiency of 50%, yielding more than 500 mW of average power at its output. We achieve spectral coverage from about 470 to 1130 nm (Fig. 1). Common servo techniques are used to phase-lock f_0 and f_R to frequency references that are calibrated by a Cs atomic clock or a more readily accessible representation of the second, for example, a quartz oscillator disciplined by the global positioning system.

Because of the large mode spacing of the comb, a simple grating spectrometer with a resolving power of $\lambda/\Delta\lambda = 6 \times 10^4$ is sufficient to resolve and spatially separate the individual comb elements. Real-color images of the resolved modes were acquired at wavelengths of 490 nm, 540 nm, 583 nm, and 632 nm, through a microscope with a digital camera (Fig. 1). Although the modes at the longest three wavelengths are clearly resolved, we are approaching the resolution limit at 490 nm. Once resolved, the modes are available as precise frequency markers, for example, in astronomic spectrograph calibration. This application should specifically benefit from the wide spectral coverage of our source extending over ~350 THz at a power level exceeding 1 nW per mode, a performance currently unachievable with existing mode-filtering approaches. Selection of individual modes via simple spatial filters or even manipulation in amplitude and phase by use of spatial light modulators is straightforward and can provide a freely programmable array of precisely defined light sources with an inherently high degree of mutual coherence. Such a device would be highly valuable for spectroscopy or Fourier synthesis of arbitrary waveforms via linear superposition and nonlinear mixing and frequency conversion.

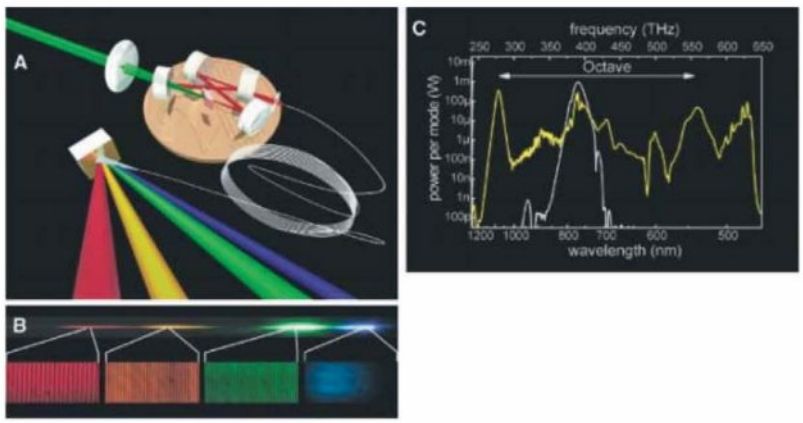

Fig. 1. (**A**) Illustration of the 10-GHz laser cavity. A 0.02-€ coin is shown for size comparison. The nonlinear fiber and diffraction grating dispersing the white light are also illustrated. (**B**) Real-color image of the spectrally dispersed visible part of the continuum and a magnified view of the individually resolved frequency comb modes at wavelengths of 490 nm, 540 nm, 583 nm, and 632 nm. (**C**) Low-resolution measurements of the direct laser output spectrum (gray line) and quasi-continuum output after broadening in nonlinear fiber (yellow line) on a power-per-mode scale.

References and Notes

1. Th. Udem, R. Holzwarth, T. W. Hänsch, *Nature* **416**, 233 (2002).
2. M. C. Stowe *et al.*, in *Advances in Atomic, Molecular and Optical Physics*, E. Arimondo, P. Berman, Eds. (Elsevier, London, 2007), vol. 55.
3. C.-H. Li *et al.*, *Nature* **452**, 610 (2008).
4. T. Steinmetz *et al.*, *Science* **321**, 1335 (2008).
5. Z. Jiang, C. B. Huang, D. E. Leaird, A. M. Weiner, *Nat. Photonics* **1**, 463 (2007).
6. A. Bartels, D. Heinecke, S. A. Diddams, *Opt. Lett.* **33**, 1905 (2008).
7. Materials and methods are available as supporting material on *Science* Online.

8. We thank T. Fortier and C. Oates for thoughtful comments on this manuscript. A.B. is chief executive officer and partial owner of Gigaoptics GmbH. NIST and Gigaoptics hold patents (6,618,423 and 6,850,543) relating to some of the technologies used in the present submission. This work is supported by the Center for Applied Photonics at the University of Konstanz and NIST.

Supporting Online Material

www.sciencemag.org/cgi/content/full/326/5953/681/DC1
Materials and Methods
SOM Text
Fig. S1
References and Notes

14 July 2009; accepted 10 September 2009
10.1126/science.1179112

[1]Center for Applied Photonics, University of Konstanz, Universitätsstraße 10, 78457 Konstanz, Germany. [2]National Institute of Standards and Technology (NIST), 325 Broadway Mail Stop 847, Boulder, CO 80305, USA.

*To whom correspondence should be addressed. E-mail: albrecht.bartels@uni-konstanz.de (A.B.); scott.diddams@nist.gov (S.A.D.)

Intergenerational Wealth Transmission and the Dynamics of Inequality in Small-Scale Societies

Monique Borgerhoff Mulder,[1*†] Samuel Bowles,[2*] Tom Hertz,[3*] Adrian Bell,[4] Jan Beise,[5] Greg Clark,[6] Ila Fazzio,[7] Michael Gurven,[8] Kim Hill,[9] Paul L. Hooper,[10] William Irons,[11] Hillard Kaplan,[12] Donna Leonetti,[13] Bobbi Low,[14] Frank Marlowe,[15] Richard McElreath,[16] Suresh Naidu,[17] David Nolin,[18] Patrizio Piraino,[19] Rob Quinlan,[20] Eric Schniter,[21] Rebecca Sear,[22] Mary Shenk,[23] Eric Alden Smith,[24] Christopher von Rueden,[25] Polly Wiessner[26]

Small-scale human societies range from foraging bands with a strong egalitarian ethos to more economically stratified agrarian and pastoral societies. We explain this variation in inequality using a dynamic model in which a population's long-run steady-state level of inequality depends on the extent to which its most important forms of wealth are transmitted within families across generations. We estimate the degree of intergenerational transmission of three different types of wealth (material, embodied, and relational), as well as the extent of wealth inequality in 21 historical and contemporary populations. We show that intergenerational transmission of wealth and wealth inequality are substantial among pastoral and small-scale agricultural societies (on a par with or even exceeding the most unequal modern industrial economies) but are limited among horticultural and foraging peoples (equivalent to the most egalitarian of modern industrial populations). Differences in the technology by which a people derive their livelihood and in the institutions and norms making up the economic system jointly contribute to this pattern.

Investigations of the dynamics of economic inequality across distinct economic systems have been limited by the paucity of data on all but contemporary market-based industrial societies. They are also hampered by the lack of an empirically based model applicable to the differing institutions and technologies characteristic of the broad range of economic systems, ranging from hunter-gatherers through pastoral and agrarian societies to modern economies. Here we present empirical estimates of the extent of inheritance of wealth across generations and of the degree of wealth inequality, along with a descriptive model of the relation between the two. We support our model with data on three distinct wealth classes—material, embodied, and relational, to be defined below—in 21 contemporary and recent hunter-gatherer, horticultural, pastoral, and agricultural populations.

The key thesis to be explored is that for some kinds of wealth and some economic systems (but not others) the parents' wealth strongly predicts the wealth of the offspring. In particular, the cattle, land and other types of material wealth of pastoral and agricultural economies are directly transmitted by simple transfers, often buttressed by social conventions of inheritance. By contrast the somatic wealth and skills and the social network ties central to foraging and horticultural livelihoods are more subject to the vagaries of learning, genetic recombination, and childhood development. Moreover, in foraging and horticultural economies, such material wealth as exists tends to circulate through broad social networks rather than being vertically transmitted to offspring. A corollary of the thesis is that, if our model is correct, economies in which material wealth is important will show substantial levels of wealth inequality.

Both the thesis and the corollary find strong support in our data. We focus on small-scale societies because they offer the greatest variation in both the technologies by which a livelihood is gained and the basic institutions that provide the incentives and constraints regulating economic life, including the dynamics of inequality and the inheritance process. (We use the term "small-scale" to refer to populations in which the influence of modern national states is limited). These societies thus provide the most powerful lens for exploring hypotheses concerning the importance of technologies (kinds of wealth) and institutions (kinds of society) in explaining the dynamics of inequality and, thus, may also illuminate long-term trends in contemporary and future economies.

The connection between wealth inheritance and wealth inequality (explained more precisely in the model below) is the following: If wealth is strongly transmitted across generations, chance shocks to the economic fortunes of a household due to disease or accident, luck in a hunt or harvest, and other environmental disturbances or windfalls will be reproduced in the next generation. These effects will thus accumulate over time and thereby counteract the widely observed inequality-dampening tendency of regression to the mean (*1*–*3*). We seek to understand the effects of this process by examining how the offsetting effects of random shocks and imperfect transmission across generations jointly determine a steady-state distribution of wealth for differing kinds of wealth and across the four different economic systems (*4*). The institutions and norms that characterize distinct economic systems and the nature of the wealth class alike will affect the degree of intergenerational transmission. The extent of shocks will also differ across wealth classes and economic systems.

For a number of modern economies, there are quantitative estimates and comparisons of the intergenerational transmission of education, occupational prestige, nonhuman physical capital, and other forms of embodied and material wealth (*3*, *5*, *6*). For small-scale populations, associations between reproductive success and material forms of wealth have been studied (*7*), and there exist piecemeal estimates of intergenerational transmission of, for example, fertility (*8*) and height (*9*). But there are no estimates allowing a comparison across populations of the inheritance of the distinctive kinds of wealth that are central to the livelihoods of small-scale communities of foragers, horticulturalists, herders, and farmers. Here we present a new set of data and conduct a quantitative comparative analysis of the transmission of distinct types of wealth among the 21 populations shown in Fig.1 and Table 1. Further information is provided in (*4*).

[1]Department of Anthropology and Center for Population Biology, University of California, Davis, CA 95616, USA. [2]Santa Fe Institute and University of Siena, Santa Fe, NM 87501, USA. [3]International University College of Turin, 10121 Turin, Italy. [4]Graduate Group in Ecology, University of California, Davis, CA 95616, USA. [5]Department of Economic and Social Affairs, United Nations, New York, NY 10017, USA. [6]Department of Economics, University of California, Davis, CA 95616, USA. [7]Center for Economic Performance, London School of Economics, London WC2A 2AE, UK. [8]Integrative Anthropological Sciences Program, University of California, Santa Barbara, CA 93106, USA. [9]School of Human Evolution and Social Change, Arizona State University, Tempe, AZ 85281, USA. [10]Department of Anthropology, University of New Mexico, Albuquerque, NM 87131, USA. [11]Department of Anthropology, Northwestern University, Evanston, IL 60208, USA. [12]Department of Anthropology, University of New Mexico, Albuquerque, NM 87131, USA. [13]Department of Anthropology, University of Washington, Seattle WA 98195, USA. [14]School of Natural Resources and Environment, University of Michigan, Ann Arbor, MI 48109, USA. [15]Department of Anthropology, Florida State University, Tallahassee, FL 32306, USA. [16]Department of Anthropology and Center for Population Biology, University of California, Davis, CA 95616, USA. [17]Harvard Academy for International Studies, Harvard University, Cambridge, MA 02138, USA. [18]Carolina Population Center, University of North Carolina, Chapel Hill, NC 27516, USA. [19]100 Tunney's Pasture Driveway, Ottawa, ON K1A 0T6, Canada. [20]Department of Anthropology, Washington State University, Pullman, WA 99164, USA. [21]Integrative Anthropological Sciences Program, University of California, Santa Barbara, CA 93106, USA. [22]Department of Social Policy, London School of Economics, London WC2A 2AE, UK. [23]Department of Anthropology, University of Missouri, Columbia, MO 65211, USA. [24]Department of Anthropology, University of Washington, Seattle, WA 98195, USA. [25]Integrative Anthropological Sciences Program, University of California, Santa Barbara, CA 93106, USA. [26]Department of Anthropology, University of Utah, Salt Lake City, UT 84112, USA.

*The first three authors contributed equally to this article. †To whom correspondence should be addressed. E-mail: mborgerhoffmulder@ucdavis.edu

The dynamics of wealth inequality. To clarify our model, we initially consider just a single type of wealth and show that the degree of inequality in its steady-state distribution depends on the extent to which wealth is transmitted across generations. Suppose that a household's wealth is acquired in two ways. The first is transmission directly from the parents, in the form of material bequests, clients, skills, private information, genotype, conditions affecting development, network connections, and so on. The second way of acquiring wealth is from the resources available to all members of the population, in the form, say, of equal access to common resources or public information.

We summarize these two influences on a household's wealth by expressing the expected wealth of household i as $\beta w_{ip} + (1 - \beta)\underline{w}$, where wealth is measured in natural logarithms, w_{ip} is the wealth level of household i's parents, and $\underline{w}$ is the population-average wealth level (normalized to be the same across generations). The intergenerational transmission coefficient, β ($0 \leq \beta < 1$), measures the extent to which the wealth of a household in one generation depends on the wealth in the previous generation, and $(1 - \beta)$ represents regression to the mean as introduced by Galton in his study of human stature (*10*).

In each generation, the realized wealth of a household is its expected wealth (above) plus a disturbance term, λ, reflecting exogenous shocks that over time are assumed to be independent of the wealth of previous generations, with mean zero and variance σ_λ^2:

$$w_i = \beta w_{ip} + (1 - \beta)\underline{w} + \lambda_i \qquad (1)$$

We are interested in the variance of the logarithm of a population's wealth (a standard unit-free measure of inequality) in the long run. To determine this, we use Eq. (1) to write the variance of wealth in generation t as:

$$\mathrm{var}(w_{it}) \equiv \mu_t = \beta^2 \mu_{t-1} + \sigma_\lambda^2 \qquad (2)$$

where μ_{t-1} is the variance of the logarithm of wealth in the parental generation. We then solve for μ, the steady-state (stationary, or long run) variance of the logarithm of wealth, by setting $\mu_{t-1} = \mu_t = \mu$, giving:

$$\mathrm{var}(w_i) \equiv \mu = \sigma_\lambda^2/(1 - \beta^2) \qquad (3)$$

This steady-state level of wealth inequality may be interpreted as the effect of stochastic shocks (the numerator), blown up by the intergenerational transmission multiplier, $(1 - \beta^2)^{-1}$, which is increasing in β, the extent of intergenerational transmission of wealth. As β approaches one, the effects of windfalls of wealth, accidents of health, theft, and the like, dissipate more slowly over time so that the shocks of even the distant past contribute to inequality in a given generation, resulting in high levels of steady-state inequality. For $\beta > 1$, there is no steady state, and inequality will increase over time. The determination of this steady state is illustrated in Fig. 2.

A population exposed to greater wealth shocks is represented by a larger intercept on the vertical axis (σ_λ^2), whereas greater intergenerational transmission of wealth is represented by a steeper solid line [the slope of which is β^2, see Eq. (2)]. To use this model, we need not assume that the steady-state wealth distribution is typically attained. What is important for our approach is that, for a given society, the fluctuations around the steady-state value are small relative to the differences in steady-state inequality across societies characterized by different economic systems and different kinds of wealth.

By a household's wealth, we mean any of its attributes that contribute to its well-being as measured by consumption levels, social status, or other ends that are valued in the particular society. To take account of many kinds of wealth simultaneously, we define the importance of each class of wealth as follows. Let E, M, and R be positive numbers representing the amount of a household's embodied, material and relational wealth. The well-being of the household, W, is a weighted product of these classes of wealth, the weights being the relative importance of each wealth class in the economic system in which the household lives:

$$W = \gamma E^e M^m R^r \qquad (4)$$

where γ is a positive constant and the exponents e, m, and r (the weights) are the derivatives of the logarithm of well-being with respect to the logarithms of the three respective wealth classes or, equivalently, the percent difference in well-being associated with a 1% difference in the amount of each class of wealth. The weighted product is preferred (to the weighted sum, for example) because it implies, plausibly, that the wealth classes are complements; that is, the contribution of each class of wealth to individual well-being is enhanced by the extent of the other classes of wealth.

We assume constant returns to scale (doubling the amount of all three classes of wealth of a household will double its well-being) implying that $e + m + r = 1$. This motivates our interpretation of these exponents as weights indicating the relative importance of each class of wealth. We refer to these weights as $\alpha \equiv \{e, m, r\}$. To combine this information on the importance of wealth classes with our measures of the extent of transmission of each wealth class across generations, we estimate an α-weighted average β for each economic system. We also calculate an α-weighted average measure of wealth inequality (the Gini coefficient) for each economic system (see below).

Ideally, one would have comparable measures of the relative importance (α) and degree of transmission (β) of each class of wealth, the degree of inequality in the distribution of each kind of wealth (Gini), and the extent of wealth shocks (σ_λ^2). Measuring the last-mentioned is difficult in any economy and impossible in the economies under study, as the estimate requires long time-

Fig. 1. Populations studied. Note: Circle indicates hunter-gatherers; star, horticulturalists; square, pastoralists; and triangle, agriculturalists.

series data for individual wealth, which, with few exceptions, are simply nonexistent. We are able, however, to measure the other three quantities, and this permits us to gauge the extent to which intergenerational wealth transmission allows the effect of shocks to accumulate over time, and to explore differences in both intergenerational wealth transmission and wealth inequality across economic systems and wealth classes.

The nature of wealth and the varieties of economic systems. Since the development of human capital theory a half-century ago, it has been conventional to treat wealth as a multidimensional attribute, as evidenced by the adjectives now routinely applied to the word "capital," namely, social, somatic, material, cultural, and network (*11*–*13*). We identified three broad classes of wealth in our populations, namely, embodied

Table 1. Population characteristics and estimates of the intergenerational transmission of 43 measures of embodied, relational, and material wealth across 5 hunter-gatherer, 4 horticultural, 4 pastoral and 8 agricultural populations. For wealth type, the number of parent-child pairs is in parentheses. β ± SE.

Economic system and population	Wealth type	Wealth class	β	General description (ref.)
Hunter-gatherer				
Ache	Hunting returns (49)	E	0.081 ± 0.273	Mobile foragers (Paraguay 1982–2008) (*30*)
Ache	Body weight (137)	E	0.509 ± 0.128	
Hadza	Body weight (227)	E	0.305 ± 0.076	Mobile foragers (Tanzania 1982–2008) (*31*)
Hadza	Grip strength (196)	E	−0.044 ± 0.050	
Hadza	Foraging returns (33)	E	0.047 ± 0.193	
Ju/'hoansi	Exchange partners (26)	R	0.208 ± 0.114	Mobile foragers (Botswana 1973–75) (*32*)
Lamalera	Quality of housing (121)	M	0.218 ± 0.099	Sedentary fishers, trade, and some farming (Indonesia 2006) (*33*)
Lamalera	Boat shares (121)	M	0.122 ± 0.093	
Lamalera	Food share partners (119)	R	0.251 ± 0.052	
Lamalera	Reproductive success (121)	E	0.161 ± 0.174	
Meriam	Reproductive success (91)	E	0.088 ± 0.247	Sedentary fishers, some farming (Australia 1998) (*34*)
Horticultural				
Dominicans	Land (62)	M	0.137 ± 0.140	Subsistence farming, fishing, bay oil production, limited wages (Dominica 2000–08) (*35*)
Gambians	Body weight (1274)	E	0.391 ± 0.041	Subsistence rice and cash farmers (Gambia 1950–80) (*36*)
Gambians	Reproductive success (967)	E	0.088 ± 0.086	
Pimbwe	House/farm utensils (283)	M	0.107 ± 0.318	Subsistence farming, some cash farming, some foraging (Tanzania 1995–2006) (*37*)
Pimbwe	Farming skill (217)	E	−0.015 ± 0.097	
Pimbwe	Body weight (148)	E	0.377 ± 0.096	
Pimbwe	Reproductive success (599)	E	−0.057 ± 0.107	
Tsimane	Household utensils (110)	M	0.024 ± 0.071	Subsistence farming, some foraging (Bolivia 2002–08) (*38*)
Tsimane	Labor cooperation (67)	R	0.181 ± 0.106	
Tsimane	Allies in conflict (45)	R	0.338 ± 0.103	
Tsimane	Knowledge/skill (181)	E	0.111 ± 0.094	
Tsimane	Grip strength (490)	E	0.070 ± 0.042	
Tsimane	Body weight (383)	E	0.253 ± 0.069	
Tsimane	Hunting returns (26)	E	0.384 ± 0.130	
Tsimane	Reproductive success (849)	E	0.128 ± 0.073	
Pastoral				
Datoga	Livestock (135)	M	0.622 ± 0.127	Transhumant pastoralism, some farming (Tanzania 1987–89) (*39*)
Datoga	Reproductive success (133)	E	0.066 ± 0.060	
Juhaina Arabs	Camels (21)	M	0.535 ± 0.226	Transhumant pastoralism (Chad 2003) (*40*)
Sangu (Ukwaheri)	Cattle (108)	M	0.957 ± 0.424	Pastoralism, some farming (Tanzania 1997–2000) (*41*)
Yomut (Charwa)	Patrimony (livestock) (22)	M	0.564 ± 0.167	Transhumant pastoralism, some farming (Turkmenistan/Iran 1965–74) (*42*)
Agricultural				
Bengali	Reproductive success (382)	E	−0.074 ± 0.057	Farmers with wage labor (India 2000–01) (*43*)
Bengaluru	In-law networks (249)	R	0.114 ± 0.073	Farmers, merchants, wage labor, urban (India 1910–1973) (*44*)
East Anglians	Estate value (land) (210)	M	0.642 ± 0.073	Farmers, wage labor, merchants; rural and urban (England 1540–1845) (*45*)
East Anglians	Reproductive success (200)	E	0.171 ± 0.150	
Khasi	Reproductive success (650)	E	0.165 ± 0.045	Farmers with wage labor (India 2000–01) (*43*)
Kipsigis	Land (270)	M	0.357 ± 0.041	Farmers with livestock (Kenya 1981–1990) (*46*)
Kipsigis	Livestock (270)	M	0.635 ± 0.098	
Kipsigis	Cattle partners (102)	R	0.041 ± 0.139	
Kipsigis	Reproductive success (270)	E	0.213 ± 0.106	
Krummhörn	Land (1602)	M	0.610 ± 0.043	Farmers with diverse off-farm occupations (German 17th to 19th century) (*47*)
Skellefteå	Reproductive success (2515)	E	0.010 ± 0.028	Farmers with diverse off-farm occupations (Sweden 1800–88) (*48*)
Yomut (Chomur)	Patrimony (land) (58)	M	0.528 ± 0.147	Farmers with livestock (Turkmenistan/Iran 1965–74) (*42*)

(body weight, grip strength, practical skills, and, in predemographic transition populations, reproductive success); material (land, livestock, and household goods); and relational (social ties in food-sharing networks and other forms of assistance). We have no measures of other heritable determinants of well-being such as ritual knowledge, an important source of institutionalized inequality in some populations. By linking the level of wealth of parents and adult offspring, measured as appropriate for individuals (e.g., body weight) or households (e.g., land), we are able to estimate the degree of intergenerational persistence for particular types of wealth and then to create averages for each broad class of wealth.

We classify economic systems according to the conventions of anthropology (*14*). Hunter-gatherer economic systems are those that make minimal use of domesticated species (either plant or animal), whereas pastoralists rely heavily, though rarely exclusively, on livestock kept for subsistence and sometimes commercial purposes. Although both horticulturalists and agriculturalists use domesticated plants and animals, horticulturalists do not typically use ploughs, their cultivation is labor- not land-limited, and land markets are absent or limited. As with all classificatory systems, there are some ambiguities of assignment of our populations to these classes, but the least improbable reclassifications do not affect our results [see (*4*), section 4].

Transmission of wealth across generations need not take the form of bequests, or the literal passing on of physical objects (such as when land is transmitted from father to son). What matters for the long-run dynamics of inequality is anything that results in a statistical association between the wealth of parents and children. This statistical association may be enhanced by positive assortment in mating or in economic pursuits as occurs when skilled hunters pursue prey together, or when successful herders cooperate in livestock management. The same is true of increasing returns or other forms of positive feedbacks, for example when those who invest a substantial amount earn higher than average returns, or when childhood developmental effects associated with modest genotypic differences result in substantial phenotypic differences. Negative feedbacks, such as sharing norms that extract substantial transfers from the wealthy, or wealth shocks that are inversely correlated with one's wealth (such as occur when cattle thieves target large herds), by contrast, heighten regression to the mean by reducing β, thereby attenuating the persistence of inequality over time and hence reducing steady-state inequality.

Our three wealth classes differ in the extent to which these transmission mechanisms—transfers, assortment, and positive feedbacks in development or accumulation—are at work. Material wealth is readily transferred to the next generation by bequests sanctioned by cultural rules. Moreover, because it is typically observable, material wealth can facilitate deliberate marital or economic assortment. For some types of material wealth (storage facilities, herds of livestock, and irrigated land, for example), the correlation of material wealth levels across generations is further enhanced by the presence of increasing returns to scale or other positive feedbacks. Network ties can easily be passed from parent to child, but the offspring of less well-connected parents can usually gain access to allies and helpers more readily than a landless son in a farming community can acquire land, for example, through savings or systems of patronage. As a result we expect the intergenerational transmission of relational wealth to be limited, at least by comparison with material wealth.

Embodied wealth is transmitted by a combination of genetic inheritance, socialization, and parent-offspring similarity in the conditions affecting childhood development. The knowledge component of embodied wealth is readily transmitted to offspring, but, unless restricted by religious or other constraints, it is typically available to other members of a population as well (the common knowledge of the behavior of prey species, for example, or farming practices). Genetic and psychometric evidence from industrial societies suggests that parent-offspring transmission of economically relevant personality and behavioral characteristics, such as risk-taking, trustworthiness, conscientiousness, and extroversion is limited (*4*). We do not have similar evidence across generations in the small-scale populations under study, but industrial-society estimates support our expectation that the degree of intergenerational transmission will differ markedly among our three wealth classes, with substantial transmission of material wealth and more limited transmission of relational and embodied wealth.

Ethnographic evidence suggests that the four economic systems also differ in the importance of

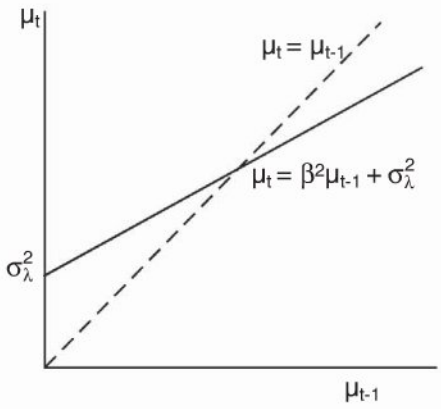

Fig. 2. Steady-state wealth distribution. The dashed line is the steady-state condition requiring wealth inequality to be unchanging from one period to the next. The solid line (Eq. 2) is the combined effect of this period's variance of shocks (the constant) augmented by the inequalities in wealth transmitted from the previous period (the slope).

Table 2. Summary statistics: Intergenerational transmission of wealth (β), by economic system and wealth class. Cell-means were estimated in a regression against a full set of dummy variables for each cell, with conventional standard errors. See (*4*), section 1, for a discussion of alternative approaches to estimating these cell-means and their standard errors, and tables S11 and S12 for the alternative results. Reported *P* values correspond to two-tailed tests of the hypothesis that the true β or Gini coefficient is zero for that cell. Averages across wealth classes (final two columns) are calculated after weighting the cell-mean β values and Ginis by the values of α shown. NA, data not available.

Economic systems		Wealth classes			α-weighted average of β values	α-weighted average of Ginis
		Embodied	Relational	Material		
Hunter-gatherer	α	0.46	0.39	0.15		
	β	0.16 ± 0.06	0.23 ± 0.11	0.17 ± 0.011	0.19 ± 0.05	0.25 ± 0.04
	P	0.01	0.04	0.12	0.00	0.00
Horticultural	α	0.53	0.26	0.21		
	β	0.17 ± 0.05	0.26 ± 0.11	0.09 ± 0.09	0.18 ± 0.04	0.27 ± 0.03
	P	0.00	0.02	0.31	0.00	0.00
Pastoral	α	0.26	0.14	0.61		
	β	0.07 ± 0.15	NA†	0.67 ± 0.07	0.43 ± 0.06†	0.42 ± 0.05†
	P	0.66		0.00	0.00	0.00
Agricultural	α	0.27	0.14	0.59		
	β	0.10 ± 0.07	0.08 ± 0.11	0.55 ± 0.07	0.36 ± 0.05	0.48 ± 0.04
	P	0.16	0.47	0.00	0.00	0.00
Average across all economic systems	α	0.38	0.23	0.39		
	β	0.12 ± 0.05	0.19 ± 0.06	0.37 ± 0.04	0.29 ± 0.03	0.35 ± 0.02
	P	0.01	0.00	0.00	0.00	0.00

†The β and Gini for Kipsigis cattle partners (see Table 1 and table S4) are used in the pastoral/relational cell for the calculation of the α-weighted average across wealth classes.

the three classes of wealth. A successful hunter-gatherer or horticulturalist depends heavily on his or her strength, practical knowledge, and social networks, while making little use of material resources that are not in the public domain. By contrast, the well-being of a herder or farmer is closely tied to the amount of stock or land under his or her command, which makes material wealth a more important influence on livelihoods in these economic systems.

Estimating the intergenerational transmission of wealth. To estimate our model of wealth transmission, we need two pieces of information: the degree of intergenerational transmission (β) for each wealth type and the importance of each wealth class in a given economic system ($\alpha \equiv \{e, m, r\}$). Note that we do not require identification of the causal paths by which transmission takes place, as might be represented in a multiequation structural model (*15*). Our model instead requires a single estimate of the magnitude of the statistical association between parental and offspring wealth (β) for each data set. This requirement, along with the absence of robust evidence of nonlinearities, motivated our consistent use of linear models. Functional forms, estimation procedures, robustness checks, weighting procedures, and other aspects of our statistical techniques and results are described in (*4*), section 1. Note that the populations studied were not selected at random; instead, we included all populations we were aware of for which intergenerational wealth transmission estimates are feasible and the researchers agreed to share data. Table 1 presents our individual estimates of β; Table 2 presents the summary statistics for both the intergenerational transmission (β) and the importance (α) of the three wealth classes in the four economic systems.

Across the four economic systems, the estimated β for 14 measures of material wealth, including agricultural and horticultural land, livestock, shares in sea mammal–hunting boats, quality of housing, and household utensils averages 0.37 (Table 2). For farm land (5 data points), the degree of transmission is substantial, averaging 0.45 (calculated from the data in Table 1), thus equaling or exceeding the intergenerational transmission of most forms of wealth in modern industrial economies (*16*). Livestock are even more highly transmitted across generations (Table 1, β values averaging 0.66).

Our 23 estimates of the transmission of embodied wealth across generations average 0.12. The highest estimates are for body weight (for which β averages 0.37). We also find a very modest level of intergenerational transmission of reproductive success (number of offspring surviving to age 5); it is entirely absent in three societies, has a maximum value of 0.21, and averages 0.09, similar to low correlations between parental and offspring fertility in many pre-demographic transition populations (*17*). Grip strength is weakly transmitted across generations. The transmission of hunting success is highly variable (0.08 for the Ache, 0.38 for the horticultural Tsimane, and 0.05 for hunting and foraging yields in the Hadza), averaging 0.17. Knowledge and skill, such as the production and management of horticultural crops in the Pimbwe or proficiency in subsistence tasks and cultural knowledge in the Tsimane, are only weakly transmitted from parents to offspring.

The six estimates of relational wealth transmission indicate that the extent to which network links are transmitted across generations is modest, averaging $\beta = 0.19$.

To measure the importance of each wealth class in the four economic systems (α) we used ethnographers' judgments (for each wealth class in the population they studied) of the percentage difference in household well-being associated with a 1% difference in the amount of a given wealth class, holding other wealth classes constant at the average for that population, and requiring these percentage effects to sum to one. The average values of α by wealth class and economic system also appear in Table 2. Consistent with descriptive ethnographies of these and other populations, embodied and relational wealth are relatively important for hunter-gatherers, whereas material wealth is key in pastoral and agricultural populations.

Statistical estimates of the importance of each class of wealth across the economic systems (α) would have been preferable, but are precluded by the absence for most populations of a single relatively homogeneous measure of well-being. However, we were able to econometrically estimate *m*—the importance of material wealth—from an equation similar to (4) using data (most of it from half a century ago) from populations not represented in our study, including one horticultural, two pastoral, and seven small-scale agricultural economies. These estimates [see (*4*) section 1] are close to our ethnographers' estimates and suggest that, if anything, we have understated the difference in the importance of material wealth between pastoral and agricultural economies, on the one hand, and horticultural economies on the other. Correcting this understatement would only strengthen our main conclusions.

Results. Our first finding is that the α-weighted averages of the β values (the importance-weighted average transmission coefficients) for the four economic systems differ markedly (Table 2). Intergenerational transmission of wealth is modest in hunter-gatherer and horticultural systems and substantial in agricultural and pastoral systems. However, even the smaller β values of the former imply that being born into the top 10% of the wealth distribution confers important advantages. In these societies, a child of parents in the highest wealth decile is on average more than three times as likely to end up in the top decile as is the child of the bottom decile [(*4*), section 3 and table S7]. Although hardly a level playing field, intergenerational transmission in these economic systems is modest when compared with the agricultural systems, where the child of the top decile is on average about 11 times more likely than the child of the poorest decile to end up in the richest decile, or to the pastoral systems, where the ratio exceeds 20.

Our second finding is that economic systems in which wealth is more heritable are indeed more unequal, as predicted by our model. For each population and type of wealth, we estimated the Gini coefficient, which is a measure of inequality ranging from 0 (equal wealth) to approximately 1 [all wealth held by a single household, see table S4 and discussion in (*4*), section 1]. To calculate an overall measure of wealth inequality for a given economic system we again weight the results for each wealth class in that system by its importance (α). These estimates of overall wealth inequality appear in the last column of Table 2, and in more detail in table S5. They exhibit the same pattern as the transmission coefficients (β values): hunter-gatherer and horticultural populations are both relatively egalitarian; pastoral and agricultural societies are characterized by substantial wealth inequality (see also fig. S2).

A third finding is that neither the overall intergenerational transmission of wealth nor the level of inequality is greater in horticultural than in hunter-gatherer populations. This result challenges a long-standing view (*18*) that foragers are uniquely egalitarian among human societies. Thus, it may be ownership rights in land and livestock, rather than the use of domesticated plants and animals per se, that are key to sustaining high levels of inequality. Our finding that pastoralists transmit wealth across generations to an extent equal to if not greater than farmers, and likewise display similar Gini coefficients, will also challenge widely held views that herders are relatively egalitarian (*19*).

Are the relative intergenerational mobility of the hunter-gatherer and horticultural systems and the high levels of intergenerational wealth transmission of the pastoral and agricultural systems due primarily to technology (the differing importance of the distinct classes of wealth across economic systems) or to institutions (differences in intergenerational transmission, independent of differences in the importance of the wealth classes)? To answer this question, we take advantage of the fact that both the importance of the wealth classes and degree of intergenerational transmission of wealth are similar in the hunter-gatherer and horticultural populations, on the one hand, and the pastoral and agricultural populations on the other. This allows us to reduce the four systems to two. Forty-five percent of the large (namely 0.21) and statistically significant difference ($P < 0.001$) between the average α-weighted β values of these two groups of economic systems is accounted for by differences in technology, reflected primarily in the greater importance of material wealth in producing the herders' and farmers' livelihoods [for the decomposition formula, see (*4*) section 1; for the paired economic systems results, see table S3]. The remaining 55% is due to differences in institutions, reflected primarily in the lesser degree of transmission of material wealth in the

horticultural and hunter-gatherer populations. Thus, although differences across economic systems in both the importance of the wealth classes and in the heritability of a given class of wealth matter, the latter is somewhat more strongly associated with differences in the extent of wealth transmission across generations, and hence the generation of inequality. This is our fourth finding.

Note that for the intergenerational transmission of wealth, the effects of technology and institutions are complementary rather than simply additive. Econometric analysis (table S13, column 2) shows that this joint (superadditive) effect of material wealth and agricultural or pastoral economic systems in the intergenerational transmission of wealth is statistically robust, even when a fixed-effects regression is used to control for all unobserved population-level characteristics (such as the distinct inheritance and marital systems and other institutional structures of the populations).

Not surprisingly in light of our fourth finding, additional econometric analysis [described in section 5 of (*4*)] shows that both wealth class and economic system significantly and independently predict the level of wealth inequality: material wealth types, and pastoral and agricultural societies, display higher Gini coefficients (table S13, column 3). Moreover, the greater inequality in material wealth is robust to the inclusion of fixed effects to control for unobservable population-level variation (table S13, column 4).

A final finding is that, in the populations studied, the more important forms of wealth are more highly transmitted across generations: The simple correlation between the 43 β values listed in Table 1 and the corresponding population and wealth-class specific α values listed in table S1 is 0.48 ($P = 0.001$). This is consistent with the view that parents differentially transmit to their offspring the forms of wealth that are most important in that society (*20*). This is most striking in the case of material wealth. In pastoral and agricultural societies, its average importance (α) is 0.60 and the average transmission coefficient (β) is 0.61; in hunter-gatherer and horticultural populations, the values, respectively, are 0.18 and 0.13 (calculated from Table 2, and see tables S2 and S4). Similarly, the less important forms of wealth in agricultural and pastoral systems (embodied and relational wealth) display significantly lower β values.

We implemented two robustness checks to make sure, first, that our results are not driven merely by the qualitative estimates of α provided by the ethnographers and, second, that these estimates are themselves plausible. The first is the above decomposition of the effects of economic system and wealth class, which shows that a substantial difference (more than half of that estimated) between economic systems in aggregate wealth transmission across generations would exist even under the unrealistic assumption that the importance of the wealth classes does not differ across economic systems. The second check is provided by our econometric estimates of the importance of material wealth mentioned above. Note that differences between the estimates of the importance of the two nonmaterial types of wealth (e and r) are modest, and that $e + m + r = 1$, so we may group embodied and relational wealth, whose importance we measure by $1 - m^*$, where m^* is the average of our econometrically estimated coefficients for material wealth in pastoral (0.84), agricultural (0.57), and horticultural (0.23) production. (We use the last-mentioned figure also for hunter-gatherers and in light of their evident similarity with horticulturalists.) Using these weights, rather than those estimated by the ethnographers, gives results similar to Table 2 [(*4*) section 5], but with even greater differences in the intergenerational transmission of wealth between the agricultural and pastoral economies, on the one hand, and the hunter-gatherer and horticultural economies, on the other.

Discussion. Our principal conclusion is that there exist substantial differences among economic systems in the intergenerational transmission of wealth and that these arise because material wealth is more important in agricultural and pastoral societies and because, in these systems, material wealth is substantially more heritable than embodied and relational wealth. By way of comparison, the degree of intergenerational transmission of wealth in hunter-gatherer and horticultural populations is comparable to the intergenerational transmission of earnings in the Nordic social democratic countries (*5*)—the average β for earnings in Denmark, Sweden, and Norway is 0.18—whereas the agricultural and pastoral societies in our data set are comparable to economies in which inequalities are inherited most strongly across generations, the United States and Italy, where the average β for earnings is 0.43. Concerning wealth inequality, the Gini measure in the hunter-gatherer and horticultural populations is almost exactly the average of the Gini measure of disposable income for Denmark, Norway, and Finland (0.24); the pastoral and agricultural populations are substantially more unequal than the most unequal of the high-income nations, the United States, whose Gini coefficient is 0.37 (*21*).

Our model explains some seeming anomalies, such as substantial wealth differences in those hunter-gatherer populations whose rich fishing sites can be defended by families or other corporate groups and transmitted across generations and which constitute an atypically important form of material wealth for those societies (*22*). Our findings also provide evidence for the view—widely held among historians, archaeologists, and other social scientists—that some influences on inequality are not captured simply by differences in technology, as measured by our α values. For example, the marked hierarchies among some Australian foragers may be due to polygyny (*23*), elite possession of ritual knowledge (*24*) that may be transmitted intergenerationally, or even to the dynamics of food sharing (*25*). Similarly, the fact that some agricultural and pastoral societies do not exhibit substantial levels of economic inequality despite their characteristic forms of wealth being in principle heritable (*26*, *27*) suggests the importance of deliberate egalitarianism, as well as other cultural influences and political choices (*28*). Examples include the lavish funeral feasting that redistributes the wealth of the elite among the Tandroy and other cattle pastoralists in Madagascar (*29*) and elsewhere (*26*). Other examples are the Nordic social democratic polities mentioned above.

One may speculate on the basis of these results that the current trend toward a knowledge-based economy that is less reliant on material wealth and more reliant on embodied and relational wealth might in the long run be associated with a concomitant reduction in intergenerational wealth transmission. But the importance in our data set of economic systems per se as a determinant of the dynamics of inequality suggests that the implications for inequality of this shift in how humans make a living will depend critically on our institutions.

References and Notes

1. A. Atkinson, in *Studies in Deprivation and Disadvantage: Parents and Children: Incomes in Two Generations*, A. B. Atkinson, A. K. Maynard, C. G. Trinder, Eds. (Heinemann Educational Books, London, 1983), pp. 94–114.
2. G. S. Becker, N. Tomes, *J. Polit. Econ.* **87**, 1153 (1979).
3. S. Bowles, H. Gintis, *J. Econ. Perspect.* **16**, 3 (2002).
4. Materials and methods and supporting text are available as supporting material on *Science* Online.
5. A. Bjorklund, M. Jantti, in *Oxford Handbook of Economic Inequality*, W. Salverda, B. Nolan, T. Smeeding, Eds. (Oxford Univ. Press, Oxford, 2009), pp. 491–521.
6. T. Hertz *et al.*, *B. E. J. Econ. Anal. Policy* **7**, 10 (2007).
7. D. Nettle, T. Pollet, *Am. Nat.* **172**, 658 (2008).
8. J. E. Pettay, L. E. B. Kruuk, J. Jokela, V. Lummaa, *Proc. Natl. Acad. Sci. U.S.A.* **102**, 2838 (2005).
9. D. F. Roberts, W. Z. Billewicz, I. A. McGregor, *Ann. Hum. Genet.* **42**, 15 (1978).
10. F. Galton, *Natural Inheritance* (Macmillan, London, 1889).
11. J. Coleman, *Foundations of Social Theory* (Harvard Univ. Press, Cambridge, MA, 1990).
12. T. W. Schultz, *Am. Econ. Rev.* **51**, 1 (1961).
13. H. Kaplan, *Yearb. Phys. Anthropol.* **39**, 91 (1996).
14. A. W. Johnson, T. Earle, *The Evolution of Human Societies: From Foraging Group to Agrarian State* (Stanford Univ. Press, Palo Alto, CA, ed. 2, 2000).
15. S. Bowles, *J. Polit. Econ.* **80**, S219 (1972).
16. K. K. Charles, E. Hurst, *J. Polit. Econ.* **111**, 1155 (2003).
17. M. Murphy, *Soc. Biol.* **46**, 122 (2007).
18. J. Woodburn, *Man (Lond)* **17**, 431 (1982).
19. H. K. Schneider, *Livestock and Equality in East Africa: The Economic Basis for Social Structure* (Indiana Univ. Press, Bloomington, IN, 1979).
20. J. Hartung, *Curr. Anthropol.* **23**, 1 (1982).
21. A. Brandolini, T. Smeeding, in *The Oxford Handbook of Economic Inequality*, W. Salverda, B. Nolan, T. Smeeding, Eds. (Oxford Univ. Press, Oxford, 2009), pp. 71–100.
22. B. Hayden, *The Pithouses of Keatley Creek* (Harcourt Brace College Publishers, New York, 1997).
23. H. Kaplan, J. Lancaster, in *Offspring: Human Fertility Behavior in Biodemographic Perspective*, K. W. Wachter, R. Bulatao, Eds. (National Academies Press, Washington, DC, 2003), pp. 170–223.
24. I. Keen, *Curr. Anthropol.* **47**, 7 (2006).
25. K. Hawkes, in *Hierarchies in Action: Cui Bono?* M. W. Diehl, Ed. (Southern Illinois Univ. Center for Archaeological Investigations, Occasional Paper 27, 2000), pp. 59–83.

26. M. Bollig, *Risk Management in a Hazardous Environment* (Springer, New York, 2006).
27. P. Wiessner, *Curr. Anthropol.* **43**, 233 (2002).
28. C. Boehm, *Hierarchy in the Forest* (Harvard Univ. Press, Cambridge, MA, 2000).
29. M. Parker Pearson, *The Archaeology of Death and Burial* (Sutton, Stroud, UK, 1999).
30. K. Hill, A. M. Hurtado, *Ache Life History: The Ecology and Demography of a Foraging People* (Aldine de Gruyter, Berlin, 1996).
31. F. W. Marlowe, *The Hadza* (Univ. of California Press, Berkeley, CA, in press).
32. P. Wiessner, in *Politics and History in Band Societies*, E. Leacock, R. Lee, Eds. (Cambridge Univ. Press, Cambridge, 1982), pp. 61–84.
33. M. Alvard, D. Nolin, *Curr. Anthropol.* **43**, 533 (2002).
34. E. A. Smith, R. B. Bird, D. W. Bird, *Behav. Ecol.* **14**, 116 (2003).
35. R. Quinlan, *Am. Anthropol.* **108**, 464 (2006).
36. R. Sear, F. Steele, I. A. McGregor, R. Mace, *Demography* **39**, 43 (2002).
37. M. Borgerhoff Mulder, *Hum. Nat.* **20**, 130 (2009).
38. M. Gurven, H. Kaplan, A. Zelada Supa, *Am. J. Hum. Biol.* **19**, 376 (2007).
39. M. Borgerhoff Mulder, *Hum. Ecol.* **20**, 383 (1992).
40. I. Fazzio, *Parental Investment Among Arab and Dazagada Herding Societies of West Chad* (VDM Verlag Dr Müller, Berlin, 2008).
41. R. McElreath, *Am. Anthropol.* **106**, 308 (2004).
42. W. Irons, *The Yomut Turkmen: A Study of Social Organization Among a Central Asian Turkic-Speaking Population* (Univ. of Michigan Museum of Anthropology, Ann Arbor, MI, 1975).
43. D. L. Leonetti, D. C. Nath, N. S. Heman, D. B. Neill, in *Grandmotherhood: The Evolutionary Significance of the Second Half of the Female Life*, E. Voland, A. Chasiotis, W. Schiefenhoevel, Eds. (Rutgers Univ. Press, New Brunswick, NJ, 2005), pp. 194–214.
44. M. K. Shenk, *Hum. Nat.* **16**, 81 (2005).
45. G. Clark, *A Farewell to Alms: A Brief Economic History of the World* (Princeton Univ. Press, Princeton, NJ, 2007).
46. M. Borgerhoff Mulder, *Curr. Anthropol.* **36**, 573 (1995).
47. E. Voland, *Behav. Ecol. Sociobiol.* **26**, 65 (1990).
48. B. S. Low, A. L. Clarke, *J. Fam. Hist.* **16**, 117 (1990).

49. The authors declare no competing interests. Financial support for this research was provided by the Behavioral Sciences Program of the Santa Fe Institute, the Russell Sage Foundation, and the NSF. We would like to thank the participating members of the populations we studied for their cooperation and M. Alexander, W. Cote, P. Lindert, C. Resnicke, T. Taylor, D. Ulibarri, and H. Wright for their contributions to this research.

Supporting Online Material

www.sciencemag.org/cgi/content/full/326/5953/682/DC1
Materials and Methods
SOM Text
Figs. S1 and S2
Tables S1 to S13
References

29 June 2009; accepted 29 September 2009
10.1126/science.1178336

The Crystal Structure of the Ribosome Bound to EF-Tu and Aminoacyl-tRNA

T. Martin Schmeing,* Rebecca M. Voorhees,* Ann C. Kelley, Yong-Gui Gao, Frank V. Murphy IV,† John R. Weir,‡ V. Ramakrishnan§

The ribosome selects a correct transfer RNA (tRNA) for each amino acid added to the polypeptide chain, as directed by messenger RNA. Aminoacyl-tRNA is delivered to the ribosome by elongation factor Tu (EF-Tu), which hydrolyzes guanosine triphosphate (GTP) and releases tRNA in response to codon recognition. The signaling pathway that leads to GTP hydrolysis upon codon recognition is critical to accurate decoding. Here we present the crystal structure of the ribosome complexed with EF-Tu and aminoacyl-tRNA, refined to 3.6 angstrom resolution. The structure reveals details of the tRNA distortion that allows aminoacyl-tRNA to interact simultaneously with the decoding center of the 30*S* subunit and EF-Tu at the factor binding site. A series of conformational changes in EF-Tu and aminoacyl-tRNA suggests a communication pathway between the decoding center and the guanosine triphosphatase center of EF-Tu.

The ribosome is the macromolecular enzyme that synthesizes proteins using aminoacyl-tRNA substrates, as directed by an mRNA template. To faithfully translate the genetic information contained in mRNA, the ribosome must select cognate tRNA by its ability to base pair with the mRNA codon, a process termed "decoding." Elongation factor Tu (EF-Tu), a translation factor with ribosome-dependent guanosine triphosphatase (GTPase) activity, delivers aminoacyl-tRNAs to the ribosome in a ternary complex (TC) of aminoacyl-tRNA•GTP•EF-Tu (where GTP is guanosine triphosphate) and plays an active role in ensuring the fidelity of decoding. Understanding the interplay between the TC and the ribosome that leads to the accurate translation of the mRNA message has been an active area of research for more than three decades.

Biochemical experiments have provided a wealth of information about the multistep process of tRNA discrimination by the ribosome. Initial binding of TC occurs independently of mRNA (*1*), after which codon-anticodon pairs are sampled at the decoding center of the 30*S* subunit. Correct codon-anticodon matching induces conformational changes in three 16*S* nucleotides—A1492, A1493, and G530 (*Escherichia coli* numbering, see table S1)—that monitor the geometry of the minor groove in the codon-anticodon helix (*2*) and accelerate the forward rate of selection (*3*). Binding of a near-cognate tRNA does not induce these changes (*4*), explaining why initial tRNA selection is more accurate than can be accounted for by the energetic differences between matched and mismatched anticodons alone (*5*). In addition to simple codon-anticodon base pairing, physical properties of the tRNA body are also important for faithful decoding (*6*–*11*). Finally, the binding energy of a cognate tRNA is used to make an important domain closure of the 30*S* subunit (*4*), moving the "shoulder" domain closer to the TC (*12*).

The signal that codon recognition has occurred must then be transmitted to the GTPase center of EF-Tu. The ribosome could stimulate GTP hydrolysis using two strategies: (i) by positioning catalytic residues in EF-Tu for GTP hydrolysis and (ii) by providing ribosomal components that function directly in catalysis. Domain 1 of EF-Tu is responsible for nucleotide binding, and rearrangements in this domain result in the opening of the hydrophobic gate, composed of residues Val^{20} in the P loop and Ile^{60} in switch I, which before activation prevents access of the catalytic His^{84} to GTP (*13*). Mutation of His^{84} results in a 10^5 decrease in the rate of GTP hydrolysis by EF-Tu, and this residue is thought to position and activate a water molecule to hydrolyze GTP (*14*). Ribosomal components implicated in GTPase activity include the sarcin-ricin loop (SRL) of 23*S* ribosomal RNA (rRNA), located adjacent to the nucleotide binding pocket of EF-Tu (*15*), ribosomal protein L7/L12, which stimulates hydrolysis 2500-fold (*16*), and the L11 protein and proximal rRNA (*17*).

Hydrolysis of GTP and release of inorganic phosphate (P_i) by EF-Tu leads to lowered affinity for aminoacyl-tRNA and release from the ribosome. tRNA is then either accommodated into the peptidyl transferase center or rejected via a "proofreading" mechanism (*18*, *19*). Proofreading and initial selection are separated by irreversible GTP hydrolysis, and their multiplicative effect accounts for the high accuracy of decoding (*3*, *20*). Despite the wealth of biochemical data, the transmission of codon recognition to the GTPase center and the activation of GTP hydrolysis is not well understood.

Crystal structures of EF-Tu and TC have been determined for complexes with guanosine diphosphate (GDP) and GTP analogs, as well as a variety of antibiotics [(Protein Data Bank identification code 1OB2) (*13*, *21*, *22*) and references therein]. Isolated structures of EF-Tu revealed the global conformational change of domain 1 that occurs upon transition between the active (GTP) and inactive (GDP) states of the protein (*13*). The

MRC Laboratory of Molecular Biology, Cambridge, CB2 0QH, UK.

*These authors contributed equally to this work.
†Present address: Northeastern Collaborative Access Team, Building 436, Argonne National Laboratory, Argonne, IL 60439, USA.
‡Present address: Max-Planck-Institut für Biochemie, Abteilung Zelluläre Strukturbiologie, Am Klopferspitz 18, Martinsried D-82152, Germany.
§To whom correspondence should be addressed. E-mail: ramakr@mrc-lmb.cam.ac.uk

conformations of switch I and switch II, which form part of the GTPase center, also depend on the nucleotide state of EF-Tu. Switch I became disordered in the complex of EF-Tu•GDP and the antibiotic methyl-kirromycin (*21*). TC structures reveal the substantial interaction surface between the tRNA and EF-Tu, including conserved interactions with A76 and the activated amino acid at the interface of domains 2 and 3 (*22*).

The complex of the TC stalled on the ribosome by the antibiotic kirromycin afforded the first visualization of EF-Tu delivering an aminoacyl-tRNA, by single particle cryo–electron microscopy (cryo-EM) (*23*). The tRNA was distorted into what was termed the "A/T" state (*24*) to interact simultaneously with the decoding center of the 30*S* subunit and EF-Tu, bound at the factor binding site in the intersubunit space (*25*). Subsequent studies produced steady improvements, and the most recent reconstructions are to beyond 7 Å resolution (*26*, *27*). These studies provided valuable information, but precise description of subtle conformational changes, the nature of the tRNA distortion, and atomic interactions, along with the mechanistic insights to which they lead, all require higher-resolution structures.

EF-Tu•tRNA Bound to the Ribosome

Here we present the crystal structure of the 70*S* ribosome from *Thermus thermophilus* in complex with $tRNA^{Phe}$ in the exit (E) and peptidyl (P) sites, mRNA, and the TC of EF-Tu•Thr-$tRNA^{Thr}$•GDP, stabilized by the antibiotics kirromycin and paromomycin, refined to 3.6 Å resolution [$I/\sigma(I) = 2$ at 3.75 Å] (Fig. 1 and table S1) (*28*). Kirromycin prevents rearrangements of EF-Tu after GTP hydrolysis and P_i release, thus trapping the complex on the ribosome (*29*). The domain conformation of EF-Tu in this state is thought to be similar to that at the GTP transition state (*30*). EF-Tu and Thr-$tRNA^{Thr}$ have been built into electron density, with many side chains of EF-Tu, bases of tRNA, both antibiotics, and GDP clearly resolved (Fig. 1A). As expected, the ribosome is in a nonratcheted state with P- and E-site tRNAs in the classic states and a similar overall conformation to the structure containing an accommodated aminoacyl-tRNA (*31*) (Fig. 1B). The largest conformational changes of the ribosome are in the L1 rRNA region and helices 43 and 44 of the 23*S* rRNA, which includes the L11 binding site, that become more ordered to interact with the elbow of the tRNA (Fig. 1C). The aminoacyl-tRNA is bound in the A/T state, and conformational changes in the 30*S* subunit indicative of cognate tRNA binding are observed including the flipping out of bases G530, A1492, and A1493 of the 16*S* rRNA and the "closing" of the 30*S* subunit (*2*). EF-Tu interacts with the factor binding site and the 30*S* "shoulder." This overall conformation is in good agreement with previous lower-resolution cryo-EM studies (*24*, *26*, *27*).

Distortion of tRNA

To adopt the A/T conformation, the aminoacyl-tRNA must be distorted substantially to allow the ~30° bend required to simultaneously bind the mRNA codon and EF-Tu. There are two distinct areas of distortion in the tRNA body: (i) a bend in a 13-nucleotide region of the anticodon stem and (ii) a change in the positioning of the D stem with respect to the acceptor- and T-stem contiguous stack. The very 3′ end of the

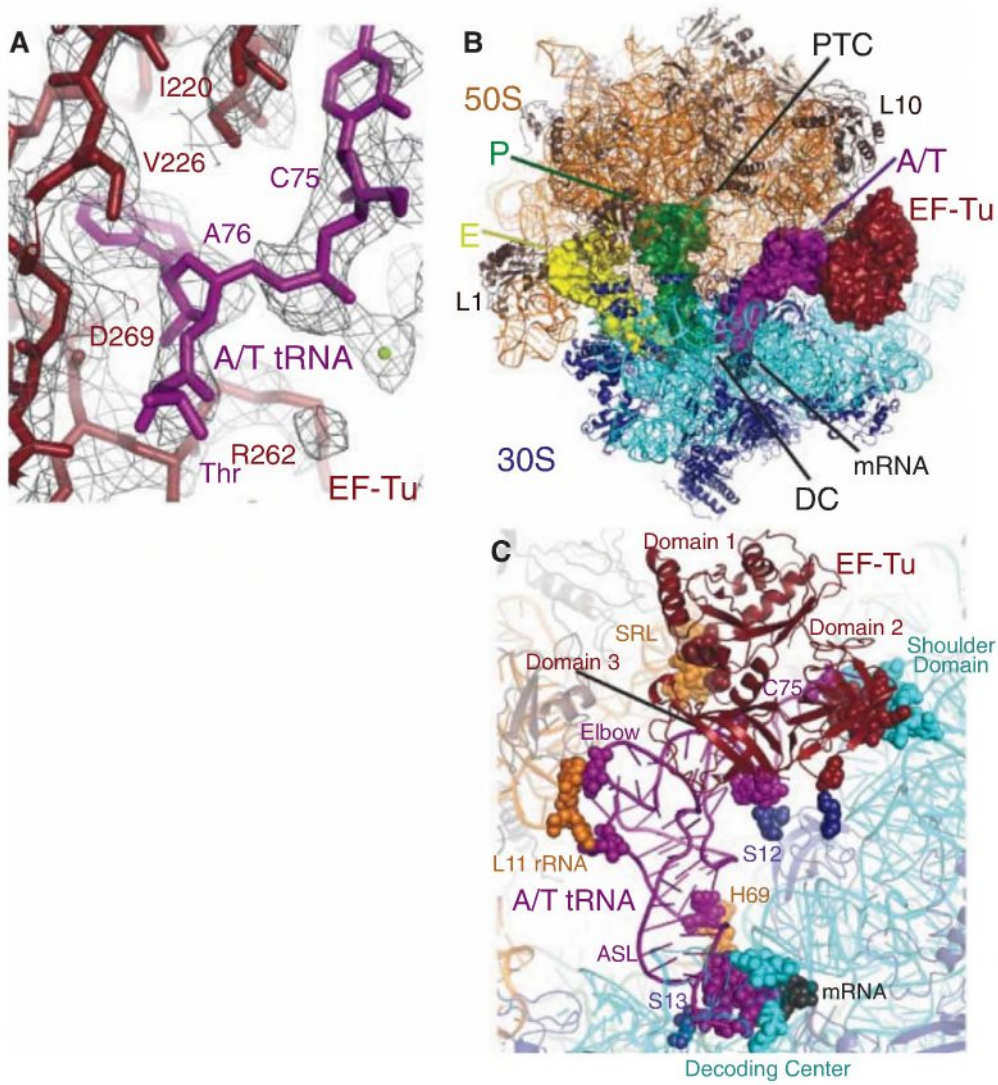

Fig. 1. Structure of EF-Tu and aminoacyl-tRNA bound to the ribosome. (**A**) Representative electron density from an unbiased difference Fourier map displayed at 1.3σ, with the refined model of EF-Tu (red) and Thr-$tRNA^{Thr}$ (purple). (**B**) Overall view of the complex, with EF-Tu and tRNAs depicted as surfaces, and rRNA and protein as cartoons. PTC, peptidyl transferase center; DC, decoding center. (**C**) Contacts between TC and the ribosome, with interacting residues shown as spheres.

tRNA is also distorted, as the backbone of residues 72 to 75 has shifted by up to 6 Å, and nucleotides C72 and C75 have swung outward. Although this conformation has an important mechanistic role (described below), it is not directly connected to the bent conformation of the tRNA body. The acceptor helix and anticodon adopt the canonical conformation, and the anticodon stem loop (ASL) of the A/T tRNA interacts with the decoding center in the same way as fully accommodated cognate aminoacyl-tRNA (A/A tRNA) (*31*) (Fig. 2A).

The anticodon stem distortion involves a reduction of helical twist and a widening of the phosphate backbone. The distortion begins at base pair 30:40, where the tRNA adopts a smooth bend involving nucleotides 25 to 30 and 40 to 48, rather then a kink as previously proposed (*24*). The helix in this region becomes under-twisted by up to 14°, from base pairs 30:40 through 25:45, to facilitate this bend (Fig. 2B). The distortion also includes a widening of the strands directly above the anticodon stem, as the phosphate-phosphate distance of nucleotides 25•45 and 26•44 are ~2 and 1 Å wider than in canonical tRNA. The observed widening explains the biochemical result that mutation of the 27:43 base pair gives an error-prone phenotype (*9*); weakening of this base pair could decrease the energy required to separate the strands at the adjacent nucleotides, allowing the distortion to occur more easily and, thus, the binding of mismatched tRNA. Indeed, the 27:43 base pair appears to be disrupted in the structure of the A/T tRNA, though the electron density for the base of C27 is not well-defined.

Ribosome binding also causes a second region of distortion, which moves the D stem away from the T- and acceptor-stem stack (Fig. 2C). This movement does not affect the canonical stack between the T and acceptor stems, which superimpose very well between the isolated and ribosomal-bound TCs (phosphorous atom root mean square deviation of 1.3 Å). The distortion of the A/T tRNA begins at the junction of the acceptor stem and D stem, around unpaired nucleotides 8 and 9, which results in a ~5 Å swing of the D arm. This rearrangement separates the 15:48 and 16:59 base pairs, but the displacement is smaller at the distal bases of the D loop (~G19), and the elbow interactions are largely unaltered.

The fact that codon recognition involves a tRNA distortion with a rearrangement of the D stem explains several experimental observations (Fig. 2D). A proflavin moiety, inserted at position 16 or 17, produces a fluorescent signal upon codon recognition (*1*), which is easily explained by the ~5 Å displacement of these nucleotides in the distorted A/T tRNA. The Hirsh suppressor tRNA is a $tRNA^{Trp}$ with a G24A mutation that allows Trp incorporation at UGA stop codons (*6*). G24 is normally base paired to C11, but in the distorted conformation the tRNA backbone across these nucleotides is ~1 Å farther apart than in a canonical tRNA, suggesting how the Hirsh suppressor can more easily sample the distorted conformation (*7*, *8*). A chemical cross-link between D-stem nucleotide 13 and nucleotide 8 (which is directly adjacent to the acceptor stem) occurs less frequently in the Hirsh tRNA background (*32*); these nucleotides separate in the distorted conformation. Conversely, the 8-to-13 cross-link would reduce the propensity for adopting the distortion required for decoding and has been shown to limit the miscoding activity of the Hirsh suppressor tRNA (*10*). The disruption of the 9:12:23 triple also gives a phenotype similar to the Hirsh suppressor (*8*). Interruption of this stabilizing interaction would facilitate deformation of the tRNA in the D-stem region. However, as the triple is intact in the A/T state, mutation of this base triple would probably allow formation of an altered distortion that achieves a similar bend to that observed for a wild-type tRNA. These mutations within the tRNA body would reduce the energetic penalty for distortion, which is normally precisely balanced against the energy derived from cognate codon-anticodon interaction. Thus, productive binding of TC and GTP hydrolysis can occur in these cases for even a near-cognate codon-anticodon interaction, as the energetic barrier for adopting the A/T conformation has been reduced.

Although the proposed nature of the tRNA distortion differed in older cryo-EM studies, its general description in the most recent cryo-EM work is similar to that observed in the present x-ray crystal structure (*26*, *27*). Although a distortion of the anticodon stem was observed, the widening of the tRNA above the anticodon stem was not detected, and the extent of the D-stem movement is considerably larger than reported.

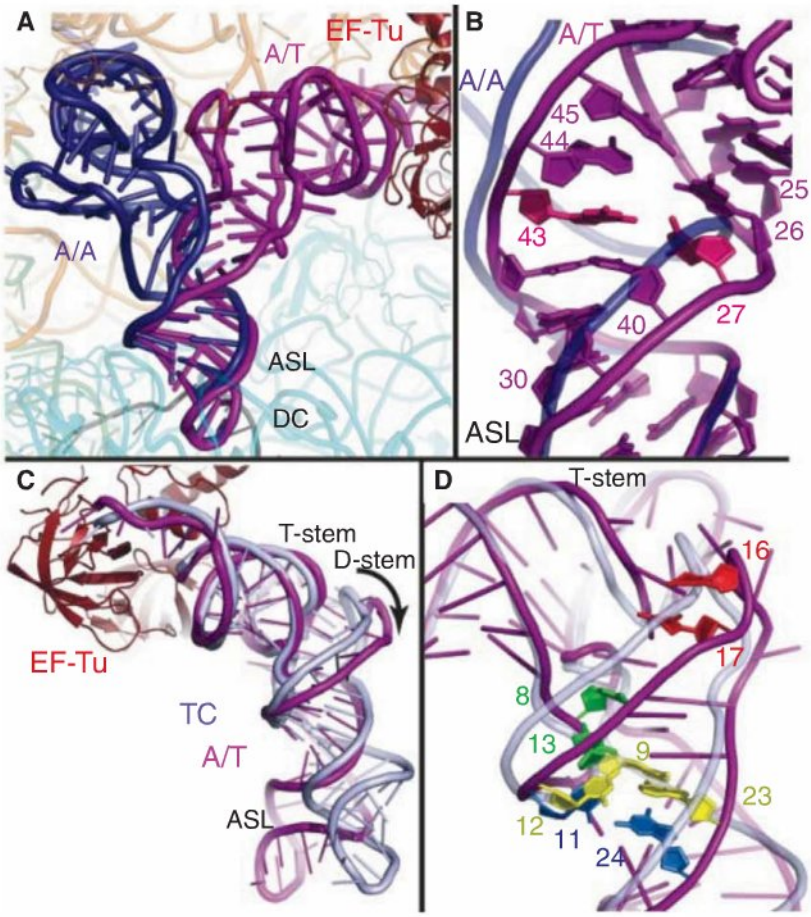

Fig. 2. Distortion of aminoacyl-tRNA in the A/T state. (**A**) Comparison of the A/T tRNA (purple) with the fully accommodated canonical A/A tRNA (dark blue) (*31*) shows the overall extent of the tRNA disortion. (**B**) The structures diverge in the ASL with a reduction of helical twist after base pair 30:40 and separation of the phosphate-sugar backbones at nucleotides 25 to 45 and 26 to 44. Disruption of the 27:43 base pair (pink) (*9*) would facilitate this strand separation. (**C**) Comparison of the A/T tRNA with tRNA of the isolated TC (light blue) (*22*) highlights the swinging out and ~5 Å shift of D-arm nucleotides. (**D**) The distortion rationalizes data pertaining to proflavin insertions at nucleotides 16 and 17 (bright red) (*1*), cross-linking of nucleotides 8 and 13 (green) (*32*), and mutations of the Hirsh base pair 24:11 (blue) (*6*, *8*) and 9:12:23 triple (yellow) (*8*).

Ribosomal Stabilization of Distorted tRNA: Few But Important Interactions

The highly distorted tRNA must be stabilized by interactions with the ribosome and EF-Tu. The structure reveals that the A/T tRNA interacts primarily with the decoding center and EF-Tu

while forming very few additional contacts with the ribosome (Fig. 1C). The decoding center interacts with the tRNA in a near identical manner to accommodated tRNA (*31*). A single additional sugar packing interaction between residue C25 of the tRNA and C1914 of 23*S* rRNA helix 69 is observed in this region.

In addition to the decoding center, the tRNA interacts with three regions of the ribosome: (i) the shoulder domain of the 16*S* rRNA, (ii) ribosomal protein S12, and (iii) the L11 region of 23*S* rRNA (Fig. 1C). Distortion in the 3′ end of the A/T tRNA involving residues 72 through 75 allows C75 to pack between EF-Tu residue 219 and the flipped base of A55, a residue that is 99.5% conserved in all species of known sequence (Fig. 3). Although A55 changes conformation, the rest of helix 5 of 16*S* rRNA is largely unaltered. S12 contacts the tRNA at the acceptor-arm/D-stem junction. In this region, the side chain of Gln^{74} is within hydrogen-bonding distance of the 2′OH of A67, and the side chain of His^{76} interacts with the sugar of residue U68. These two S12 residues form part of the highly conserved QEH sequence (*33*). Mutation of His^{76} leads to streptomycin-resistance, suggesting that this contact is important for proper TC binding (*34*). The S12 interactions were previously reported to be with tRNA residue 69 (*26*). In addition, EF-Tu contacts S12 with a single salt bridge between Glu^{249} of domain 2 of EF-Tu and Lys^{119} of S12.

The L11 rRNA interacts with the tRNA elbow at residue dihydroU20 (which is within hydrogen-bonding distance of U1068) and C56 through a packing interaction with A1067. The latter interaction is consistent with biochemical data showing that mutation of A1067U resulted in a threefold decrease in the rate of TC binding to the ribosome and a twofold decrease in the rate of GTP hydrolysis for cognate tRNA (*35*).

Considering only these few interactions outside the decoding center, the surface area of the A/T tRNA buried by the ribosome is only 482 $Å^2$. The most extensive interactions of the tRNA are those with EF-Tu, which bury 1540 $Å^2$ of surface area. The movement of the strained tRNA into the peptidyl transferase center upon release of EF-Tu would require disruption of only a few interactions with the ribosome, an energetic barrier that should be easily surmountable by the potential energy stored in the strained tRNA.

An Important Interaction Between Domain 2 and the 16*S* rRNA

The overall domain orientation of the ribosome-bound EF-Tu is very similar to that of the isolated methyl-kirromycin structure (*21*, *27*); however, a small concerted conformational change is observed in surface residues of domain 2 (Fig. 3A). Whereas those residues forming the interface between domains 2 and 3 remain unaltered, domain 2 residues 256 to 273 and 219 to 226, the latter composing a β turn near the 3′ end of the A/T tRNA, shift to allow two loops of EF-Tu to contact the 16*S* rRNA shoulder (Fig. 3, A and B). These interactions are facilitated by the domain closure of the 30*S* subunit, which moves the 16*S* rRNA toward EF-Tu. As these movements are not observed in the isolated structures of EF-Tu, even when similarly bound to both GDP and kirromycin, they are presumably a result of ribosome binding. Residues 278 to 281 interact with 16*S* rRNA residues 367 and 368 via packing, in addition to hydrogen bonding between Arg^{279} and U368. The second of these loops of EF-Tu packs into a pocket of 16*S* rRNA made by residues 55 and 56, 357 and 358, and 368. Hydrophobic interactions include those between Thr^{221} and 16*S* residues A55 and U56 and between Gly^{222} and U368, whereas hydrogen-bonding interactions occur between Arg^{223} and Gly^{222} and U368 and G357, respectively. This loop undergoes the most marked change upon ribosome binding, and the contacts may be of particular importance, as four of the seven residues between 219 and 226 are more than 99% conserved in all species, including humans. Furthermore, hydrogen-bonding interactions with both loops of EF-Tu occur with residue U368, which is 99.7% conserved across all species.

Mutational and biochemical data highlight the importance of the interaction between domain 2 of EF-Tu and the shoulder of the 30*S* subunit. Mutation of Gly^{222} to an aspartate prevents hydrolysis of GTP by EF-Tu, and thus

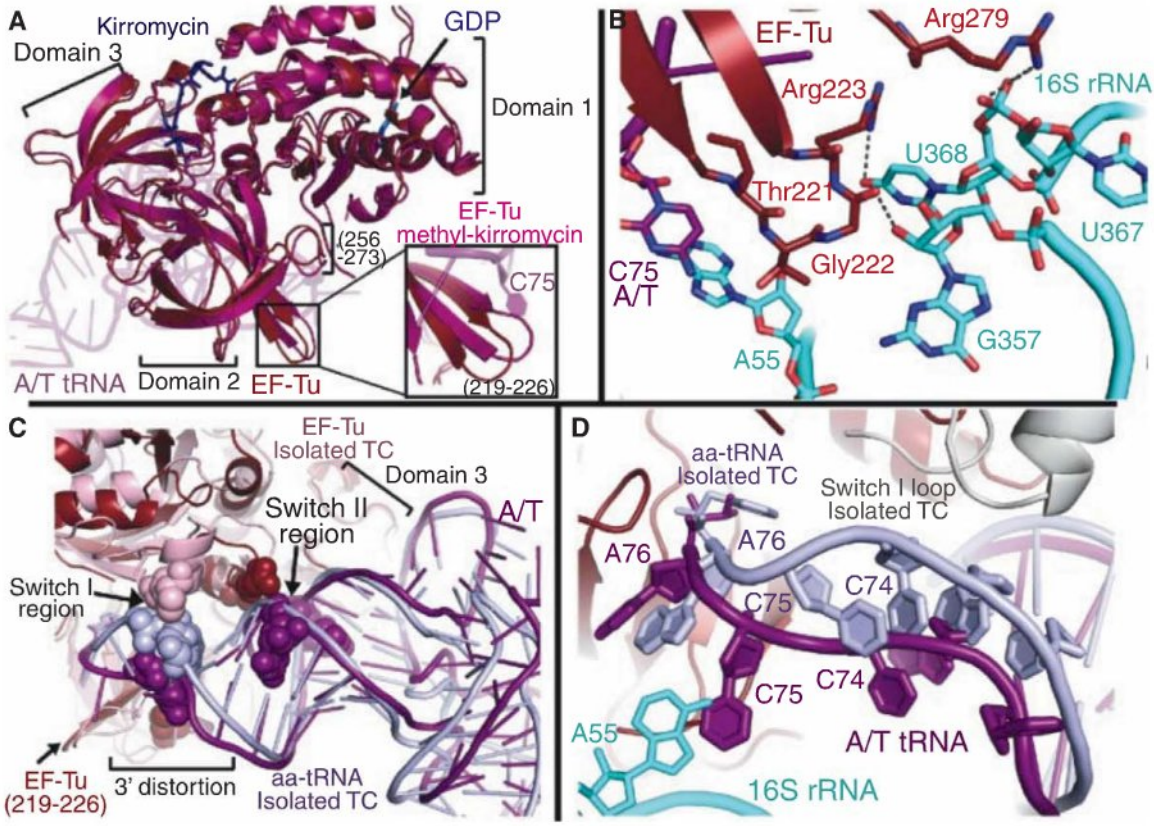

Fig. 3. Changes of EF-Tu upon ribosome binding. **(A)** EF-Tu bound to the ribosome (red) adopts a similar conformation to the isolated EF-Tu methyl-kirromycin complex (hot pink) (*21*), but ribosome binding induces a shift in domain 2 loops, including residues 256 to 273 and 219 to 226 (inset). **(B)** The detailed interactions between EF-Tu domain 2 and the shoulder domain of 16*S* rRNA (light blue). **(C)** Ribosome binding alters some of the contacts between EF-Tu and tRNA. Interaction of domain 3 with the T stem is largely unchanged when compared to the isolated TC (*22*), but that of switch II with the 5′ end of tRNA is altered, and the switch I contact with the 3′ end is abolished. **(D)** Interaction with the 30*S* shoulder distorts the 3′ end of tRNA, separating it from switch I, which becomes disordered. The ordered switch I from the isolated TC (gray) is shown for comparison.

protein synthesis, at physiological Mg^{2+} concentrations (*36*, *37*). At Mg^{2+} concentrations above 10 mM, the $Gly^{222} \rightarrow Asp^{222}$ (G222D) mutant EF-Tu can hydrolyze GTP and allow tRNA accommodation, although via a somewhat altered pathway (*36*). Further, kinetic data suggested that the G222D mutant EF-Tu was specifically deficient in its ability to transmit codon-anticodon recognition to the GTPase center, perhaps by preventing a conformational change in EF-Tu (*36*). Replacement of the highly conserved Gly^{222} would probably prevent the conformational change in this loop required for interaction with the 16*S* rRNA. Additionally, placing a large, negatively charged aspartate in a position that abuts the phosphate backbone of the 16*S* rRNA would be electrostatically unfavorable. However, at Mg^{2+} concentrations above 10 mM, this negative charge is probably screened by the divalent cations, partially rescuing the deficiency of the G222D mutant EF-Tu.

Shoulder Binding Alters Certain Interactions of EF-Tu with tRNA

Upon ribosome binding, local conformational changes of EF-Tu in both domain 2 and switch II alter the nature of a specific subset of the contacts between EF-Tu and the tRNA (Fig. 3C). Despite the suggestion from a cryo-EM study (*26*), the contacts between EF-Tu and the aminoacyl-tRNA are similar to those observed in the isolated structure of TC for much of the binding surface, including those involving the tRNA T-stem and parts of the acceptor stem (*22*). Likewise, interactions with the activated amino acid of aminoacyl-tRNA are maintained, including a hydrogen bond between Arg^{262} and the backbone carbonyl and Asn^{273} with the primary amine, as well as several hydrogen bonds with A76.

In solution, EF-Tu protects the labile ester bond of aminoacyl-tRNA and must continue to prevent hydrolysis of this bond upon binding to the ribosome. Maintaining these interactions with the amino acid while also allowing the conformational change of domain 2 toward the 16*S* rRNA may in part require the observed distortion of the 3′ end of the A/T tRNA (Fig. 3) and the previously unseen EF-Tu/tRNA interactions. This distortion of the tRNA between residues 72 and 75 moves the bases of C74 and C75 to interact with Arg^{283} and Thr^{219}-Ile^{220}, respectively (fig. S1), and shifts the tRNA backbone 5 to 6 Å away from the position of switch I in the isolated GDPNP•TC (GDPNP is a GTP analog) (Fig. 3D) (*22*). This would disrupt the interaction of tRNA residues 73 and 74 with switch I, perhaps leading to the disordering of switch I, for which we see no electron density.

Ribosome binding shifts the switch II loop toward the backbone of the tRNA [this motion is also mimicked by binding of kirromycin (Protein Data Bank identification code 1OB2)], allowing interaction between the phosphate oxygen of C65 with the side chain of Lys^{89}. In a recent cryo-EM study, however, the authors suggested, based on a comparison with the isolated kirromycin-TC structure, that upon ribosome binding the acceptor arm of the tRNA shifted closer to switch II of EF-Tu, facilitating formation of an interaction between the conserved Asp^{86} and the tRNA (*26*). However, a negatively charged Asp side chain would interact with the phosphate backbone in a repulsive manner. We find the acceptor arm of the tRNA not to be distorted from the canonical structure, evidenced by the superimposition of this region with that from the isolated TC (*22*) (Fig. 3C). With this comparison, it is instead a local movement of the switch II loop (including Asp^{86}) that allows the altered interaction of switch II with the acceptor stem.

GTPase Activation by the Ribosome

Along with the P loop, switch I and switch II are functional components of the GTPase center of EF-Tu. GTP is protected from hydrolysis by a hydrophobic gate of Ile^{60} (switch I) and Val^{20} (P loop) (*13*). During ribosome-induced GTP hydrolysis, this gate is opened, allowing putative catalytic residues Gly^{83} and His^{84} of switch II to interact with the γ-phosphate or nucleophilic

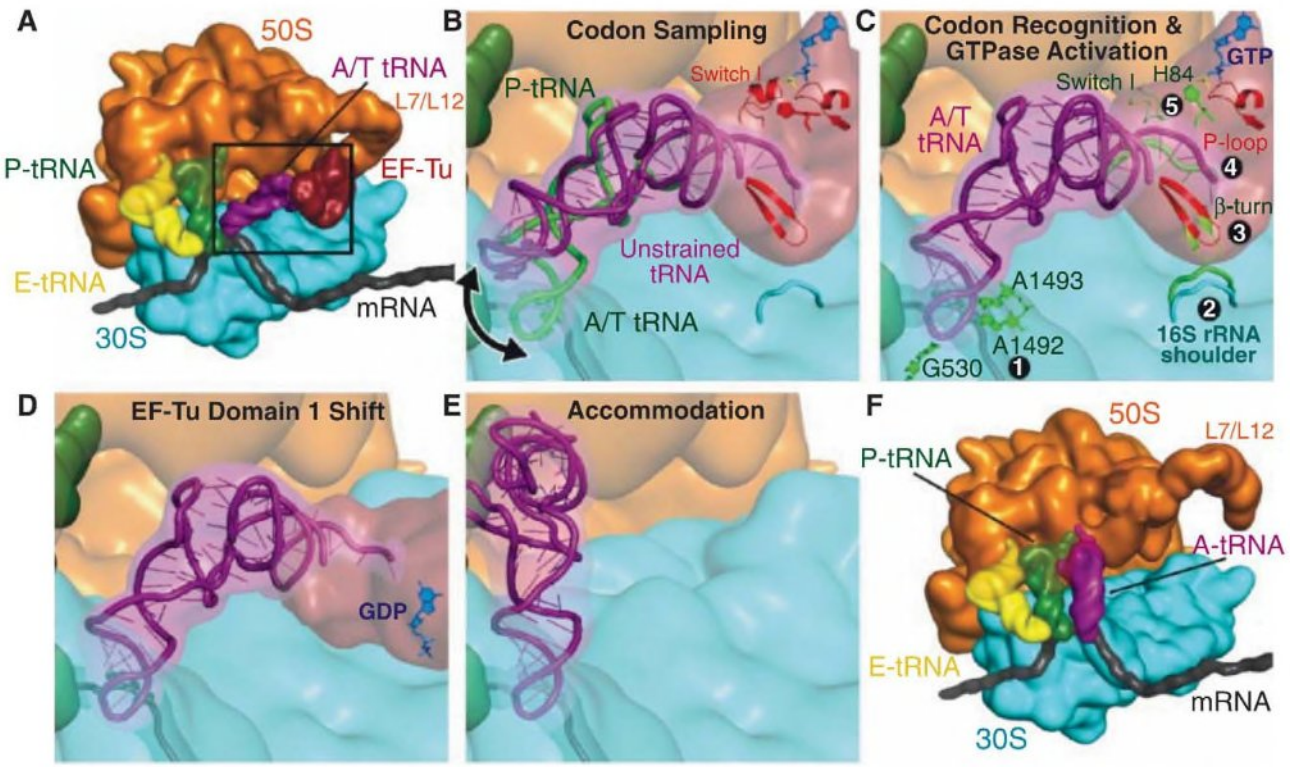

Fig. 4. Schematic representation of the decoding pathway. (**A**) The L7/L12 stalk recruits TC to a ribosome with deacylated tRNA in the E site and peptidyl-tRNA in the P site. The black frame represents the enlarged area depicted in (B) to (E). (**B**) The tRNA samples codon-to-anticodon pairing until a match (**C**) is sensed, by decoding center nucleotides 530, 1492, and 1493 (1). Codon recognition triggers domain closure of the 30*S* subunit (2), bringing the shoulder domain into contact with EF-Tu and shifting the β loop at 230 to 237 of domain 2 (3). This changes the conformation of the acceptor end of the tRNA (4), disrupting its contacts with switch I, which becomes disordered (5), opening the hydrophobic gate to allow His^{84} to catalyze GTP hydrolysis. (**D**) GTP hydrolysis and P_i release cause domain rearrangement of EF-Tu, leading to its release from the ribosome and (**E** and **F**) accommodation of aminoacyl-tRNA.

water (*13*, *14*). In the present structure, the catalytic His^{84} is positioned away from the G nucleotide in its inactivated position (*22*), consistent with the post-GTPase state of this complex (fig. S2). The switch II loop and the P loop are well ordered, but no density is observed for the switch I region from residues 42 to 65, including Ile^{60} of the hydrophobic gate. This disordering of switch I may be the mechanism of opening the hydrophobic gate, as observed in the isolated structure of EF-Tu in complex with GDP and methylkirromycin (*21*).

The disorder of switch I seen here is in contrast to the recent cryo-EM structure of the ribosome bound to the TC in the same state (*26*) that reports weak density for an alternate conformation of switch I interacting with helices 8 and 14 of the 16*S* rRNA. There is no evidence for this conformation in the current study, even in electron density maps calculated to low resolution and displayed at low threshold, consistent with another cryo-EM structure (*27*).

Perhaps because the reported structure does not depict the transition state of the GTP hydrolysis reaction, we cannot identify ribosomal components that could directly function in catalysis, despite the proposal that additional catalytic groups may be involved (*38*). No density was observed for ribosomal protein L7/L12, which is known to be important for stimulating GTP hydrolysis by the ribosome, although perhaps through indirect action (*16*). Also important for GTP hydrolysis is the SRL of the 23*S* rRNA, which interacts with domain 1 of EF-Tu. No conformational changes of the SRL are observed when compared to that containing an ASL in the A site (*39*). However, the catalytic His^{84} interacts with the 2′OH of G2661, probably holding the residue in its inactivated state (fig. S2). Additionally, EF-Tu residue His^{19} is within hydrogen-bonding distance of a phosphate oxygen of G2661 of the SRL. Mutation of SRL residue G2661C results in hyperaccurate ribosomes, perhaps by disrupting an interaction between EF-Tu and the SRL, further destabilizing the binding of near-cognate tRNA (*40*). Though Val^{20} (P loop), one part of the hydrophobic gate, is positioned close to these interactions, the SRL does not seem to be directly involved in opening the hydrophobic gate. Furthermore, the closest nucleotide of the SRL is ~5.5 Å from the GDP sugar, which would be too far to be directly involved in stimulating GTP hydrolysis.

Insights into the Decoding Pathway

The crystal structure of EF-Tu trapped on the ribosome provides an opportunity to analyze the complete decoding pathway in its structural context and to propose the mechanism by which codon-anticodon recognition is communicated to the GTPase center more than 80 Å away (Fig. 4 and movie S1).

Initial binding and sampling. The multimeric L7/L12 recruits TC for initial reversible and mRNA-independent binding (Fig. 4A) (*1*, *41*). In the initial TC conformation, the position of the tRNA allows sampling of codon-anticodon matches without excessive tRNA strain (Fig. 4B and fig. S3) (*36*).

Codon recognition and GTPase activation. The aminoacyl-tRNA samples a strained conformation until codon-anticodon recognition takes place (*42*), which results in the 30*S* subunit domain closure (Fig. 4C) (*2*). The precisely tuned flexibility of the tRNA facilitates its distortion (*11*). EF-Tu is pulled into its productive conformation by interactions with the distorted tRNA and by contacts with the ribosome.

Binding of EF-Tu induces a shift of regions of domain 2—including the β turn composed of residues 219 to 226—toward the now closed 16*S* rRNA. This leads to a ~5 Å distortion of the 3′ end of the tRNA (residues 72 to 75), which disrupts interactions between the tRNA and switch I loop. Loss of these stabilizing interactions leads to disordering of switch I, which opens the hydrophobic gate, thereby transmitting the signal that codon recognition has taken place to the heart of the GTPase center. This proposal explains why cleavage of switch I between residues Arg^{57} and Gly^{58} or Lys^{51} and Ala^{52} causes defects in ribosome-induced GTP hydrolysis by EF-Tu (*43*), as these cleavages would prevent transmission of the signal from the 3′ end of the tRNA to the GTPase center.

Opening of the hydrophobic gate allows putative catalytic residues Gly^{83} and His^{84} of switch II to interact with the γ-phosphate and/or activate a water molecule, triggering GTP hydrolysis (*13*, *14*, *44*).

Nucleotide-induced conformation change of EF-Tu. After GTP hydrolysis and P_i release, EF-Tu undergoes a conformational change to its GDP form, which involves a ~100° swing of the domain 1 relative to domains 2 and 3 (Fig. 4D) (*13*). This movement would disrupt the interactions of domain 1 with the SRL, as well as those between switch II and the tRNA acceptor arm, separating TC and leading to dissociation of EF-Tu from the ribosome.

Accommodation and proofreading. In the absence of EF-Tu, the few interactions between the distorted tRNA and the ribosome leave a largely clear path to the peptidyl transferase center (PTC) (Figs. 1C and 4E). The energetics of accommodation must be finely balanced, as near-cognate tRNAs are discriminated against at this second checkpoint in decoding (*3*). A near-cognate tRNA would have weaker interactions with the decoding center, as it cannot induce the closed 30*S* conformation that is characteristic of cognate tRNA binding (*4*). Therefore, as the tRNA reverts to its relaxed form, near-cognate tRNA might more easily disengage from the decoding center rather then swing into the PTC, providing the molecular mechanism for proofreading (*4*, *45*). Once accommodation is complete, peptide bond formation is very rapid, and the proper incoming amino acid is added to the nascent peptide chain, thus achieving the goal of decoding.

References and Notes

1. M. V. Rodnina, T. Pape, R. Fricke, L. Kuhn, W. Wintermeyer, *J. Biol. Chem.* **271**, 646 (1996).
2. J. M. Ogle *et al.*, *Science* **292**, 897 (2001).
3. K. B. Gromadski, M. V. Rodnina, *Mol. Cell* **13**, 191 (2004).
4. J. M. Ogle, F. V. Murphy, M. J. Tarry, V. Ramakrishnan, *Cell* **111**, 721 (2002).
5. T. Xia *et al.*, *Biochemistry* **37**, 14719 (1998).
6. D. Hirsh, *Nature* **228**, 57 (1970).
7. L. Cochella, R. Green, *Science* **308**, 1178 (2005).
8. D. Smith, M. Yarus, *J. Mol. Biol.* **206**, 503 (1989).
9. D. W. Schultz, M. Yarus, *J. Mol. Biol.* **235**, 1381 (1994).
10. J. Vacher, R. H. Buckingham, *J. Mol. Biol.* **129**, 287 (1979).
11. O. Piepenburg *et al.*, *Biochemistry* **39**, 1734 (2000).
12. J. M. Ogle, V. Ramakrishnan, *Annu. Rev. Biochem.* **74**, 129 (2005).
13. H. Berchtold *et al.*, *Nature* **365**, 126 (1993).
14. T. Daviter, H. J. Wieden, M. V. Rodnina, *J. Mol. Biol.* **332**, 689 (2003).
15. D. Moazed, J. M. Robertson, H. F. Noller, *Nature* **334**, 362 (1988).
16. D. Mohr, W. Wintermeyer, M. V. Rodnina, *Biochemistry* **41**, 12520 (2002).
17. H. R. Bourne, D. A. Sanders, F. McCormick, *Nature* **349**, 117 (1991).
18. R. C. Thompson, P. J. Stone, *Proc. Natl. Acad. Sci. U.S.A.* **74**, 198 (1977).
19. T. Ruusala, M. Ehrenberg, C. G. Kurland, *EMBO J.* **1**, 741 (1982).
20. S. C. Blanchard, R. L. Gonzalez, H. D. Kim, S. Chu, J. D. Puglisi, *Nat. Struct. Mol. Biol.* **11**, 1008 (2004).
21. L. Vogeley, G. J. Palm, J. R. Mesters, R. Hilgenfeld, *J. Biol. Chem.* **276**, 17149 (2001).
22. P. Nissen *et al.*, *Science* **270**, 1464 (1995).
23. H. Stark *et al.*, *Nature* **389**, 403 (1997).
24. M. Valle *et al.*, *EMBO J.* **21**, 3557 (2002).
25. D. Moazed, H. F. Noller, *Cell* **57**, 585 (1989).
26. E. Villa *et al.*, *Proc. Natl. Acad. Sci. U.S.A.* **106**, 1063 (2009).
27. J. C. Schuette *et al.*, *EMBO J.* **28**, 755 (2009).
28. Materials and methods are available as supporting material on *Science* Online.
29. U. Kothe, M. V. Rodnina, *Biochemistry* **45**, 12767 (2006).
30. M. V. Rodnina, R. Fricke, W. Wintermeyer, *Biochemistry* **33**, 12267 (1994).
31. R. M. Voorhees, A. Weixlbaumer, D. Loakes, A. C. Kelley, V. Ramakrishnan, *Nat. Struct. Mol. Biol.* **16**, 528 (2009).
32. A. Favre, R. Buchingham, G. Thomas, *Nucleic Acids Res.* **2**, 1421 (1975).
33. Single-letter abbreviations for the amino acid residues are as follows: A, Ala; C, Cys; D, Asp; E, Glu; F, Phe; G, Gly; H, His; I, Ile; K, Lys; L, Leu; M, Met; N, Asn; P, Pro; Q, Gln; R, Arg; S, Ser; T, Thr; V, Val; W, Trp; and Y, Tyr.
34. S. T. Gregory, J. F. Carr, A. E. Dahlberg, *RNA* **15**, 208 (2009).
35. U. Saarma, J. Remme, M. Ehrenberg, N. Bilgin, *J. Mol. Biol.* **272**, 327 (1997).
36. E. Vorstenbosch, T. Pape, M. V. Rodnina, B. Kraal, W. Wintermeyer, *EMBO J.* **15**, 6766 (1996).
37. G. W. Swart, A. Parmeggiani, B. Kraal, L. Bosch, *Biochemistry* **26**, 2047 (1987).
38. M. V. Rodnina, *Proc. Natl. Acad. Sci. U.S.A.* **106**, 969 (2009).
39. M. Selmer *et al.*, *Science* **313**, 1935 (2006); published online 7 September 2006 (10.1126/science.1131127).
40. N. Bilgin, M. Ehrenberg, *J. Mol. Biol.* **235**, 813 (1994).
41. M. Diaconu *et al.*, *Cell* **121**, 991 (2005).
42. T. H. Lee, S. C. Blanchard, H. D. Kim, J. D. Puglisi, S. Chu, *Proc. Natl. Acad. Sci. U.S.A.* **104**, 13661 (2007).
43. W. Zeidler *et al.*, *Eur. J. Biochem.* **239**, 265 (1996).
44. C. Knudsen, H. J. Wieden, M. V. Rodnina, *J. Biol. Chem.* **276**, 22183 (2001).
45. T. Pape, W. Wintermeyer, M. Rodnina, *EMBO J.* **18**, 3800 (1999).

46. We thank M. M. Babu and P. Lukavski for help with data analysis, G. Leonard and S. Brockhauser for their guidance and advice with data collection at the European Synchrotron Light Source beamline ID14.4,

C. Schulze-Briese and A. Pauluhn for help with initial diffraction studies performed at the Swiss Light Source, and L. Ulisko for preparation of additional images. This work was supported by the Medical Research Council U.K., the Wellcome Trust, the Agouron Institute, and the Louis-Jeantet Foundation. R.M.V. is the recipient of a Gates-Cambridge scholarship; T.M.S. received support from the Human Frontiers Science Program Organization and Emmanuel College, University of Cambridge; and V.R. holds stock options and is on the Scientific Advisory Board of Rib-X Pharmaceuticals, a company dedicated to making antibiotics that target the ribosome. The structure has been deposited at the Protein Data Bank with accession codes 2WRN, 2WRO, 2WRQ, and 2WRR.

Supporting Online Material

www.sciencemag.org/cgi/content/full/1179700/DC1
Materials and Methods
Figs. S1 to S3
Tables S1 and S2
References
Movie S1

27 July 2009; accepted 9 September 2009
Published online 15 October 2009;
10.1126/science.1179700
Include this information when citing this paper.

The Structure of the Ribosome with Elongation Factor G Trapped in the Posttranslocational State

Yong-Gui Gao, Maria Selmer,* Christine M. Dunham,† Albert Weixlbaumer,‡ Ann C. Kelley, V. Ramakrishnan§

Elongation factor G (EF-G) is a guanosine triphosphatase (GTPase) that plays a crucial role in the translocation of transfer RNAs (tRNAs) and messenger RNA (mRNA) during translation by the ribosome. We report a crystal structure refined to 3.6 angstrom resolution of the ribosome trapped with EF-G in the posttranslocational state using the antibiotic fusidic acid. Fusidic acid traps EF-G in a conformation intermediate between the guanosine triphosphate and guanosine diphosphate forms. The interaction of EF-G with ribosomal elements implicated in stimulating catalysis, such as the L10-L12 stalk and the L11 region, and of domain IV of EF-G with the tRNA at the peptidyl-tRNA binding site (P site) and with mRNA shed light on the role of these elements in EF-G function. The stabilization of the mobile stalks of the ribosome also results in a more complete description of its structure.

The ribosome is the large molecular machine that uses an mRNA template to synthesize proteins, in a process referred to as translation. Ribosomes from all species consist of a large and a small subunit, which are termed 50*S* and 30*S* subunits in bacteria and consist of roughly two-thirds RNA and one-third protein. The last decade has seen a revolutionary change in our understanding of translation, largely as a result of the determination of high-resolution structures of the ribosomal subunits, as well as, more recently, the entire ribosome (*1*). Protein factors play crucial roles in all stages of translation, which can be divided roughly into initiation, elongation, and termination. The hydrolysis of guanosine 5′-triphosphate (GTP) by factors is required in all three stages of translation.

At the heart of translation is the elongation cycle, which consists of sequential addition of amino acids to the growing polypeptide chain directed by the mRNA codons. This process is catalyzed by two guanosine triphosphatase (GTPase) factors, elongation factors Tu (EF-Tu) and G (EF-G). At the beginning of the cycle, a nascent peptide chain linked to a tRNA is bound in the peptidyl-tRNA binding site (P site) of the ribosome, whereas the A site remains empty. The incoming aminoacyl-tRNA is delivered to the aminoacyl-tRNA site (A site) of the ribosome as a ternary complex with EF-Tu and GTP. After GTP hydrolysis and peptidyl transfer, the nascent peptide chain is linked to the new amino acid on the A-site tRNA through the formation of a peptide bond, leaving the P-site tRNA deacylated.

This assembly of tRNAs and mRNA must then move with respect to the ribosome by one codon in a process known as translocation, which is catalyzed by EF-G. In the first step of translocation, the aminoacyl ends of the tRNAs move with respect to the 50*S* subunit, so that the P- and A-site tRNAs move to the E (exit) and P sites, respectively, creating hybrid P/E and A/P states of the tRNAs (*2*). The formation of the intermediate states of tRNA is coupled to a rotation or ratcheting of about 6° of the 30*S* and 50*S* subunits relative to each other (*3*, *4*). The binding of EF-G to this ratcheted state catalyzes the second step of translocation, which involves movement of the mRNA and the anticodon stem-loops of the tRNAs with respect to the 30*S* subunit, accompanied by a resetting of the ratchet. The hydrolysis of GTP by EF-G is known to precede and accelerate this second step (*5*). Translocation completes the elongation cycle and leaves the ribosome with tRNAs in the E and P sites and an empty A site ready for the next amino-acyl tRNA. In addition to its role in translocation, EF-G is also required for ribosome recycling, where it acts in conjunction with ribosome recycling factor (*1*).

Although biochemical studies have elucidated the overall role of EF-G in translocation, understanding the detailed mechanism of the process requires knowledge of the precise interactions EF-G makes with the ribosome in various states of translocation. Crystal structures of EF-G with and without bound guanosine diphosphate (GDP) have been determined (*6*, *7*). The structure of the ternary complex of EF-Tu with tRNA and the GTP analog GDPNP showed a surprising similarity in shape to that of EF-G (*8*). The GTPase domains of the two factors are similar, and domain IV of EF-G protrudes from the body of the molecule in a manner similar to that of the tRNA anticodon stem-loop, which suggests that EF-G and the ternary complex bind the ribosome in a similar way.

To date, the main structural data on the binding of any GTPase factors to the ribosome come from cryo–electron microscopy (cryo-EM). The complex of EF-G with the ribosome has been solved in both the GTP and GDP states of the factor (*9*–*13*). These structures show that the conformation of EF-G on the ribosome is significantly altered from that of the isolated crystal structures. They also reveal the orientation of the factor on the ribosome in the pre- and post-GTP hydrolysis states and the conformational changes in the ribosome itself that accompany binding of EF-G. Further details of the mechanism of translocation require higher-resolution structures, but crystallization of the ribosome in complex with any GTPase factor has been elusive.

In this study, we report a new crystal form of the 70*S* ribosome made possible by use of a mutant ribosome that eliminates the steric clash that excludes GTPase factors in all previously published crystal forms (*14*). We have used this form to determine the structure of the posttranslocation state of the ribosome in complex with EF-G and fusidic acid, an antibiotic that allows GTP hydrolysis and translocation by EF-G but prevents its release from the ribosome. The structure, which is refined to 3.6 Å (I/σ = 2 at 3.7 Å), reveals conformational changes in the ribosome involved in GTPase activation; details of the interaction of domain IV of EF-G with the ribosome, mRNA, and tRNA; and insights into the mechanism of fusidic acid, which functions only in complex with EF-G bound to the ribosome.

MRC Laboratory of Molecular Biology, Hills Road, Cambridge, CB2 0QH, UK.

*Present address: Department of Cell and Molecular Biology, Uppsala University, Box 596, Uppsala, SE 751 24, Sweden.
†Present address: Department of Biochemistry, Emory University School of Medicine, Atlanta, GA 30322, USA.
‡Present address: The Rockefeller University, Box 224, New York, NY 10065, USA.
§To whom correspondence should be addressed. E-mail: ramak@mrc-lmb.cam.ac.uk

Crystallization and structure determination of the ribosome in the posttranslocation state with EF-G and fusidic acid. In all previously reported crystal forms of the ribosome from both *Escherichia coli* and *Thermus thermophilus* (*15*–*17*), a lattice contact with ribosomal protein L9 from a neighboring molecule would result in a steric clash with a bound GTPase factor. This interaction of L9 is so strong that our previous attempts to crystallize EF-G in complex with the ribosome resulted in a high-resolution crystal form in which the L9 contact had displaced the factor from the ribosome (*17*). This prompted us to truncate the gene for L9 in *T. thermophilus*. Previously established methods for genetic manipulation in this species (*18*) were used to generate the strain *T. thermophilus* HB8-MRC-MSAW1. Ribosomes from this strain were used to crystallize the posttranslocational state with mRNA, deacylated tRNA in the P and E sites, and EF-G with GDP and fusidic acid. This complex crystallized in the space group $P2_1$ with cell dimensions of 291.8 by 270.4 by 402.4 Å and $\beta = 91.7°$ and diffracted to beyond 3.5 Å resolution. The structure was solved by molecular replacement using the empty ribosome [from ref. (*17*)] as a starting model. Clear difference Fourier density was seen for the tRNAs, mRNA, GDP, and EF-G, in which well-ordered side chains of the factor were clearly distinguishable (Fig. 1A). Difference Fourier maps also clearly showed the locations of GDP and fusidic acid (Fig. 1B). The final structure after inclusion of all ligands was refined by using data to 3.6 Å resolution with a final R/R_{free} of 0.227/0.260 [table S1; details in (*14*)].

Overall structure of EF-G in the ribosome. The overall conformation of EF-G in the ribosome (Fig. 2A) agrees with previous cryo-EM studies either on an EF-G fusidic acid complex (*9*, *11*, *12*) or EF-G with a nonhydrolyzable GTP analog bound to the ratcheted ribosome (*12*, *13*). As expected, in the crystal structure here, the ribosomal subunits are in the canonical rather than ratcheted state. The binding of EF-G has made mobile elements of the ribosome better ordered, so that the L1 stalk and the N-terminal domain (NTD) of L10 are visible even in high-resolution maps, which allowed us to build them in their entirety (Fig. 2B). Maps calculated at lower resolution (5.0 Å) allowed us to place the helical extension of L10, four copies of the NTD of L12, as well as a copy of the C-terminal domain (CTD) of L12 that makes contact with EF-G and L11. The ordering of the L1 stalk, which makes contact with E-site tRNA on the other side of P-site tRNA, must be indirect, because EF-G does not directly contact it.

The conformation of EF-G on the ribosome (Fig. 2C) is different from that of the isolated EF-G with or without GDP (*6*, *7*, *19*) and the structure of EF-G-2 bound to the GTP analog GDPNP (*13*). An alignment using the G domain, which contains the nucleotide-binding site, shows that the most striking conformational change from the isolated structures is a reorientation of domain IV, although domains III and V have also moved significantly (fig. S1). A sequence alignment with *E. coli* EF-G is shown in fig. S2. Throughout this paper, RNA helices are numbered with the standard Brimacombe nomenclature, prefixed by H for 23*S* RNA and h for 16*S* RNA, and RNA residues are numbered with the *E. coli* sequence.

EF-G is held in position by contacts with both the 50*S* and 30*S* subunits (Fig. 2A and fig. S3A). The G domain, domain III, and domain V all surround the sarcin-ricin loop (SRL; 2660 loop or H95), the ribosomal element closest to the nucleotide-binding site, as inferred from previous cryo-EM studies (fig. S3B). The binding of EF-G also appears to have ordered the C terminus of L6 near the SRL and domain V. The β-barrel domain II contacts h5 and h15 (360 to 380) in the shoulder of the 30*S* subunit (fig. S3C). Domain III, which is required for GTP hydrolysis (*20*), makes contact with both the 30*S* subunit through interactions with h5 and protein S12, and the SRL in the 50*S* subunit (fig. S3D). Domain V makes several contacts with the 50*S* subunit, including the L11-binding region (H43/44; 1070/1095 loops) and the adjacent H89 (2475 loop) (fig. S3E). Finally, domain IV is inserted into the 30*S* decoding center where it contacts P-site tRNA and mRNA, and the EF-G–specific G′ domain makes a contact with a copy of the L12 CTD, which bridges it to the NTD of L11. These two interactions are discussed in detail below.

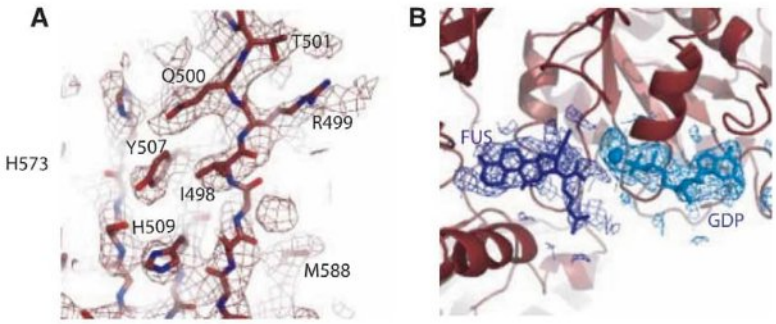

Fig. 1. Unbiased difference Fourier electron density maps for (**A**) EF-G and (**B**) the ligands fusidic acid (FUS) and GDP with its coordinated Mg^{2+} ion in the ribosome. All figures were made by using PyMol (*48*).

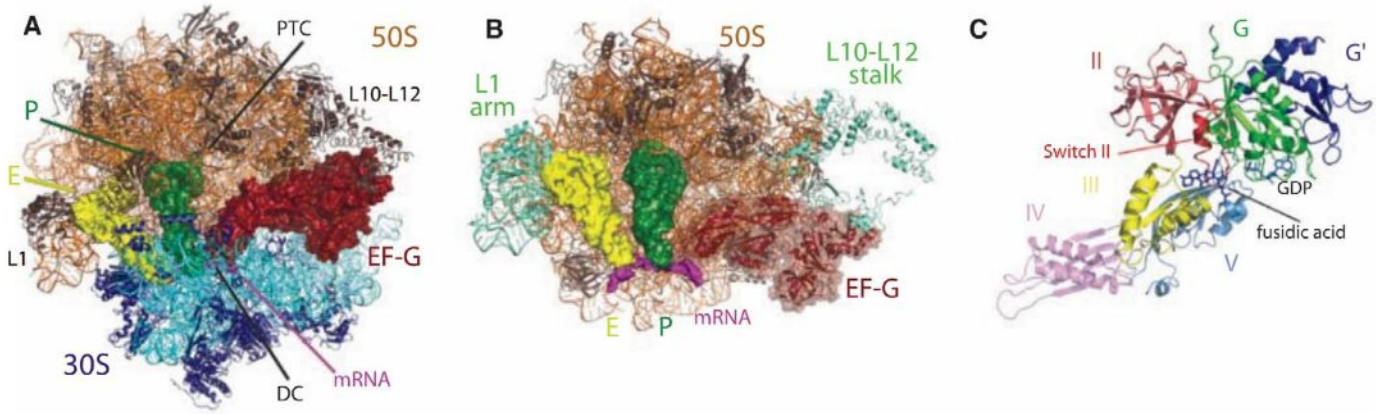

Fig. 2. EF-G in the posttranslocational state of the ribosome. (**A**) Overall view of EF-G in the ribosome. EF-G is shown in reddish-brown, the 50*S* subunit on top is shown in orange, the 30*S* subunit below is shown in cyan, P-site tRNA in green, and E-site tRNA in yellow, and the mRNA in purple. The decoding center (DC) in the 30*S* subunit and the peptidyl transferase center (PTC), and the L1 and L10-L12 stalks are indicated as shown. (**B**) Global changes in the 50*S* subunit as a result of EF-G binding. The mobile regions of the 50*S* subunit are indicated in teal and include the L1 stalk (both RNA and protein) and the L10-L12 stalk, as well as the adjacent L11 region (not labeled). (**C**) The structure of EF-G bound to fusidic acid and GDP in the ribosome. The various domains of EF-G are colored as shown.

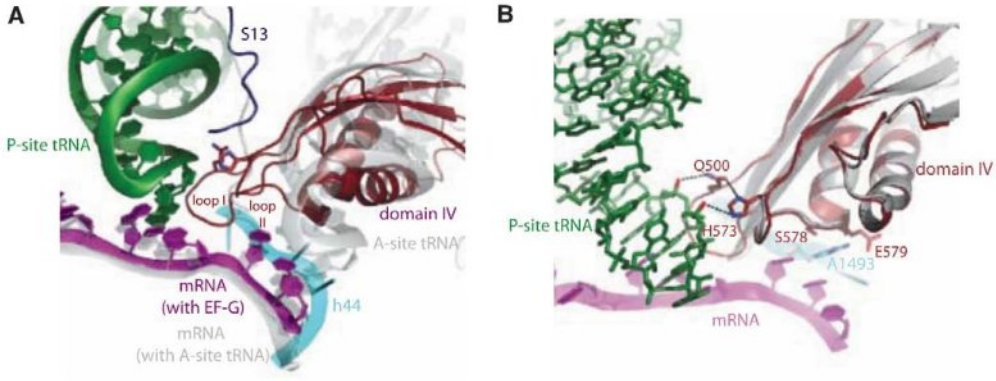

Fig. 3. Interactions of domain IV of EF-G with tRNA and mRNA. **(A)** Interactions of domain IV of EF-G with P-site tRNA and mRNA. Loop I is inserted into the minor groove between P-site tRNA and its codon. In gray are shown elements from a superposition of the 70*S* structure with A-site tRNA (*22*), showing conformational changes in the mRNA and protein S13 on EF-G binding. Unlike A-site tRNA, domain IV of EF-G does not make extensive interactions with the A-site codon. **(B)** Details of interactions with domain IV in the decoding site. The residues Q500 from loop I and H573 from loop II form a network of interactions with P-site tRNA and each other; loop I has changed conformation relative to its structure in domain IV of the isolated protein (gray) [2BM0 from ref. (*19*)], to insert into the minor groove between P-site tRNA and mRNA. Residues S578 and E579 make interactions with the universally conserved A1493 of 16*S* RNA.

Interaction of domain IV with mRNA and tRNA in the decoding center. Domain IV, which occupies the A site of the 30*S* subunit, makes extensive contacts with mRNA, P-site tRNA, and the decoding center of the 30*S* subunit (Fig. 3). Unlike A-site tRNA (*21*), the contacts of domain IV are made with the P-site tRNA and codon rather than with the A-site codon (Fig. 3A).

Domain IV contains two loops at its tip, loop I (496 to 509) and loop II (567 to 579). The two conserved glycines (502 and 503) facilitate a tight turn of loop I that allows it to be inserted into the minor groove between P-site tRNA and codon (Fig. 3A). When bound to the ribosome, the highly conserved loop I is in a different conformation from that in isolated structures (Fig. 3B). Two conserved residues, Q500 in loop I and H573 in loop II participate in a network of interactions (*22*) (Fig. 3B). H573 can form hydrogen bonds with a phosphate oxygen of U37 of the P-site tRNA, as well as with the carbonyl oxygen of Q500. The amide of Q500 can, in turn, form a hydrogen bond with a phosphate oxygen of A38 of P-site tRNA. Finally, S578 and E579 are both within hydrogen-bonding distance of the universally conserved A1493 of 16*S* RNA (Fig. 3B).

The structure clearly rationalizes the previous finding that mutation of H573 or insertions in loop II between 576 and 579 substantially reduce translocation without affecting EF-G binding or GTP hydrolysis (*23*, *24*). In addition to these interactions with tRNA and mRNA, domain IV also makes contacts with both h35 in the head of the 30*S* subunit and with h44 at the decoding center. Thus, although domain IV and A-site tRNA both bind in the same location in the 30*S* subunit, their interactions are quite different; in particular, there appear to be no direct contacts of domain IV with the A-site codon, at least in the posttranslocational state. This is not unexpected, because the codon that has been translocated into the A site would not be accessible to EF-G before translocation. It is possible that the contacts of the tip of domain IV with the P-site tRNA and codon, as seen in the current structure, initially occur when they are in the A site and are maintained throughout their translocation into the P site, which helps to avoid a frameshift during the process. If so, one of the early events in translocation by EF-G must be the displacement by loop I of the ribosomal bases G530, A1492, and A1493 that line the minor groove of the A-site codon-anticodon helix during decoding (*25*), and this may explain why antibiotics that stabilize those bases in the minor groove also inhibit translocation (*26*).

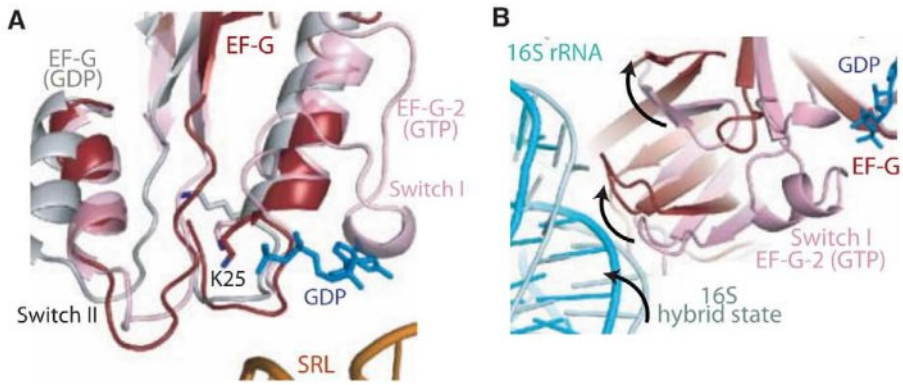

Fig. 4. The environment of the nucleotide-binding site in EF-G bound to the ribosome in the presence of fusidic acid. **(A)** A superposition shows that the switch I region of EF-G-2 in the GTP-bound form (pink) (*13*) has become disordered in the fusidic acid–complex structure. However switch II (red) in the structure is close to the GTP form of EF-G-2, and different from the altered conformation of the GDP form of EF-G in isolation (gray) [2BM0 from ref. (*19*)]. Similarly, K25, which interacts with the γ-phosphate in the GTP form, remains in that form in this structure rather than adopt the altered conformation (gray) of the GDP form of EF-G. **(B)** Conformational changes of the β hairpins and 16*S* movement in domain II relative to the GTP form of EF-G-2 (*13*). This movement is in the same direction as the movement of 16*S* RNA (cyan) relative to that of the ratcheted ribosome (light blue) that was aligned by using the 50*S* subunit (*49*).

Catalytic activity of EF-G. Translocation is a highly complex process involving large-scale movements of the ribosomal subunits and mRNA and tRNA. The structure presented here represents the posttranslocational state after GTP hydrolysis trapped with fusidic acid. Interestingly, it retains some features of the GTP state of EF-G and thereby sheds light on the catalysis of GTP hydrolysis.

The structure reveals atomic details of the environment of the catalytic site. The GDP molecule is clearly visible along with a coordinated Mg^{2+} ion (Fig. 1B). The closest ribosomal element to the catalytic site is the sarcin-ricin (2660) loop of 23*S* RNA, as expected from cryo-EM studies (*12*, *13*). In the GTP state, as represented by the structure of EF-G-2 with GDPNP (*13*), the nucleotide is protected from hydrolysis by two switch regions (40 to 66 and 80 to 102) which are ordered. In the structure here, the switch I loop has changed conformation, becoming disordered in the process, which allows access by water to the γ-phosphate. However, the switch II loop (80 to 102) is in the same conformation as the GTP state of EF-G-2 rather than of other GDP structures of EF-G, where this loop has moved away from the nucleotide (Fig. 4A) (*7*, *19*, *27*). This suggests that the factor has been frozen in an intermediate state between GTP hydrolysis and the GDP-bound conformation after release from the ribosome.

EF-G lacking domain III has reduced GTPase activity, although it binds GTP normally (*20*). Domain III interacts with both S12 and h5 (360 stem) of 16*S* RNA in the 30*S* subunit, as well as the SRL in the 50*S* subunit (fig. S3d). Thus by contacting both subunits, domain III can sense

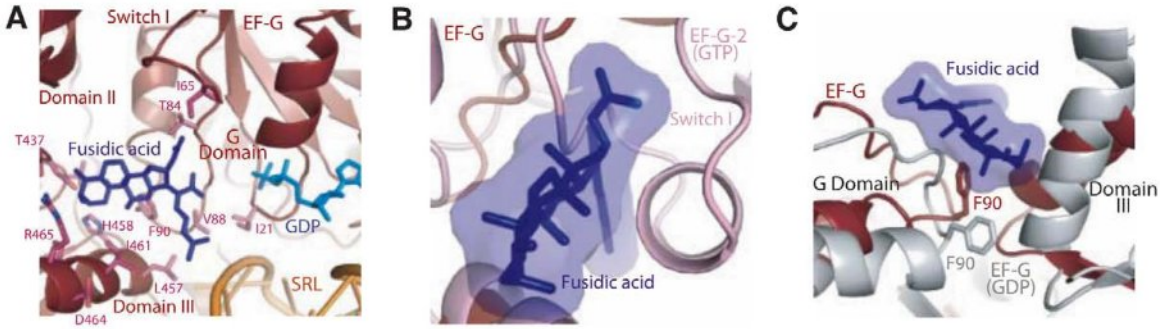

Fig. 5. Fusidic acid bound to EF-G in the ribosome. (**A**) Interactions of fusidic acid in a pocket lined by domains of EF-G, showing amino acids whose mutation gives rise to fusidic acid resistance. (**B**) A superposition of switch I from the GTP form of EF-G-2 (*13*) shows it would clash with fusidic acid. (**C**) Conformational changes between the fusidic acid–bound structure compared with the GDP-bound form of EF-G in isolation [2BM0 from ref. (*19*)] (gray). F90, switch II of the G domain, and domain III are all in a conformation that is different from the GDP form of EF-G.

the conformation of the ribosome, in particular the difference between ratcheted and nonratcheted subunits. These contacts may play a role in triggering GTP hydrolysis, in a manner similar to what has been proposed for EF-Tu (*28*).

The β-hairpins (314 to 328 and 354 to 366) in domain II have moved relative to the GTP form of EF-G-2 and are similar to the GDP form of EF-G (Fig. 4B). In the GTP form, these hairpins would make contact with the switch I helix, and their movement may be correlated with the destabilization of the switch I region during GTP hydrolysis. It is interesting to note that at least one of the hairpins interacts with the shoulder of 16*S* RNA, so their movement away from the switch I helix could track a rotation of the 30*S* relative to the 50*S* subunit. This may therefore hint at how GTP hydrolysis is coupled to the movement of the ribosomal subunits from the ratcheted form back to the canonical form during the second step of translocation.

A detailed understanding of the mechanism of GTPase activation and GTP hydrolysis by EF-G will require high-resolution structures of the pretranslocational ribosome with EF-G before and just after GTP hydrolysis. Remarkably, to date, there is no such structure by any method; reported cryo-EM structures of the ribosome complexed with EF-G and a GTP analog do indeed show a ratcheted state of the ribosome but do not contain an A-site tRNA [e.g., refs. (*12*, *13*)]. Moreover, domain IV of EF-G in these structures is in almost the same conformation as the structure here and would be incompatible with the A-site tRNA that would be present in a pretranslocated state.

Fusidic acid. Fusidic acid prevents the release of EF-G after GTP hydrolysis and translocation. It was originally thought to allow only a single round of GTP hydrolysis by EF-G (*29*), but recent studies suggest that multiple rounds of GTP hydrolysis can occur before trapping the ribosome in the posttranslocational state (*30*). However, fusidic acid has low affinity for isolated EF-G, so it has not previously been possible to visualize it directly when bound to the factor alone.

Clear density can be seen for fusidic acid (Fig. 1B) in a pocket surrounded by the switch II region of the G domain, as well as domains II and III (Fig. 5A). We have placed the molecule in the most plausible orientation, taking into account the shape of the density and the nature of potential interactions; however, alternative orientations that are rotated or flipped by 180° are also possible. The location is consistent with predictions from analysis of mutational data on fusidic acid (*19*, *31*). Fusidic acid would clash with the closed conformation of the switch I loop as observed in the GTP-bound form of EF-G-2 (Fig. 5B) (*13*), and binding must therefore require an open, disordered form of the switch I loop. The opening of the switch I loop would expose the γ-phosphate to water, which suggests that the binding of fusidic acid must occur after GTP hydrolysis.

Two EF-G mutations, T84A and G16V, give rise to fusidic acid resistance and hypersensitivity, respectively (*32*). T84 is involved in a direct contact with fusidic acid. Meanwhile, the mutation of G16 to valine stabilizes the loop that is part of switch II in a conformation (*19*) similar to the fusidic acid–bound structure described here, which leads to increased fusidic acid affinity and thus sensitivity. Mutation of F90 greatly reduces fusidic acid sensitivity (*33*, *34*). This residue interacts directly with fusidic acid in a manner similar to that observed in other fusidic acid–binding proteins (*35*, *36*).

The conformation of F90 is similar to that in the GTP form of EF-G-2, but different from that in the GDP bound EF-G structures (Fig. 5C) (*7*, *19*, *27*) where it interacts with a helix of domain III. The direct interaction of F90 with fusidic acid would thus prevent the conformational change of switch II that would normally occur after GTP hydrolysis and the transmission of this change to domain III. In addition, K25, which interacts with the γ-phosphate in the GTP form of EF-G-2 (*13*), remains in a similar conformation rather than in the altered form observed in the GDP structures (Fig. 4A) (*7*, *19*, *27*), where it makes a hydrogen bond with T84 of the switch II loop. Finally, fusidic acid also makes direct interactions with domain III, stabilizing a conformation that is different from that of the normal GDP form (Fig. 5, A and C). The altered conformations of the switch II region and domain III relative to domain II would result in stabilization of domain IV in the 30*S* subunit–binding pocket. Without fusidic acid, the conformation of domain IV that is preferred in the GDP form would result in the disruption of its contacts with the 30*S* subunit and could destabilize the factor on the ribosome and lead to its release.

Thus, the main effect of fusidic acid appears to be to lock switch II in a conformation similar to the GTP form even after GTP hydrolysis and, as a result, to prevent the transmission of conformational changes to domains III and IV. Although the location of fusidic acid is different from that of sordarin, which blocks the release of EF-2, the eukaryotic counterpart of EF-G (*37*), or of aurodox, which, like kirromycin, blocks the release of EF-Tu after GTP hydrolysis (*38*), all three antibiotics may act by preventing large-scale conformational changes in the elongation factors that are required for their release from the ribosome after GTP hydrolysis.

The L10-L12 stalk and the L11 region. Although at some distance from each other on the ribosome, both the L10-L12 stalk and the L11 region have been implicated in EF-G function. Both EF-Tu and EF-G have greatly diminished GTPase activity on ribosomes lacking the CTD of L12 (*39*, *40*). The L11 region of the 50*S* subunit (including protein L11 and the 1065/1096 stem loops of 23*S* RNA) is the binding site of the antibiotic thiostrepton, which inhibits steps in translocation after GTP hydrolysis, such as phosphate release (*30*, *41*). Kinetic measurements suggest that thiostrepton does not prevent binding of EF-G or GTP hydrolysis, but it inhibits subsequent steps such as the release of inorganic phosphate and translocation (*41*, *42*).

The structure shows that EF-G interacts directly with both the L11 region and the CTD of L12 (Fig. 6A). In the presence of bound EF-G, the long alpha helix at the C terminus of L10 is bent relative to its structure in the isolated L10-$(L12)_6$ complex (*40*) (Fig. 6A). This allows the L10-L12 stalk to bend toward the L11 region, and as a result, a copy of the CTD of L12 interacts with both the NTD of L11 and the G′ domain of EF-G (Fig. 6B), in agreement with previous cryo-EM data (*43*). The conformation of the G′ domain is similar to that in the GDP structures of EF-G and brings it into closer contact with the CTD of L12 as compared with the

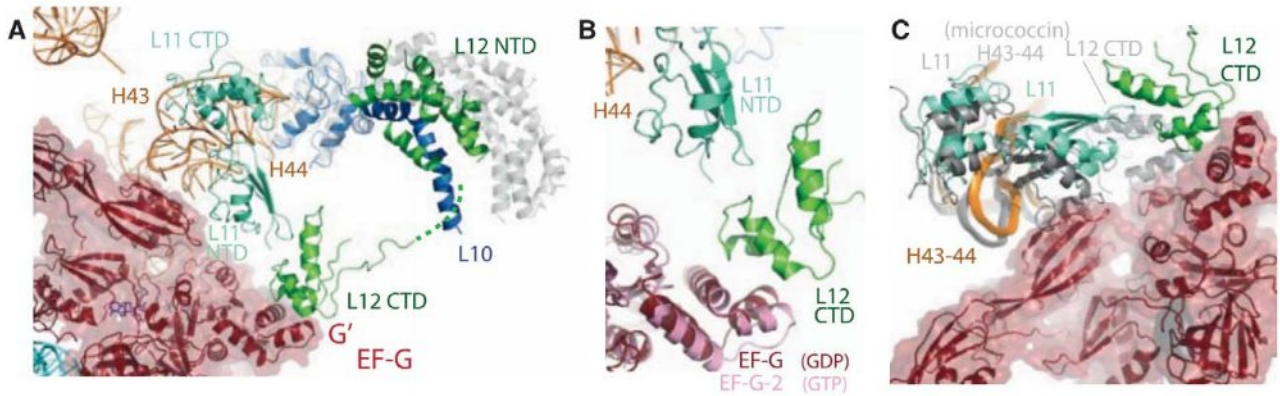

Fig. 6. Interaction of EF-G with the L11 region and the L10-L12 stalk. (**A**) Overview showing that EF-G interacts directly with the L11 RNA (helices 43 and 44) through domain V. The L10-L12 stalk has bent towards the L11 region relative to the structure of the isolated stalk (gray) (*40*) as judged by superimposing the globular part of L10. As a result, a copy of the CTD of L12 bridges the G′ domain of EF-G and the NTD of L11 by interacting with both of them. (**B**) Conformational changes in the G′ and G domains of EF-G in the GDP-fusidic acid form in the ribosome (reddish-brown) as compared with the GTP form (pink) (*13*). (**C**) Comparison of the structure of EF-G trapped in the posttranslocational state of the ribosome with the structure of the 50*S* subunit bound to micrococcin (*46*). Domain V of EF-G interacts with helices 43 and 44 of 23*S* RNA that bind L11. A superposition of the micrococcin-bound 50*S* structure (gray) using all of 23*S* RNA shows that helices 43 and 44 (gray) superimpose reasonably well on the EF-G ribosome complex, but the NTD of L11 would clash with domain V of EF-G. The CTD of L12 is in the micrococcin-bound 50*S* structure and is also in a different location and orientation compared with the current structure, where it interacts with the G′ domain.

GTP form of EF-G-2, consistent with previous mutagenesis data (*44*). It is possible that this movement of the G′ domain may transmit conformational changes required for phosphate release, and as seen in Fig. 6b, there is also a shift in the G domain adjacent to the G′ domain, which provides a path to the nucleotide-binding site.

Domain V of EF-G interacts with the tip of the 1067 and 1095 loops of the L11 region of 23*S* RNA. The conformation of this region of 23*S* RNA appears to have only minimal changes compared with the isolated L11-RNA complex (*45*) or a native 50*S* structure (*46*). The binding of micrococcin, which binds to the L11 region and enhances GTPase activity by EF-G, also stabilizes a CTD of L12 near L11 (*46*). Superposition of the micrococcin-bound 50*S* structure shows that the L11 CTD and RNA superimpose reasonably well, but the L11 NTD is in a different orientation that would clash with domain V of EF-G in the current structure (Fig. 6C). Note that the location of the CTD of L12 in the micrococcin structure is different from its location here in the presence of EF-G (Fig. 6C) and is closer to the SRL and the nucleotide-binding site.

In the presence of thiostrepton, which also binds to the L11 region but inhibits EF-G function, the L11 NTD would also be brought closer to EF-G rather than away from it, which would result in a similar clash with EF-G as micrococcin (*46*). Thus, as suggested previously (*46*), the thiostrepton-bound form of the L11 region may allow EF-G binding and GTP hydrolysis, but in the absence of a compensating stabilization of the CTD of L12, may be suboptimal for other functions, such as phosphate release, and may reduce the overall affinity of EF-G, which would explain its loss from ribosomes on centrifugation (*47*).

The role of the CTD of L12 appears to be complex. It appears to be required for initial binding and GTPase activation for both EF-Tu and EF-G, even in single-turnover experiments (*39*, *40*). However, mutations that would disrupt its interactions with the G′ domain inhibit phosphate release without affecting GTPase activation (*44*). Given the two different locations for the CTD of L12 in the micrococcin bound 50*S* structure (*46*) and the EF-G complex of the ribosome here (Fig. 6C), it is tempting to speculate that the former location, which could be common to EF-Tu and EF-G, may be involved in GTPase activation, whereas the latter location, which specifically involves the G′ domain, is involved in the release of inorganic phosphate. Clearly, studies with the 70*S* ribosome in other states, as well as with micrococcin, will help to clarify this issue.

Conclusion. This work reports a crystal form, obtained from ribosomes lacking protein L9, that allows crystallization of the ribosome in the presence of GTPase factors. The structure reported here reveals details of the ribosome complexed with EF-G trapped in the posttranslocational state by the antibiotic fusidic acid. It reveals many aspects of EF-G function, in addition to providing a more complete model of the ribosome that includes the entire L1 stalk and much of the L10-L12 stalk. The close interactions of domain IV of EF-G with the 30*S* subunit suggest how it could facilitate translocation without slippage of the reading frame. The structure shows changes in the crucial switch regions around the nucleotide-binding pocket that accompany GTP hydrolysis and may couple it to movement of the subunits. It reveals the location of fusidic acid and shows how the antibiotic may trap EF-G on the ribosome by preventing conformational changes required for its release after translocation. The structure also sheds light on the interactions of EF-G with the L12 stalk and the L11 binding region. Further understanding of EF-G function in translation will require its structure in complex with the ribosome in other states, e.g., before GTP hydrolysis and translocation, as well as in posttermination complexes with ribosome-recycling factor. Finally, this work paves the way for the study of other GTPase factors bound to the ribosome.

References and Notes

1. V. Ramakrishnan, *Cell* **108**, 557 (2002).
2. D. Moazed, H. F. Noller, *Nature* **342**, 142 (1989).
3. J. Frank, R. K. Agrawal, *Nature* **406**, 318 (2000).
4. D. N. Ermolenko *et al.*, *Nat. Struct. Mol. Biol.* **14**, 493 (2007).
5. M. V. Rodnina, A. Savelsbergh, V. I. Katunin, W. Wintermeyer, *Nature* **385**, 37 (1997).
6. A. Aevarsson *et al.*, *EMBO J.* **13**, 3669 (1994).
7. J. Czworkowski, J. Wang, T. A. Steitz, P. B. Moore, *EMBO J.* **13**, 3661 (1994).
8. P. Nissen *et al.*, *Science* **270**, 1464 (1995).
9. R. K. Agrawal, P. Penczek, R. A. Grassucci, J. Frank, *Proc. Natl. Acad. Sci. U.S.A.* **95**, 6134 (1998).
10. R. K. Agrawal, A. B. Heagle, P. Penczek, R. A. Grassucci, J. Frank, *Nat. Struct. Biol.* **6**, 643 (1999).
11. H. Stark, M. V. Rodnina, H. J. Wieden, M. van Heel, W. Wintermeyer, *Cell* **100**, 301 (2000).
12. M. Valle *et al.*, *Cell* **114**, 123 (2003).
13. S. R. Connell *et al.*, *Mol. Cell* **25**, 751 (2007).
14. Materials and methods are available as supporting material on *Science* Online.
15. B. S. Schuwirth *et al.*, *Science* **310**, 827 (2005).
16. A. Korostelev, S. Trakhanov, M. Laurberg, H. F. Noller, *Cell* **126**, 1065 (2006).
17. M. Selmer *et al.*, *Science* **313**, 1935 (2006).
18. D. M. Cameron *et al.*, *J. Bacteriol.* **186**, 5819 (2004).
19. S. Hansson, R. Singh, A. T. Gudkov, A. Liljas, D. T. Logan, *J. Mol. Biol.* **348**, 939 (2005).
20. K. A. Martemyanov, A. T. Gudkov, *J. Biol. Chem.* **275**, 35820 (2000).
21. R. M. Voorhees, A. Weixlbaumer, D. Loakes, A. C. Kelley, V. Ramakrishnan, *Nat. Struct. Mol. Biol.* **16**, 528 (2009).
22. Single-letter abbreviations for the amino acid residues are as follows: A, Ala; C, Cys; D, Asp; E, Glu; F, Phe; G, Gly; H, His; I, Ile; K, Lys; L, Leu; M, Met; N, Asn; P, Pro; Q, Gln; R, Arg; S, Ser; T, Thr; V, Val; W, Trp; and Y, Tyr.

23. A. Savelsbergh, N. B. Matassova, M. V. Rodnina, W. Wintermeyer, *J. Mol. Biol.* **300**, 951 (2000).
24. K. A. Martemyanov, A. S. Yarunin, A. Liljas, A. T. Gudkov, *FEBS Lett.* **434**, 205 (1998).
25. J. M. Ogle *et al.*, *Science* **292**, 897 (2001).
26. F. Peske, A. Savelsbergh, V. I. Katunin, M. V. Rodnina, W. Wintermeyer, *J. Mol. Biol.* **343**, 1183 (2004).
27. S. al-Karadaghi, A. Aevarsson, M. Garber, J. Zheltonosova, A. Liljas, *Structure* **4**, 555 (1996).
28. T. M. Schmeing *et al.*, *Science* 15 October 2009 (10.1126/science.1179700).
29. J. W. Bodley, F. J. Zieve, L. Lin, *J. Biol. Chem.* **245**, 5662 (1970).
30. H. S. Seo *et al.*, *Biochemistry* **45**, 2504 (2006).
31. M. Laurberg *et al.*, *J. Mol. Biol.* **303**, 593 (2000).
32. K. A. Martemyanov, A. Liljas, A. S. Yarunin, A. T. Gudkov, *J. Biol. Chem.* **276**, 28774 (2001).
33. U. Johanson, D. Hughes, *Gene* **143**, 55 (1994).
34. I. Nagaev, J. Bjorkman, D. I. Andersson, D. Hughes, *Mol. Microbiol.* **40**, 433 (2001).
35. I. A. Murray *et al.*, *J. Mol. Biol.* **254**, 993 (1995).
36. P. A. Zunszain, J. Ghuman, A. F. McDonagh, S. Curry, *J. Mol. Biol.* **381**, 394 (2008).
37. R. Jorgensen *et al.*, *Nat. Struct. Biol.* **10**, 379 (2003).
38. L. Vogeley, G. J. Palm, J. R. Mesters, R. Hilgenfeld, *J. Biol. Chem.* **276**, 17149 (2001).
39. D. Mohr, W. Wintermeyer, M. V. Rodnina, *Biochemistry* **41**, 12520 (2002).
40. M. Diaconu *et al.*, *Cell* **121**, 991 (2005).
41. M. V. Rodnina *et al.*, *Proc. Natl. Acad. Sci. U.S.A.* **96**, 9586 (1999).
42. D. Pan, S. V. Kirillov, B. S. Cooperman, *Mol. Cell* **25**, 519 (2007).
43. P. P. Datta, M. R. Sharma, L. Qi, J. Frank, R. K. Agrawal, *Mol. Cell* **20**, 723 (2005).
44. A. Savelsbergh, D. Mohr, U. Kothe, W. Wintermeyer, M. V. Rodnina, *EMBO J.* **24**, 4316 (2005).
45. B. T. Wimberly, R. Guymon, J. P. McCutcheon, S. W. White, V. Ramakrishnan, *Cell* **97**, 491 (1999).
46. J. M. Harms *et al.*, *Mol. Cell* **30**, 26 (2008).
47. D. M. Cameron, J. Thompson, P. E. March, A. E. Dahlberg, *J. Mol. Biol.* **319**, 27 (2002).
48. W. L. DeLano, www.pymol.org (2006).
49. X. Agirrezabala *et al.*, *Mol. Cell* **32**, 190 (2008).
50. We thank C. Schulze-Briese, M. Fuchs, and M. Wang for help with data collection at the Swiss Light Source; J. Frank for coordinates of the ratcheted ribosome obtained from modeling into cryo-EM maps; J. Hentschel for help with crystallization trials; M. Schmeing and R. Voorhees for help with data collection, making figures, and critical feedback; and C. Neubauer and L. Ng for useful discussions. V.R. was supported by the U.K. Medical Research Council, a Wellcome Trust program grant, and awards from the Agouron Institute and the Louis-Jeantet Foundation. Coordinates for the structure have been deposited in the Protein Data Bank as four split entries with codes 2wri, 2wrj, 2wrk, and 2wrl.

Supporting Online Material

www.sciencemag.org/cgi/content/full/1179709/DC1
Materials and Methods
Figs. S1 to S3
Table S1
References

27 July 2009; accepted 9 September 2009
Published online 15 October 2009;
10.1126/science.1179709
Include this information when citing this paper.

High-Temperature Superconductivity in a Single Copper-Oxygen Plane

G. Logvenov, A. Gozar, I. Bozovic*

The question of how thin cuprate layers can be while still retaining high-temperature superconductivity (HTS) has been challenging to address, in part because experimental studies require the synthesis of near-perfect ultrathin HTS layers and ways to profile the superconducting properties such as the critical temperature and the superfluid density across interfaces with atomic resolution. We used atomic-layer molecular beam epitaxy to synthesize bilayers of a cuprate metal ($La_{1.65}Sr_{0.45}CuO_4$) and a cuprate insulator (La_2CuO_4) in which each layer is just three unit cells thick. We selectively doped layers with isovalent Zn atoms, which suppress superconductivity and act as markers, to show that this interface HTS occurs within a single CuO_2 plane. This approach may also be useful in fabricating HTS devices.

Some of the cuprate materials that show high-temperature superconductivity (HTS) are extremely anisotropic, which raises the question of how thin a cuprate layer can be while still retaining HTS. Can a single CuO_2 layer be superconducting, and if this is the case, how does its maximal critical temperature (T_c) compare to that in bulk samples? In two-dimensional (2D) systems, true long-range order is not possible (*1*), but a quasi–long-range order (and, in particular, superconductivity) may occur (*2*–*4*). The above question is also of fundamental importance because much of the current HTS theory is based on purely 2D models (*5*, *6*). To answer this question experimentally, an essentially perfect ultrathin HTS film is needed, but this objective has proven hard to reach (*7*–*14*). The problem is that in ultrathin cuprate films, T_c can be reduced for many reasons, including surface roughness, cation interdiffusion across the interface, strain arising from mismatch in the lattice constants, structure reconstruction caused by electrostatic incongruity between the two ionic crystals, and charge depletion or accumulation driven by the difference in chemical potentials. Within the La-Sr-Cu-O family of compounds, the highest T_c reported (*13*) is ~10 K in a $La_{1.9}Sr_{0.1}CuO_4$ layer two unit cells thick—the total of nominally four superconducting CuO_2 planes. (In $La_{2-x}Sr_xCuO_4$ compounds, one unit cell contains two CuO_2 layers.)

Another way to approach this problem emerges from a recent discovery of high-T_c interface superconductivity (*15*) that occurs in bilayers consisting of an insulating La_2CuO_4 (LCO) layer and a nonsuperconducting metallic $La_{1.65}Sr_{0.45}CuO_4$ (LSCO) layer; in such heterostructures, the HTS fluid is confined near the interface. However, a full understanding of interface superconductivity requires atomic-resolution measurements of the variations along the z axis (i.e., perpendicular to the substrate and to the CuO_2 planes) of the chemical composition (e.g., the Sr dopant concentration), the crystallographic structure, the free charge-carrier density (n), and the superfluid density (n_s).

This challenge has already triggered several innovative technical approaches. The chemical composition profile has been measured by ion-scattering spectroscopy as well as electron energy-loss spectroscopy in scanning transmission electron microscopy (EELS-STEM) (*15*). The crystallographic structure has been profiled with the use of synchrotron x-ray diffraction and coherent Bragg rod analysis (COBRA), a phase-retrieval technique that provides accurate positions of atoms within the unit cell in ultrathin films (*16*). The hole density profile in LSCO-LCO superlattices has been determined from soft resonant x-ray scattering (SRXRS) (*17*). An alternative and very promising approach, cross-section atomic force microscopy with a conducting tip, has been pioneered by Basletic *et al.* (*18*), but so far it has not been applied to cuprate superconductors.

The outstanding challenge has been profiling the superconducting properties with atomic resolution; the standard techniques are inherently limited by much larger length scales such as the penetration depth and the coherence length. Here, we accomplish this goal with a method inspired by the so-called δ-doping technique used in semiconductor technology, which amounts to placing the dopant atoms in a single atomic layer. For complex oxides, the feasibility of the technique has been demonstrated and verified by STEM (*19*).

To synthesize films, we used an oxide molecular beam epitaxy (MBE) system equipped with 16 metal sources and a 16-channel atomic absorption spectroscopy system that monitors the atomic fluxes in real time (*20*, *21*). This information is fed to the computer that controls the pneumatic shutters that chop the atomic beams, allowing for atomic layer-by-layer (ALL) film synthesis. A pure ozone source was used to ensure high oxidation power under high-vacuum conditions, so that ad-

Brookhaven National Laboratory, Upton, NY 11973, USA.
*To whom correspondence should be addressed. E-mail: bozovic@bnl.gov

vanced in situ surface analysis tools such as reflection high-energy electron diffraction (RHEED) and time-of-flight ion scattering and recoil spectroscopy (TOF-ISARS) systems could be used, to control the quality of film growth in real time (*21*). Using ALL-MBE, we reproducibly fabricated single-crystal films with atomically smooth surfaces and interfaces, digitally controlling the film thickness. Film stoichiometry was controlled to the 1% level and could be changed on a layer-by-layer basis, enabling us to dope a single, specified layer at will. Figure 1A shows the schematic of such δ-doping in an LSCO-LCO heterostructure.

In the present experiment, doping was achieved by replacing a small amount (3%) of Cu by Zn. The presence of zinc suppresses superconductivity very efficiently (*21*–*25*): 3% Zn doping in $La_{1.85}Sr_{0.15}CuO_4$ reduces T_c by a factor of ~2. However, specific heat (*22*) and nuclear magnetic resonance shift (*23*) measurements show that the carrier density is not affected; Zn is isovalent with Cu. The suppression has been ascribed to pair breaking caused in part by in-plane scattering across the parts of the Fermi surface where the order parameter is out of phase (*21*–*25*). However, for our experiment, the detailed microscopic mechanism is not critical. The Zn → Cu substitution works, as illustrated in Fig. 1B, where we contrast the temperature dependence of resistance in our optimally doped $La_2CuO_{4+\delta}$ and $La_{1.85}Sr_{0.16}CuO_4$ films with their 3% Zn-doped analogs, $La_2Cu_{0.97}Zn_{0.03}O_{4+\delta}$ and $La_{1.85}Sr_{0.16}Cu_{0.97}Zn_{0.03}O_4$.

The ALL synthesis method allows us to dope just a single, predetermined CuO_2 layer with Zn. In this regard, we can perform "δ-doping tomography" and compare a series of samples in which we vary systematically, in increments of 0.5 unit cells, the position of the CuO_2 layer δ-doped by Zn. By studying the transport properties in such a set of samples, we could pinpoint which CuO_2 layers are superconducting. With this motivation, we prepared a set of LSCO-LCO bilayers, with each LSCO or LCO layer exactly three unit cells thick, so that each bilayer film contains 12 CuO_2 planes (Fig. 1A). This thickness is sufficient to reach the maximal T_c in LSCO-LCO bilayers (*15*). Apart from a few undoped control samples, in every bilayer one CuO_2 plane is doped with 3% Zn. The position of the Zn-doped CuO_2 layer is varied systematically from the CuO_2 plane closest to the $LaSrAlO_4$ substrate ($N = -6$) to the one nearest to the free film surface ($N = 6$). The nominal geometric boundary between the metal and the insulator is located between the planes $N = -1$ and $N = 1$.

We studied the superconducting transport properties of these films by measuring the magnetic penetration depth $\lambda(T)$ by mutual inductance technique and the temperature-dependent dc resistance $R(T)$ between 4.2 and 300 K. Typical $R(T)$ characteristics in this set of samples are shown in Fig. 2A. Most of the $R(T)$ curves almost coincide, indicating $T_c = 32 \pm 4$ K; this spread is similar to what we observe in single-phase films. However, one $R(T)$ curve, for the $N = 2$ sample,

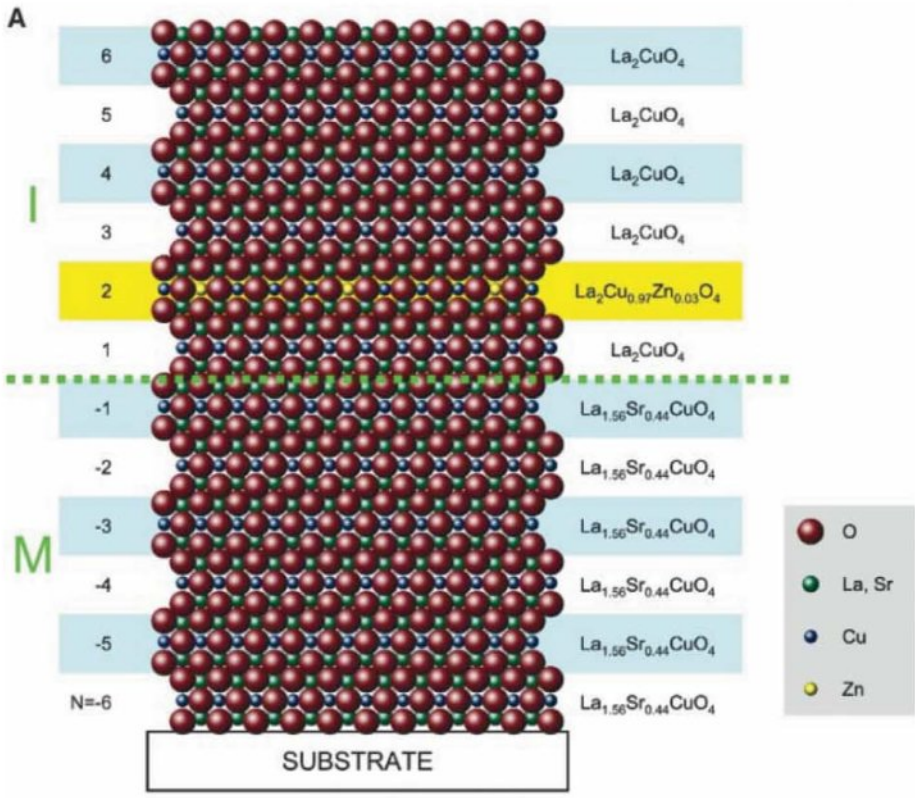

Fig. 1. (**A**) Schematic illustration of δ-doping using atomic layer-by-layer molecular beam epitaxy (ALL-MBE). The model represents a LSCO-LCO bilayer six unit cells thick, such as the ones studied in this work; one unit cell contains two CuO_2 planes. In bulk, LSCO is a non-superconducting metal (M) and LCO is an insulator (I). The green dashed line indicates the position of the nominal geometrical LSCO-LCO interface between the layers $N = -1$ and $N = 1$. By virtue of digital layer-by-layer synthesis, one can dope the selected layer(s) with Zn, which substitutes for Cu. Here, the $N = 2$ CuO_2 plane (the second above the interface) contains some Zn dopant atoms. (**B**) Effect of Zn doping on superconductivity in single-phase LSCO films grown by MBE. The temperature dependence of resistance is shown for LSCO = $La_{1.85}Sr_{0.15}CuO_4$ and LCO* = $La_2CuO_{4+\delta}$ (doped by excess interstitial oxygen) as well as for their analogs doped with 3% Zn, namely Zn-LSCO = $La_{1.85}Sr_{0.15}Cu_{0.97}Zn_{0.03}O_4$ and Zn-LCO* = $La_2Cu_{0.97}Zn_{0.03}O_{4+\delta}$. To facilitate comparison, the resistance of each film is normalized to its value at $T = 45$ K.

is unusual and shows a much lower $T_c \approx 18$ K. In Fig. 2B, we show the measured T_c as a function of the position ($N = -6, -5, \ldots, -1, 1, 2, \ldots, 6$) of the CuO_2 plane doped with Zn. A pronounced depression of T_c, roughly by a factor of 2, occurs when the Zn dopant atoms are placed in the $N = 2$ layer (i.e., in the second CuO_2 plane above the LSCO-LCO interface). The small sample-to-sample variations in T_c could originate from small and uncontrolled variations in any of the factors mentioned above: stoichiometry, surface roughness, cation interdiffusion, strain, structure reconstruction, and charge depletion or accumulation. Nonetheless, the depression of superconductivity observed in $N = 2$ samples, where $T_c = 18 \pm 3$ K, was reproduced in six bilayer samples without exception and is much greater than these random variations. We conclude that this particular CuO_2 layer is responsible for the interface superconductivity with $T_c = 32 \pm 4$ K. Moreover, the data also imply that no other layer has $T_c > 18$ K, if any of them is superconducting at all.

The magnetic measurements show the same dependence on N (Fig. 3). Both T_c and the magnitude of superconducting screening of the magnetic field are markedly reduced only in $N = 2$ samples. The screening can be quantified by the inverse of the perpendicular penetration depth $\lambda_\perp = \lambda^2/d$ (where λ is the usual 3D penetration depth and d is the layer thickness), which is directly proportional to the superfluid density $n_s = (m^*/\mu_0 e^2 d)(1/\lambda_\perp)$, where m^* is the charge carrier effective

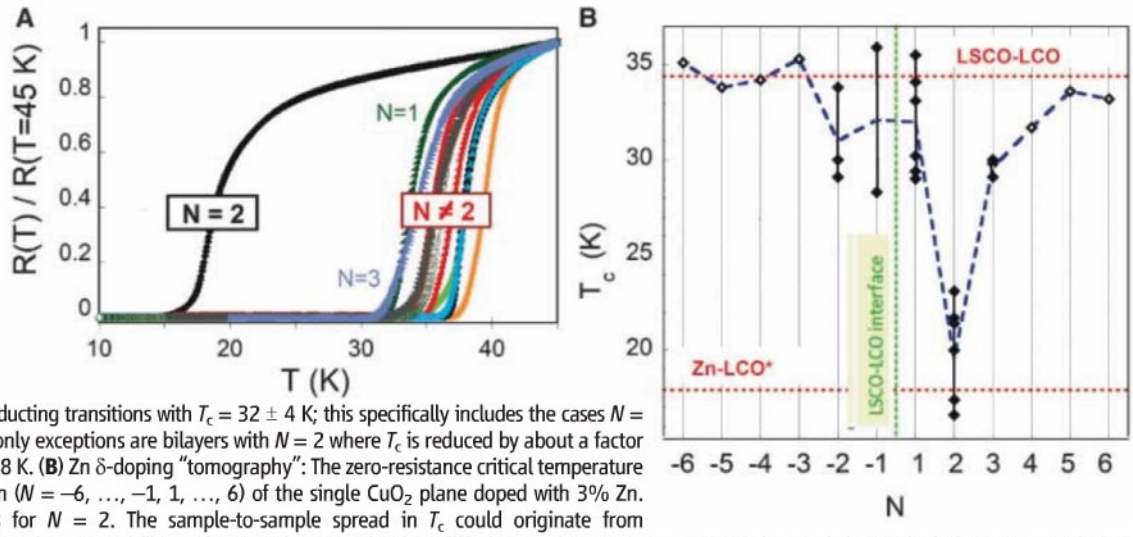

Fig. 2. **(A)** Effect of δ-doping with Zn on superconductivity in LSCO-LCO bilayer films grown by MBE. As defined in the text, LSCO = $La_{1.65}Sr_{0.45}CuO_4$, which is overdoped and metallic but not superconducting per se; LCO = La_2CuO_4, which is an antiferromagnetic insulator. The number N indicates which CuO_2 plane is doped by substituting 3% of Cu by Zn. All the bilayers with $N \neq 2$, including films without any Zn doping, show superconducting transitions with $T_c = 32 \pm 4$ K; this specifically includes the cases $N = 1$ and $N = 3$ as indicated. The only exceptions are bilayers with $N = 2$ where T_c is reduced by about a factor of two; in the one shown $T_c \approx 18$ K. **(B)** Zn δ-doping "tomography": The zero-resistance critical temperature T_c as a function of the position ($N = -6, \ldots, -1, 1, \ldots, 6$) of the single CuO_2 plane doped with 3% Zn. Strong T_c suppression occurs for $N = 2$. The sample-to-sample spread in T_c could originate from uncontrolled small variations in substrate and film surface roughness, cation interdiffusion, strain, structure reconstruction, and charge depletion or accumulation. The open black diamonds (connected by the blue dashed line as a guide to the eye) are the average T_c values for a given N. The red dashed lines indicate typical T_c in LSCO-LCO bilayers without any Zn and in single-phase Zn-LCO* films, respectively. The green dashed line marks the nominal LSCO-LCO interface.

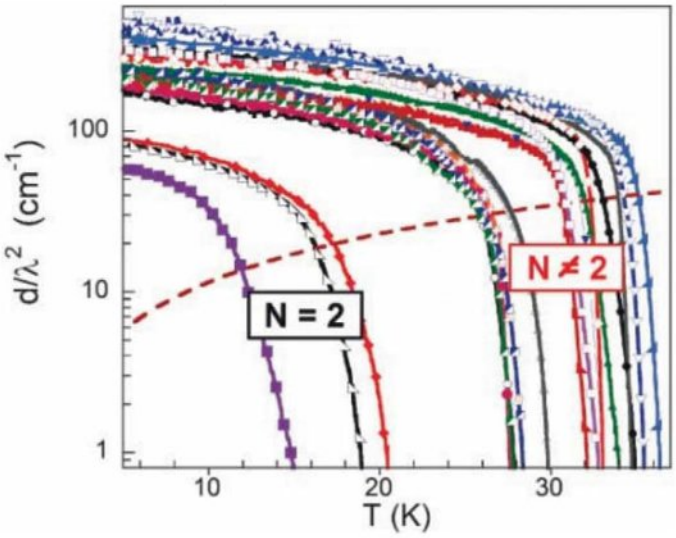

Fig. 3. Effect of Zn δ-doping on superconducting screening (the Meissner effect) in LSCO-LCO bilayer films grown by MBE. The mutual inductance technique (*21*) was used to determine the perpendicular (2D) penetration depth $\lambda_\perp = \lambda^2/d$, which is proportional to the superfluid density $n_s = (m^*/\mu_0 e^2 d)(1/\lambda_\perp)$. Different symbols correspond to different samples. Multiple samples are shown for the three critical doping locations, $N = 1$, $N = 2$ and $N = 3$; detailed sample information is provided in (*21*). The number N indicates which CuO_2 plane is doped by substituting 3% of Cu by Zn. The bilayer with $N = 2$ is again the only exception, showing the reduction in T_c by about a factor of 2 and the reduction of $n_s(T \to 0)$ by a factor of 4.

mass, μ_0 is the vacuum magnetic permeability, and e is the electron charge. The N dependence of $\lambda_\perp$ is particularly informative. The inferred profile of the superfluid carrier density n_s is essentially a δ-function centered at $N = 2$. This conclusion is consistent with all of our experiments so far (*15*–*17*) as well as with numerical simulations.

To be more precise, what we measure is $\lambda_\perp$ rather than n_s; to determine the exact absolute value of the latter, we need to know accurately the values of both d and m^*. This information does not follow directly from our data alone, but because the effect of Zn is just pair breaking (*21*–*25*), we can assume that the thickness of the superconducting layer is independent of whether a tiny amount of Zn has been placed in layer $N = 1$, $N = 2$, $N = 3$, or in none whatsoever. The same should be true of m^* as well (*21*–*25*). Under these assumptions, we can compare the data measured in samples δ-doped with Zn in different layers. The superfluid density decreases in LSCO single crystals and thin films upon Zn doping (*24*, *25*); for a Zn-doping level of 3%, $n_s(T \to 0)$ is reduced by about a factor of 4 to 5. If our metal-insulator bilayer contained two CuO_2 layers with equal superfluid density, we would expect n_s in the sample with no Zn to be ~65% greater than in the sample with 3% Zn in the $N = 2$ layer. If three CuO_2 planes were superconducting, the difference would be even smaller, ~35%, and even less for more planes. However, the effect in Fig. 3 is an order of magnitude greater; once Zn is placed outside the $N = 2$ layer, $1/\lambda_\perp$ increases by ~300 to 400%. This difference shows that most of the superfluid density is confined within the single $N = 2$ layer, whereas the contribution to Meissner screening from all other CuO_2 planes is small.

In Fig. 4A, we show the profile of charge-carrier (hole) density across the LSCO-LCO interface determined from model calculations (*21*) where we take into account the hole depletion or accumulation as well as the smearing of Sr concentration. Hole redistribution arises from the difference between the chemical potentials in LSCO and LCO, and it has been quantified by SRXRS (*17*), whereas the Sr concentration profile has been measured by TOF-ISARS and EELS-STEM (*15*); these data have been used here as the input information. Although the model is simple and approximate, the predictions agree with the experimental data in three key aspects: (i) The highest T_c exceeds 30 K; (ii) HTS occurs in a single CuO_2 plane; and (iii) the "hot" layer is $N = 2$. The CuO_2 layer immediately below ($N = 1$) is overdoped and the one above ($N = 3$) is quite underdoped, and renders $T_c <$ 10 K in either of these two layers. This result is fully consistent with our transport measurement data that show the dip in T_c only when Zn is δ-doped in the $N = 2$ layer. Note that if we assume that the Sr profile is a perfectly sharp step function, from charge transfer alone we infer that near-optimum doping and the highest T_c should occur in the first layer CuO_2 after the interface. We arrive at the same inference if we use the experimentally determined Sr profile but assume that there is no charge depletion or accumulation. Only by the concurrence of both effects is the highest T_c pushed to the second CuO_2 plane above the interface.

From a practical viewpoint, δ-doping in superconducting oxide heterostructures opens path to fabricating HTS electronic devices with modulated superconducting properties. For example, because insertion of few layers doped to this low level does not disrupt epitaxial growth, a trilayer film with Zn-doped barrier with near-perfect interfaces could be synthesized and used to fabricate HTS sandwich Josephson junctions with improved properties and uniformity. One can also envisage devices (such as superconducting field-effect

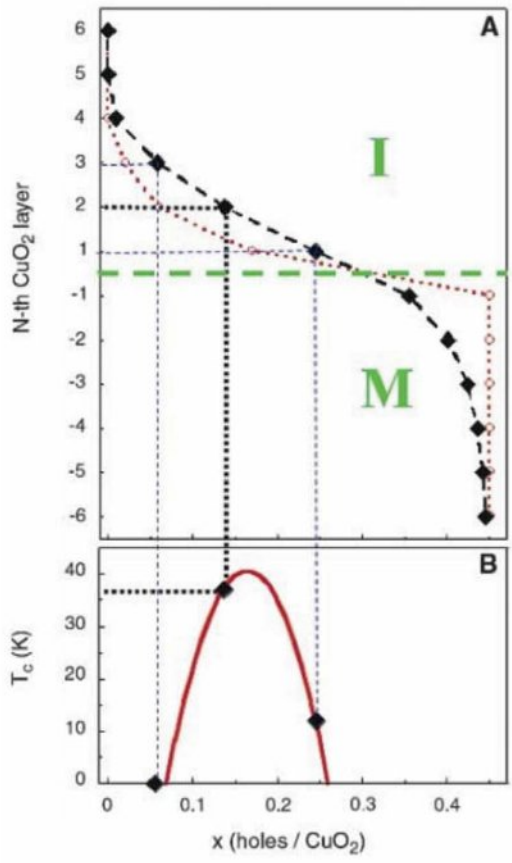

Fig. 4. Profile of charge carrier density across the LSCO-LCO interface. (**A**) The open dots represent the measured Sr concentration profile due to diffusion of Sr atoms from the LSCO layer to the LCO layer. Solid black dots show the charge carrier density in individual CuO_2 layers, as determined in this work. The nominal LSCO-LCO interface is between the layers $N = -1$ and $N = 1$. (**B**) The so-called generic phase diagram of HTS, i.e., the dependence of T_c on the carrier density. The dashed lines between (A) and (B) show interrelation between the charge profile across the interface and the corresponding T_c in the respective CuO_2 planes. Apparently, only the $N = 2$ CuO_2 plane is expected to have the value of T_c near that in optimally doped LSCO, whereas the overdoped $N = 1$ plane can have T_c as low as 10 K and the $N = 3$ plane is underdoped and may not be superconducting at all.

transistors) with ultrathin HTS electrodes transparent to electric and magnetic fields.

Apart from superconductivity (*15*, *26*), strongly correlated oxide heterostructures show a range of other fascinating interface electronic phenomena, including formation of high-mobility 2D electron gases, the quantum Hall effect, and magnetism (*27*–*29*). With the proper choice of dopant atoms to which the property of interest is most sensitive, our δ-doping tomography technique can also be applied to profile with atomic resolution these electronic states and to engineer the interface properties.

References and Notes

1. N. D. Mermin, H. Wagner, *Phys. Rev. Lett.* **17**, 1133 (1966).
2. V. L. Ginzburg, *Phys. Scr.* **T27**, 76 (1989).
3. V. L. Berezinskii, *Sov. Phys. JETP* **32**, 493 (1971).
4. J. M. Kosterlitz, D. J. Thouless, *J. Phys. Chem.* **6**, 1181 (1973).
5. E. Dagotto, *Rev. Mod. Phys.* **66**, 763 (1994).
6. P. A. Lee, N. Nagaosa, X. G. Wen, *Rev. Mod. Phys.* **78**, 17 (2006).
7. I. Bozovic, J. N. Eckstein, in *Physical Properties of Superconductors, Vol. 5*, D. M. Ginsberg, Ed. (World Scientific, Singapore, 1996), pp. 99–207.
8. J. M. Triscone, Ø. Fischer, *Rep. Prog. Phys.* **60**, 1673 (1997).
9. T. Sugimoto *et al.*, *Appl. Phys. Lett.* **58**, 1103 (1991).
10. T. Terashima *et al.*, *Phys. Rev. Lett.* **67**, 1362 (1991).
11. I. Bozovic, J. N. Eckstein, G. F. Virshup, *Physica C* **235–240**, 178 (1994).
12. M. Calame *et al.*, *Phys. Rev. Lett.* **86**, 3630 (2001).
13. A. Rüfenacht *et al.*, *Solid State Electron.* **47**, 2167 (2003).
14. I. Hetel, T. R. Lemberger, M. Randeria, *Nat. Phys.* **3**, 700 (2007).
15. A. Gozar *et al.*, *Nature* **455**, 782 (2008).
16. H. Zhou *et al.*, http://arxiv.org/abs/0903.2097 (2009).
17. S. Smadici *et al.*, *Phys. Rev. Lett.* **102**, 107004 (2009).
18. M. Basletic *et al.*, *Nat. Mater.* **7**, 621 (2008).
19. A. Ohtomo, D. A. Muller, J. L. Grazul, H. Y. Hwang, *Nature* **419**, 378 (2002).
20. I. Bozovic, *IEEE Trans. Appl. Supercond.* **11**, 2686 (2001).
21. See supporting material on *Science* Online.
22. J. W. Loram, K. A. Mirza, P. F. Freeman, *Physica C* **171**, 243 (1990).
23. H. Alloul *et al.*, *Phys. Rev. Lett.* **67**, 3140 (1991).
24. C. Bernhard *et al.*, *Phys. Rev. Lett.* **77**, 2304 (1996).
25. K. Karpinska *et al.*, *Phys. Rev. Lett.* **84**, 155 (2000).
26. N. Reyren *et al.*, *Science* **317**, 1196 (2007); published online 1 August 2007 (10.1126/science.1146006).
27. A. Ohtomo, H. Y. Hwang, *Nature* **427**, 423 (2004).
28. A. Tsukazaki *et al.*, *Science* **315**, 1388 (2007); published online 24 January 2007 (10.1126/science.1137430).
29. A. Brinkman *et al.*, *Nat. Mater.* **6**, 493 (2007).

30. We thank V. L. Ginzburg, D. Schlom, B. Halperin, and S. Kivelson for useful discussions. Supported by the U.S. Department of Energy under contract MA-509-MACA.

Supporting Online Material

www.sciencemag.org/cgi/content/full/326/5953/699/DC1
Materials and Methods
Figs. S1 to S7
References

9 July 2009; accepted 24 August 2009
10.1126/science.1178863

Reconstruction of Molecular Orbital Densities from Photoemission Data

Peter Puschnig,[1]* Stephen Berkebile,[2] Alexander J. Fleming,[2] Georg Koller,[2] Konstantin Emtsev,[3] Thomas Seyller,[3] John D. Riley,[4] Claudia Ambrosch-Draxl,[1] Falko P. Netzer,[2] Michael G. Ramsey[2]

Photoemission spectroscopy is commonly applied to study the band structure of solids by measuring the kinetic energy versus angular distribution of the photoemitted electrons. Here, we apply this experimental technique to characterize discrete orbitals of large π-conjugated molecules. By measuring the photoemission intensity from a constant initial-state energy over a hemispherical region, we generate reciprocal space maps of the emitting orbital density. We demonstrate that the real-space electron distribution of molecular orbitals in both a crystalline pentacene film and a chemisorbed *p*-sexiphenyl monolayer can be obtained from a simple Fourier transform of the measurement data. The results are in good agreement with density functional calculations.

Highest occupied and lowest unoccupied electronic orbitals of molecules are the prime determinants of the respective compounds' chemical, electronic, and optical properties. The electronic states of extended periodic systems are described by band structures, allowed energies E for given momentum values k, and the orbitals are Bloch wave functions associated with a particular k point. For finite systems, such as molecules, the orbitals are viewed as a particular spatial distribution of the electron density at discrete energies. Several experimental methods have enabled imaging of molecular orbitals under certain conditions (*1*). For simple diatomic molecules in the gas phase, high harmonic generation using femtosecond laser pulses allows a tomographic reconstruction of the highest occupied molecular orbital (HOMO) (*2*). Electron momentum spectroscopy, also applied to molecules in the gas phase, can provide the spherically averaged orbital electron density in momentum space (*3*). In the solid state, scanning tunneling microscopy (STM) is a powerful technique for mapping orbital structures of more complex molecules, particularly at cryogenic temperatures on inert decoupling layers (*4*). However, strong bonding interactions with the substrate complicate interpretation of the

[1]Chair of Atomistic Modelling and Design of Materials, University of Leoben, 8700 Leoben, Austria. [2]Institute of Physics, Karl-Franzens University Graz, 8010 Graz, Austria. [3]Lehrstuhl für Technische Physik, Universität Erlangen-Nürnberg, 91058 Erlangen, Germany. [4]Department of Physics, La Trobe University, Victoria 3086, Australia.

*To whom correspondence should be addressed. E-mail: peter.puschnig@unileoben.ac.at

images (*5*), making complementary experimental techniques desirable. Here we demonstrate that ultraviolet angle-resolved photoelectron spectroscopy (ARPES) allows molecular orbital densities to be reconstructed in real space in a rather simple way, as exemplified by analyses of a crystalline pentacene film and a chemisorbed monolayer, *p*-sexiphenyl on Cu (110).

In ARPES (schematically depicted in Fig. 1), an incident photon of energy $\hbar\omega$ excites an electron from a bound initial state, described by wave function ψ_i and energy E_i, to a final electron state ψ_f with kinetic energy E_{kin}. Because energy and momentum parallel to the surface are conserved during the photoemission process, the measurement of the emitted electron's energy and momentum probes the band structure of solids. ARPES is commonly used to study band dispersions, Fermi surfaces, and many-body correlations in a wide range of materials (*6*). A theoretical description of the angle-resolved photocurrent intensity is generally rather involved, and attempts to analyze it in a quantitative manner are rather scarce.

In this work, we treat the photo-excitation as a single coherent process from a molecular orbital to the final state, which is referred to as the one-step model of photoemission (PE). The PE intensity $I(\theta,\phi;E_{kin})$ is given by a Fermi golden rule formula (*7*).

$$I(\theta,\phi;E_{kin}) \propto \sum_i |\langle\psi_f(\theta,\phi;E_{kin})|\mathbf{A}\cdot\mathbf{p}|\psi_i\rangle|^2 \times \delta(E_i + \Phi + E_{kin} - \hbar\omega) \quad (1)$$

Here, the polar and azimuthal emission angles defined in Fig. 1 are denoted by θ and ϕ, respectively. The photocurrent I is given by a sum over all transitions from occupied initial states i described by wave functions ψ_i to the final state ψ_f characterized by the direction (θ,ϕ) and the kinetic energy of the emitted electron. The δ function ensures energy conservation, where Φ denotes the sample work function. The transition matrix element is given in the dipole approximation, where $\mathbf{p}$ and $\mathbf{A}$, respectively, denote the momentum operator and the vector potential of the exciting electro-magnetic wave. The difficulty in evaluating Eq. 1 lies in the proper treatment of the final state. In the most simple approach, it is approximated by a plane wave (PW) characterized only by the direction and wave number of the emitted electron. This has already been proposed more than 30 years ago (*8*), with some success in explaining the observed PE distribution from atoms and small molecules adsorbed at surfaces. Using a PW approximation is appealing because the evaluation of Eq. 1 renders the photocurrent I_i arising from one particular initial state i proportional to the Fourier transform (FT) $\tilde{\psi}_i(\mathbf{k})$ of the initial-state wave function corrected by the polarization factor $\mathbf{A}\cdot\mathbf{k}$:

$$|\tilde{\psi}_i(\mathbf{k})| \propto \frac{\sqrt{I_i(\theta,\phi)}}{|\mathbf{A}\cdot\mathbf{k}|} \quad (2)$$

Thus, if the angle-dependent photocurrent of individual initial states can be selectively measured (as it can for organic molecules where the intermolecular band dispersion is often smaller than the energetic separation of individual orbitals), a one-to-one relation between the photocurrent and the molecular orbitals in reciprocal space can be established. This allows the measurement of the absolute value of the initial-state wave function in reciprocal space and, via a subsequent FT, a reconstruction of molecular orbital densities in real space.

However, attempts to explain ARPES data of oriented films of large polyatomic molecules by a PW final state led to the conclusion that it should not be used in this context (*9*, *10*) because it does not take into account spherical wave effects of the outgoing wave. Thus, the independent atomic center (IAC) approximation was adopted by calculating the emission as an independent, but coherent, sum from individual atomic centers (*11*). The IAC approximation has been used to account for the observed take-off angle dependence of the photocurrent of thin films of organic molecules (*12*). As a further improvement over the IAC, single-scattering (SS) events of the emitted electron have also been taken into account and shown to be important in some applications (*13*, *14*). Here we argue that, despite the obvious simplification of the PW final-state assumption over the more accurate IAC and SS theories, the PW assumption can still lead to a meaningful description of the observed PE intensity of large π-conjugated molecules. As already noted by Grobman (*11*), the IAC expression for the photocurrent can be considerably simplified if the initial molecular orbital comprises atomic orbitals of the same chemical and orbital character. This situation is met by a π molecular orbital of a planar polyatomic molecule for which the contributing atomic orbitals are all of p_z character. For such a case, we show in the supporting online material (SOM) that the angular-dependent photocurrent, computed within the IAC approximation, is given by the FT of the initial state modulated only by a weakly angular-dependent function (*15*). Furthermore, for the special case where the electric field vector of the photon is parallel to the direction of the emitted electron, the IAC reduces exactly to Eq. 2 (*15*, *16*). Thus, the PW final-state assumption can be expected to be valid if the following conditions are fulfilled: (i) π-orbital emissions from large planar molecules; (ii) an experimental geometry in which the angle between the polarization vector $\mathbf{A}$ and the direction of the emitted electron $\mathbf{k}$ is rather small

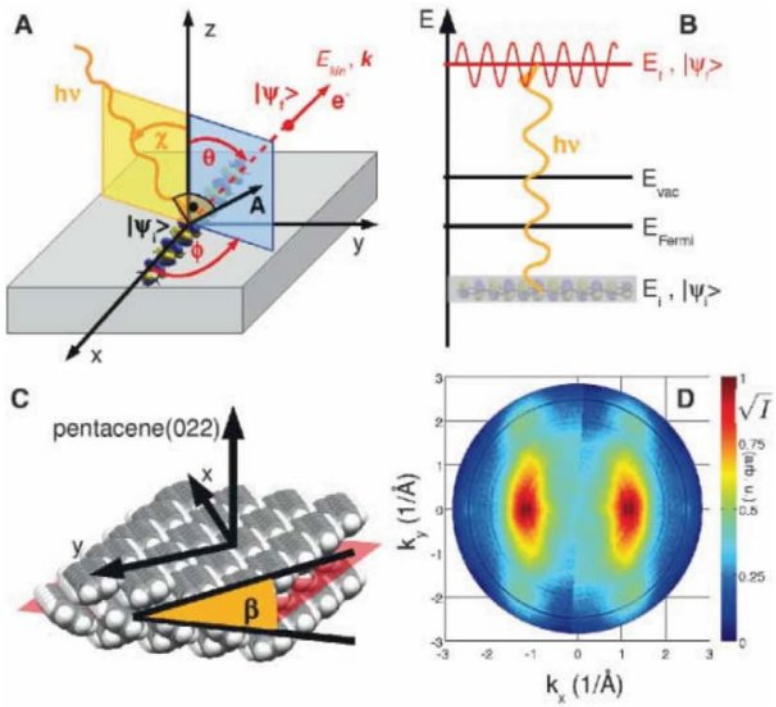

Fig. 1. Momentum maps in angle-resolved PE experiments. (**A**) The incident photon with energy $h\nu$ and vector potential **A** excites an electron from the initial state ψ_i to the final state ψ_f characterized by the kinetic energy E_{kin} and the momentum vector **k**. The polar and azimuthal angles θ and ϕ, respectively, define the direction of the photoemitted electron. (**B**) Schematic energy-level diagram showing the energy of the initial state E_i, the Fermi level E_{Fermi}, the vacuum level E_{vac}, and the final-state energy E_f. (**C**) Model of the pentacene multilayer arrangement on a Cu(110)-(2 × 1)O surface: The long molecular axis points along the *x* axis, and the (022) surface (indicated by the red plane) features pentacene molecules tilted by $\beta = 26°$ out of the *xy* plane. (**D**) Square root of the PE intensity as a function of azimuthal and polar angle after conversion to momentum (azimuthal scan) at a constant binding energy of 1.3 eV ($h\nu$ = 35 eV) corresponding to the pentacene HOMO.

(Fig. 1A); and (iii) molecules consisting of many light atoms (H, C, N, O). The third requirement is a result of the small scattering cross section of light atoms and the presence of many scattering centers expected to lead to a rather weak and structureless angular pattern (*14*, *17*). In the SOM, we compare the PW approach with calculations within the framework of the IAC and SS theories from the literature for a typical π-conjugated organic molecule satisfying the above-mentioned conditions, thereby demonstrating the agreement among the theoretical results as well as with the experimental data (*15*).

We continue by demonstrating the viability of the PW approach for both reciprocal space mapping as well as real-space reconstructions of relatively complicated molecular orbitals. We first present results for the organic π-conjugated molecular semiconductor pentacene in a multilayer thin film, focusing on the emission from the HOMO. As a second example, we show that the approach allows reconstruction of the orbitals of *p*-sexiphenyl bonded to the Cu (110) surface. Not only do we reconstruct a real-space image of the HOMO, but we also show that the PE intensity at the Fermi level that appears on adsorption has the orbital structure of the lowest unoccupied molecular orbital (LUMO).

Pentacene is a planar aromatic molecule consisting of five linearly edge-fused phenyl rings, and has been extensively studied owing to its interesting optoelectronic properties. Its electronic structure, in particular the intermolecular HOMO dispersion, has been analyzed by means of both PE experiments (*18*–*20*) and calculations within the framework of density functional theory (DFT) (*21*–*23*). When the molecule is vacuum deposited on the p(2 × 1) oxygen-reconstructed Cu(110) surface, its long axis orients parallel to the oxygen rows, resulting in crystalline pentacene(022) films (*24*) (Fig. 1C). The (022) surface termination exhibits molecules with their long axis parallel to the surface but with the π face tilted out of the surface plane by an angle of β = 26°. Figure 1D shows a momentum map at the HOMO energy of a pentacene multilayer using a toroidal electron energy analyzer at the synchrotron radiation facility BESSY II (*25*). As a function of the momentum vector parallel to the molecular axis, k_x, there is a pronounced intensity maximum of the PE intensity centered at 1.15 Å^{-1}, as observed previously (*20*). In the momentum maps, these intense features extend about ±0.8 Å^{-1} in the k_y direction, and in addition, there are weaker-intensity lobes at about the same k_x value around $k_y \approx \pm 2$ Å^{-1}.

To illustrate the relation between the measured PE intensity and the FT of the emitting orbital, we calculate the electronic structure of an isolated pentacene molecule using DFT (*26*). The resulting HOMO orbital is depicted in Fig. 2A, and its corresponding three-dimensional FT in Fig. 2B. Because the momentum maps are measured at constant binding energy, we evaluate the FT on a hemisphere of radius $k = \sqrt{(2m/\hbar^2)E_{kin}}$ (indicated in red). The value of the FT on that hemisphere for a kinetic energy of 29.8 eV is shown in Fig. 2C. However, a comparison with the photoelectron momentum map (Fig. 1D) appears to be unsatisfactory. In particular, the minimum at $k_y = 0$, reflecting the nodal structure of the pentacene HOMO, seems to be absent in the measurement. The reason for this apparent discrepancy is a geometric one: the presence of both +26° and −26° tilt angles β in the film structure. Once this factor is taken into account, the agreement between experiment (Fig. 1D) and theory (Fig. 2D) is excellent. Both the strong maxima at $k_y = 0$ and the weak peaks at $k_y = 2$ Å^{-1} result from the out-of-plane tilt angle of the pentacene molecules (*15*). Clearly, the FT approach describes the PE intensity well and therefore allows molecular orientations to be determined with a precision comparable to that of standard in situ techniques such as near-edge x-ray absorption fine structure (NEXAFS). By varying the tilt angle β in the simulations, we estimate the accuracy of the ARPES approach to be better than 5° (fig. S3). A comparison between the PE intensity and the FT has the added advantage that rather than giving an average orientation, multiple orientations are immediately apparent and can be resolved. Moreover, ARPES works at low photon energies, minimizing damage to the sample, and does not require a tunable photon source.

We next apply the approach to an adsorbed monolayer bound to a metal surface. *p*-Sexiphenyl adsorbs on the Cu(110) surface with its molecular planes parallel to the surface, and orients with its long axis parallel to the Cu rows (*27*), as seen in the STM image in fig. S2B. Upon the adsorption of the molecules, we recognize two new features in the low–binding energy region in the ARPES data acquired parallel to the molecular axis (fig. S2C): one centered at 0.3 eV below the Fermi level, and the other at a binding energy of 1.9 eV at the intersection of the Cu sp and d bands. Momentum maps at these two binding energies (Fig. 3, A and C, respectively) compare well to the calculated FTs of the HOMO and LUMO from an isolated sexiphenyl (Fig. 3, B and D). The main characteristics, maxima at $k_x^{HOMO} \approx \pm 1.45$ Å^{-1} reflecting the spatial periodicity set by the length of one phenyl ring ($2\pi/k_x^{HOMO} \approx 4.3$ Å) (*28*), are observed in the data as well as in the calculation. Also, the width Δk_x, which is inversely proportional to the length of the molecule, appears consistent in the PE data. The same holds for the extension in *y* direction, Δk_y, which is related to the width of a phenyl ring. These findings are

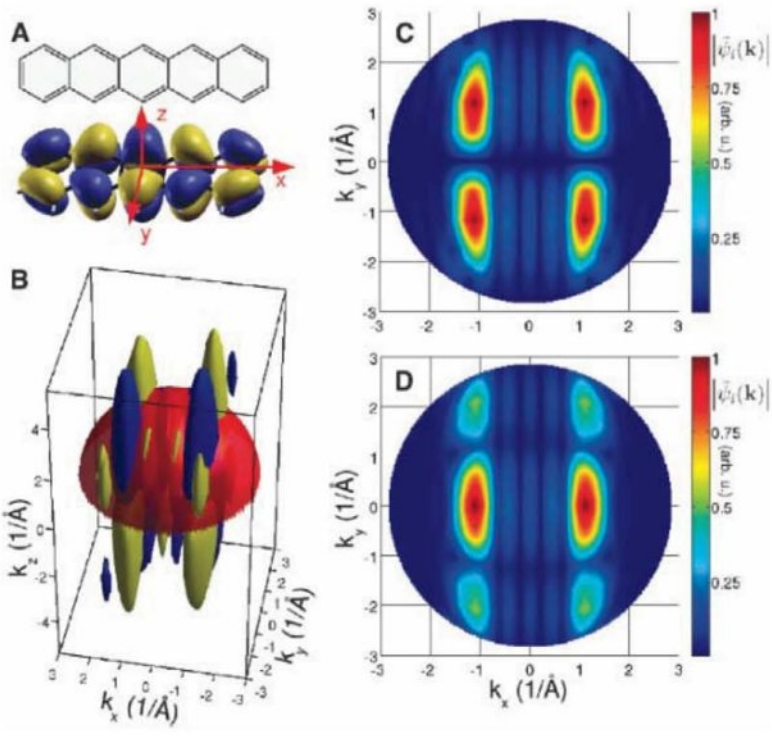

Fig. 2. Calculation of the PE intensity from the FT of the molecular orbital. (**A**) Line drawing and HOMO of pentacene as obtained from a DFT calculation for an isolated molecule. The choice of the coordinate system is indicated, where *x* and *y* are parallel to the long and short molecular axis, respectively, and *z* is perpendicular to the molecular plane. (**B**) Three-dimensional FT of the HOMO as an isosurface plot; blue indicates negative and yellow, positive values, together with a hemisphere of radius $k = \sqrt{(2m/\hbar^2)E_{kin}}$ with a kinetic energy $E_{kin} = 29.8$ eV (see text). (**C**) Absolute value of the HOMO FT on the hemisphere shown in (B). (**D**) Simulation of PE intensity of the pentacene multilayer film, taking into account molecules with tilt angles of β = +26° and β = −26° out of the *xy* plane (see text).

strong evidence that the molecular feature observed at a binding energy of 1.9 eV can indeed be attributed to the sexiphenyl HOMO and, moreover, that its character is preserved even in a strongly interacting monolayer on a metal surface. In a similar manner, we unambiguously assign the intensity close to the Fermi level to an emission from the filled LUMO (Fig. 3, C and D). This emission thus indicates electron transfer from the metal into the former LUMO of the isolated molecule; as was the case for the HOMO, the nodal structure of the LUMO is found to be preserved on adsorption. Thus, PE momentum maps provide fingerprints of molecular states, allowing for their unique identification even in cases where there is a rather strong bonding interaction.

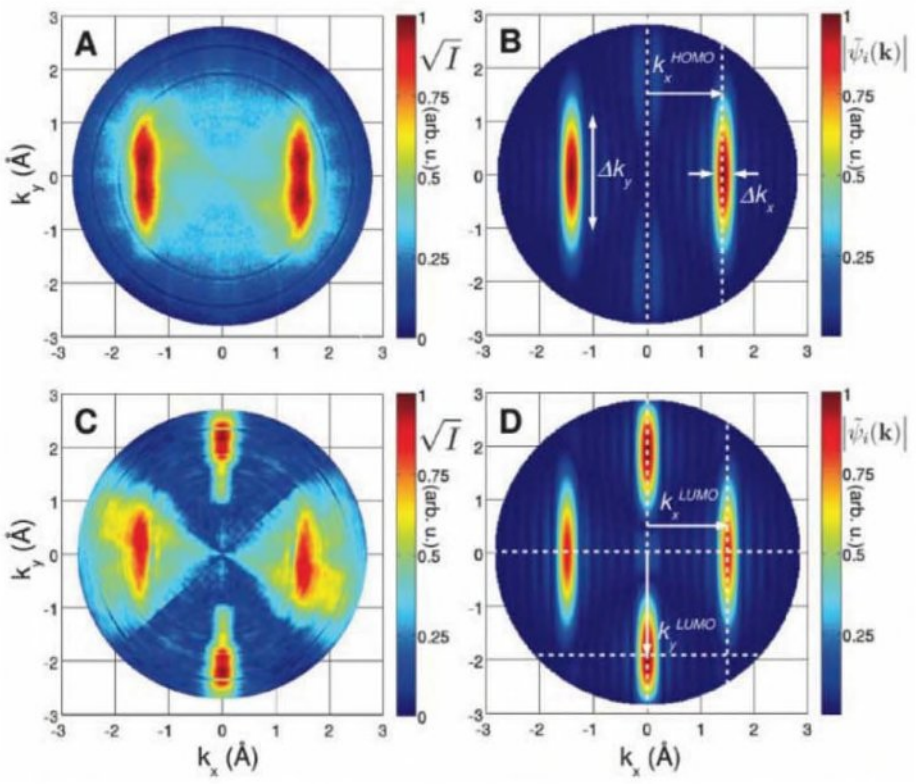

Fig. 3. Measured PE intensities compared to calculated FTs. (**A**) PE momentum map (square root of the intensity) from a monolayer of sexiphenyl on Cu(110) at a binding energy of 1.9 eV, which corresponds to the sexiphenyl HOMO. (**B**) Absolute value of the FT of the sexiphenyl HOMO calculated for an isolated molecule within DFT. (**C**) Same as in (A) but for a binding energy of 0.3 eV. (**D**) Same as in (B) but for the sexiphenyl LUMO. Characteristic features in the computed FTs are indicated by the white arrows, as described in the text.

The ability to reproduce the PE momentum maps with FTs of the initial-state wave functions encouraged us to reconstruct real-space images of the molecular orbital densities from the experimental PE data. From Eq. 2, we take the square root of the PE data and divide it by the polarization factor $|\mathbf{A} \cdot \mathbf{k}| \propto |\sin\theta \cos\chi - \cos\theta \sin\chi|$. Restricting the data to positive k_x values and considering the incidence angle $\chi = -40°$ of the p-polarized photons (Fig. 1A), this function has a maximum for a take-off angle $\theta = 50°$ and a minimum value of 0.64 at normal emission. Before performing the inverse FT of the processed PE data, we mirror the data to the negative k_x plane and change its sign (or leave it unchanged) according to the parity of the wave function, which is even for the HOMO (and odd for the LUMO). By the latter procedure, we restore phase information on the wave function to facilitate the comparison with calculated orbitals. The inverse FTs of the PE data for the adsorbed sexiphenyl HOMO and LUMO are compared with the DFT calculated orbitals of the isolated molecule in Fig. 4. Spatial periodicities and nodal structure are well conserved across theory and experiment. Because the resolution Δx in the reconstructed images is inversely proportional to the PW cutoff k_{max} (thus $\Delta x = \pi/k_{max}$), kinetic energies of around 30 eV as used in our experiments lead to $\Delta x \approx 1$ Å.

Compared to the DFT orbitals, both the HOMO and LUMO electron densities obtained from photoemission are more weighted around the center of the molecule, a distinction we tentatively attribute to the interaction with the Cu surface. Indeed, in sexiphenyl charge-transfer salts, the local distortions and the transferred electrons are located around the center of the molecule (*29*). Further-

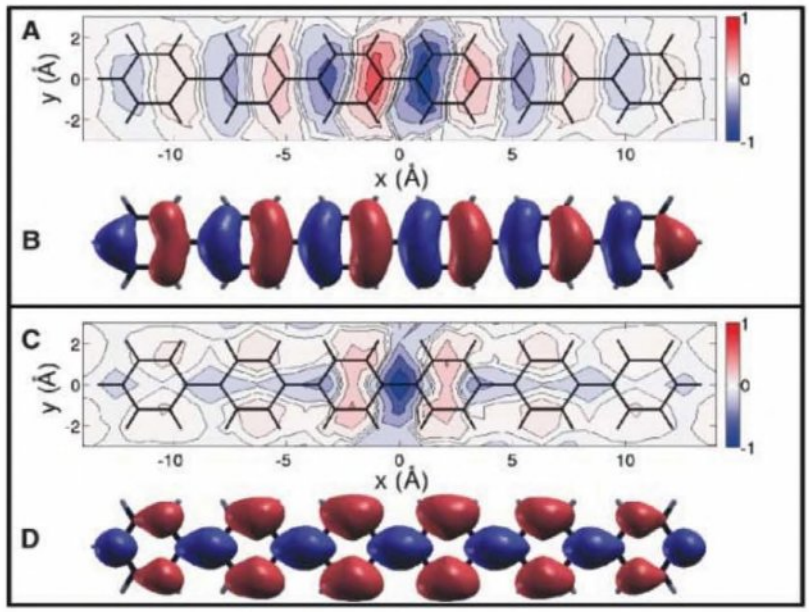

Fig. 4. Molecular orbitals reconstructed from PE data as compared to DFT orbitals. (**A**) The HOMO of sexiphenyl reconstructed from the PE momentum map at a binding energy of 1.9 eV. (**B**) HOMO of an isolated sexiphenyl molecule from DFT. (**C**) The LUMO of sexiphenyl reconstructed from the momentum map at a binding energy of 0.3 eV. (**D**) LUMO of an isolated sexiphenyl molecule from DFT. Experimentally determined orbitals are displayed as density plots, where red colors indicate positive and blue, negative values. For clarity, isolines (dashed lines) are also included. The DFT orbitals are represented as isosurface plots using the same color code. The molecular backbone is indicated by black lines.

more, although STM images typically do not match molecular orbital images exactly, an STM image of a monolayer of sexiphenyl adsorbed on Cu (110) does show an electron density distribution that is weighted toward the center of the molecules (fig. S2B). Nonetheless, improvements in the PE signal-to-background ratio are necessary before any strong conclusions can be reached concerning the extent of orbital distortion introduced by the metal surface.

The demonstrated simple relation between the PE intensity and the FT of the molecular orbital should be a valuable tool for further investigation of organic molecular films and monolayers.

References and Notes

1. W. H. E. Schwarz, *Angew. Chem. Int. Ed.* **45**, 1508 (2006).
2. J. Itatani *et al.*, *Nature* **432**, 867 (2004).
3. C. E. Brion, G. Cooper, Y. Zheng, I. V. Litvinyuk, I. E. McCarthy, *Chem. Phys.* **270**, 13 (2001).
4. J. Repp, G. Meyer, S. M. Stojkovic, A. Gourdon, C. Joachim, *Phys. Rev. Lett.* **94**, 026803 (2005).
5. R. Temirov, S. Soubatch, O. Neucheva, A. C. Lassise, F. S. Tautz, *N. J. Phys.* **10**, 053012 (2008).
6. A. Damascelli, *Phys. Scr.* **T109**, 61 (2004).
7. P. J. Feibelman, D. E. Eastman, *Phys. Rev. B* **10**, 4932 (1974).
8. J. W. Gadzuk, *Phys. Rev. B* **10**, 5030 (1974).
9. T. Permien, R. Engelhardt, C. A. Feldmann, E. E. Koch, *Chem. Phys. Lett.* **98**, 527 (1983).
10. N. V. Richardson, *Chem. Phys. Lett.* **102**, 390 (1983).
11. W. D. Grobman, *Phys. Rev. B* **17**, 4573 (1978).
12. S. Hasegawa *et al.*, *Phys. Rev. B* **48**, 2596 (1993).
13. N. Ueno *et al.*, *J. Chem. Phys.* **107**, 2079 (1997).
14. S. Kera *et al.*, *Chem. Phys.* **325**, 113 (2006).
15. Additional details of sample preparation, experimental setup, and computational methods are available as supporting online material on *Science* Online.
16. S. M. Goldberg, C. S. Fadley, S. Kono, *Solid State Commun.* **28**, 459 (1978).
17. E. L. Shirley, L. J. Terminello, A. Santoni, F. J. Himpsel, *Phys. Rev. B* **51**, 13614 (1995).
18. N. Koch *et al.*, *Phys. Rev. Lett.* **96**, 156803 (2006).
19. H. Kakuta *et al.*, *Phys. Rev. Lett.* **98**, 247601 (2007).
20. S. Berkebile *et al.*, *Phys. Rev. B* **77**, 115312 (2008).
21. M. L. Tiago, J. E. Northrup, S. G. Louie, *Phys. Rev. B* **67**, 115212 (2003).
22. K. Hummer, C. Ambrosch-Draxl, *Phys. Rev. B* **72**, 205205 (2005).
23. D. Nabok *et al.*, *Phys. Rev. B* **76**, 235322 (2007).
24. M. Koini *et al.*, *Thin Solid Films* **517**, 483 (2008).
25. L. Broekman *et al.*, *J. Electron. Spectrosc. Relat. Phenom.* **144–147**, 1001 (2005).
26. X. Gonze *et al.*, *Comput. Mater. Sci.* **25**, 478 (2002).
27. M. Oehzelt *et al.*, *ChemPhysChem* **8**, 1707 (2007).
28. G. Koller *et al.*, *Science* **317**, 351 (2007).
29. M. G. Ramsey, M. Schatzmayr, S. Stafström, F. P. Netzer, *Europhys. Lett.* **28**, 85 (1994).

30. This work was supported by the Austrian Science Foundation (FWF) within the National Research Network S97 "Interface Controlled and Functionalized Organic Films." The ARPES data for this work were measured at the beamline TGM4 of the Helmholtz Zentrum Berlin—Electron storage ring BESSY II supported by the European Community–Research Infrastructure Action under FP7 Programme for Research and Technical Development through the Integrated Infrastructure Initiative "European Light Sources Activities–Synchrotrons and Free Electron Lasers–Grant Agreement 226716."

Supporting Online Material

www.sciencemag.org/cgi/content/full/1176105/DC1
SOM Text
Figs. S1 to S5
References

11 May 2009; accepted 6 August 2009
Published online 10 September 2009;
10.1126/science.1176105
Include this information when citing this paper.

Synergic Sedation of Sensitive Anions: Alkali-Mediated Zincation of Cyclic Ethers and Ethene

Alan R. Kennedy,[1] Jan Klett,[1] Robert E. Mulvey,[1]* Dominic S. Wright[2]

Deprotonation of alkyl and vinyl carbon-hydrogen bonds for synthetic purposes is often hindered not merely by the need for an exceptionally strong base, but by the inherent instability of the resultant anion. Metalation of cyclic ethers adjacent to oxygen, for example, has invariably initiated a ring-opening decomposition pathway. Here, we show that the use of a bimetallic base can overcome such instability through a cooperative combination of zinc-carbon and sodium-oxygen bonding. Both tetrahydrofuran and tetrahydropyran reacted cleanly over days at room temperature to yield α-zinc–substituted products that were sufficiently stable to be isolated and crystallographically characterized. A related zincation-anion trapping strategy, with sodium replaced by potassium, induced clean deprotonation of ethene to yield a stable product. Preliminary electrophilic quenching experiments with the α-zinc–substituted cyclic ethers and benzoyl chloride gave satisfactory yields of the tetrahydrofuran-derived ketone but only trace amounts of the tetrahydropyran-derived ketone.

Transforming relatively inert carbon-hydrogen bonds to more reactive, more useful carbon-metal bonds, or metalation, is an essential tool for constructing compounds. Metalation is usually performed with organolithium reagents because the high electropositivity of lithium leads to polar, reactive $C^{\delta-}$- $Li^{\delta+}$ bonds, which can metalate C-H bonds in organic compounds. Despite their widespread use, organolithium reagents (*1*, *2*) have major limitations, including an inability to metalate low-acidity hydrocarbons (that is, those with high pK_a values, where K_a is the acid dissociation constant). A pertinent example would be ethene, the simplest alkene, which has very weakly acidic H atoms (its estimated pK_a is ~44) (*3*); and although ethene's carbometalation (RLi addition across the C=C bond) and polymerization are common, its metalation in contrast is exceedingly difficult and to date has only been achieved in a few select cases with aggressive, structurally ill-defined superbasic mixtures. Other common drawbacks with organolithium reagents are poor functional group tolerance and low stability of lithiohydrocarbon intermediates. Seeking improved metalating agents, a few groups worldwide have recently pioneered bimetallic alternatives. Notable examples include the lithium zincate $LiZn^tBu_2(TMP)$ [where TMP = 2,2,6,6-tetramethylpiperidide, *cyclo*-$NC(Me)_2(CH_2)_3C(Me)_2$] made by Kondo and Uchiyama and colleagues (*4*) and the lithium magnesiate (TMP)MgCl.LiCl made by Knochel and colleagues (*5*), both of which can selectively metalate a wide variety of aromatic compounds. Bimetallic bases can also effect unusual regioselectivities, as we have shown with the sodium magnesiate [(TMEDA)Na(TMP)(^{n}Bu)Mg(TMP)] (where TMEDA = N,N,N',N'-tetramethylethylenediamine, $Me_2NCH_2CH_2NMe_2$), which metalates toluene in the meta position (*6*), in contrast to the common lateral- and ortho-metalation of aromatic compounds that occurs with conventional bases.

Metalation of ethers is also particularly challenging because metalated ethers are generally highly unstable and rapidly cleave. Such metal-induced ether cleavage is extremely complicated, with several different pathways possible (*7*). With strong bases such as organolithium reagents, metalation (exchange of a C-H bond for a C-metal bond) is generally the opening attack leading to the breakdown of the ether ("protophilic ether cleavage") (*8*). Specifically with the cyclic tetrahydrofuran (THF), metalation at the α-position localizes a high degree of negative charge on the α-C atom adjacent to the electron-rich O atom, causing a severe destabilization that incites a spontaneous ring opening. The final decomposition products depend on conditions, but a mixture of ethene and the enolate of acetaldehyde is common (Fig. 1) (*9*).

Synthetically useful controlled metalation of THF would therefore appear to be an insurmountable challenge. However, we report successful metalation achieved by using a synergic mixed-metal strategy that has far-reaching implications for metalation and organometallic chemistry in general. By mixing an alkali metal with zinc in the same coordination compound, or "alkali-metal–mediated zincation" (AMM*Zn*) (*10*–*12*), we show that not only is it possible to directly metalate (zincate) the

[1]WestCHEM, Department of Pure and Applied Chemistry, University of Strathclyde, Glasgow G1 1XL, UK. [2]Chemistry Department, Cambridge University, Lensfield Road, Cambridge CB2 1EW, UK.

*To whom correspondence should be addressed. E-mail: r.e.mulvey@strath.ac.uk

sensitive cyclic ether with zinc (a metal of low electropositivity that has been long considered too kinetically inert for C-H metalation applications), but also that it can be accomplished with the hypersensitive α-metalated THF fragment staying intact at ambient temperature without any ring opening or cleavage. Extending the scope of this advance, we additionally report an identical reaction with a second cyclic ether, the six-membered heterocyclic homolog tetrahydropyran (THP) (*13*), as well as zincation of ethene (*14*) and the synergic entrapment of its deprotonated fragment, the vinyl anion, by similar alkali metal-zinc cooperativity.

To take on the challenge of a delicate zincation of THF, we designed a milder AMM*Zn* reagent than that previously used for the zincation of several aromatic compounds (*11*). Accordingly, the aggressive $^{t}Bu^{-}$ carbanions within the established AMM*Zn* reagent [(TMEDA)Na(μ-TMP)(μ-^{t}Bu)Zn(^{t}Bu)] (*12*) were replaced with gentler trimethylsilylmethyl ($Me_3SiCH_2^-$) ligands, in which the α-silyl substituent stabilizes the carbanion (*15*). The resulting complex [(TMEDA)Na(μ-TMP)(μ-CH_2SiMe_3)Zn(CH_2SiMe_3)] **1** was characterized by means of a combination of x-ray crystallographic and nuclear magnetic resonance (NMR) spectroscopic studies (*16*). For the reaction with THF, **1** was prepared in situ in hexane solution, and all solvent was removed in vacuo so as to leave a colorless/yellowish residue. This residue was redissolved in neat THF to form a pale yellow solution that was stirred for an extended period. After the removal of some solvent, addition of *n*-hexane to the oily residue, and cooling of the solution to –30°C, colorless block crystals in a best yield of 52.7% (after a 2-week stir; though yields of 42 and 47% were achieved after only a 2-day and 7-day stir, respectively) were obtained. This crystalline product was identified as the α-zincated THF compound [(TMEDA)Na(μ-TMP)(μ-C_4H_7O)Zn(CH_2SiMe_3)] **2**.

Figure 2 shows the molecular structure of **2** as determined with x-ray crystallographic studies (*16*). Its salient feature is the retention of the C_4H_7O cyclic framework of THF with the missing equatorial H atom at one α-C position replaced by a zinc atom. This substitution renders the α-C1 a chiral center (though overall the crystals are racemic), with distorted tetrahedral coordination of C, H, O, and Zn atoms. Stabilization of the trapped THF fragment is provided by bimetallic (Na and Zn) chelation from the (TMEDA)Na(μ-TMP)Zn(CH_2SiMe_3) residue of reagent **1** through Na-O and Zn-C interactions. To effect this deprotonation, **1** has ultimately used one alkyl (Me_3SiCH_2) ligand, which reacts to form tetramethylsilane Me_4Si, though the TMP ligand may be involved at an intermediate stage as observed in other AMM*Zn* reactions (*17*, *18*). The structure of **2** observed in the crystal fits the ^{1}H and ^{13}C NMR spectroscopic data gleaned from [D_6]-benzene solution. Most revealingly, the methylene Me_3SiCH_2 atoms are diastereotopic, appearing as two distinct doublets [at –0.27 and –0.31 parts per million (ppm)], which is a consequence of the chirality of the neighboring α-C center, and all four α-CH_3 groups of TMP are inequivalent (at 1.09, 1.14, 1.43, and 1.48 ppm), as are the two α-$C(Me)_2$ groups in the ^{13}C NMR spectrum (at 31.0 and 34.2 ppm).

Confirmation that this direct zincation-synergic entrapment strategy can be applied to other saturated cyclic ethers comes from the successful reaction of **1** with THP. The isolated crystalline product [(TMEDA)Na(μ-TMP)(μ-C_5H_9O)Zn(CH_2SiMe_3)] **3** (Fig. 3) (*16*) essentially mimics **2** in all of its gross structural features, with the obvious exception that the five-element (NaNZnCO) ring is now fused to a six-atom (OC_5) heterocycle rather than a five-atom homolog. After a 5-day reaction time, a 1:1 mixture of **1** and **3** was obtained in a 29% overall crystalline yield. Despite the mixture that can be ascertained by the superposition of two NMR spectra, the ^{1}H NMR spectrum of a [D_6]-benzene solution shows characteristic signals of the Me_3SiCH_2 atoms (–0.35 and –0.33 ppm of diastereotopic CH_2 and 0.49 ppm of $SiMe_3$) as well as the signals of the α-protons of THP (3.29 and 3.59 ppm).

Turning to the alkene ethene, treatment of its gaseous form in *n*-hexane at 50°C with the synergic potassium zinc reagent (PMDETA)K(TMP)(CH_2SiMe_3)Zn(CH_2SiMe_3) [where PMDETA = N,N,N′N″,N″–pentamethyldiethylenetriamine, $(Me_2NCH_2CH_2)_2NMe$] **4** accomplished the elusive deprotonation in 2 hours; the corresponding sodium zincate **1** proved insufficiently reactive (under the same conditions, only traces of metalated product were found). In the fully characterized crystalline product [(PMDETA)K(μ-TMP)(μ-CH=CH_2)Zn(CH_2SiMe_3)] **5** (Fig. 4) (*16*), the vinyl CH_2=CH^- anion is entrapped by bimetallic chelation via Zn, forming a σ-bond to the deprotonated C atom and K engaging with the π-system of the unsaturated C_2 unit. In contrast, the metal vinyl MCH=CH_2 products of the aforementioned aggressive metal-hydrogen exchange reactions were never isolated or characterized (*19*–*21*) but were invariably used in situ in subsequent reactions. Unlike vinyllithium (*22*), **5** exhibits good solubility in hydrocarbon solvents and is non-pyrophoric.

Some preliminary reactivity studies of the α-zincated ether compounds **2** and **3** have been performed with the common electrophile benzoyl chloride. After a standard electrophilic quenching procedure, the reaction of an in situ mixture of **2** with three molar equivalents of the acid chloride in THF solution gave the desired product phenyl tetrahydrofuran-2-yl ketone (*23*) in an isolated

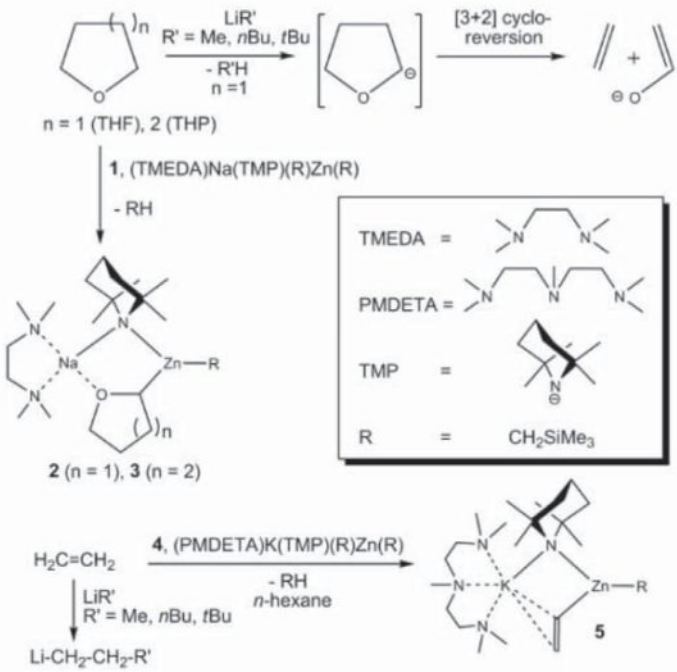

Fig. 1. Formation of compounds **2**, **3**, and **5** as well as alternative reactions with conventional organolithium reagents.

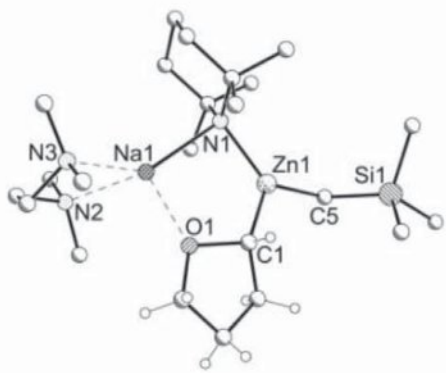

Fig. 2. Molecular structure of **2**. Selected hydrogen atoms and minor disordered groups have been omitted for clarity. Selected bond lengths (in angstroms) and angles (in degrees) are Zn(1)-C(1), 2.040(2); Zn(1)-C(5), 2.0217(17); Zn(1)-N(1), 2.0071(12); Na(1)-N(1), 2.4333(13); Na(1)-O(1), 2.2636(13); O(1)-C(1), 1.495(3); C(1)-Zn(1)-C(5), 117.14(8); C(5)-Zn(1)-N(1), 128.60(6); N(1)-Zn(1)-C(1), 114.26(7); Na(1)-N(1)-Zn(1), 91.45(5); and O(1)-C(1)-Zn(1), 115.20(15).

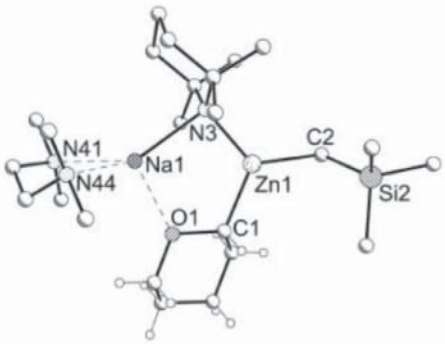

Fig. 3. Molecular structure of **3**. Selected hydrogen atoms and minor disordered groups have been omitted for clarity. Selected bond lengths (in angstroms) and angles (in degrees) are Zn(1)-C(2), 2.027(2); Zn(1)-C(11), 2.037(3); Zn(1)-N(3), 2.008(2); Na(1)-N(3), 2.423(2); Na(1)-O(1), 2.278(2); O(1)-C(11), 1.470(3); C(11)-Zn(1)-C(2), 119.52(11); C(2)-Zn(1)-N(3), 123.98(10); N(3)-Zn(1)-C(11), 116.29(10); Na(1)-N(3)-Zn(1), 95.38(8); and O(1)-C(11)-Zn(1), 114.11(17).

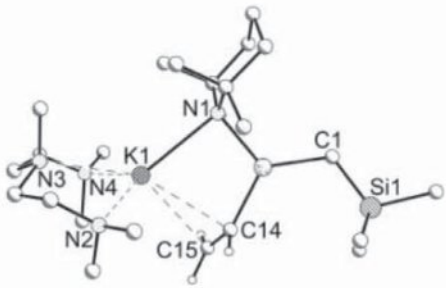

Fig. 4. Molecular structure of one crystallographically independent unit of **5**. Selected hydrogen atoms and minor disordered groups have been omitted for clarity. Selected bond lengths (in angstroms) and angles (in degrees) are Zn(1)-C(11), 2.020(4); Zn(1)-C(2), 2.021(4); C(11)-C(12), 1.330(6); Zn(1)-N(31), 2.016(2); K(1)-N(31), 2.765(3); K(1)-C(11), 2.985(4); K(1)-C(12), 3.167(4); C(11)-Zn(1)-C(2), 125.02(15); C(2)-Zn(1)-N(31), 122.29(14); N(31)-Zn(1)-C(11), 112.68(12); K(1)-N(31)-Zn(1), 91.06(9); and Zn(1)-C(11)-C(12), 129.1(3).

yield of 37.5%. The yield was increased to 71.0% when a crystalline sample of **2** was employed in a similar reaction. Attempts to produce phenyl tetrahydropyran-2-yl ketone from the corresponding reaction with **3** have so far afforded only trace amounts of the planned product. We suspect that in both cases, but especially in the case of **3**, the cyclic ether-functionalized ketones, once formed, partially decompose, leading to a lowering of the observed yields. These promising but contrasting results demand that the reactivities of **2** and **3** are explored with a wide range of electrophiles and in different types of C-C bond–forming reactions.

References and Notes

1. M. Schlosser, Ed., *Organometallics in Synthesis—A Manual* (Wiley, Chichester, ed. 2, 2002).
2. J. Clayden, *Organolithiums: Selectivity for Synthesis* (Elsevier, Oxford, 2002).
3. A. Streitwieser, D. W. Boerth, *J. Am. Chem. Soc.* **100**, 755 (1978).
4. Y. Kondo, M. Shilai, M. Uchiyama, T. Sakamoto, *J. Am. Chem. Soc.* **121**, 3539 (1999).
5. A. Krasovskiy, V. Krasovskaya, P. Knochel, *Angew. Chem. Int. Ed.* **45**, 2958 (2006).
6. P. C. Andrikopoulos *et al.*, *Angew. Chem. Int. Ed.* **44**, 3459 (2005).
7. J. Clayden, S. A. Yasin, *N. J. Chem.* **26**, 191 (2002).
8. A. Maercker, *Angew. Chem. Int. Ed. Engl.* **26**, 972 (1987).
9. R. B. Bates, L. M. Kroposki, D. E. Potter, *J. Org. Chem.* **37**, 560 (1972).
10. R. E. Mulvey, F. Mongin, M. Uchiyama, Y. Kondo, *Angew. Chem. Int. Ed.* **46**, 3802 (2007).
11. R. E. Mulvey, *Acc. Chem. Res.* **42**, 743 (2009).
12. R. E. Mulvey, *Organometallics* **25**, 1060 (2006).
13. T. W. Green, P. G. M. Wuts, *Protective Groups in Organic Synthesis* (Wiley, New York, 1999).
14. Estimated world production of ethene can be found in (*24*).
15. W. Mowat *et al.*, *J. Chem. Soc., Dalton Trans.* 533 (1972).
16. Materials and methods are available as supporting material on *Science* Online.
17. D. Nobuto, M. Uchiyama, *J. Org. Chem.* **73**, 1117 (2008).
18. W. Clegg *et al.*, *J. Am. Chem. Soc.* **131**, 2375 (2009).
19. A. A. Morton *et al.*, *J. Am. Chem. Soc.* **72**, 3785 (1950).
20. L. Brandsma, H. D. Verkruijsse, C. Schade, P. v. R. Schleyer, *J. Chem. Soc. Chem. Commun.* 260 (1986).
21. D. Seyferth, *Organometallics* **28**, 2 (2009).
22. W. Bauer, F. Hampel, *J. Chem. Soc. Chem. Commun.* 903 (1992).
23. E. J. Enholm, J. A. Schreier, *J. Heterocycl. Chem.* **32**, 109 (1995).
24. M. McCoy *et al.*, *Chem. Eng. News* **86 (27)**, 61 (2008).

25. We are indebted to the UK Engineering and Physical Sciences Research Council for financial support (through grant award EP/F0637/1) and the Royal Society/Wolfson Foundation for a research merit award (to R.E.M.). K. W. Klinkhammer, E. Hevia, and C. O'Hara are also thanked for their valuable input through many discussions. Metrical data for **1**, **2**, **3**, and **5** are freely available from the Cambridge Crystallographic Database Center (CCDC) (codes 735270 to 735273).

Supporting Online Material

www.sciencemag.org/cgi/content/full/326/5953/706/DC1
Materials and Methods
Figures
References

23 June 2009; accepted 10 September 2009
10.1126/science.1178165

4D Nanoscale Diffraction Observed by Convergent-Beam Ultrafast Electron Microscopy

Aycan Yurtsever and Ahmed H. Zewail*

Diffraction with focused electron probes is among the most powerful tools for the study of time-averaged nanoscale structures in condensed matter. Here, we report four-dimensional (4D) nanoscale diffraction, probing specific site dynamics with 10 orders of magnitude improvement in time resolution, in convergent-beam ultrafast electron microscopy (CB-UEM). As an application, we measured the change of diffraction intensities in laser-heated crystalline silicon as a function of time and fluence. The structural dynamics (change in 7.3 ± 3.5 picoseconds), the temperatures (up to 366 kelvin), and the amplitudes of atomic vibrations (up to 0.084 angstroms) are determined for atoms strictly localized within the confined probe area (10 to 300 nanometers in diameter). We anticipate a broad range of applications for CB-UEM and its variants, especially in the studies of single particles and heterogeneous structures.

In fields ranging from cell biology to materials science, structures can be imaged in real-space by using electron microscopy. Atomic-scale resolution of structures is usually available from Fourier-space diffraction (*1*–*3*) data, but this approach suffers from the averaging over the selected specimen area which is typically on the micrometer scale. Substantial progress in techniques has enabled localization of diffraction to nanometer- and even angstrom-sized areas by focusing a condensed electron beam onto the specimen. Parallel illumination with a single electron wave vector is reshaped to a convergent beam with a span of incident wave vectors. This method of convergent-beam electron diffraction (CBED) or electron microdiffraction (*1*, *4*) has made possible determination of structures in three dimensions with highly precise localization to areas reaching below one unit cell. The applications have been wide-ranging, from revealing bonding charge distribution (*5*, *6*) and local defects and strains in solids (*7*) to detecting local atomic vibrations and correlations (*8*, *9*). Today, aberration-corrected, atomic-sized convergent electron beams enable analytical probing by using electron-energy-loss spectroscopy (EELS) (*10*) and scanning transmission electron microscopy (STEM) (*11*).

The above-mentioned studies all probed static, or time-averaged, structures. In order to resolve structural dynamics with appropriate spatiotemporal resolution, femtosecond (fs) and picosecond (ps) electron pulses are ideal probes because of their picometer wavelength and their large cross section, resulting from the effective Coulomb interaction with atomic nuclei and core

Physical Biology Center for Ultrafast Science and Technology, Arthur Amos Noyes Laboratory of Chemical Physics, California Institute of Technology, Pasadena, CA 91125, USA.

*To whom correspondence should be addressed. E-mail: zewail@caltech.edu

and valence electrons of matter. Typically, ultrafast electron diffraction is achieved by initiating the physical or chemical change with a pulse of photons (pump) and observing the ensuing dynamics with electron pulses (probe) at later times. By recording sequentially delayed diffraction frames, a "movie" can be produced to reveal the temporal evolution of the transient structures involved in the processes under study. In our laboratory (*12*–*16*), studies in ultrafast electron diffraction and crystallography have spanned phases ranging from isolated molecules to interfaces and macromolecular structures. Other research groups (*17*–*20*) have invoked the techniques, primarily for the study of nonequilibrium melting, lattice distortion, and phonon dynamics.

The spatial resolution in all these time-resolved investigations corresponds to atomic (and subatomic) length scale, but the probed specimen area is on the order of square micrometers, as mentioned above, albeit with a substantially reduced volume when compared with x-ray diffraction [see overviews in (*21*, *22*)]. Thus, these techniques, as with those based on parallel beam illumination, lack the capability of resolving nanometric heterogeneity, for instance in nanometer-sized particles or specific sites in an extended material. Real-space ultrafast electron microscopy (*23*, *24*) can resolve such objects by selected-area imaging, but the diffraction from a selected area is typically averaged over micrometers or more. Accordingly, the analytical and quantitative information available from this parallel-beam diffraction within such areas is somewhat limited. It follows that nanoscale (and finer) time-resolved, convergent-beam diffraction would be of great use in materials science and biology for structural dynamics studies in heterogeneous media.

Here, we report the development of convergent-beam ultrafast electron microscopy (CB-UEM) with applications in the study of nanoscale, site-

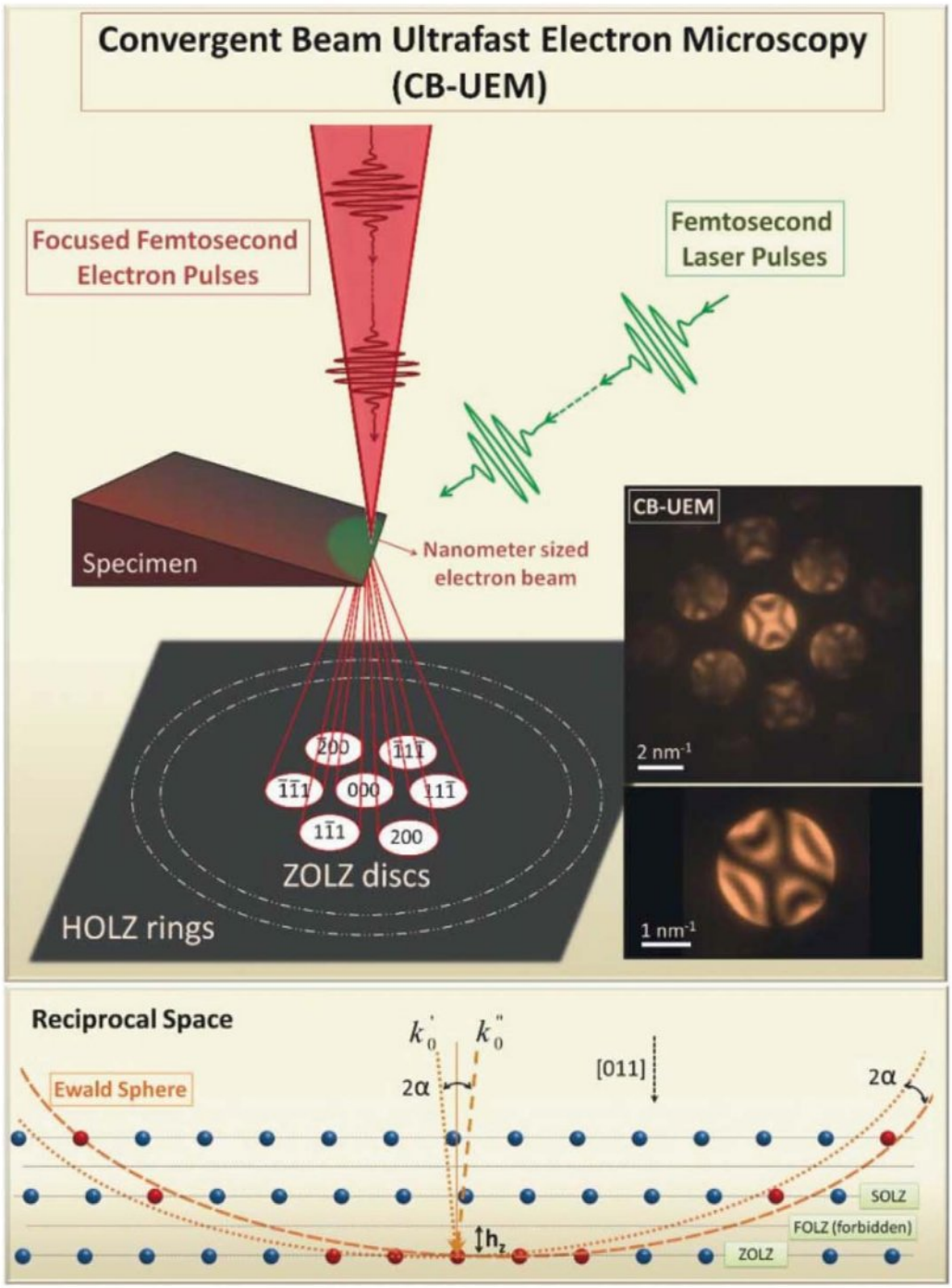

Fig. 1. Schematic of the CB-UEM setup (**top**) and observed low-angle diffraction discs. Femtosecond electron pulses are focused on the specimen to form a nanometer-sized electron beam. Structural dynamics are determined by initiating a change with a laser pulse and then observing the consequences by using electron packets delayed in time. Insets (right) show the CB-UEM patterns taken along the Si [011] zone axis at different magnifications. At the high camera length used, only the ZOLZ discs indexed in the figure are visible; the kinematically forbidden 200 disc appears as a result of dynamic scattering. In the reciprocal space representation of the diffraction process (**bottom**), the Ewald sphere has an effective thickness of 2α, the convergence angle of the electron beam. The diamond structure of Si forbids any reflections from odd-numbered Laue planes when the zone axis is [011].

selected structural dynamics initiated by ultrafast laser heating (10^{14} K s^{-1}). Because of the femtosecond pulsed-electron capability, the time resolution is 10 orders of magnitude improved from that of conventional TEM, which is milliseconds; and, because of beam convergence, high-angle Bragg scatterings are visible with their positions and intensities being very sensitive to both the three-dimensional (3D) structural changes and amplitudes of atomic vibrations. The CB-UEM configuration is shown in Fig. 1; our chosen specimen is a crystalline silicon slab, a prototype material for such investigations. From these experiments, we found that the structural change within the locally probed site occurs with a time constant of 7.3 ± 3.5 ps, which is on the time scale of the rise of lattice temperature known for bulk silicon from the detailed spectroscopic studies of Sjodin *et al.* (*25*). For these local sites, the temperatures measured at different laser fluences range from 299 to 366 K, corresponding to vibrational amplitude changes from 0.077 to 0.084 Å, respectively.

The electron microscope is integrated with a fs oscillator and amplifier laser system in California Institute of Technology's (Caltech's) UEM-2. The fundamental mode of the laser at 1036 nm was split into two beams: The first was frequency doubled to 518 nm and used to initiate the heating of the specimen, whereas the second, which was frequency tripled, was directed to the microscope for extracting electrons from the cathode. The time delay between pump and probe was adjusted by changing the relative optical path lengths of these two pulses. The pulses were sufficiently separated in time (5 μs) to allow for cooling of the specimen.

The electron packets were accelerated to 200 keV (corresponding to a de Broglie wave vector of 39.9 $Å^{-1}$), demagnified, and lastly focused (with a 6-mrad convergence angle) to an area of 10- to 300-nm diameter on the wedge-shaped specimen, as shown in Fig. 1. A wide range of thicknesses, starting from ~2 nm, was accessible simply by moving the electron beam laterally. The silicon specimen was prepared by mechanical polishing of a wafer along the (011) planes, followed by Ar ion milling for final thinning and smoothing; the wedge angle was 2°. In the microscope, Kikuchi lines were observed and used as a guide to orient the specimen with the [011] zone axis being either parallel or tilted relative to the incident electron beam direction.

In Fig. 1, we display typical high-magnification (high-value camera length) CB-UEM patterns of Si obtained when the specimen is unexcited and the zone axis is very close to [011]; the relative magnification can be seen by comparing the disc length scale in Fig. 1 and circle radius in Fig. 2. Unlike parallel-beam diffraction, which yields spots, convergent-beam diffraction produces discs in reciprocal space (back focal plane of the objective lens) with their diameter given by the convergence angle (2α) of the electron pulses. These discs form the zero-order Laue zone (ZOLZ) of the pattern; they show white contrast with thin specimens and exhibit the interference patterns displayed in Fig. 1 when the thickness is increased, as expected (*1*, *4*, *5*).

In the reciprocal space, the effective thickness of the Ewald sphere is 2α (bottom image of Fig. 1), giving rise to multiple spheres that can intersect with higher-order Laue zone (HOLZ) reflections, the focus of this study (Fig. 2) and the key to 3D structural information; the first and second zones, FOLZ and SOLZ, are examples of such zones or rings. The interference patterns in the discs are the result of dynamical scattering in silicon (*1*, *4*, *5*) and are reproduced in our CB-UEM patterns (Fig. 1).

The scattering vectors of HOLZ rings (R) are related to the interzone spacing in the reciprocal space (h_z in $Å^{-1}$) by the tilt angle from the zone axis (η) and by the magnitude of the incident electron's wave vector (k_0). In the plane of the detector and for our tilt geometry, the HOLZ ring scattering vector is given by

$$R \cong \left[k_0^2 \sin^2(\eta) + 2k_0 h_z\right]^{1/2} - k_0 \sin(\eta) \quad (1)$$

where, for our case of the [011] zone axis, $h_z = n/(a\sqrt{2})$; $n = 1,2,3...$ for the different Laue zones with a being the lattice constant. Additionally, for this zone axis, $k + l = n$, where (hkl) are the Miller indices of the reciprocal space. When $k + l = 1$ for FOLZ, k and l must have different parity, which is forbidden by the symmetry of the diamond Si structure. Therefore, the FOLZ along the [011] zone axis should be absent, and the first visible ring should belong to SOLZ; in general, all odd numbered zones will be forbidden. Here, HOLZ indexing is defined according to the face-centered cubic unit cell and not to the primitive one (*1*).

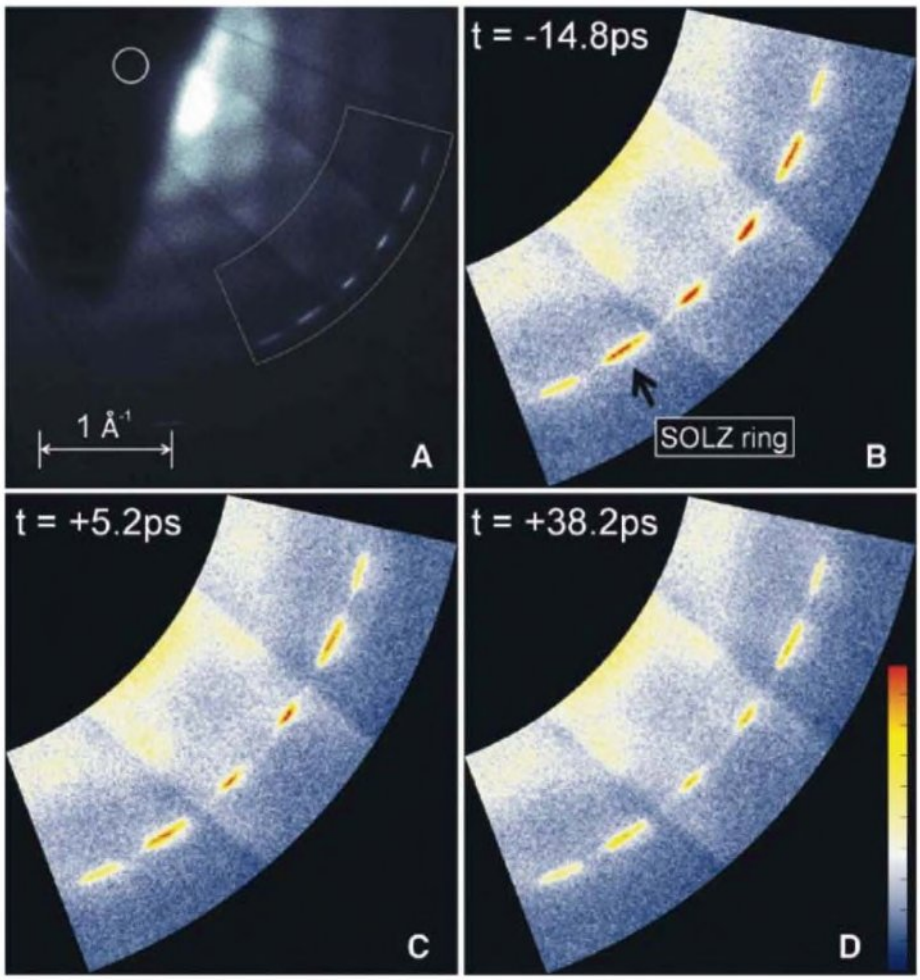

Fig. 2. Temporal frames of CB-UEM. (**A**) High-angle SOLZ ring obtained for a tilt angle of 5.15° from the [011] zone axis. Besides SOLZ, Kikuchi lines and periodic bands (resulting from atomic correlations) are visible. The ZOLZ discs are blocked (top left) to enhance the dynamic range in the area of interest, indicated by the curved box; the disc of the direct beam (the center one in Fig. 1 discs) is indicated by a circle. The intensity scale is logarithmic. (**B** to **D**) Time frames of the SOLZ ring are shown by color mapping for visualization of dynamics. The intensity of the ring changes within picoseconds, but the surrounding background remains at the same level.

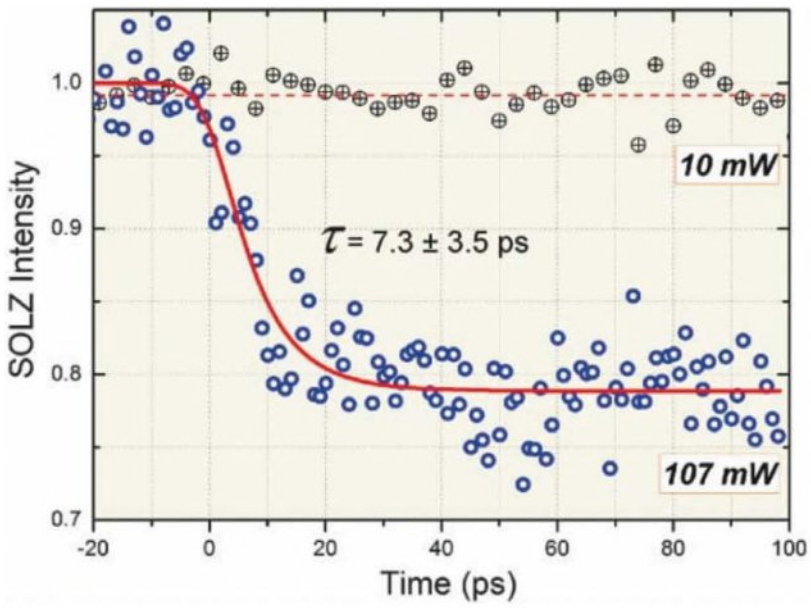

Fig. 3. Diffraction intensities at different times and fluences. Normalized, azimuthally integrated intensity changes of the SOLZ ring are shown, with time ranging from −20 ps to +100 ps, for two different laser powers. Whereas the 10-mW response does not show noticeable dynamics, the 107-mW transient has an intensity change with a characteristic time (τ) of 7.3 ± 3.5 ps. The range of fluences studied was 1.2 to 15 mJ cm^{-2} (Fig. 4). The red curve is a monoexponential fit based on the Debye-Waller effect, as discussed in the text. The red dashed line through the 10 mW data is an average of the points after +20 ps. The dependence on fluence is given in Fig. 4.

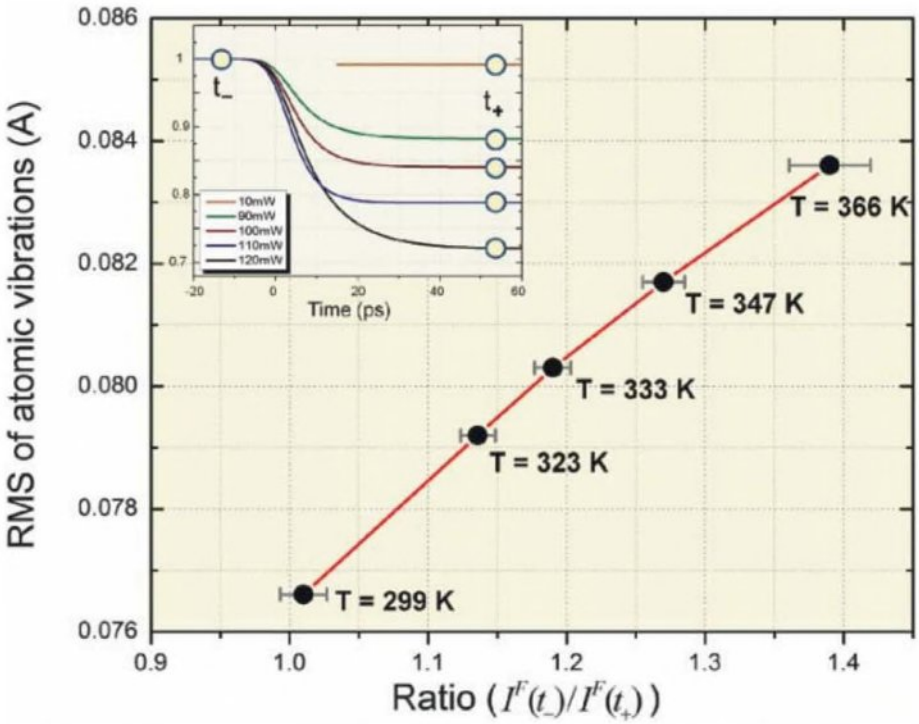

Fig. 4. Amplitudes of atomic vibrations (rms) plotted against the observed intensity change at different fluences. (**Inset**) The monoexponential temporal behavior, with the asymptotes highlighted (circles) for their values at different fluences. The fluence was varied from 1.2 to 15 mJ cm^{-2}. The configuration of the laser excitation is similar to that given in (*23*). This comparative study of the effect of the fluence was performed at a slightly different sample tilt (corresponding to $s = 2.7$ Å^{-1}), corresponding to a thickness of ~80 nm. For each fluence, the temperature represents the effective value for the lattice structural change. The error bars given were obtained from the fits at the asymptotes shown in the inset, and they are determined by the noise level of temporal scans.

The HOLZ ring taken with the CB-UEM is presented in Fig. 2. In order to reduce the strong on-zone-axis dynamic scattering (and to bring the high scattering angles into the range of the recording camera), the slab was tilted 5.15° away from the [011] zone axis, along the [02$\bar{2}$] direction. The scattering vector of the Bragg points of the ring, from the direct beam position, was measured to be 2.2 Å^{-1}, close to the value of 2.22 Å^{-1} obtained by using Eq. 1 for $n = 2$, which identifies the spots shown as part of the SOLZ. From this value, the known lattice separation of 5.4 Å was obtained for silicon.

In addition to the SOLZ ring, Kikuchi lines and some oscillatory bands are also visible in the CB-UEM, as seen in Fig. 2A. Kikuchi lines arise from elastic scatterings of the inelastically scattered electrons, whereas the oscillatory bands in the thermal diffuse scattering (TDS) background result from correlations between the atoms (*9*). We also observed deficit HOLZ lines and interference fringes in ZOLZ discs (*1*, *4*). Although the dynamics in these features may reveal additional intriguing behavior, this report is primarily concerned with the relative intensity change of the SOLZ spots of the ring.

The temporal behavior is displayed in Fig. 2, with three CB-UEM frames taken at time delays of $t = -14.8$ ps, +5.2 ps, and +38.2 ps, together with a static image; the zero of time is defined by the coincidence of the pump and probe pulses in space and time. The frame at negative time has a higher ring intensity than that observed at +38.2 ps, whereas the +5.2 ps frame shows an intermediate intensity value. The results indicate that the intensity change is visible within the first 5 ps of the structural dynamics. For quantification, the intensities in each frame were normalized to the area of azimuthally integrated background. The normalization of the HOLZ ring intensities to the TDS background makes the atomic vibration estimations insensitive to the thickness changes of the probed area (*8*), which may result from slight beam jittering.

Figure 3 depicts the transient behavior of the SOLZ ring intensity for two different laser power, 10 mW and 107 mW, corresponding to pulse fluence of 1.2 and 13 mJ cm^{-2}, respectively, after correcting for power losses; the heating laser beam diameter on the specimen is 60 μm (*23*). The intensities were normalized to the average value obtained at negative times. Whereas the intensity change is essentially absent in the 10-mW data, the results for the 107-mW set show a transient behavior with a characteristic time of 7.3 ± 3.5 ps obtained from the monoexponential fit shown in red in the figure. The temporal response of UEM-2 is on the fs time scale, as obtained by EELS, and it is much shorter than the 7 ps reported here (*26*, *27*).

The local heating of the lattice is responsible for the SOLZ intensity change with time. A pump laser, in our case at 518 nm (2.4 eV), excites the valance electrons of Si to the conduction band; one-photon absorption occurs through

the indirect bandgap at 1.1 eV, and multiphoton absorption excites electron-hole pairs through the direct gap. The excited carriers thermalize within 100 fs (*28*), via carrier-carrier scatterings, and then electron cooling takes place in ~1 ps, by electron-phonon coupling. During this time, lattice heating occurs through increased atomic vibration, reducing SOLZ intensity. The effective lattice temperature is ultimately established with a time constant of a few picoseconds depending on density of carriers or fluence (*25*). However, in CB-UEM measurements the lattice-temperature rise could be slower than in bulk depending on the dimension of the specimen relative to the mean free path of electrons in the solid.

The dynamical change can be quantified by considering a time-dependent Debye-Waller factor with an effective temperature describing the decrease in the Bragg spot intensity with time. If the root mean square (rms) displacement of the atoms, $\langle u_x^2 \rangle^{1/2}$, along one of the three principle axes is denoted by u_x for simplicity and the scattering vector by s, then the HOLZ ring intensity can be expressed as

$$I^F_{\mathrm{Ring}}(t) = I_0(t_-)\exp\left[-4\pi^2 s^2 u_x^2(t)\right] \quad (2)$$

where $I^F_{\mathrm{Ring}}(t)$ is the measured intensity for a given fluence, F, and the vibrational amplitude is now time dependent. Note that u_x^2 is one-third of the total, u^2_{total} (*29*).

In the Einstein model of atomic vibrations, which has been used successfully for silicon (*8*, *30*), the atoms are treated as independent harmonic oscillators, with the three orthogonal components of the vibrations decoupled. As a result, a single frequency (ω) is sufficient to specify the energy eigenstates of the oscillators. The relationship of the vibrational amplitude to temperature can be established by simply considering the Boltzmann average over the populated eigenstates. Consequently, the probability distribution of atomic displacements is derived to be of Gaussian form, with a standard deviation corresponding to the rms (u_x) of the vibration involved (*8*, *30*)

$$u_x = \left[(\hbar/2\omega m)\coth(\hbar\omega/2k_{\mathrm{B}}T_{\mathrm{eff}})\right]^{1/2} \quad (3)$$

where $\hbar$ is Planck's constant, k_{B} the Boltzmann constant, T_{eff} in our case the effective temperature, and m the mass of the oscillator. In the high-temperature limit, that is, when $\hbar\omega/2k_{\mathrm{B}}T << 1$, Eq. 3 simplifies to $m\omega^2 u_x^2 = k_{\mathrm{B}}T$, which is the classical limit for a harmonic oscillator; the zero-point energy, which contributes almost half of the mean vibration amplitude at room temperature, is included in Eq. 3. The value of $\hbar\omega$ is 25.3 meV. Despite its simplicity, the Einstein model in Eq. 3 was remarkably successful in predicting the HOLZ rings and TDS intensities by multislice simulations (*8*, *30*), although it was not as successful in predicting the oscillatory bands in the background, which are due to correlations (*9*).

In Fig. 4, we present the change in the asymptotic intensity with fluence (inset) and the derived vibrational amplitudes for the different temperatures. The amplitudes are directly obtained from Eq. 2 because s is experimentally measured. The relative temperature change (from t_- to t_+) is then derived from Eq. 3, taking the value of u_x at room temperature (297 K) to be 0.076 Å [from both CBED (*30*) and x-ray (*31*) measurements] for the unexcited specimen. The amplitude of atomic vibrations, and hence the temperature, increases as the fluence of the initiating pulse increases. Although the trend is expected for an increased u_x with temperature, the absolute values, from 0.077 to 0.084 Å, correspond to a large 3.2% to 3.6% change in nearest neighbor separation; these values are still well below the 15% criterion for a melting phase transition.

The linear thermal expansion coefficient has been accurately determined for silicon (*32*), and for a value of $2.6 \times 10^{-6}\ \mathrm{K}^{-1}$ at room temperature the vibrational amplitudes reported here are much higher than the equilibrium thermal values at the same temperature. This is because the effective temperature applies to a lattice arrested in a picosecond time window; at longer times, the vibrations equilibrate to a lower temperature (*33*). As such, measuring nanoscale local temperatures on the ultrashort time scale enhances the sensitivity of the probe thermometer by orders of magnitude. Moreover, the excitation per site is substantially enhanced. For a single-photon absorption at the fluence used, we estimate, for a 60-nm-thick specimen, the number of absorbed photons per Si atom (for the fs pulse used) to be ~0.01, as opposed to 10^{-9} photons per atom if the experiments were conducted in the time-averaged mode.

The achievement of nanoscale diffraction with CB-UEM opens the door to exploration of different structural, morphological, and electronic phenomena. The spatially focused and timed electron packets enable studies of single particles and structures of heterogeneous media. Extending the methodology reported here to other variants, such as EELS (*26*), STEM (*11*), and nanotomography (*34*), promises possibilities for mapping individual unit cells and atoms on the ultrashort time scale of structural dynamics.

References and Notes

1. J. C. H. Spence, J. M. Zuo, *Electron Microdiffraction* (Plenum, New York, 1992).
2. J. M. Cowley, *Diffraction Physics* (Elsevier, Amsterdam, ed. 3, 1995).
3. Z. L. Wang, *Elastic and Inelastic Diffraction and Imaging* (Plenum, New York, 1995).
4. D. B. Williams, C. B. Carter, *Transmission Electron Microscopy* (Plenum, New York, 1996), vol. II.
5. P. A. Midgley, M. Saunders, R. Vincent, J. W. Steeds, *Ultramicroscopy* **59**, 1 (1995).
6. J. M. Zuo, M. Kim, M. O'Keefe, J. C. H. Spence, *Nature* **401**, 49 (1999).
7. P. Zhang *et al.*, *Appl. Phys. Lett.* **89**, 161907 (2006).
8. R. F. Loane, P. R. Xu, J. Silcox, *Acta Crystallogr. A* **47**, 267 (1991).
9. D. A. Muller, B. Edwards, E. J. Kirkland, J. Silcox, *Ultramicroscopy* **86**, 371 (2001).
10. D. A. Muller *et al.*, *Science* **319**, 1073 (2008).
11. K. A. Mkhoyan, P. E. Batson, J. Cha, W. J. Schaff, J. Silcox, *Science* **312**, 1354 (2006).
12. H. Ihee *et al.*, *Science* **291**, 458 (2001).
13. C.-Y. Ruan, V. A. Lobastov, F. Vigliotti, S. Chen, A. H. Zewail, *Science* **304**, 80 (2004).
14. P. Baum, D.-S. Yang, A. H. Zewail, *Science* **318**, 788 (2007).
15. N. Gedik, D.-S. Yang, G. Logvenov, I. Bozovic, A. H. Zewail, *Science* **316**, 425 (2007).
16. F. Carbone, P. Baum, P. Rudolf, A. H. Zewail, *Phys. Rev. Lett.* **100**, 035501 (2008).
17. H. E. Elsayed-Ali, T. B. Norris, M. A. Pessot, G. A. Mourou, *Phys. Rev. Lett.* **58**, 1212 (1987).
18. M. Harb *et al.*, *Phys. Rev. Lett.* **100**, 155504 (2008).
19. S. Nie, X. Wang, H. Park, R. Clinite, J. Cao, *Phys. Rev. Lett.* **96**, 025901 (2006).
20. R. K. Raman *et al.*, *Phys. Rev. Lett.* **101**, 077401 (2008).
21. J. M. Thomas, *Angew. Chem. Int. Ed.* **43**, 2606 (2004).
22. C. Bressler, M. Chergui, *Chem. Rev.* **104**, 1781 (2004); and references therein.
23. B. Barwick, H. S. Park, O.-H. Kwon, J. S. Baskin, A. H. Zewail, *Science* **322**, 1227 (2008); and references therein.
24. A. H. Zewail, J. M. Thomas, *4D Electron Microscopy* (Imperial College Press, London, 2009); and references therein.
25. T. Sjodin, H. Petek, H. Dai, *Phys. Rev. Lett.* **81**, 5664 (1998).
26. F. Carbone, O.-H. Kwon, A. H. Zewail, *Science* **325**, 181 (2009).
27. For this study, we used 500 to 1000 electrons per pulse, and care was taken to account for any instrumental broadening in fitting the transient response by proper convolution with the two pulse-widths involved. By measuring the energy spread of the photoelectron packets with EELS in the same microscope (UEM-2), we obtained a maximum temporal width of 0.7 ps. The path difference caused by the condenser lens system, at 10 mrad convergence angle, is 0.3 ps.
28. J. R. Goldman, J. A. Prybyla, *Phys. Rev. Lett.* **72**, 1364 (1998).
29. In the standard formula for the Debye-Waller effect, three components of vibrational amplitudes are considered, and the exponent becomes $\exp[-(4/3)\pi^2 s^2 u^2_{\mathrm{total}}]$. All three components in the Einstein model are equal, and hence $u_x^2 = 1/3u^2_{\mathrm{total}}$. From an experimental point of view, the intensities could be expressed as $I^F_{\mathrm{Ring}}(t) \sim \exp[-4\pi^2 s^2 u_x^2(t)]/\{1 - \exp[-4\pi^2 s^2 u_x^2(t)]\}$ where the denominator represents the TDS background (*30*). However, under our experimental conditions, this background is insignificant in the narrow angular range studied. Moreover, we note that TDS and other background contributions, such as inelastic plasmon scattering, which can be filtered out (*30*), are not of concern here because we are monitoring the temporal change in reference to frames recorded at negative delay times.
30. P. Xu, R. F. Loanne, J. Silcox, *Ultramicroscopy* **38**, 127 (1991); and references therein.
31. P. J. E. Aldred, M. Hart, *Proc. R. Soc. London Ser. A* **332**, 239 (1973).
32. Y. Okada, Y. Tokumaru, *J. Appl. Phys.* **56**, 314 (1984).
33. J. Yang, N. Gedik, A. H. Zewail, *J. Phys. Chem. C* **111**, 4889 (2007).
34. P. A. Midgley, E. P. W. Ward, A. B. Hungria, J. M. Thomas, *Chem. Soc. Rev.* **36**, 1477 (2007) and references therein.

35. This work was supported by the NSF and the Air Force Office of Scientific Research in the Gordon and Betty Moore Center for Physical Biology at CalTech. We thank O.-H. Kwon and H. S. Park for the experimental aid in UEM-2 laboratory and acknowledge the helpful use of the Cornell TEM sample preparation facility. Caltech has filed a provisional patent application for variants of 4D microscopy.

17 July 2009; accepted 27 August 2009
10.1126/science.1179314

A Late Archean Sulfidic Sea Stimulated by Early Oxidative Weathering of the Continents

Christopher T. Reinhard,[1] Rob Raiswell,[2] Clint Scott,[1] Ariel D. Anbar,[3] Timothy W. Lyons[1]*

Iron speciation data for the late Archean Mount McRae Shale provide evidence for a euxinic (anoxic and sulfidic) water column 2.5 billion years ago. Sulfur isotope data compiled from the same stratigraphic section suggest that euxinic conditions were stimulated by an increase in oceanic sulfate concentrations resulting from weathering of continental sulfide minerals exposed to an atmosphere with trace amounts of photosynthetically produced oxygen. Variability in local organic matter flux likely confined euxinic conditions to midportions of the water column on the basin margin. These findings indicate that euxinic conditions may have been common on a variety of spatial and temporal scales both before and immediately after the Paleoproterozoic rise in atmospheric oxygen, hinting at previously unexplored texture and variability in deep ocean chemistry during Earth's early history.

The first two billion years of Earth's history were characterized by little to no free atmospheric oxygen (*1*, *2*). A large body of evidence points to a sharp rise in the concentration of atmospheric O_2 during the Paleoproterozoic between 2.45 and 2.32 billion years ago (Ga) (*1*–*3*), but the history of deep ocean oxygenation is less well-known. The deposition of banded iron formations (BIF) during the Archean and early Proterozoic (~3.8 to 1.8 Ga) has been taken to imply that deep ocean water masses were anoxic and rich in dissolved ferrous iron (Fe^{2+}) derived from high-temperature weathering of seafloor basalt under low oceanic sulfate (SO_4^{2-}) concentrations (*4*, *5*). Reducing and iron-rich (ferruginous) deep ocean conditions are thought to have persisted for most of Earth's early history, although a relative paucity of BIF between 2.4 and 2.0 Ga (*6*) has rendered deep ocean chemistry during this period obscure. In any case, the cessation of BIF deposition at ~1.8 Ga is generally linked to the accumulation of oxygen in the atmosphere through the eventual removal of Fe^{2+} from the ocean either as ferric (hydr)oxides (*7*) or as pyrite in euxinic basins (*8*). A corollary of the latter model is that oxidative delivery of sulfate to the ocean was not sufficient to remove reactive iron through microbial sulfide production before ~1.8 Ga. However, recent studies of the late Archean Mount McRae Shale suggest that oxidative sulfur cycling may have preceded the Paleoproterozoic rise in atmospheric oxygen (*9*) and that conditions sufficient to authigenically enrich molybdenum (Mo) in marine sediments existed at ~2.5 Ga (*10*). On the modern Earth, substantial enrichment of Mo into sediments occurs after the conversion of soluble molybdate (MoO_4^{2-}) to particle-reactive thiomolybdates ($MoO_{4-x}S_x^{2-}$) in stable sulfidic environments (*11*), indicating that the Mo enrichments seen in the Mount McRae Shale may have resulted from the development of a euxinic water column in association with increased oxidative transport of crustal sulfur as SO_4^{2-}.

To examine the possibility of euxinia during the late Archean, we analyzed iron mineral speciation in the Mount McRae Shale (*12*). The distribution of iron among different biogeochemically labile mineral phases ("highly reactive iron") can reveal local redox conditions (*13*, *14*). Highly reactive iron (Fe_{HR}) is defined as the sum of pyrite iron (Fe_{PY}) and iron in phases that are reactive to hydrogen sulfide (H_2S) on short diagenetic time scales, such as ferric oxides (Fe_{ox}), magnetite (Fe_{mag}), and iron present as carbonate (Fe_{carb}). In modern sediments from oxic continental margins and the deep sea, Fe_{HR} makes up 6 to 38% of the total sedimentary iron (Fe_T) (i.e., Fe_{HR}/Fe_T = 0.06 to 0.38); an average Fe_{HR}/Fe_T ratio of 0.26 ± 0.08 defines the modern siliciclastic baseline (*13*). Values for Fe_{HR}/Fe_T that are elevated above this siliciclastic background suggest reactive iron input that is decoupled from detrital sources, an indication of iron transport and scavenging within an anoxic water column (*15*). We also look toward total iron enrichments (expressed as Fe_T/Al ratios) as an indicator of water column anoxia (*16*, *17*).

If Fe_{HR}/Fe_T and Fe_T/Al data provide evidence for anoxia, the ratio Fe_{PY}/Fe_{HR} can be used to distinguish between anoxic but nonsulfidic conditions and anoxic water columns containing free H_2S (euxinic). This approach is based on the simple premise that under anoxic conditions dissolved Fe^{2+} and dissolved H_2S cannot coexist in abundance in solution because of the insolubility of iron sulfide phases, and therefore high values for Fe_{PY}/Fe_{HR} indicate H_2S-dominated water column chemistry. For confirmation, we also measured degree of pyritization (DOP) as a conservative indicator of iron-limited pyrite formation and euxinia (*12*, *17*). The distribution of highly reactive Fe species in the Mount McRae Shale is shown in Fig. 1, along with Fe_T/Al, bulk molybdenum (Mo), and organic carbon (TOC) concentrations from (*10*). We focus here on the pyritic and organic-rich lower shale interval (LSI) and upper shale interval (USI). Ferric oxides make up a small proportion of Fe_{HR} for the entire sequence analyzed here, indicating water column and/or pore fluid conditions that were reducing with respect to iron (Fig. 1). Values for Fe_{HR}/Fe_T and Fe_T/Al are elevated throughout, suggesting that the entire sequence was deposited beneath an anoxic water column. In a few instances, Fe_{PY}/Fe_{HR} values in the LSI approach a threshold ($Fe_{PY}/Fe_{HR} \geq 0.8$) interpreted to reflect euxinia when paired with evidence for anoxic deposition (*14*, *18*); however, the average Fe_{PY}/Fe_{HR} for this unit (0.55 ± 0.20) suggests a predominance of ferruginous conditions. Variations in Fe_{HR} within the LSI are governed by differences in Fe_{carb} rather than Fe_{PY} (fig. S2). These data are consistent with sulfate reduction and pyrite formation within or beneath an anoxic water column, but with reactive Fe in excess of dissolved H_2S such that H_2S did not persist in the pore fluids or water column during LSI deposition.

The USI shows pronounced enrichment in Fe_{HR}, indicating extensive reactive Fe scavenging beneath an anoxic water column (Fig. 1). Values for Fe_T/Al, although lower than those seen in the underlying siderite-facies, remain elevated. In contrast to the LSI, Fe_{PY}/Fe_{HR} values are persistently high (0.85 ± 0.17), as is DOP (0.78 ± 0.23). A strong linear relation between Fe_{HR} and Fe_{PY} for the USI (fig. S2) demonstrates that variations in the amount of Fe_{HR} are governed by differences in Fe_{PY} content and that Fe_{HR} is all but completely pyritized. This combination of parameters (elevated values for Fe_{HR}/Fe_T, Fe_T/Al, Fe_{PY}/Fe_{HR}, and DOP) indicates that the water column was euxinic for a substantial portion of USI deposition.

To examine whether euxinia occurred in association with a transient or secular change in the oxidative transport of MoO_4^{2-} and SO_4^{2-} (*19*), we turn to the sulfur isotope composition of syngenetic and early diagenetic pyrite from deep-water facies (shales and BIF) of the Neoarchean-Paleoproterozoic (2.7 to 2.45 Ga) Hamersley Basin (Fig. 2). Neoarchean samples below the USI, including those from the LSI and the siderite-facies BIF directly beneath the USI, show large $\Delta^{33}S$ values and positive covariation between $\Delta^{33}S$ and $\delta^{34}S$ (Fig. 2). This pattern has been hypothesized to reflect a primary atmospheric array in the isotopic composition of elemental sulfur aerosols (*20*). The corresponding linearity and large positive $\Delta^{33}S$ anomalies of these data suggest a tight isotopic coupling between atmospherically derived reduced sulfur species and sedimentary pyrite formation and also indicate that the transfer and mixing mechanisms that contributed to the signal ultimately preserved in the sediments were similar on at

[1]University of California–Riverside, Department of Earth Sciences, Riverside, CA 92521, USA. [2]University of Leeds, School of Earth and Environment, Leeds, UK LS2 9JT. [3]Arizona State University, School of Earth and Space Exploration and Department of Chemistry and Biochemistry, Tempe, AZ 85287, USA.

*To whom correspondence should be addressed. E-mail: timothyl@ucr.edu

least a basinal scale and through large periods of Archean time (*9*, *20*).

The sulfur isotope composition of pyrite in the USI and the overlying Brockman BIF shows a different distribution (Fig. 2). Values for $\Delta^{33}S$ are attenuated during euxinic deposition, with the largest positive $\Delta^{33}S$ values in the USI found in intervals that are transitional with the siderite-facies BIF unit below or the overlying carbonate unit. The linear array that characterizes the data before deposition of the USI is no longer evident, and a linear regression through the USI/Brockman data is closely aligned with the mass-dependent fractionation array in $\delta^{34}S$-$\delta^{33}S$ space. This shift is accompanied by predominantly small negative $\Delta^{33}S$ values and relatively depleted $\delta^{34}S$ values within the USI, followed by subdued variability in $\Delta^{33}S$ and a wide spread in $\delta^{34}S$ values [from −5 per mil (‰) to +35‰] in the overlying Brockman BIF. We interpret this isotopic shift to reflect increased SO_4^{2-} availability during deposition of the USI and Brockman BIF accompanied by mixing of photolytically produced sulfur and isotopically normal crustal sulfur oxidatively mobilized under an atmosphere that remained O_2-poor (*12*). A transient or secular increase in the oxidative transport of MoO_4^{2-} and SO_4^{2-} during USI deposition is also supported by the contrasting strong non–mass-dependent (NMD) signal (*20*) and essential lack of Mo enrichment (*21*) preserved in pyritic shales of the Jeerinah Formation underlying the Mount McRae—analogous to the signals seen in the LSI and the siderite-facies BIF beneath the USI. The persistence of distinct NMD anomalies, despite the overall shift in isotopic arrays, requires the formation and burial of sulfur with NMD isotope composition throughout this period. Ground-level atmospheric O_2 concentrations of less than 2 parts per million by volume (ppmv) (i.e., below 10^{-5} the present atmospheric level) are therefore implied (*22*), and concentrations throughout most of the troposphere may have been substantially lower than this (*22*, *23*). This assertion is also supported by $\Delta^{33}S/\Delta^{36}S$ relationships (*9*).

Combined, the high-resolution Fe speciation, Mo enrichment, and sulfur isotope data for the Mount McRae Shale indicate the development of euxinia during deposition of the USI and that these conditions were contemporaneous with a change in sedimentary sulfur isotope systematics. However, the stratigraphic position of the USI between two BIFs, coupled with Fe_T/Al ratios that are persistently and substantially elevated above crustal values (Fig. 1), suggest that hydrothermal iron fluxes to the deep basin were important at this time. Our interpretation therefore implies a water column structure that would allow for both the accumulation of dissolved H_2S and the subsequent or coeval deposition of voluminous BIF.

To reconcile these observations, we postulate locally enhanced microbial H_2S production, stimulated by organic matter (OM) delivery and facilitated by an increased flux of dissolved SO_4^{2-} to the basin. Local loading of OM would have fueled vigorous sulfate reduction along the basin margin, resulting in an oxidant minimum zone in which dissolved H_2S accumulated and quantitatively removed dissolved Fe^{2+} from the water column (Fig. 3). Euxinia would have expanded or contracted periodically as a function of the balance between reactive Fe input and OM flux, with the possibility of dissolved H_2S transiently accumulating on a basin scale or receding beneath the sediment-water interface. This lateral redox structure is similar to the basin-scale lithofacies framework hypothesized for contemporaneous strata from the South African Transvaal basin (*24*), indicating that such conditions may have been common during this period.

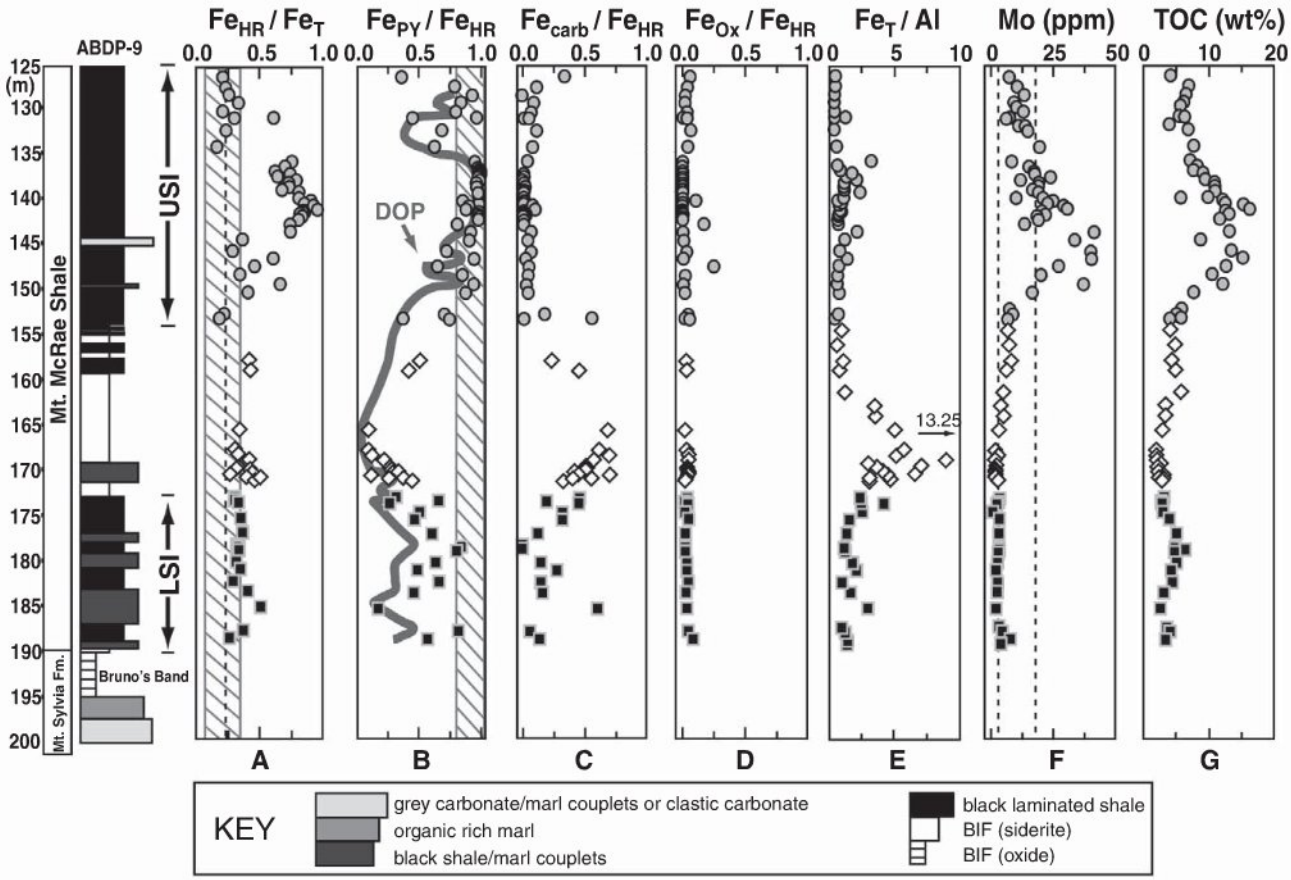

Fig. 1. (**A** to **G**) Stratigraphic profiles for iron speciation data from the ADBP-9 core. Squares, diamonds, and circles represent the LSI, siderite-facies BIF, and USI, respectively. The striped box in (A) represents the range of Fe_{HR}/Fe_T values seen in modern oxic continental margin and deep-sea sediments (*13*). The dotted line in (A) represents the mean Fe_{HR}/Fe_T value (0.26) for normal (oxic) marine settings (*13*). The striped box in (B) represents Fe_{PY}/Fe_{HR} values that are above 0.8. Euxinia is implied when both of these thresholds are exceeded and Fe_T/Al values exceed 0.5. The dark line in (B) is the best fit through DOP values (not shown). The two dotted lines in (E) reflect average bulk Mo enrichments for the Archean [3 parts per million (ppm)] and Proterozoic (18 ppm) (*21*). Data for (E) and (F) from (*10*).

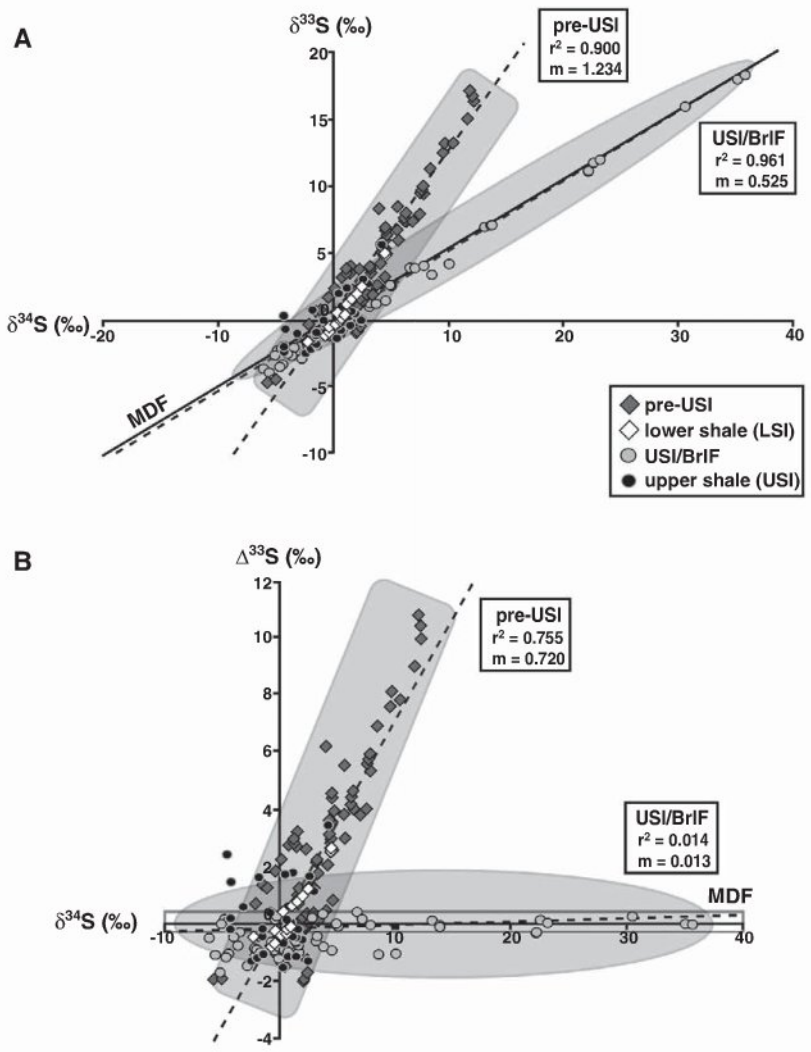

Fig. 2. Sulfur isotope data for deep-water Hamersley Basin pyrite samples spanning 2.7 to 2.45 Ga, displayed as $\delta^{34}S$ versus $\delta^{33}S$ (**A**) and $\delta^{34}S$ versus $\Delta^{33}S$ (**B**). Pre-USI data are from the Jeerinah Formation and lower Mount McRae Shale (*20*, *27*); the LSI and siderite-facies BIF beneath the USI (*9*); and the Marra Mamba BIF (*27*), which was deposited between the Jeerinah Formation and the Mount McRae Shale. USI/Brockman BIF (BrIF) data are from the USI (*9*) and the overlying BrIF (*27*, *28*). The line labeled "MDF" in (A) is the mass-dependent fractionation line, defined as $\delta^{33}S = 0.515 \times \delta^{34}S$ (*29*). The gray box in (B) represents the range of $\Delta^{33}S$ values attainable by mass-dependent processes (*30*, *31*).

Although OM delivery was the proximate cause of euxinia, we propose that it was the increased availability of SO_4^{2-} attendant to oxidative weathering that ultimately allowed microbial H_2S production to overwhelm reactive Fe, at least locally, during USI deposition. Elevated total sulfur concentrations in this interval, coincident with increased TOC and high Fe_T values (*9*, *10*), also point to increasing availability of water column SO_4^{2-} such that microbial sulfate reduction was able to keep pace with substantial OM flux and relatively high reactive Fe availability. It is possible that mid-water column euxinia existed subsequent to USI deposition, with the stratigraphic transition to Brockman BIF recording a change in water depth rather than a temporal change in basin chemistry.

Our findings suggest that weak oxidative forcing could have stimulated the development of euxinia 50 to 100 million years before the Paleoproterozoic rise in atmospheric oxygen and that stable and persistent euxinia could have developed at least locally, and perhaps on a much larger scale, even within BIF-forming basins. Sulfur isotope data indicate that the weathering flux of SO_4^{2-} to the ocean increased substantially after the rise in atmospheric oxygen between 2.45 and 2.32 Ga (*8*, *25*). The lack of BIF between 2.4 and 2.0 Ga may therefore reflect the frequent or sustained development of euxinia within Paleoproterozoic basins (*1*), presaging the possibly widespread and protracted development of similar oceanographic conditions hypothesized previously for the Mesoproterozoic (~1.8 to 1.0 Ga) (*8*). Constraints on deep ocean redox during this intervening period are sparse, but existing data intimate that euxinic deep basins were much more common than ferruginous ones between 2.4 and 2.0 Ga (*21*).

More generally, we argue that deposition of BIFs represented episodic pulses of reducing power from Earth's interior (*6*) rather than persistent deep-water conditions. Significant spatial variability in water column chemistry is indicated for intervals of BIF deposition, with intervening periods throughout the Archean and Paleoproterozoic during which at least portions of the water column may have been euxinic. Vacillation be-

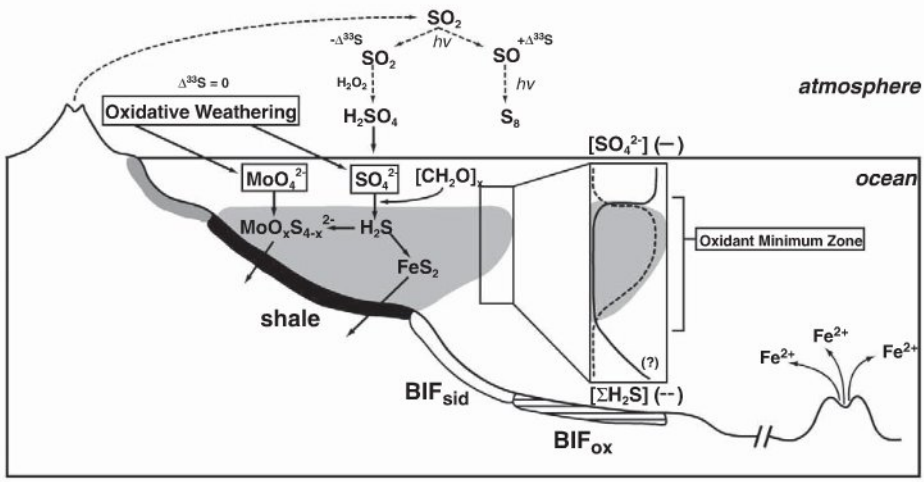

Fig. 3. Schematic representation of the Hamersley Basin during the deposition of the upper Mount McRae Shale (USI). Oxidative delivery of SO_4^{2-} and MoO_4^{2-}, combined with a high local organic matter flux, resulted in the accumulation of free H_2S in the water column in excess of dissolved Fe^{2+} (euxinia), supporting authigenic Mo enrichment. Atmospheric O_2 concentrations below 2 ppmv could have driven the enhanced oxidative weathering recorded in the USI but would still have allowed for SO_2 photolysis and the preservation of NMD sulfur isotope anomalies (*12*). Atmospheric photochemistry simplified from (*32*).

tween euxinic and ferruginous conditions would have favored the early evolution and ecological expansion of a variety of anoxygenic photosynthetic metabolisms in pelagic environments. Expressions of biological oxygen production (such as those seen in the upper Mount McRae and Brockman BIF) would then have varied with the extent to which episodic or sustained pulses of reductants from the Earth's interior would have buffered photosynthetic oxygen, contributing to the protracted nature of Earth surface oxygenation during the Archean and Proterozoic (*26*).

References and Notes

1. D. E. Canfield, *Annu. Rev. Earth Planet. Sci.* **33**, 1 (2005).
2. H. D. Holland, *Geochim. Cosmochim. Acta* **66**, 3811 (2002).
3. A. Bekker *et al.*, *Nature* **427**, 117 (2004).
4. A. E. Isley, *J. Geol.* **103**, 169 (1995).
5. L. R. Kump, W. E. Seyfried, *Earth Planet. Sci. Lett.* **235**, 654 (2005).
6. A. E. Isley, D. H. Abbott, *J. Geophys. Res.* **104**, 15461 (1999).
7. P. E. Cloud, *Am. J. Sci.* **272**, 537 (1972).
8. D. E. Canfield, *Nature* **396**, 450 (1998).
9. A. J. Kaufman *et al.*, *Science* **317**, 1900 (2007).
10. A. D. Anbar *et al.*, *Science* **317**, 1903 (2007).
11. B. E. Erickson, G. R. Helz, *Geochim. Cosmochim. Acta* **64**, 1149 (2000).
12. Materials and methods are available as supporting material on *Science* Online.
13. R. Raiswell, D. E. Canfield, *Am. J. Sci.* **298**, 219 (1998).
14. S. W. Poulton, P. W. Fralick, D. E. Canfield, *Nature* **431**, 173 (2004).
15. J. W. M. Wijsman, J. J. Middelburg, C. H. R. Heip, *Mar. Geol.* **172**, 167 (2001).
16. Interpretation of this measurement follows the same rationale as that for Fe_{HR}/Fe_T (i.e., enrichments above the average Fe_T/Al ratio for continental crust of ~0.5 imply transport and scavenging of iron under anoxic conditions), but Fe_T/Al is immune to concerns regarding authigenic iron-silicate formation or metamorphic repartitioning of reactive iron phases into poorly reactive silicate mineralogies.
17. T. W. Lyons, S. Severmann, *Geochim. Cosmochim. Acta* **70**, 5698 (2006).
18. T. F. Anderson, R. Raiswell, *Am. J. Sci.* **304**, 203 (2004).
19. Because Mo enrichments require both an oceanic Mo reservoir and the accumulation of free H_2S, it is possible that the metal enrichments recorded in the USI point only to the development of euxinia rather than a temporally constrained increase in the flux of MoO_4^{2-} and SO_4^{2-} to the Hamersley Basin during USI deposition.
20. S. Ono *et al.*, *Earth Planet. Sci. Lett.* **213**, 15 (2003).
21. C. Scott *et al.*, *Nature* **452**, 456 (2008).
22. A. A. Pavlov, J. F. Kasting, *Astrobiology* **2**, 27 (2002).
23. K. Zahnle, M. Claire, D. Catling, *Geobiology* **4**, 271 (2006).
24. C. Klein, N. J. Beukes, *Econ. Geol.* **84**, 1733 (1989).
25. E. M. Cameron, *Nature* **296**, 145 (1982).
26. L. R. Kump, M. E. Barley, *Nature* **448**, 1033 (2007).
27. M. Partridge, S. D. Golding, K. A. Baublys, E. Young, *Earth Planet. Sci. Lett.* (2008).
28. S. J. Mojzsis, C. D. Coath, J. P. Greenwood, K. D. McKeegan, T. M. Harrison, *Geochim. Cosmochim. Acta* **67**, 1635 (2003).
29. J. R. Hulston, H. G. Thode, *J. Geophys. Res.* **70**, 3475 (1965).
30. J. Farquhar *et al.*, *Geobiology* **1**, 27 (2003).
31. S. Ono, B. Wing, D. Johnston, J. Farquhar, D. Rumble, *Geochim. Cosmochim. Acta* **70**, 2238 (2006).
32. J. F. Kasting, K. J. Zahnle, J. P. Pinto, A. T. Young, *Orig. Life Evol. Biosph.* **19**, 95 (1989).

33. The NASA Astrobiology Institute and Exobiology Program and the NSF Geobiology and Low Temperature Geochemistry Program provided financial support. The authors thank B. Gill, S. Severmann, N. Planavsky, M. Claire, J. Kaufman, and R. Buick for helpful discussions, and G. Arnold for handling of core material.

Supporting Online Material

www.sciencemag.org/cgi/content/full/326/5953/713/DC1
Materials and Methods
Figs. S1 to S3
Table S1
References

22 May 2009; accepted 31 August 2009
10.1126/science.1176711

Improved Attribution of Climate Forcing to Emissions

Drew T. Shindell,* Greg Faluvegi, Dorothy M. Koch, Gavin A. Schmidt, Nadine Unger, Susanne E. Bauer

Evaluating multicomponent climate change mitigation strategies requires knowledge of the diverse direct and indirect effects of emissions. Methane, ozone, and aerosols are linked through atmospheric chemistry so that emissions of a single pollutant can affect several species. We calculated atmospheric composition changes, historical radiative forcing, and forcing per unit of emission due to aerosol and tropospheric ozone precursor emissions in a coupled composition-climate model. We found that gas-aerosol interactions substantially alter the relative importance of the various emissions. In particular, methane emissions have a larger impact than that used in current carbon-trading schemes or in the Kyoto Protocol. Thus, assessments of multigas mitigation policies, as well as any separate efforts to mitigate warming from short-lived pollutants, should include gas-aerosol interactions.

Multicomponent climate change mitigation strategies are likely to be much more cost effective than carbon dioxide (CO_2)–only strategies (*1*, *2*) but require quantification of the relative impact of different emissions that affect climate. Because globally and annually averaged radiative forcing (RF) is generally a good predictor of global mean surface temperature change, a scale related to RF is a logical choice for comparing emissions. The most widely used, and that adopted in the Kyoto Protocol, is the global warming potential (GWP), defined as the integrated global mean RF out to a chosen time of an emission pulse of 1 kg of a compound relative to that for 1 kg of CO_2. GWPs are thus based on radiative impact and atmospheric residence time and can include both the direct radiative effect of emitted species and radiative effects from indirect chemical responses. Previous studies, including the Intergovernmental Panel on Climate Change (IPCC) Fourth Assessment Report (AR4), provide estimates of RF and GWPs of short-lived gas emissions (*3*–*5*). However, except for the indirect effect of NO_x emissions on nitrate aerosol, gas-aerosol interactions were not included. These interactions occur primarily through ozone precursors altering the availability of oxidants, influencing aerosol formation rates, and through sulfate-nitrate competition for ammonium.

We used the composition-climate model Goddard Institute for Space Studies (GISS) Model for Physical Understanding of Composition-Climate Interactions and Impacts (G-PUCCINI) (*6*) to calculate the response to removal of all anthropogenic methane, carbon monoxide (CO) plus volatile organic compounds (VOCs), NO_x, SO_2, and ammonia emissions. This model couples gas-phase, sulfate (*7*), and nitrate (*8*) aerosol chemistry within the GISS ModelE general circulation model (GCM). Anthropogenic emissions are from a 2000 inventory (*9*). We calculated both the "abundance-based" RF owing to the net atmospheric composition response by species when all emissions are changed simultaneously and the "emissions-based" forcing attributable to the responses of all species to emissions of a single pollutant (Fig. 1). The sum of the forcings that take place via response of a particular species in the emissions-based analysis (each represented by a different color in Fig. 1) is approximately equal to the forcing due to that species in the abundance-based analysis. Likewise, the sums of all emissions-based and all abundance-based forcings are similar. Hence, the two viewpoints provide different but compatible pictures of how emissions and composition changes influence RF.

Emissions of NO_x, CO, and methane have substantial impacts on aerosols by altering the abundance of oxidants, especially hydroxyl, which convert SO_2 into sulfate. Global burdens of hydroxyl and sulfate change by 18% and 13% for increased NO_x, by –13% and –9% for CO, and by –26% and –11% for methane (sulfate forcing closely follows the sulfate burden change). Coupling in the other direction is very weak because reactions of gas-phase species upon aerosol surfaces have only a small effect on the global burden of the radiatively active species ozone and methane (e.g., anthropogenic SO_2 emissions enhance the removal of NO_x through reactions on particulate

NASA Goddard Institute for Space Studies and Columbia University, New York, NY 10025, USA.

*To whom correspondence should be addressed. E-mail: drew.t.shindell@nasa.gov

surfaces, causing ozone to decrease, but the RF is only –0.004 W/m^2). Increased SO_2 leads to substantially reduced nitrate aerosol, however, owing to greater ammonium sulfate formation at the expense of ammonium nitrate (*10*, *11*). We group CO and VOCs together for RF because they play similar roles in atmospheric chemistry, but the effects of historical CO emissions are ~3 to 7 times as great.

Methane emissions provide the second-largest contribution to historical warming after carbon dioxide. Including direct and indirect chemical effects and only the direct radiative effects of aerosols, NO_x emissions are the most powerful cooling agents (Fig. 1). However, adding in aerosol indirect effects (AIE) on clouds, which are highly uncertain (*12*), could make SO_2 emissions the stronger contributor to negative historical forcing. Atmospheric responses to individual species emissions changes are largely additive, with increases of 15% or less in the response of methane, ozone, sulfate, and hydroxyl when all pollutants are changed simultaneously, compared with the summed response to individual changes. Nitrate shows a greater discrepancy (~0.04 W/m^2), but the difference is well within uncertainty (0.10 W/m^2) (see Fig. 1 caption).

We present the results of several calculations of 100-year GWPs, the most commonly used time horizon, first reporting values without including indirect chemical responses of aerosols or CO_2 (as in the AR4, although the indirect responses of CO_2 are only 0.04 W/m^2 for CO and 0.02 W/m^2 for methane), then adding in the radiative effects resulting from the aerosol response to oxidant changes (Fig. 2). Reference CO_2 forcing is taken from the AR4, whereas the RF for all other gases and the direct radiative effects of aerosols are calculated within the GISS GCM for current conditions using the model's radiative transfer calculation and simulated composition response to 1-year pulse emissions. We also computed GWP, including a rough estimate of AIE, assuming they augment the sulfate aerosol direct radiative effects calculated here by 150%, taking the uncertainty range as 75 to 225% (*13*). Uncertainties in GWP are otherwise based on the RF uncertainties from AR4 (as in Fig. 1). We report GWPs for CO alone, because GWPs for different VOCs vary by an order of magnitude (*14*).

Our value for the 100-year GWP of methane when including only the responses of methane, ozone, and stratospheric water vapor is almost identical to the comparable AR4 value. The GWP is substantially larger when the direct radiative effects of the aerosol responses are included, however. It becomes larger still, including aerosol-cloud interactions, although uncertainties increase as well. Although results are not statistically different at the 95% confidence level, the best estimate is nonetheless substantially larger when gas-aerosol interactions are included. The 100-yr GWP for CO was 1.9 in AR4, with a 1.0 to 3.0 range based on the third IPCC assessment and subsequent results (*3*, *14*). As with methane, our GWP is similar to those in previous work when aerosol responses are neglected but is substantially larger when these responses are included. GWPs become extremely difficult to define for shorter-lived species because they depend strongly on the location and time (season and day) of the emission pulse (*15*). Estimates of 100-year GWPs for global surface NO_x emissions report values of roughly –10 to –30, including the indirect responses of methane and ozone only (*16*, *17*), in very rough accord with our results, but differences in the imposed emissions changes preclude a rigorous comparison.

Although our calculations are more complete than previous studies, additional processes should be included as they become better understood. These include mixing between aerosol types (*18*), formation of secondary organic aerosols, which are sensitive to both organic aerosol emissions and oxidant levels (*19*), and interactions between pollutants and ecosystems. The latter includes suppression of CO_2 uptake by increased surface ozone concentrations (*20*), aerosols enhancing the ratio of diffuse to direct radiation reaching the biosphere leading to increased CO_2 uptake (*21*) (at least for some plant types when aerosol loading is not so large as to dramatically reduce total surface irradiance), and the effects of nitrogen and sulfur deposition on ecosystems. These effects may be important but are highly uncertain at present. Ecosystem-chemistry interactions add both positive and negative forcing terms to the GWP of NO_x (NO_x leads to increased ozone, causing increased CO_2, but also leads to increased aerosol, causing decreased CO_2), adding to an already complex set of multiple, sometimes opposing, forcings (Fig. 1). For CO and methane, however, increased emissions lead to increased CO_2 from both the ozone-ecosystem interactions and the aerosol-ecosystem interactions, so would simply increase their positive GWPs still further.

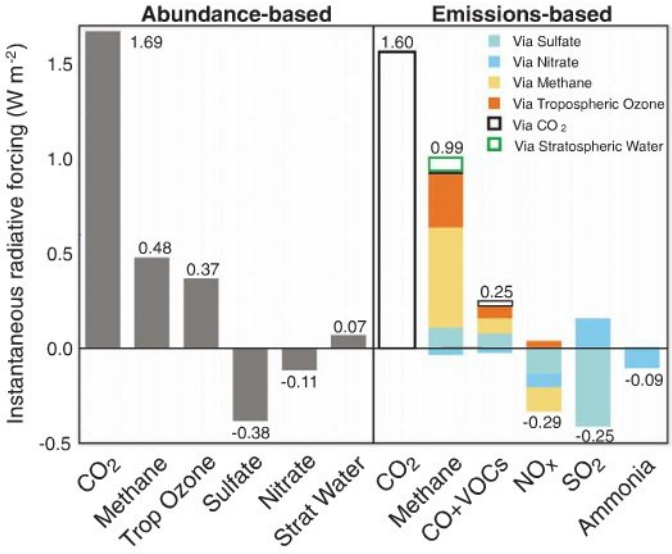

Fig. 1. Radiative forcing from 1750 to 2000. Numerical values within the figure give the net forcing (instantaneous at the tropopause). Uncertainties in the abundance-based values are 0.16 for CO_2, 0.05 for methane, +0.15 to –0.10 for ozone, 0.20 for sulfate, 0.10 for nitrate, and 0.05 for stratospheric water (*5*). For emissions-based values, we estimate uncertainties by adding the forcing uncertainties for each component in quadrature, yielding 0.14 for methane, 0.04 for CO+VOCs, 0.09 for NO_x, 0.23 for sulfate, and 0.10 for ammonia. AIE are not included. All forcing values are from this work except those from CO_2 and stratospheric water, which are based on the IPCC AR4 (*5*).

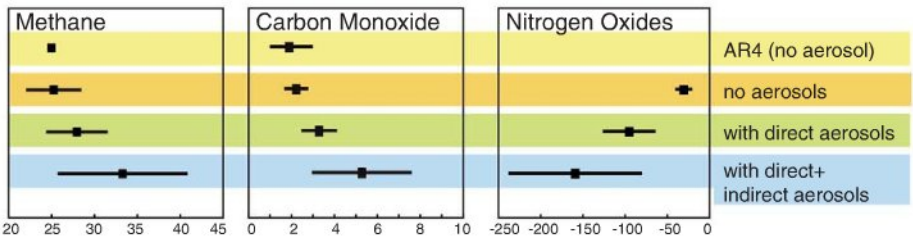

Fig. 2. The 100-year GWPs for methane, CO, and NO_x (per Tg N) as given in the AR4 and in this study when including no aerosol response, the direct radiative effect of aerosol responses, and the direct+indirect radiative effects of aerosol responses. The AR4 did not report uncertainties for methane or CO and gave no mean estimate for NO_x. The range for the GWP of CO is from the third IPCC assessment and encompasses values reported up through the AR4. Our calculations for the shorter 20-year GWP, including aerosol responses, yield values of 79 and 105 for methane, 11 and 19 for CO, and –335 and –560 for NO_x, including direct and direct+indirect radiative effects of aerosols in each case. The 100-yr GWPs for SO_2 (per Tg SO_2) and ammonia would be –22 and –19, respectively, including direct aerosol radiative effects only, and –76 and –15 adding indirect aerosol radiative effects. GWPs for very short-lived NO_x, SO_2, and ammonia will vary widely by emission location and timing, and hence global values are of limited use.

Hence, the uncertainty in quantifying these processes implies only that the larger estimates of CO and methane GWPs presented here may still be too low.

Although we focus on global mean results, the effects of oxidant changes on sulfate are stronger in areas with high SO_2 emissions that are more oxidant-limited. This is in accord with previous results showing a strong sulfate response over high-emission regions in Asia to perturbations in North American emissions attributable to NO_x emissions changes followed by long-range ozone transport (*22*). The global sulfate response to oxidant changes can be large, because much of the industrialized Northern Hemisphere is oxidant-limited, especially during winter (*23*), but the oxidant-aerosol interactions may show greater sensitivity to emission trends in peak emission regions. Consistent with this, the ratio of the sulfate to hydroxyl burden changes is greater in response to NO_x and CO emissions, generally colocated with SO_2 emissions, than for methane. Our previous results showed a small global mean net impact of all ozone precursors on sulfate forcing despite large regional forcings (*24*). Although that study used different emissions (a future scenario), those results seem reasonably consistent because the sum of the sulfate responses to all historical ozone precursors in this work is only 0.06 W/m^2.

Our results indicate that NO_x emissions cause a substantial net cooling at all time scales. In contrast, CO emissions cause warming. The 100-year GWP for methane is ~10% greater (~20 to 40%, including AIE) than earlier estimates (*5*) that neglected interactions between oxidants and aerosols. GWPs for methane and CO would likely be further increased by including ecosystem responses. Decreased emissions of SO_2 warm climate, but including the sulfate-nitrate interaction makes the climate impact less severe than might otherwise have been thought.

There are many limitations to the GWP concept (*25*). It includes only physical properties, and its definition is equivalent to an unrealistic economic scenario of no discounting through the selected time horizon followed by discounting to zero value thereafter. The 100-year time horizon conventionally chosen strongly reduces the influence of species that are short-lived relative to CO_2. Additionally, GWPs assume that integrated global mean RF is a useful indicator of climate change. Although this is generally reasonable at the global scale, GWP does not take into account the rate of change, and it neglects that the surface temperature response to regionally distributed forcings depends on the location of the RF (*26*) and that precipitation and circulation responses may be even more sensitive to RF location (*27*). Along with their dependence on emission timing and location, this makes GWPs particularly ill-suited to very short-lived species such as NO_x, SO_2, or ammonia, although they are more reasonable for longer-lived CO. Inclusion of short-lived species in agreements alongside long-lived greenhouse gases is thus problematic (*28*, *29*). Hence, emissions of short-lived species have traditionally been, and will likely continue to be, primarily regulated by local- to regional-scale policies targeting air quality. Should policies aim to mitigate climate change by separately targeting short-lived species emissions, however, they should consider effects across gas-phase and aerosol species. Furthermore, assessment of policies affecting particular sectors that emit both long- and short-lived species should include the overall impact rather than simply the impact of long-lived gases.

Despite their limitations, GWPs are widely used for comparison among long-lived gases, forming the basis for worldwide political agreements on climate and carbon trading. Because the latter was a $126 billion/year market in 2008 (*30*), even small differences in GWPs can have large economic consequences. Our results suggest that gas-aerosol interactions play an important role in methane's GWP, and hence our larger value would allow better optimization of climate change mitigation policies. Methane's GWP may also change with time as air quality regulations alter the background state of tropospheric chemistry. Finally, our results demonstrate that improving our knowledge of aerosol-climate interactions is important not only for better understanding the aerosol contribution to past and future climate change, but even for correctly evaluating the effects of long-lived greenhouse gas emissions from methane-oxidant-aerosol interactions.

References and Notes

1. J. Jensen, M. Thelle, *What Are the Gains from a Multi-Gas Strategy?* (Fondazione Eni Enrico Mattei, Milano, Italy, 2001).
2. J. Reilly *et al.*, *Nature* **401**, 549 (1999).
3. T. K. Berntsen *et al.*, *Tellus B Chem. Phys. Meterol.* **57**, 283 (2005).
4. D. T. Shindell, G. Faluvegi, N. Bell, G. A. Schmidt, *Geophys. Res. Lett.* **32**, L04803, 10.1029/2004GL021900 (2005).
5. P. Forster *et al.*, *Climate Change 2007: The Physical Science Basis*, S. Solomon, Ed. (Cambridge Univ. Press, New York, 2007).
6. D. T. Shindell *et al.*, *Atmos. Chem. Phys.* **6**, 4427 (2006).
7. D. Koch, G. Schmidt, C. Field, *J. Geophys. Res.* **111**, D06206, 10.1029/2004JD005550 (2006).
8. S. E. Bauer *et al.*, *Atmos. Chem. Phys.* **7**, 5043 (2007).
9. F. J. Dentener *et al.*, *Atmos. Chem. Phys.* **5**, 1731 (2005).
10. D. K. Henze, J. H. Seinfeld, D. T. Shindell, *Atmos. Chem. Phys.* **9**, 5877 (2009).
11. H. O. T. Pye *et al.*, *J. Geophys. Res.* **114**, D01205, 10.1029/2008JD010701 (2009).
12. J. E. Penner *et al.*, *Atmos. Chem. Phys.* **6**, 3391 (2006).
13. M. M. Kvalevåg, G. Myhre, *J. Clim.* **20**, 4874 (2007).
14. W. J. Collins, R. G. Derwent, C. E. Johnson, D. S. Stevenson, *Clim. Change* **52**, 453 (2002).
15. K. P. Shine, T. K. Berntsen, J. S. Fuglestvedt, S. R. *Proc. Natl. Acad. Sci. U.S.A.* **102**, 15768 (2005).
16. R. G. Derwent, W. J. Collins, C. E. Johnson, D. S. Stevenson, *Clim. Change* **49**, 463 (2001).
17. O. Wild, M. Prather, H. Akimoto, *Geophys. Res. Lett.* **28**, 1719 (2001).
18. J. Haywood, O. Boucher, *Rev. Geophys.* **38**, 513 (2000).
19. K. Tsigaridis *et al.*, *Atmos. Chem. Phys.* **6**, 5143 (2006).
20. S. Sitch, P. M. Cox, W. J. Collins, C. Huntingford, *Nature* **448**, 791 (2007).
21. L. M. Mercado *et al.*, *Nature* **458**, 1014 (2009).
22. D. Shindell *et al.*, *Atmos. Chem. Phys.* **8**, 7101 (2008).
23. T. F. Berglen, T. K. Berntsen, I. S. A. Isaksen, J. K. Sundet, *J. Geophys. Res.* **109**, D19310, 10.1029/2003JD003948 (2004).
24. N. Unger, D. T. Shindell, D. M. Koch, D. Streets, *Proc. Natl. Acad. Sci. U.S.A.* **103**, 4377 (2006).
25. O. Godal, *Clim. Change* **58**, 243 (2003).
26. D. Shindell, G. Faluvegi, *Nature Geosci.* **2**, 294 (2009).
27. Y. Ming, V. Ramaswamy, *J. Clim.* **22**, 1329 (2009).
28. T. C. Bond, H. Sun, *Environ. Sci. Technol.* **39**, 5921 (2005).
29. K. Rypdal *et al.*, *Environ. Sci. Policy* **8**, 29 (2005).
30. K. Capoor, P. Ambrosi, *State and Trends of the Carbon Market 2009* (The World Bank, Washington, DC, 2009).

31. We thank the NASA Atmospheric Chemistry Modeling and Analysis Program for supporting this work.

9 April 2009; accepted 9 September 2009
10.1126/science.1174760

Control of Iron Homeostasis by an Iron-Regulated Ubiquitin Ligase

Ajay A. Vashisht,[1] Kimberly B. Zumbrennen,[2] Xinhua Huang,[1] David N. Powers,[1] Armando Durazo,[3] Dahui Sun,[4] Nimesh Bhaskaran,[5] Anja Persson,[6] Mathias Uhlen,[6] Olle Sangfelt,[5] Charles Spruck,[4] Elizabeth A. Leibold,[2] James A. Wohlschlegel[1]*

Eukaryotic cells require iron for survival and have developed regulatory mechanisms for maintaining appropriate intracellular iron concentrations. The degradation of iron regulatory protein 2 (IRP2) in iron-replete cells is a key event in this pathway, but the E3 ubiquitin ligase responsible for its proteolysis has remained elusive. We found that a SKP1-CUL1-FBXL5 ubiquitin ligase protein complex associates with and promotes the iron-dependent ubiquitination and degradation of IRP2. The F-box substrate adaptor protein FBXL5 was degraded upon iron and oxygen depletion in a process that required an iron-binding hemerythrin-like domain in its N terminus. Thus, iron homeostasis is regulated by a proteolytic pathway that couples IRP2 degradation to intracellular iron levels through the stability and activity of FBXL5.

Iron regulatory proteins 1 and 2 (IRP1 and IRP2) function as RNA-binding proteins during iron-limiting conditions in order to regulate the translation and stability of mRNAs encoding proteins required for iron homeostasis (*1*, *2*). In iron-replete cells, IRP RNA binding is reduced because of the assembly of a 4Fe-4S cluster in IRP1 (*3*) and the proteasomal degradation of IRP2 (*4*–*7*). Despite the importance of IRP2 in iron metabolism, the ubiquitin ligase

responsible for its degradation remains unclear. Early studies suggested that a unique 73-amino-acid region of IRP2 was a substrate for the haem-oxidized IRP2 ubiquitin ligase (HOIL-1) (*8*, *9*). Other studies, however, showed that deletion of the 73-amino-acid region or HOIL-1 silencing did not affect the iron-dependent degradation of IRP2 (*10*–*12*).

Human FBXL5 is a member of the F-box family of adaptor proteins that confer substrate specificity to SCF (SKP1-CUL1-F-box) ubiquitin ligases (*13*, *14*). FBXL5 contains a hemerythrin-like domain, a F-box domain that mediates its association with SKP1, and four leucine-rich repeats that probably function in substrate binding (fig. S1). Affinity purification followed by multi-dimensional protein identification technolology (MudPIT) (*15*, *16*) was used to identify proteins that interact with a mutant form of FBXL5 lacking the F-box domain, which cannot assemble into an active SCF complex (*17*). Because this mutant retains the ability to interact with substrates but is unable to catalyze their ubiquitination, it functions as a substrate-trapping reagent. IRP1 and IRP2 were identified as FBXL5-interacting proteins in this analysis (table S1). A reciprocal proteomic analysis showed that FBXL5, SKP1, and CUL1 copurify with IRP2 (table S1).

We confirmed the interaction of FBXL5 with SCF components and IRPs using coimmunoprecipitation analyses (*17*). Human embryonic kidney (HEK) 293 cells stably expressing hemagglutinin (HA)–FLAG-FBXL5 were transfected with Myc-CUL1 or Myc-SKP1. HA-FLAG-FBXL5 copurified with immunoprecipitated Myc-CUL1 and Myc-SKP1 (Fig. 1A). For the FBXL5-IRP interactions, HA-FLAG-FBXL5 was immunoprecipitated from stable HEK293 cells. Endogenous IRP1 and IRP2 copurified only in extracts containing HA-FLAG-FBXL5 (Fig. 1B). We found that the 73-amino-acid region of IRP2 was not required for the interaction with FBXL5 (fig. S2). Thus, FBXL5 is a component of a bona fide SCF complex that interacts with IRP1 and IRP2.

To determine whether the FBXL5-IRP2 interaction is regulated by iron, we immunoprecipitated FLAG-IRP2 from HEK293 cells coexpressing either Myc-FBXL5 or Myc-FBXL5-ΔF-box after treatment with ferric ammonium citrate (FAC) or the iron chelator desferrioxamine (DFO). FLAG-IRP2 interacted with Myc-FBXL5 and Myc-FBXL5-ΔF-box more strongly in cells treated with FAC as compared with those treated with DFO, suggesting that the interaction is iron-regulated (Fig. 1C). In addition, we found that expression of Myc-FBXL5 but not Myc-FBXL5-ΔF-box strongly reduced the abundance of co-expressed IRP2, which is consistent with a role for FBXL5 in promoting IRP2 degradation and FBXL5-ΔF-box acting as a dominant negative mutant. The interaction of Myc-FBXL5 and Myc-FBXL5-ΔF-box with IRP1 and an IRP1-C3S mutant, which is sensitive to iron-dependent degradation because of its inability to form a 4Fe-4S cluster, was also iron-regulated (fig. S3) (*18*, *19*).

Coimmunoprecipitation analyses showed that FBXL5 overexpression reduced the levels of co-transfected IRP2 in an iron-regulated manner (Fig. 1C). Stable expression of HA-FLAG-FBXL5 in HEK293 cells also reduced endogenous IRP2 levels in an iron-dependent manner (Fig. 2A). Reduced IRP2 was associated with an increase in the iron-storage protein ferritin, indicating that ferritin was translationally derepressed (*1*, *2*). FBXL5 depletion by small interfering RNA (siRNA) in HEK293 cells increased IRP2 and decreased ferritin protein levels independently of iron treatment (Fig. 2B). Similar results were found when FBXL5 was depleted from IMR90 human diploid fibroblasts (fig. S4), indicating that IRP2 regulation by FBXL5 is not limited to transformed cells.

To determine whether FBXL5 regulates IRP2 iron-dependent degradation, pulse-chase experiments were performed in order to measure the half-life of endogenous IRP2 in control HEK293 cells or cells expressing HA-FLAG-FBXL5 or HA-FLAG-FBXL5-ΔF-box with or without FAC (*17*). Expression of HA-FLAG-FBXL5 reduced the half-life of IRP2 in both untreated and FAC-treated cells, whereas expression of HA-FLAG-FBXL5-ΔF-box increased IRP2 half-life (Fig. 2C). Depletion of FBXL5 by siRNA inhibited FLAG-IRP2 degradation as compared with that of cells treated with nonspecific siRNA (Fig. 2D). FBXL5 depletion also prevented the iron-dependent degradation of FLAG-IRP1-C3S (fig. S5).

To determine whether FBXL5 catalyzes IRP2 ubiquitination, we analyzed the abundance of IRP2-ubiquitin conjugates after FBXL5 overexpression (*17*). FLAG-IRP2, HA-ubiquitin (HA-Ub), and Myc-FBXL5 or Myc-FBXL5-ΔF-box were coexpressed in HEK293 cells, and Ub-conjugates were immunoprecipitated under denaturing conditions by use of antibodies to HA. Overexpression of Myc-FBXL5, but not Myc-FBXL5-ΔF-box, increased FLAG-IRP2 poly-ubiquitination (Fig. 2E). Similarly, Myc-FBXL5, but not Myc-FBXL5-ΔF-box, increased the ubiquitination of FLAG-IRP1 and FLAG-IRP1-C3S (fig. S6).

Our data suggest that FBXL5 protein stability may be iron-regulated (Figs. 1C and 3, A and

[1]Department of Biological Chemistry, David Geffen School of Medicine, University of California, Los Angeles, CA 90095, USA. [2]Departments of Medicine and Oncological Sciences, University of Utah, Salt Lake City, UT 84112, USA. [3]Department of Chemistry and Biochemistry, University of California, Los Angeles, CA 90095, USA. [4]Sidney Kimmel Cancer Center, San Diego, CA 92121, USA. [5]Cancer Center Karolinska, Department of Oncology and Pathology, Karolinska Hospital, SE-171 76 Stockholm, Sweden. [6]School of Biotechnology, Department of Proteomics, Royal Institute of Technology/AlbaNova, SE-106 91 Stockholm, Sweden.

*To whom correspondence should be addressed. E-mail: jwohl@mednet.ucla.edu

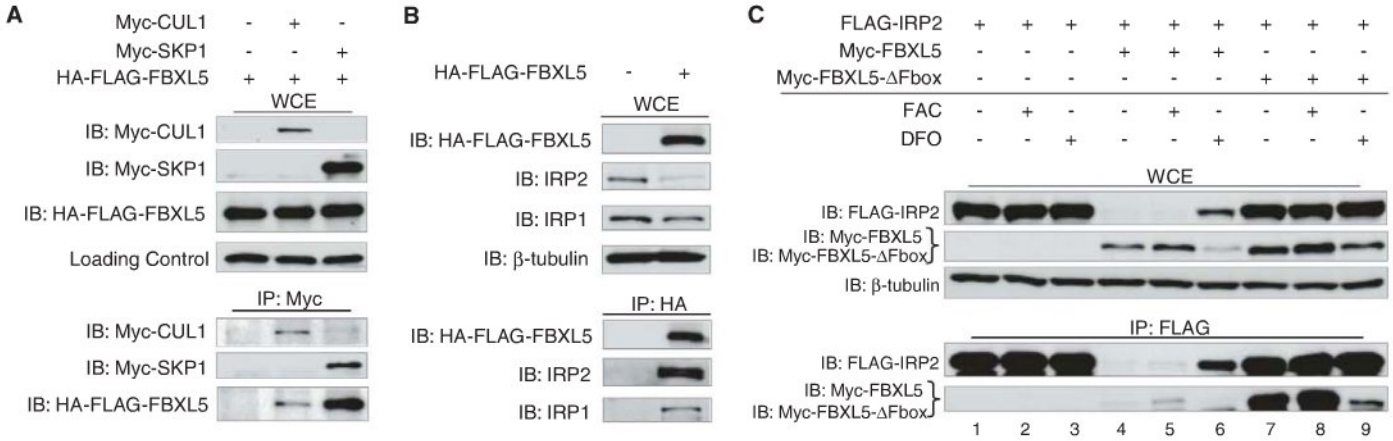

Fig. 1. FBXL5 forms a SCF complex that associates with IRP1 and IRP2. (**A**) Flp-In TREx-293 cells (Invitrogen, Carlsbad, CA) stably expressing HA-FLAG-FBXL5 were transfected with Myc-CUL1, Myc-SKP1, or empty vector. Myc-CUL1 and Myc-SKP1 were immunoprecipitated with antibody to c-Myc. Whole-cell extracts (WCEs) and immunoprecipitates (IPs) were immunoblotted with antibodies to FLAG and c-Myc. (**B**) HA-FLAG-FBXL5 was immunoprecipitated from stable Flp-In TREx-293 cells using antibody to HA. WCEs and IPs were immunoblotted with antibodies to FLAG, IRP1, IRP2, and β-tubulin. (**C**) HEK293 cells were cotransfected with FLAG-IRP2 and Myc-FBXL5, Myc-FBXL5-ΔF-box, or empty vector and treated for 8 hours with FAC or DFO. FLAG-IRP2 was immunoprecipitated using antibodies to FLAG. WCEs and IPs were immunoblotted with antibodies to FLAG, c-Myc, and β-tubulin.

B). We hypothesized that oxygen levels may also affect FBXL5 stability because IRP2 is stabilized during hypoxia (*10*, *20*). We tested these hypotheses by analyzing endogenous FBXL5 levels in cells treated with FAC, DFO, or hypoxia (1% O_2). FBXL5 levels increased with FAC and decreased with DFO and hypoxia (Fig. 3A). Reduction of FBXL5 protein by DFO or hypoxia was blocked by treatment with the proteasome inhibitor MG132, suggesting that FBXL5 is targeted for proteasomal degradation under these conditions (Fig. 3B). Pulse-chase experiments at 21% O_2 showed that FBXL5 half-lives were increased with FAC treatment (5.8 hours) and decreased by DFO (2.5 hours) as compared with that of untreated cells (4.3 hours) (Fig. 3C). The half-life of HA-FLAG-FBXL5 was also decreased in untreated cells exposed to 1% O_2 (Fig. 3C). Thus, FBXL5 stability is dependent on cellular iron and oxygen concentrations.

We next examined the role of the putative hemerythrin-like binding domain (PFAM01814) in regulating FBXL5 stability and function. Hemerythrins are oxygen carriers that bind to oxygen through a diiron metal center (*21*). The hemerythrin-like domain of FBXL5 could therefore function as a cellular iron and oxygen "sensor" by directly binding iron and oxygen. The protein-threading algorithm HHpred (*22*) revealed that the FBXL5 N terminus is structur-

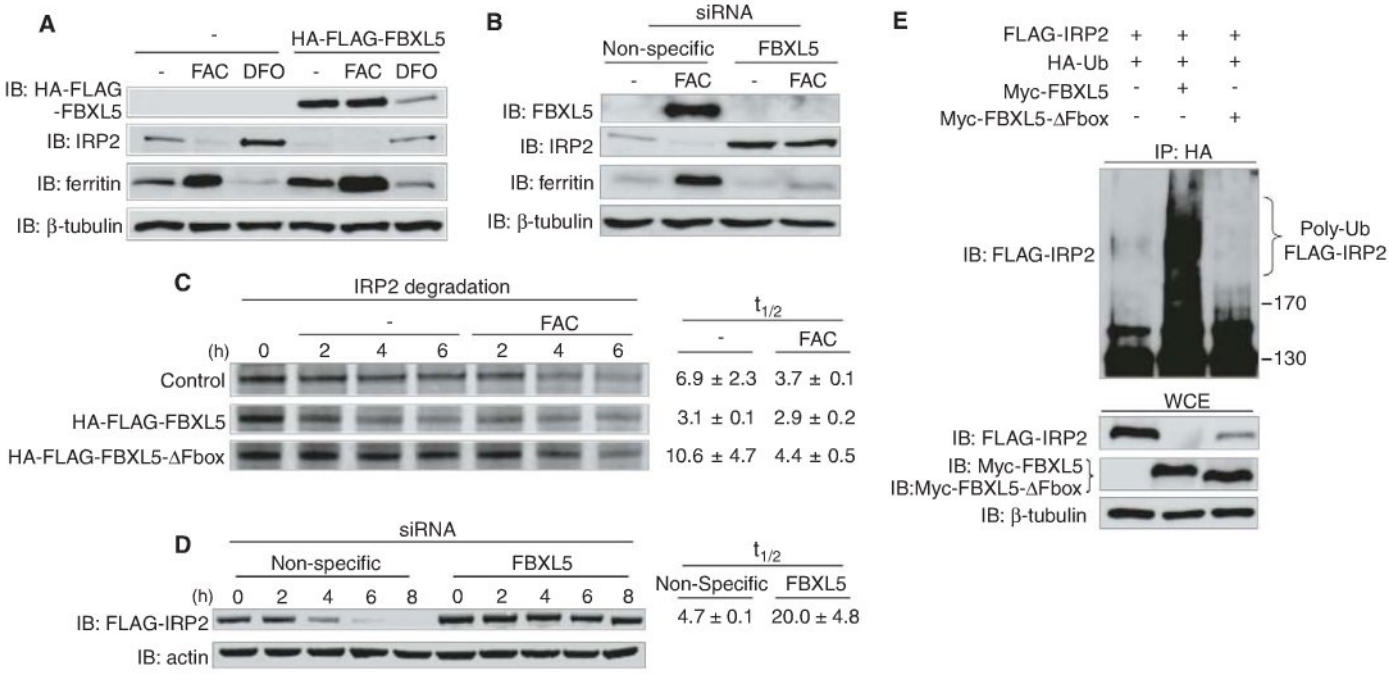

Fig. 2. FBXL5 regulates IRP2 ubiquitination and iron-dependent degradation. (**A**) Flp-In TREx-293 cells stably expressing HA-FLAG-FBXL5 or control cells were treated for 8 hours with FAC or DFO. WCEs were probed with antibodies to FLAG, IRP2, ferritin, and β-tubulin. (**B**) HEK293 cells were transfected with nonspecific or FBXL5 siRNAs and then treated with or without FAC for 8 hours. WCEs were immunoblotted with the specified antibodies. (**C**) Flp-In TREx-293 cells stably expressing HA-FLAG-FBXL5 or HA-FLAG-FBXL5-ΔF-box or control cells were pulsed with ^{35}S-met/cys for 1 hour and then chased in medium supplemented with or without additional FAC. ^{35}S-labeled endogenous IRP2 was immunoprecipitated with antibody to IRP2 and half-lives (t 1/2) are shown as average ± SD (n = 2 independent experiments). (**D**) Flp-In TREx-293 cells stably expressing FLAG-IRP2 were treated with nonspecific or FBXL5 siRNAs, pulsed with doxycycline overnight so as to induce FLAG-IRP2 expression, and then chased in medium supplemented with FAC. WCEs were probed with antibodies to FLAG and actin. FLAG-IRP2 half-lives (t 1/2) are shown as average ± SEM (n = 3 independent experiments). (**E**) HEK293 cells were cotransfected with HA-Ub, FLAG-IRP2 and Myc-FBXL5, Myc-FBXL5-ΔF-box, or empty vector and then treated with FAC and MG132 for 4 hours and ubiquitin conjugates immunoprecipitated by using antibodies to HA. HA-immunoprecipitates (IP: HA) and WCEs were immunoblotted with antibodies to FLAG, c-Myc, and β-tubulin.

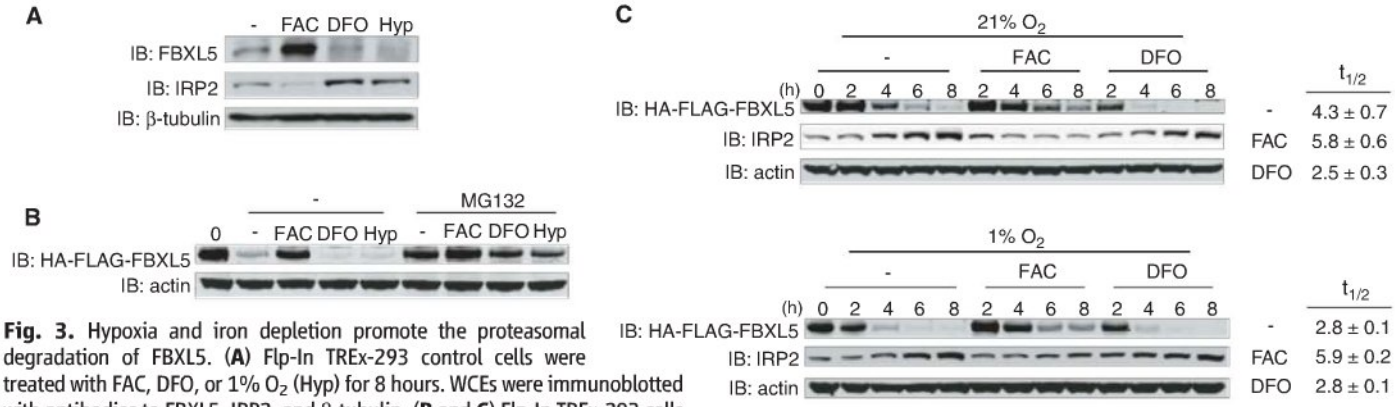

Fig. 3. Hypoxia and iron depletion promote the proteasomal degradation of FBXL5. (**A**) Flp-In TREx-293 control cells were treated with FAC, DFO, or 1% O_2 (Hyp) for 8 hours. WCEs were immunoblotted with antibodies to FBXL5, IRP2, and β-tubulin. (**B** and **C**) Flp-In TREx-293 cells stably expressing HA-FLAG-FBXL5 were treated overnight with doxycycline so as to induce HA-FLAG-FBXL5 expression and then chased in control medium (–) in 21% O_2 or 1% O_2 (hypoxia) or in medium supplemented with FAC or DFO. (B) Cells were supplemented with or without MG132 for 6 hours. WCEs were immunoblotted with antibodies to FLAG and actin. (C) WCEs were immunoblotted with antibodies to FLAG, IRP2, and actin. HA-FLAG-FBXL5 half-lives (t 1/2) are shown as average ± SEM (n = 3 independent experiments).

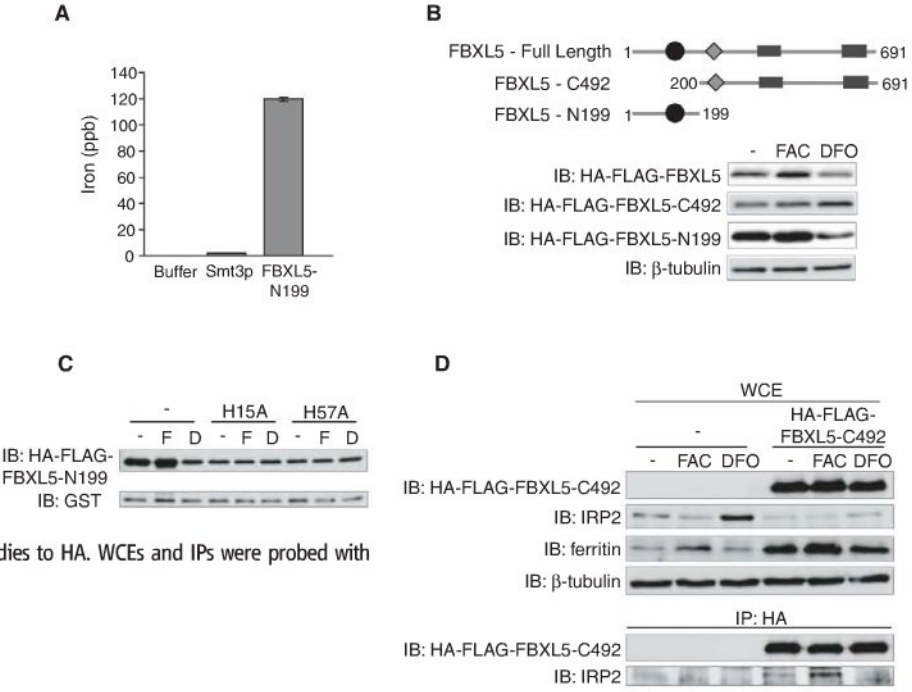

Fig. 4. FBXL5 stability is regulated by an iron-binding hemerythrin-like domain. (**A**) An N-terminal fragment of FBXL5 encompassing amino acids 1 to 199 (FBXL5-N199) or Smt3p (negative control) was expressed in *Escherichia coli*, and the amount of copurifying iron was measured by means of ICP-MS. (**B**) HEK293 cells were transfected with HA-FLAG-FBXL5, HA-FLAG-FBXL5-N199, or HA-FLAG-FBXL5-C492 (amino acids 200 to 691) and treated with FAC or DFO for 8 hours. WCEs were immunoblotted with antibodies to FLAG or β-tubulin. (**C**) HEK293 cells were cotransfected with HA-FLAG-FBXL5-N199, HA-FLAG-FBXL5-N199-H15A, or HA-FLAG-FBXL5-N199-H57A, and a plasmid expressing glutathione *S*-transferase (GST) as a marker for transfection efficiency, and treated with FAC (F) or DFO (D) for 8 hours. WCEs were immunoblotted with antibodies to FLAG and GST. (**D**) Flp-In TREx-293 cells stably expressing HA-FLAG-FBXL5-C492 or control cells were treated for 8 hours with FAC or DFO. HA-FLAG-FBXL5-C492 was immunoprecipitated by use of antibodies to HA. WCEs and IPs were probed with antibodies to FLAG, IRP2, ferritin, and β-tubulin.

ally homologous to other hemerythrin family members, with the highest-scoring hit ($P = 1.6 \times 10^{-17}$) belonging to a hemerythrin-like domain protein from *Neisseria meningitides* (Uniprot, Q9JYL1) (fig. S7). Inductively coupled plasma mass spectrometry (ICP-MS) analysis showed that iron copurified with a recombinant fragment of FBXL5 (FBXL5-N199), which encompasses the hemerythrin-like domain, but not buffer alone or His-Smt3p, an unrelated control protein (Fig. 4A) (*17*). Thus, the N terminus of FBXL5 can function as a hemerythrin domain to coordinate iron and oxygen binding.

Based on the FBXL5 domain structure, we hypothesized that the C-terminal 492 amino acids of FBXL5 (FBXL5-C492) containing both the F-box domain and the leucine-rich repeats function in substrate recognition and ubiquitin conjugation, whereas the N-terminal 199 amino acids regulate FBXL5 stability. We expressed the HA-FLAG-FBXL5-N199 and -C492 fragments in HEK293 cells and analyzed their abundance after FAC and DFO treatments (Fig. 4B). HA-FLAG-FBXL5 and HA-FLAG-FBXL5-N199 protein levels were iron-dependent, whereas HA-FLAG-FBXL5-C492 abundance was not iron-regulated. We also found that the mutation of two putative iron-binding residues in the hemerythrin-like domain, H15A and H57A, reduced the abundance and iron-dependent stability of FBXL5 as compared with the wild-type protein (Fig. 4C). Collectively, these data indicate the hemerythrin-like domain regulates FBXL5 stability through iron-coordination.

Because FBXL5-C492 is stable in iron-depleted cells but retains the ability to interact with IRP2, we used this C-terminal fragment to determine whether iron regulates the FBXL5-IRP2 interaction beyond controlling FBXL5 stability. Expression of HA-FLAG-FBXL5-C492 in HEK293 cells reduced endogenous IRP2 levels, indicating that this C-terminal fragment can promote IRP2 degradation (Fig. 4D). IRP2 levels in the HA-FLAG-FBXL5-C492–expressing cells remain partially iron-regulated (stabilized in DFO compared FAC), suggesting that intracellular iron concentrations are still capable of influencing this pathway. Moreover, HA-FLAG-FBXL5-C492 associates with IRP2 more strongly in FAC-treated cells as compared with DFO-treated cells (Fig. 4D). Thus, an iron-dependent mechanism promotes the physical association of FBXL5 with IRP2. By analogy to other F-box proteins in which substrate binding is dependent upon the post-translational modification of the target, these data could be explained by an iron-regulated modification on IRP2 that stimulates its association with FBXL5.

Our study demonstrates that IRP2 protein levels are controlled by an iron-regulated SKP1-CUL1-FBXL5 complex (fig. S8). In the presence of iron and oxygen, the FBXL5 hemerythrin-like domain binds iron, resulting in the stabilization of a SKP1-CUL1-FBXL5 complex that catalyzes IRP2 ubiquitination and proteasomal degradation. Conversely, loss of iron and/or oxygen binding by the hemerythrin-like domain renders FBXL5 susceptible to proteasomal degradation. These studies identify an iron sensor that functions as a key regulator of iron homeostasis in eukaryotes.

References and Notes

1. M. U. Muckenthaler, B. Galy, M. W. Hentze, *Annu. Rev. Nutr.* **28**, 197 (2008).
2. M. L. Wallander, E. A. Leibold, R. S. Eisenstein, *Biochim. Biophys. Acta* **1763**, 668 (2006).
3. T. A. Rouault, *Nat. Chem. Biol.* **2**, 406 (2006).
4. B. Guo, J. D. Phillips, Y. Yu, E. A. Leibold, *J. Biol. Chem.* **270**, 21645 (1995).
5. B. Guo, Y. Yu, E. A. Leibold, *J. Biol. Chem.* **269**, 24252 (1994).
6. K. Iwai, R. D. Klausner, T. A. Rouault, *EMBO J.* **14**, 5350 (1995).
7. F. Samaniego, J. Chin, K. Iwai, T. A. Rouault, R. D. Klausner, *J. Biol. Chem.* **269**, 30904 (1994).
8. H. Ishikawa *et al.*, *Mol. Cell* **19**, 171 (2005).
9. K. Yamanaka *et al.*, *Nat. Cell Biol.* **5**, 336 (2003).
10. E. S. Hanson, M. L. Rawlins, E. A. Leibold, *J. Biol. Chem.* **278**, 40337 (2003).
11. J. Wang *et al.*, *Mol. Cell. Biol.* **24**, 954 (2004).
12. K. B. Zumbrennen, E. S. Hanson, E. A. Leibold, *Biochim. Biophys. Acta* **1783**, 246 (2008).
13. T. Cardozo, M. Pagano, *Nat. Rev. Mol. Cell Biol.* **5**, 739 (2004).
14. M. D. Petroski, R. J. Deshaies, *Nat. Rev. Mol. Cell Biol.* **6**, 9 (2005).
15. M. P. Washburn, D. Wolters, J. R. Yates 3rd, *Nat. Biotechnol.* **19**, 242 (2001).
16. D. A. Wolters, M. P. Washburn, J. R. Yates 3rd, *Anal. Chem.* **73**, 5683 (2001).
17. Materials and methods are available as supporting material on *Science* Online.
18. S. L. Clarke *et al.*, *EMBO J.* **25**, 544 (2006).
19. J. Wang *et al.*, *Mol. Cell. Biol.* **27**, 2423 (2007).
20. E. G. Meyron-Holtz, M. C. Ghosh, T. A. Rouault, *Science* **306**, 2087 (2004).
21. R. E. Stenkamp, *Chem. Rev.* **94**, 715 (1994).
22. J. Soding, A. Biegert, A. N. Lupas, *Nucleic Acids Res.* **33**, W244 (2005).

23. This work was supported by grants from NIH (GM45201 to E.A.L), the Swedish Cancer Society (N.B. and O.S.), the Swedish Children Cancer Foundation (O.S.), the Swedish Research Council (O.S.), the Cancer Society in Stockholm (O.S.), the Knut and Alice Wallenberg Foundation (A.P. and M.U.), the Stein-Oppenheimer Foundation (J.A.W.), and the Jonsson Comprehensive Cancer Center (J.A.W.). We thank D. Lim for graphic support.

Supporting Online Material

www.sciencemag.org/cgi/content/full/1176333/DC1
Materials and Methods
Figs. S1 to S8
Table S1
References

15 May 2009; accepted 14 August 2009
Published online 17 September 2009;
10.1126/science.1176333
Include this information when citing this paper.

An E3 Ligase Possessing an Iron-Responsive Hemerythrin Domain Is a Regulator of Iron Homeostasis

Ameen A. Salahudeen,* Joel W. Thompson,* Julio C. Ruiz, He-Wen Ma, Lisa N. Kinch, Qiming Li, Nick V. Grishin, Richard K. Bruick†

Cellular iron homeostasis is maintained by the coordinate posttranscriptional regulation of genes responsible for iron uptake, release, use, and storage through the actions of the iron regulatory proteins IRP1 and IRP2. However, the manner in which iron levels are sensed to affect IRP2 activity is poorly understood. We found that an E3 ubiquitin ligase complex containing the FBXL5 protein targets IRP2 for proteasomal degradation. The stability of FBXL5 itself was regulated, accumulating under iron- and oxygen-replete conditions and degraded upon iron depletion. FBXL5 contains an iron- and oxygen-binding hemerythrin domain that acted as a ligand-dependent regulatory switch mediating FBXL5's differential stability. These observations suggest a mechanistic link between iron sensing via the FBXL5 hemerythrin domain, IRP2 regulation, and cellular responses to maintain mammalian iron homeostasis.

Although iron is an essential cofactor for many proteins, its chemical properties also promote side reactions that damage macromolecules. Failure to maintain proper iron homeostasis can lead to a variety of diseases including anemia and iron overload disorders (*1*–*4*). When cellular iron bioavailability is low, the iron regulatory proteins IRP1 and IRP2 coordinate the posttranscriptional regulation of many genes affecting cellular and systemic iron homeostasis by binding to iron response elements (IREs) found within their mRNAs (*5*, *6*). For example, when IRPs bind to the IRE located within the 5′ untranslated region (UTR) of the ferritin mRNA, initiation of protein synthesis is repressed (*1*, *2*). Conversely, IRP binding to IREs within the transferrin receptor 1 (TfR1) 3′UTR stabilizes the mRNA and increases its expression (*7*). When cellular iron bioavailability is high, IRP1 assembles an iron-sulfur cluster and loses its affinity for IREs (*6*), whereas IRP2 is preferentially degraded by the proteasome (*8*, *9*). However, the underlying mechanism(s) by which cells directly sense iron (as well as oxygen) bioavailability and relate those changes to differences in IRP2 stability remain controversial (*10*–*15*).

To address these questions, we performed a small interfering RNA (siRNA) screen to identify an E3 ubiquitin ligase that regulates IRP2 stability (*16*). A clonal human embryonic kidney (HEK)

Department of Biochemistry, University of Texas Southwestern Medical Center, Dallas, TX 75390, USA.

*These authors contributed equally to this work.
†To whom correspondence should be addressed. E-mail: richard.bruick@utsouthwestern.edu

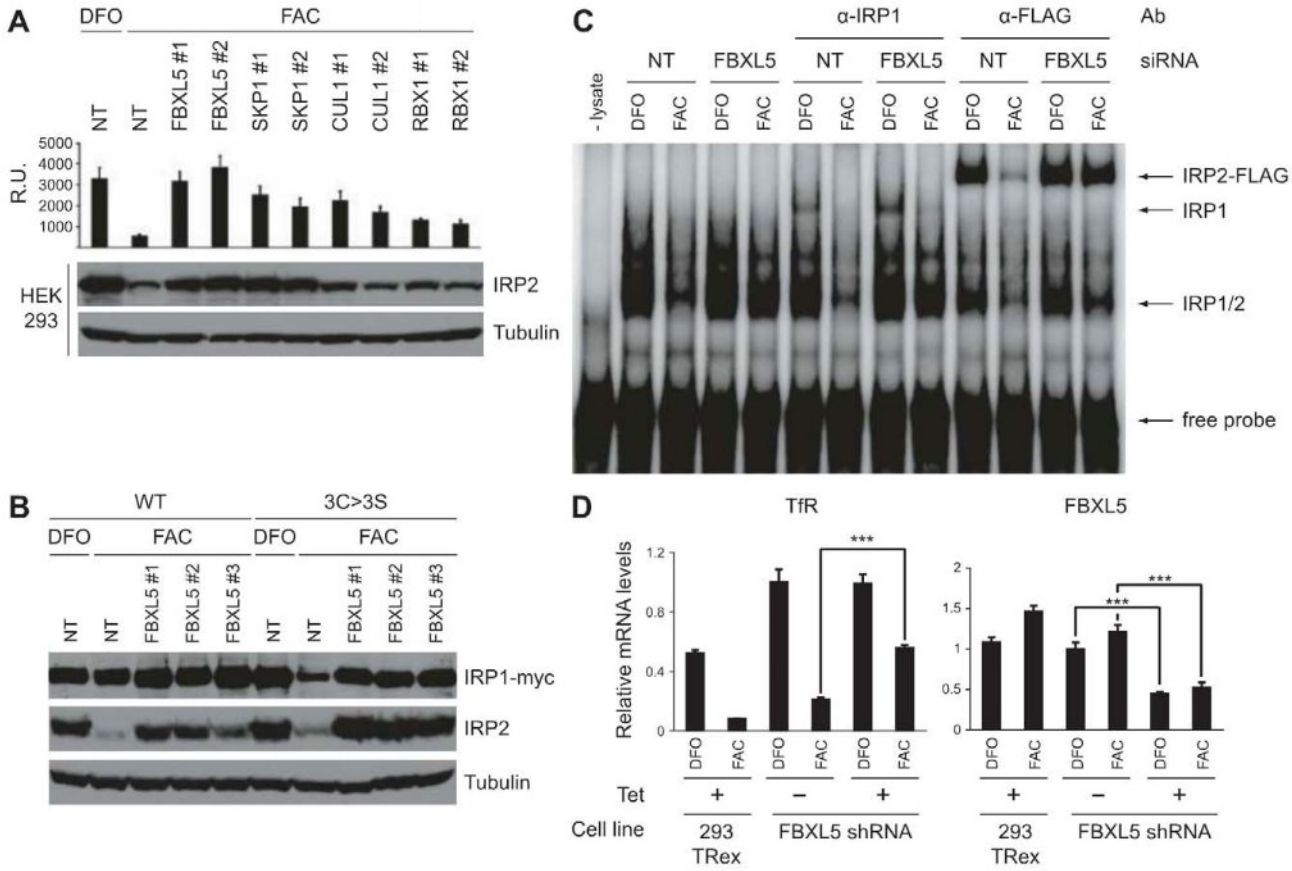

Fig. 1. IRP2 is stabilized under iron-replete conditions after siRNA-mediated suppression of SCF^{FBXL5}. (**A**) IRP2 accumulation was assessed using the AlphaScreen assay (top) or by immunoblot analysis of endogenous IRP2 (bottom). Knockdown efficiency of the SKP1, CUL1, and RBX1 siRNAs is shown in fig. S2D. (**B**) IRP1 stabilization under iron-replete conditions after siRNA-mediated suppression of FBXL5, as measured by immunoblot analysis of HEK 293 cell lines stably transfected with either a myc-tagged wild-type (WT) or 3C>3S IRP1 Tet-inducible expression construct. (**C**) Measurement of RNA binding activity from lysates after siRNA-mediated suppression of FBXL5 in cells expressing HA-IRP2-FLAG. Because human IRP1-IRE and IRP2-IRE complexes migrate similarly, antibodies were added to supershift individual complexes. (**D**) Relative TfR1 and FBXL5 mRNA accumulation levels measured by qRT-PCR. Assays were performed in triplicate with data represented as the mean ± SE with *P* values determined using Student's unpaired *t* test (***$P < 0.001$).

293 cell line stably transfected with a plasmid constitutively expressing N-terminal hemagglutinin (HA)–tagged and C-terminal FLAG-tagged IRP2 accumulated high levels of HA-IRP2-FLAG in cells depleted of iron upon treatment with the chelator deferoxamine mesylate (DFO). As observed for endogenous IRP2, low levels of HA-IRP2-FLAG accumulated in cells incubated in the presence of excess iron [ferric ammonium citrate (FAC); fig. S1B]. As an alternative to immunoblots, HA-IRP2-FLAG accumulation levels could be assessed using a high-throughput luminescent proximity assay (AlphaScreen; fig. S1A).

Inappropriate accumulation of HA-IRP2-FLAG under iron-replete conditions, consistent with reduced E3 ligase activity, was best observed with siRNAs targeting expression of the F-box–containing FBXL5 protein (*17*). Compared with a nontargeting (NT) control siRNA, knockdown of FBXL5 expression by either of two independent siRNAs (FBXL5 1 or 2) led to complete stabilization of HA-IRP2-FLAG under iron-replete conditions (Fig. 1A). Similar results were observed for endogenous IRP2 in HEK 293 cells (Fig. 1A), HeLa cells (fig. S2A), nontumorigenic HBEC-30 cells (fig. S2B), and a clonal cell line containing a tetracycline (Tet)–inducible FBXL5 short hairpin RNA (shRNA) (see below). F-box–containing proteins typically assemble within SCF E3 ubiquitin ligase complexes containing SKP1, Cullin 1 (CUL1), and RBX1 (*18*), each of which were also identified in the unbiased siRNA screen and whose knockdown partially stabilized IRP2 (Fig. 1A).

Despite a greater than 60% amino acid identity, IRP1 and IRP2 are regulated differently. Such differences are not attributable to the 73–amino acid insert unique to IRP2 (*19*), as deletion of this region does not preclude iron-dependent IRP2 degradation or sensitivity to FBXL5 knockdown (fig. S2C). Moreover, when IRP1 is not bound to an iron-sulfur cluster, it can be targeted for proteasomal degradation under iron-replete conditions, similar to IRP2 (*20*, *21*). Although little change in IRP1 levels was observed in FAC-treated HEK 293 cell lines stably expressing myc-tagged wild-type (WT) IRP1 after transfection with three independent FBXL5 siRNAs, a myc-tagged IRP1 (3C > 3S) lacking three cysteines required for Fe-S cluster assembly (*20*) responded in an analogous manner to endogenous IRP2 (Fig. 1B). Together, these data suggest that FBXL5 can recognize both apo-IRP1 and IRP2, likely through a common element.

We performed electrophoretic mobility shift assays to demonstrate that this accumulated IRP2 upon FBXL5 knockdown is functional. Knockdown of FBXL5 expression under iron-replete conditions increased total IRE binding activity (IRP1/2) to levels similar to those observed under iron-deficient conditions (Fig. 1C). Although IRP1's RNA binding activity is sensitive to cellular iron availability, FBXL5 knockdown had little effect on IRP1's IRE binding activity, which suggests that it does not simply reduce cellular iron uptake or availability. In contrast, the increased IRP2-FLAG levels upon FBXL5 knockdown in FAC-treated cells elevated total IRP2 RNA binding activity (Fig. 1C). Furthermore, in Tet-inducible FBXL5 shRNA cells, loss of FBXL5 expression (+Tet) resulted in a factor of ~2.5 increase in TfR1 mRNA accumulation under iron-replete conditions (Fig. 1D) consistent with the increased IRP2 levels (see below). Thus, reduced FBXL5 expression results in inappropriate accumulation of IRP2 under iron-replete conditions and increased IRP2 IRE binding activity with concomitant misregulation of IRP target genes.

A physical interaction between FBXL5 and IRP2 was observed as antibodies to FLAG coimmunoprecipitated FBXL5-V5 with IRP2-FLAG (Fig. 2A) and FLAG-tagged FBXL5 coimmunoprecipitated endogenous IRP2 (Fig. 2B). To investigate whether this interaction reflected an E3 ligase–substrate relationship, we prepared recombinant SCF^{FBXL5}. Affinity-purified FLAG-tagged WT FBXL5, but not FBXL5 lacking the F-box domain, assembled into a stoichiometric (fig. S3, A and B) SCF^{FBXL5} complex (Fig. 2C). Purified SCF^{FBXL5}, but not the ΔF-box FBXL5 variant (fig. S3C), was able to ubiquitinate recombinant IRP2 in vitro (Fig. 2D).

To reveal the mechanism by which SCF^{FBXL5} targets IRP2 for degradation in both an iron- and oxygen-dependent manner (*2*, *6*), we conducted an immunoblot analysis, which revealed that both FBXL5-FLAG (Fig. 3A) and endogenous FBXL5 (Fig. 3C) protein levels were low when iron is limiting but increased by more than an order of magnitude under iron-replete conditions. This difference was attenuated by addition of the proteasome inhibitor MG132 (Fig. 3A). Interestingly, FBXL5-FLAG protein levels were inversely regulated with respect to IRP2 (Fig. 3B). Because FBXL5 mRNA levels did not change significantly as a function of iron (Fig. 1D) and iron-dependent regulation of exogenous FBXL5-FLAG did not require elements from the FBXL5 promoter or UTRs, these data indicate that FBXL5 is posttranslationally targeted for proteasomal degradation in an iron-dependent manner. FBXL5-FLAG levels from iron-replete cells were also substantially lower when incubated under low-O_2 conditions (Fig. 3D). Thus, both

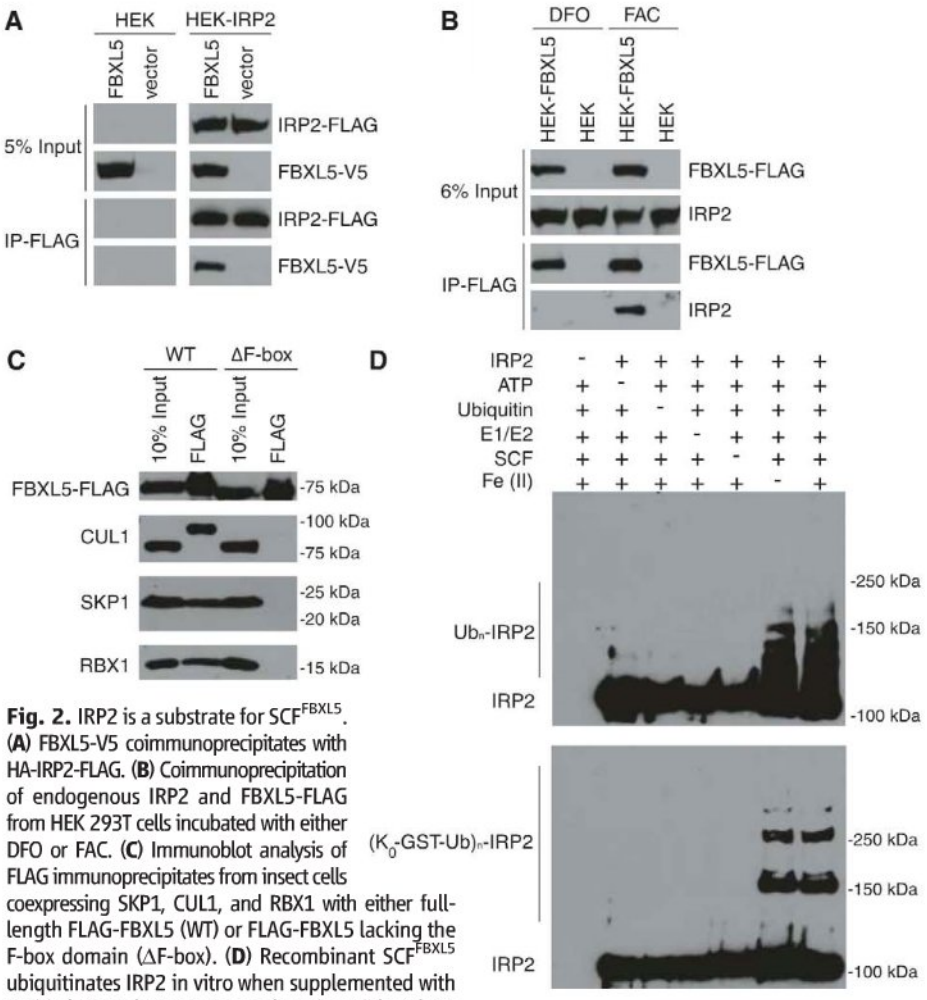

Fig. 2. IRP2 is a substrate for SCF^{FBXL5}. **(A)** FBXL5-V5 coimmunoprecipitates with HA-IRP2-FLAG. **(B)** Coimmunoprecipitation of endogenous IRP2 and FBXL5-FLAG from HEK 293T cells incubated with either DFO or FAC. **(C)** Immunoblot analysis of FLAG immunoprecipitates from insect cells coexpressing SKP1, CUL1, and RBX1 with either full-length FLAG-FBXL5 (WT) or FLAG-FBXL5 lacking the F-box domain (ΔF-box). **(D)** Recombinant SCF^{FBXL5} ubiquitinates IRP2 in vitro when supplemented with purified E1 and E2 enzymes, adenosine triphosphate (ATP), and WT ubiquitin (top) or glutathione *S*-transferase (GST)–tagged ubiquitin lacking lysines (K_0-GST-Ub) and thus unable to form polyubiquitin chains (bottom).

iron- and O_2-dependent regulation of IRP2 may be mediated by reciprocal effects on FBXL5's stability.

To identify the region of FBXL5 that confers such regulation, we transfected a series of V5-tagged FBXL5 deletion mutants (fig. S4) into HEK 293T cells followed by incubation with DFO or FAC. As observed for the full-length protein, all but one deletion construct showed preferential accumulation under conditions of excess iron. In contrast, the FBXL5 ΔN-term protein accumulated at constitutively high levels under both conditions (Fig. 3E). Moreover, expression of FBXL5 residues 1 to 161 demonstrated that this region was sufficient to recapitulate iron-dependent degradation (Fig. 3F).

Residues 1 to 161 of the human FBXL5 protein are predicted to contain five α helices encompassing several conserved histidine and glutamic acid residues (figs. S5 and S6A), similar to hemerythrin-like four-helix up and down bundles with an additional C-terminal helix packed against the core (fig. S6B). Although not previously reported in mammalian proteins, hemerythrin domains have been frequently reported to contain μ-oxo diiron centers (*22*) that reversibly bind oxygen (fig. S6C) and often function as O_2-transport proteins, O_2 sensors, or metal storage depots in marine invertebrates and bacteria (*23*). Recombinantly expressed (fig. S6D) FBXL5 hemerythrin domain (WT) copurified with iron, whereas mutation of one of the predicted bridging carboxylates (E61A) was sufficient to abolish iron binding (Fig. 4A). UV-visible absorbance spectroscopy of the WT domain also showed a broad absorbance peak around 330 nm, characteristic of oxidized μ-oxo diiron centers in hemerythrins (*24*), that decreased upon reduction with dithionite to remove oxygen (Fig. 4B). Circular dichroism spectrometry showed that the WT domain is largely α-helical with minima at 207 and 222 nm (*25*). In contrast, the spectrum of the E61A mutant is indicative of an unstructured protein (Fig. 4C). Thermal denaturation experiments (Fig. 4D) revealed that treatment of the hemerythrin domain with dithionite and the iron chelator *o*-phenanthroline lowers both the melting temperature and cooperativity of unfolding, which indicates that these reagents destabilize the tertiary fold of the domain (*25*). Thus, the FBXL5 N terminus folds into an α helix–rich structure capable of binding both iron and oxygen.

To determine whether the FBXL5 hemerythrin (Hr) domain could regulate a heterologous protein, we transfected HEK 293T cells with constructs expressing the domain fused to either the N terminus (Hr-Luc) or C terminus (Luc-Hr) of firefly luciferase. Unlike unmodified luciferase (Luc), both Hr-Luc (~2.5x) and Luc-Hr (~2.0x) luciferase activities were higher in lysates from FAC-treated cells and correlated with changes in fusion protein accumulation (Fig. 4E). Incubation under low-oxygen conditions also reduced fusion protein luciferase activity and accumulation under iron-replete conditions (Fig. 4E).

Because deletion of the hemerythrin domain resulted in constitutive FBXL5 accumulation (Δ1-161; Fig. 4F) and fusion of the domain conferred iron- and O_2-dependent regulation of stability in the context of a heterologous protein (Fig. 4E), a recognition motif for an E3 ubiquitin ligase (degron) likely resides within this domain. Several F-box proteins mediate their own stability through autoubiquitination (*26*), which may contribute to the partial stabilization of the ΔF-box variant (Fig. 3E). However, knockdown of FBXL5 expression has no effect on the iron-dependent accumulation of the hemerythrin domain itself (fig. S7), indicating that its degron is likely recognized by an as yet unidentified E3 ligase. In the folded iron- and oxygen-bound state, this degron may be efficiently sequestered from the E3 ligase within the hemerythrin fold, promoting FBXL5 accumulation and subsequent IRP2 degradation.

If the hemerythrin domain is unable to assemble a diiron center (e.g., iron-deficient conditions), the domain may unfold to reveal the degron. Degradation of FBXL5 would then preclude the assembly of the SCF complex allowing IRP2 to

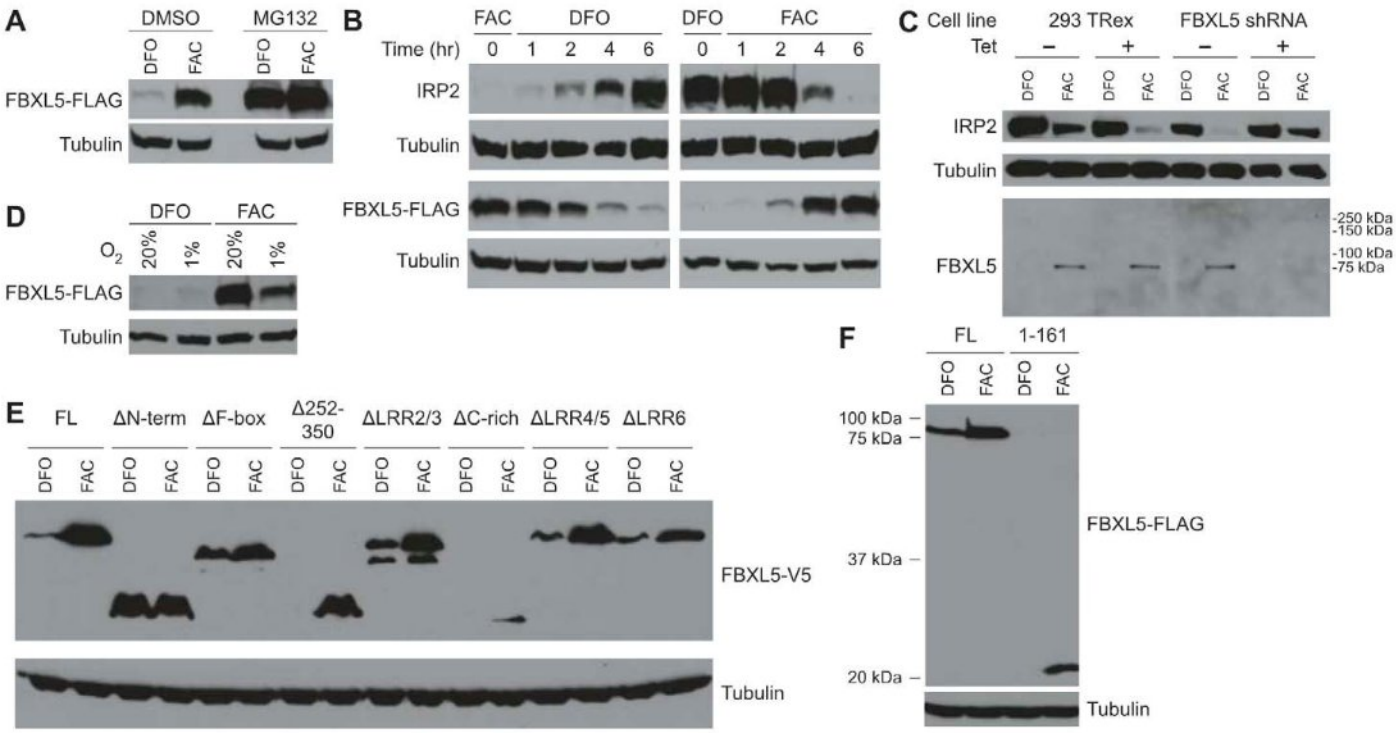

Fig. 3. FBXL5 protein accumulation is dependent on iron and oxygen availability. (**A**) Immunoblot analysis of stably transfected FBXL5-FLAG protein accumulation under iron-deplete (DFO) or iron-replete (FAC) conditions. (**B**) Time course of IRP2 and FBXL5 responses to changes in iron availability. HEK FBXL5-FLAG cells were incubated 16 hours with either FAC or DFO, then switched to low- or high-iron conditions, respectively. Quantitation is provided in table S1. (**C**) Endogenous IRP2 and FBXL5 levels were assessed by immunoblot analysis in WT cells (293 TRex) or in a clonal cell line stably expressing a Tet-inducible FBXL5 shRNA. (**D**) Accumulation of FBXL5 under iron-replete conditions is attenuated (by a factor of 2.5) in cells incubated under low-oxygen conditions (1% O_2) for 16 hours. (**E** and **F**) Residues 1 to 161 mediate iron- and oxygen-dependent regulation of FBXL5 accumulation. Assessment of FBXL5 protein accumulation under iron-deplete (DFO) or iron-replete (FAC) conditions by immunoblot analysis of transiently transfected FBXL5 constructs. Quantitation is provided in table S2.

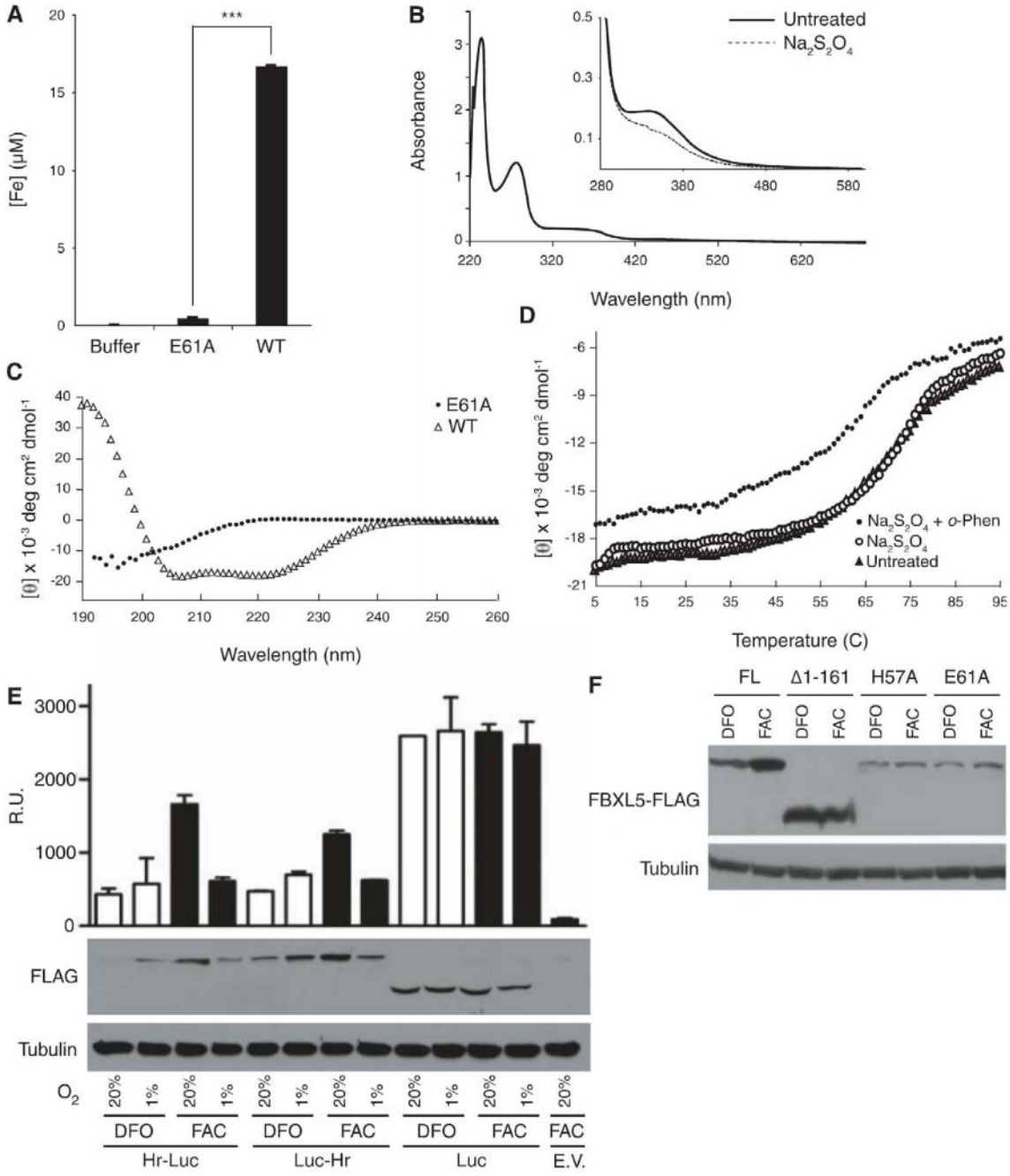

Fig. 4. FBXL5 contains an iron- and oxygen-binding hemerythrin domain that regulates its stability. (**A**) Iron content of recombinant WT or variant (E61A) FBXL5 hemerythrin domains. Assays were performed in triplicate with data represented as the mean ± SE, with *P* values determined using Student's unpaired *t* test (***$P < 0.001$). (**B**) UV chromatogram of the FBXL5 hemerythrin domain before and after dithionite addition. (**C**) Circular dichroism spectra of purified FBXL5 hemerythrin domains. (**D**) Measurement of mean molar residual ellipticity at 222 nm as a function of thermal denaturation of the WT domain treated with dithionite and iron chelator (*o*-Phen). (**E**) Luciferase activity (upper panels) and protein accumulation levels (lower panels; quantitation provided in table S3) in HEK 293T cells transiently transfected with fusion protein expression constructs. E.V., empty vector. Assays were performed in triplicate with data represented as the mean ± SE. (**F**) Immunoblot analysis of protein accumulation from transiently transfected FBXL5 expression constructs.

accumulate and bind IREs. Indeed, prior studies have implicated the involvement of such a labile protein in IRP2 degradation (*8*). Consistent with this model, mutation of iron-binding ligands prevented FBXL5 accumulation (Fig. 4F), suggesting an iron-insensitive, and unfolded, hemerythrin domain in which the degron is constitutively exposed. In contrast, ΔN-term FBXL5 overexpression partially circumvented iron-dependent IRP2 regulation, as observed by a reduction of IRP2 accumulation under iron-deplete conditions (fig. S8). However, the inability of ΔN-term FBXL5 overexpression to fully block IRP2 accumulation in DFO-treated cells may indicate the presence of additional mechanism(s) by which iron and oxygen regulate SCF^{FBXL5}. Underscoring this possibility is the observation that FBXL5 and IRP2 failed to coimmunoprecipitate in lysates from DFO-treated cells, which suggests that iron availability may also affect substrate recognition (Fig. 2B). We did not observe a further increase in ubiquitination activity when additional iron was added to recombinant SCF^{FBXL5} in vitro (Fig. 2D), which suggests two possibilities: Either there was sufficient iron present during purification, or the minimal reconstitution assay presented here did not fully recapitulate all aspects of SCF^{FBXL5} regulation.

Like several F-box–containing proteins reported to act as ligand-regulated effector proteins in plants (*27*), FBXL5 is an example of a ligand-regulated F-box protein in metazoans. Our observations suggest a direct mechanistic link between sensing iron and oxygen availability via FBXL5's hemerythrin domain, IRP2 induction, and the regulation of mammalian iron homeostasis.

References and Notes

1. M. U. Muckenthaler, B. Galy, M. W. Hentze, *Annu. Rev. Nutr.* **28**, 197 (2008).
2. M. L. Wallander, E. A. Leibold, R. S. Eisenstein, *Biochim. Biophys. Acta* **1763**, 668 (2006).
3. E. Beutler, *Annu. Rev. Med.* **57**, 331 (2006).
4. D. M. Wrighting, N. C. Andrews, *Curr. Top. Dev. Biol.* **82**, 141 (2008).
5. M. W. Hentze, M. U. Muckenthaler, N. C. Andrews, *Cell* **117**, 285 (2004).
6. T. A. Rouault, *Nat. Chem. Biol.* **2**, 406 (2006).
7. D. M. Koeller *et al.*, *Proc. Natl. Acad. Sci. U.S.A.* **86**, 3574 (1989).

8. B. Guo, J. D. Phillips, Y. Yu, E. A. Leibold, *J. Biol. Chem.* **270**, 21645 (1995).
9. F. Samaniego, J. Chin, K. Iwai, T. A. Rouault, R. D. Klausner, *J. Biol. Chem.* **269**, 30904 (1994).
10. K. Iwai *et al.*, *Proc. Natl. Acad. Sci. U.S.A.* **95**, 4924 (1998).
11. K. Yamanaka *et al.*, *Nat. Cell Biol.* **5**, 336 (2003).
12. E. Bourdon *et al.*, *Blood Cells Mol. Dis.* **31**, 247 (2003).
13. E. S. Hanson, M. L. Rawlins, E. A. Leibold, *J. Biol. Chem.* **278**, 40337 (2003).
14. J. Wang *et al.*, *Mol. Cell. Biol.* **24**, 954 (2004).
15. K. B. Zumbrennen, E. S. Hanson, E. A. Leibold, *Biochim. Biophys. Acta* **1783**, 246 (2008).
16. See supporting material on *Science* Online.
17. N. Zhang *et al.*, *Biochem. Biophys. Res. Commun.* **359**, 34 (2007).
18. A. R. Willems, M. Schwab, M. Tyers, *Biochim. Biophys. Acta* **1695**, 133 (2004).
19. K. Iwai, R. D. Klausner, T. A. Rouault, *EMBO J.* **14**, 5350 (1995).
20. S. L. Clarke *et al.*, *EMBO J.* **25**, 544 (2006).
21. C. Fillebeen, D. Chahine, A. Caltagirone, P. Segal, K. Pantopoulos, *Mol. Cell. Biol.* **23**, 6973 (2003).
22. R. E. Stenkamp, *Chem. Rev.* **94**, 715 (1994).
23. C. E. French, J. M. Bell, F. B. Ward, *FEMS Microbiol. Lett.* **279**, 131 (2008).
24. J. H. Zhang, D. M. Kurtz Jr., Y. M. Xia, P. G. Debrunner, *Biochemistry* **30**, 583 (1991).
25. N. J. Greenfield, *Nat. Protocols* **1**, 2876 (2007).
26. J. M. Galan, M. Peter, *Proc. Natl. Acad. Sci. U.S.A.* **96**, 9124 (1999).
27. D. E. Somers, S. Fujiwara, *Trends Plant Sci.* **14**, 206 (2009).
28. We thank R. Eisenstein for IRP1 reagents and helpful discussions; Z. Chen for SCF expression plasmids; W. Gao for K_0-GST-Ubiquitin and helpful discussions; M. Brown and J. Goldstein for E2 expression constructs; K. Gardner and F. Correa for assistance with circular dichroism; the UTSW HTS facility for assistance with siRNA screening; and L. Wang, G. Pineda, S. Laxman, X. Du, and J. Wang for helpful discussions. R.K.B. is the Michael L. Rosenberg Scholar in Medical Research and was supported by the Burroughs Wellcome Fund, the Robert A. Welch Foundation, the Texas Advanced Research Program, and NIH grant CA115962. This investigation was conducted in a facility constructed with support from the Research Facilities Improvement Program (grant C06 RR 15437-01) from the NIH National Center for Research Resources.

Supporting Online Material

www.sciencemag.org/cgi/content/full/1176326/DC1
Materials and Methods
Figs. S1 to S8
Tables S1 to S6
References

14 May 2009; accepted 26 August 2009
Published online 17 September 2009;
10.1126/science.1176326
Include this information when citing this paper.

Quantifying the Impact of Immune Escape on Transmission Dynamics of Influenza

Andrew W. Park,[1,2]* Janet M. Daly,[3,4] Nicola S. Lewis,[3,5,6] Derek J. Smith,[5,7,8] James L. N. Wood,[6] Bryan T. Grenfell[7,9,10]

Influenza virus evades prevailing natural and vaccine-induced immunity by accumulating antigenic change in the haemagglutinin surface protein. Linking amino acid substitutions in haemagglutinin epitopes to epidemiology has been problematic because of the scarcity of data connecting these scales. We use experiments on equine influenza virus to address this issue, quantifying how key parameters of viral establishment and shedding increase the probability of transmission with genetic distance between previously immunizing virus and challenge virus. Qualitatively similar patterns emerge from analyses based on antigenic distance and from a published human influenza study. Combination of the equine data and epidemiological models allows us to calculate the effective reproductive number of transmission as a function of relevant genetic change in the virus, illuminating the probability of influenza epidemics as a function of immunity.

As well as occasional pandemics caused by novel virus subtypes against which the population has no natural immunity, influenza virus causes annual epidemics in man, resulting in considerable morbidity and mortality (*1*). The recurring dynamics of annual influenza arises largely from the evolution of the virus (*2*) [particularly gradual changes in the surface antigens, haemagglutinin (HA), and neuraminidase, which determine the influenza subtype]. The mutation rate of the H3N2 subtype of human influenza A virus, which has caused most morbidity and mortality between 1968 and 2009, results in the appearance of antigenically novel viruses every 2 to 5 years (*3*). These viruses have amino acid substitutions at key antigenic sites, allowing them to escape the humoral immunity of individuals vaccinated or infected with preceding strains.

Integration of the epidemiological and evolutionary dynamics (phylodynamics) of influenza viruses is much studied (*3*–*7*). However, a crucial gap in our knowledge is that we do not know how changes in viral HA translate into immune escape in previously infected or vaccinated hosts, in terms of increases in the effective reproductive number (*8*). To quantify this relationship, we need data from controlled seasonal influenza infections, preferably of a natural mammalian host with manipulated prior immunity. A series of experimental infection studies with equine influenza virus (EIV) provides this opportunity (table S1).

Equine influenza vaccines have been used, particularly in racehorses, since the 1960s. For more than 40 years, all equine influenza infections have been caused by strains of the H3N8 subtype, which has a similar course of infection to seasonal influenza A in humans (*9*). In the late 1980s, and in contrast to influenza A in humans, the equine H3N8 subtype diverged into two lineages (*10*). Experiments in which homologous and heterologous equine influenza vaccines were tested (*11*) allow us to relate the impact of differences between vaccine and challenge strains on key epidemiological parameters. We begin with the simplest model, using amino acid substitutions (genetic distance) to measure heterology of different strain pairs (*11*). Our focus here is on relating broad patterns of heterology to epidemic risk. Outbreaks can occur in a wholly susceptible population when the basic reproductive number (R_0) exceeds one; that is, an infectious individual gives rise, on average, to more than one new infection (*8*). In populations that are not wholly susceptible (for example, a partially vaccinated population), the effective reproductive number, R, which takes into account that infectious individuals may make contact with nonsusceptible individuals, is the more appropriate measure of outbreak risk (*8*). The effective reproductive number can be calculated as $R = R_0\, pqd / d_{max}$, where p and q are the probabilities of becoming infected and infectious, respectively, and d is the infectious period (*11*). The parameter d_{max} is the maximum infectious period (estimated as the sample mean of the control animals).

The equine data (Fig. 1) show that even when the HAs of the vaccine and challenge strains are identical, the nonadjuvanted vaccines used are imperfect; animals vaccinated with a homologous strain have ~55% chance of becoming infected (p) and, if infected, have ~65% chance of becoming infectious (q), and are infectious (d) for an average of 2.8 days. Figure 1 also shows that p, q, and d increase with increasing number of amino acid differences in antigenic sites, a [supported by regression analyses (table S2)]. For mismatches of five or more amino acids in

[1]Odum School of Ecology, University of Georgia, Athens, GA 30602, USA. [2]Department of Infectious Diseases, College of Veterinary Medicine, University of Georgia, Athens, GA 30602, USA. [3]Animal Health Trust, Lanwades Park, Newmarket, Suffolk CB8 7UU, UK. [4]School of Veterinary Medicine and Science, The University of Nottingham, Sutton Bonington, Leicestershire LE12 5RD, UK. [5]Department of Zoology, University of Cambridge CB2 3EJ, UK. [6]Cambridge Infectious Diseases Consortium, Department of Veterinary Medicine, Cambridge CB3 0ES, UK. [7]Fogarty International Center, National Institutes of Health, Bethesda, MD 20892, USA. [8]Department of Virology, Erasmus Medical Center, Rotterdam, Netherlands. [9]Center for Infectious Disease Dynamics, The Pennsylvania State University, University Park, PA 16802, USA. [10]Department of Ecology and Evolutionary Biology and Woodrow Wilson School, Princeton University, Princeton, NJ 08540, USA.

*To whom correspondence should be addressed. Email: awpark@uga.edu

epitopes of the HA, the probabilities of becoming infected and infectious are close to 1. The infectious period shows a steady increase with degree of mismatch, increasing to around 5 days in unvaccinated control animals. All control (naïve) animals became infected and infectious. Reanalysis of a human influenza challenge study (*12*) reveals a qualitatively similar trend between p and a [see (*11*) for details].

Deterministic and stochastic models (*11*), parameterized from the equine data (Fig. 1), were used to explore the risk of outbreaks in vaccinated populations, as a function of immune escape. We consider the spread of infection in populations where all 1000 hosts are given the same imperfect vaccine and one infectious individual is introduced into the population; R begins to exceed 1.0 at $a \geq 2$ (i.e., at least two amino acid differences). Coinciding with this, the deterministic model and the worst-case scenario from the stochastic model begin to show large outbreaks (Fig. 2A), which increase in size as a increases. For $a < 2$, we only see stuttering chains of transmission, with ~5% of the population infected in the worst-case scenario. The stochastic model shows that large outbreaks only become the more likely outcome (50th percentile for outbreak size) for $a \geq 7$ (Fig. 2A).

Because the switch from small to large outbreaks being more likely is a qualitative phenomenon (*13*), we can readily use it to demonstrate how the target vaccine coverage to attain herd immunity (*14*) increases as a between the vaccine and circulating strains increases (Fig. 2B). Similarly, when all hosts are vaccinated, there is a trade-off between a and the minimum value of R_0 required to overcome the herd immunity effect (fig. S3).

Although influenza A demonstrates a strong correlation between genetic changes in HA and resulting antigenic phenotype (*3*), punctuation in the antigenic evolution of human influenza viruses indicates that certain amino acid changes have a greater antigenic effect than others (*3*, *7*). The trends observed in the epidemiological traits measured in the equine challenge studies were still evident when antigenic distances (table S4) rather than amino acid differences in antigenic sites were used as the explanatory variable (fig. S4).

Equine influenza strains from the Eurasian (n = 17 strains) and American (n = 24 strains) H3N8 lineages (table S5) were used to compare the use of genetic or antigenic distance to characterize epidemic probability (*11*). Distances were calculated from Newmarket/2/93, which was chosen as a reference strain because it represents the central point of the Eurasian antigenic cluster (Fig. 3A) and was used in several of the challenge studies. These data were used with the stochastic population model to consider the scenario in which a population of 1000 individuals is vaccinated with the reference strain and one individual (infectious with another strain) is introduced into the population. Sizing and coloring the infecting strain according to model predictions of outbreak probability (Fig. 3B) clearly shows the differential risk depending on whether the vaccine and infecting strains are from the same antigenic cluster. When the vaccine and infecting strains come from within a cluster, large outbreaks are rare. Conversely, when the two strains are from different clusters, large outbreaks occur with a probability approaching 0.5 and can result in infection of around 70% of the population (fig. S6). This finding mirrors the observation that unexpectedly large outbreaks occur in vaccinated equine populations when infecting and vaccine strains are from different antigenic clusters (*15*). Sometimes a strain may be predicted to cause a large epidemic on the basis of genetic data despite a vaccine and infecting strain pair appearing to be antigenically similar (Fig. 3B, I) and vice versa (Fig. 3B, II). Overall, though, the model's risk predictions based on genetic distance between vaccine and challenge strains form low and high-risk groups, which are generally consistent with the strain groupings based on antigenic distance.

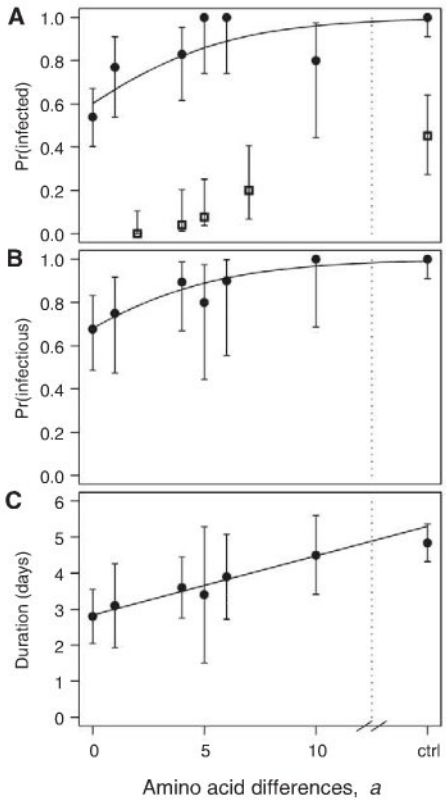

Fig. 1. Results from experimental infection of vaccinated hosts. Increasing the number of amino acid differences in HA epitopes between vaccine and challenge strains affects (**A**) the probability of becoming infected, (**B**) the probability of becoming infectious, and (**C**) the infectious period. Closed circles show the group means from the equine challenge studies and open squares the group means for probability of becoming infected in the human challenge study of Potter *et al.* (*12*). Error bars represent 95% confidence intervals. Solid lines are logistic [(A) and (B)] and linear (C) regressions, with parameters given in table S4. Control (unvaccinated) data are shown but were not used in the regression parameter estimation.

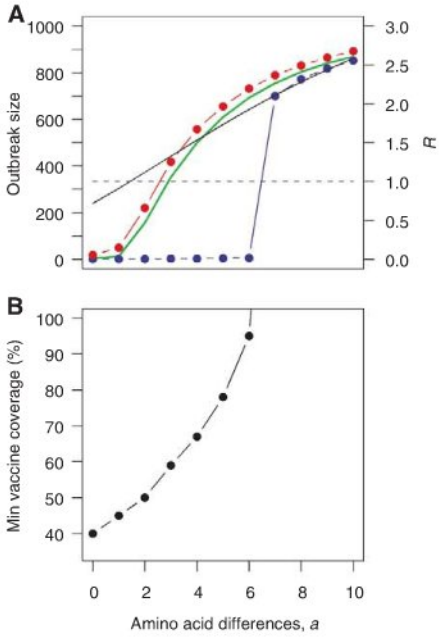

Fig. 2. Results from population models. (**A**) Outbreak size and effective reproductive number (R) in a vaccinated population of 1000 individuals as a function of the number of amino acid differences in HA epitopes of the vaccine and circulating strains. The green line shows the deterministic model prediction for outbreak size, and the solid black line shows the value of R. Five thousand stochastic simulations were ranked by outbreak size. Red circles denote 95th percentiles and blue circles 50th percentiles (median). (**B**) Closed circles show the minimum vaccine coverage necessary to prevent large outbreaks from being the most likely outcome as a function of the number of amino acid differences between the vaccine and circulating strains (assuming $R_0 = 3.0$). Details of model implementation are given in (*11*).

For seasonal influenza, previous exposure to virus as a result of vaccination and infection results in a heterogeneous profile of population immunity. We derive an expression for R when the host population is heterogeneous with respect to partial cross-immunity to a circulating strain (*11*) which shows how R depends on the mean and variance of the number of amino acid differences between the infecting strain and the strains against which a given host's immune system is primed. In addition, R depends on the term $\frac{\partial^2 R}{\partial a^2}$, which captures the details of how the important components of cross-immunity change as a function of the number of amino acid differences. The degree of heterogeneity in the population, measured by var(a), can play a crucial role in determining epidemic risk (*11*) (fig. S6).

This research is also pertinent to the use of vaccines to control pandemic influenza. Baseline predictions of a pandemic with no intervention could be estimated using the model parameterized with data from experimental infection of immunologically naïve animals. Prepandemic vaccines have the advantage that they can be used prophylactically, and can be rapidly dispatched to at-risk populations in the event of a crisis, but are unlikely to be a perfect match to circulating strains (*16*). Our work shows that even these vaccines can provide a benefit to the population (providing a is not too large); increasing the proportion of the population vaccinated can offset an imperfect match between strains (Fig. 2B). In other models, a trade-off has been demonstrated between vaccine coverage and efficacy (foot-and-mouth disease) (*17*), or dose (pandemic influenza) (*18*). Also, models using vaccination in conjunction with antivirals to control pandemic influenza show that low-efficacy vaccines augment population-level protection (*19*).

This study illustrates the power of in vivo infections of natural hosts to illuminate the dynamics of incompletely immunizing pathogens. Specifically, it is the first to explicitly measure how heterology between prevailing immunity and a viral escape mutant influences transmission (through components of the effective reproductive number) and hence epidemic potential in a natural host. This calibration should reinforce modeling studies that relate genetic and antigenic change of influenza virus to ensuing large-scale patterns, including cluster transition rates, seasonal attack rates, and refractory periods (*7*).

Although the model uses data to estimate the dependence of key epidemiological parameters on the genetic distance between vaccine and infecting strains, certain assumptions were necessary (*11*). Because transmission was not explicitly measured in the experiments, we need to assume a baseline transmission rate; this corresponds to $R_0 = 3.0$, which is in line with upper-bound estimates for human influenza A (*20*, *21*) and is in the range of a recent estimate for EIV in stabled racehorses (*22*). Qualitative predictions of the model are robust to changes in this parameter (e.g., fig. S3). The infectious period may be overestimated because it is measured as duration of viral shedding, which ignores the possibility that titers of virus shed may be below an infectious dose, particularly in the early and late stages of this period (*23*). The model assumes that parameters p, q, and d vary independently with a. The data suggest that this is generally true (*11*). There is some evidence of correlation between q and d (possibly mediated by some unmeasured immunological effect). Consequently, an alternative population model is tested embodying this covariance; it shows that results are unaffected by this modification (*11*). The antibody-binding epitopes of H3 HA were proposed for human influenza A (*24*). Although the antigenic sites of equine H3 HA have not been mapped completely, from the data available to date, it is believed that they are equivalent to those proposed for human H3 HA because the human and equine H3 influenza viruses share a common ancestry (*25*).

The synthesis of disease data at different scales (amino acids up to group-level infection studies) has illustrated how herd immunity and immune escape are related in systems with antigenically complex pathogen and host structures. The ultimate goal is to directly link these results to epidemic dynamics, which is a realistic objective as influenza sequence data continues to accumulate. The ideas presented here could extend to a broad class of infections, including emerging, reemerging and extant infectious diseases.

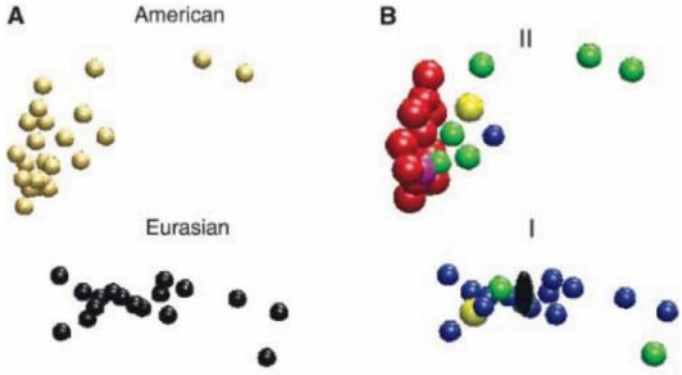

Fig. 3. A sample of equine influenza strains positioned in a three-dimensional antigenic space, where the antigenic phenotype is determined by antigenic cartography of haemagglutination inhibition assay titers (*3*). Strains are colored according to (**A**) phylogenetic grouping [black strains belong to the "Eurasian" lineage and gold strains to the "American" lineage (*10*)] and (**B**) stochastic model predictions for the probability (s) of a large outbreak (determined by a histogram analysis of 1000 replications of the model) in a population of 1000 individuals vaccinated with the strain shown as a black ellipsoid in cluster I, into which one individual (infectious with one of the strains shown in the figure) is introduced. Increasing sphere size represents increasing probability of a large outbreak. This is also color coded where probabilities are blue, $s = 0.0$; green, $0.1 < s < 0.2$; yellow, $0.2 < s < 0.3$; red, $0.3 < s < 0.4$; magenta, $0.4 < s < 0.5$.

References and Notes

1. N. J. Cox, K. Subbarao, *Annu. Rev. Med.* **51**, 407 (2000).
2. D. Hobson, R. L. Curry, A. S. Beare, A. Ward-Gardner, *J. Hyg. (London)* **70**, 767 (1972).
3. D. J. Smith *et al.*, *Science* **305**, 371 (2004).
4. N. M. Ferguson, A. P. Galvani, R. M. Bush, *Nature* **422**, 428 (2003).
5. J. R. Gog, J. Swinton, *J. Math. Biol.* **44**, 169 (2002).
6. B. T. Grenfell *et al.*, *Science* **303**, 327 (2004).
7. K. Koelle, *Science* **314**, 1898 (2006).
8. R. M. Anderson, R. M. May, *Infectious Diseases of Humans: Dynamics and Control* (Oxford Univ. Press, New York, 1991).
9. M. J. Studdert, *Virus Infections of Invertebrates* (Elsevier, New York, 1996).
10. J. M. Daly *et al.*, *Vaccine* **22**, 4101 (2004).
11. Materials and methods are available as supporting material on *Science* Online.
12. C. W. Potter, R. Jennings, J. Nicholson, D. A. J. Tyrrell, K. G. Dickinson, *J. Hyg. (London)* **79**, 321 (1977).
13. I. Nåsell, *Epidemic Models: Their Structure and Relation to Data* (Cambridge Univ. Press, Cambridge, 1995).
14. P. E. M. Fine, *Epidemiol. Rev.* **15**, 265 (1993).
15. J. R. Newton, K. Verheyen, J. L. N. Wood, P. J. Yates, J. A. Mumford, *Vet. Rec.* **145**, 449 (1999).
16. N. M. Ferguson *et al.*, *Nature* **442**, 448 (2006).
17. M. J. Keeling, M. E. J. Woolhouse, R. M. May, G. Davies, B. T. Grenfell, *Nature* **421**, 136 (2003).
18. S. Riley, J. T. Wu, G. M. Leung, *PLoS Med.* **4**, e218 (2007).
19. I. M. Longini *et al.*, *Science* **309**, 1083 (2005).
20. C. Mills, J. Robins, M. Lipsitch, *Nature* **432**, 904 (2004).
21. J. Wallinga, M. Lipsitch, *Proc. R. Soc. London Ser. B. Biol. Sci.* **274**, 599 (2007).
22. K. Satou, H. Nishiura, *J. Eq. Vet. Sci.* **26**, 310 (2006).
23. D. C. Wiley, J. J. Skehel, *Annu. Rev. Biochem.* **56**, 365 (1987).
24. J. A. Mumford, D. Hannant, D. M. Jessett, *Equine Vet. J.* **22**, 93 (1990).
25. R. S. Daniels, J. J. Skehel, D. C. Wiley, *J. Gen. Virol.* **66**, 457 (1985).

26. We are grateful to R. Pyhälä, National Public Health Institute, Finland, for providing the HA1 sequence for A/Finland/74 (H3N2) and L. Yipu, National Institute for Medical Research, UK, for providing a sample of A/Scotland/74 (H3N2) from which we obtained the HA1 sequence. We also thank J. Gog, S. Gandon, J. Drake, P. Rohani, and Y. Michalakis for helpful discussions. Financial support came from Horserace Betting Levy Board (A.P. and J.D.), University of Georgia (A.P.), Cambridge Infectious Diseases Consortium (N.L.), NIH Director's pioneer award DP1-OD000490-01 (D.S.), European Union 223498 (D.S.), Human Frontiers Science Program (D.S.), Defra grant VT0105 (J.W.), Alborada Trust (J.W.), Research and Policy for Infectious Disease Dynamics program of the Science and Technology Directorate, Department of Homeland Security (J.W. and B.G.), NIH grant R01GM083983-02 (B.G.), NSF grant 0742373 (B.G.), Fogarty International Center, and NIH (B.G., D.S., J.W.). The authors declare no competing financial interests.

Supporting Online Material

www.sciencemag.org/cgi/content/full/326/5953/726/DC1
Materials and Methods
Figs. S1 to S7
Tables S1 to S5
References

7 May 2009; accepted 15 September 2009
10.1126/science.1175980

The Transmissibility and Control of Pandemic Influenza A (H1N1) Virus

Yang Yang,[1] Jonathan D. Sugimoto,[1,2] M. Elizabeth Halloran,[1,3] Nicole E. Basta,[1,2] Dennis L. Chao,[1] Laura Matrajt,[4] Gail Potter,[5] Eben Kenah,[1,3,6] Ira M. Longini Jr.[1,3]*

Pandemic influenza A (H1N1) 2009 (pandemic H1N1) is spreading throughout the planet. It has become the dominant strain in the Southern Hemisphere, where the influenza season has now ended. Here, on the basis of reported case clusters in the United States, we estimated the household secondary attack rate for pandemic H1N1 to be 27.3% [95% confidence interval (CI) from 12.2% to 50.5%]. From a school outbreak, we estimated that a typical schoolchild infects 2.4 (95% CI from 1.8 to 3.2) other children within the school. We estimated the basic reproductive number, R_0, to range from 1.3 to 1.7 and the generation interval to range from 2.6 to 3.2 days. We used a simulation model to evaluate the effectiveness of vaccination strategies in the United States for fall 2009. If a vaccine were available soon enough, vaccination of children, followed by adults, reaching 70% overall coverage, in addition to high-risk and essential workforce groups, could mitigate a severe epidemic.

Pandemic H1N1, which first emerged in Mexico in April 2009, had spread worldwide, resulting in more than 130,000 laboratory-confirmed cases and 800 deaths in over 100 countries, by mid-July (*1*). The global distribution of this novel strain prompted the World Health Organization to declare the first influenza pandemic of the 21st century in June 2009 (*2*). Initially, most cases were clustered in households (*3*–*6*) and schools (*7*), with over 50% of the reported cases in schoolchildren in the 5- to 18-year-old age range. A recent analysis of data from the United States, Canada, the United Kingdom, and the European Union suggests upper bounds on case fatality ratios ranging from 0.20% to 0.68% in these regions and a possibly higher case fatality ratio in Mexico of 1.23% [95% confidence interval (CI) from 1.03% to 1.47%] (*8*).

Both pandemic and seasonal influenza cause sustained epidemics in the upper Northern Hemisphere (above latitude ~20°N) and lower Southern Hemisphere (below latitude ~20°S) during the respective late fall to early spring months, with epidemics in the more tropical regions (between latitudes ~20°S and 20°N) occurring spo-

[1]Center for Statistics and Quantitative Infectious Diseases, Fred Hutchinson Cancer Research Center and the University of Washington, Seattle, WA 98109, USA. [2]Department of Epidemiology, School of Public Health, University of Washington, Seattle, WA 98195, USA. [3]Department of Biostatistics, School of Public Health, University of Washington, Seattle, WA 98195, USA. [4]Department of Applied Mathematics, University of Washington, Seattle, WA 98195, USA. [5]Department of Statistics, University of Washington, Seattle, WA 98195, USA. [6]Department of Global Health, University of Washington, Seattle, WA 98195, USA.

*To whom correspondence should be addressed. E-mail: longini@scharp.org

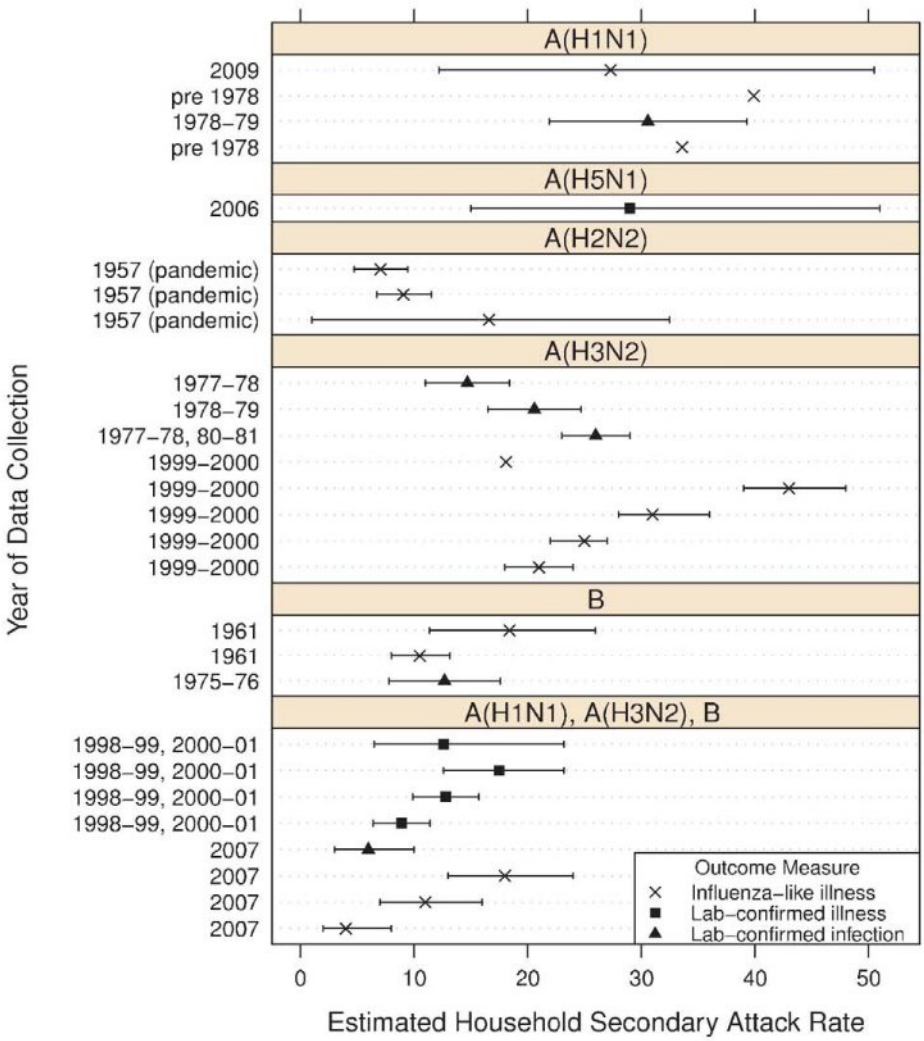

Fig. 1. Estimated influenza illness and infection household secondary attack rates from this study and a PubMed literature search. Detailed information on the search references is given in section 2 of (*15*) and table S8. The household illness secondary attack rate has its basis in the onset date of an influenza-like illness. Lab-confirmed illness is confirmed through a virus-positive nasopharyngeal or throat swab taken at the time of the influenza-like illness. The household infection secondary attack rate has its basis in paired sera bracketing the usual influenza season, where an infection is defined as a substantial rise in hemagglutination-inhibition titer comparing the preinfluenza season sample to the postinfluenza season sample. The 95% CIs are taken from the referenced paper or calculated by the authors if sufficient information was presented. Estimates from pandemic strains include the current estimate and those from Asian influenza A (H2N2) in 1957. The influenza A (H1N1) strain of 1978–1979 reemerged after being absent since 1957. The influenza A (H5N1) strain in 2006 was an avian strain that did not spread beyond the initial family clusters.

radically, but sometimes corresponding to the rainy season. The last influenza pandemic was the Hong Kong influenza A (H3N2) 1968–1969 pandemic. At that time, the first large epidemic was in Hong Kong in July 1968, followed by epidemics in Southeast Asia in August to September 1968, in the upper Northern Hemisphere between September 1968 and April 1969 (peaking in late December 1968 and early January 1969), and in the lower Southern Hemisphere between June and September 1969 (*9*). In the United States and the upper Northern Hemisphere, shifted (i.e., pandemic) or drifted strains of influenza tend to have a relatively small spring "herald wave" before returning in the fall (*10*). In the upper Northern Hemisphere, the 1918–1919 influenza A (H1N1) pandemic had a mild spring 1918 herald wave, followed by a severe second wave in the fall of 1918. Pandemic Asian influenza A (H2N2), 1957–1958, caused mid-summer 1957 outbreaks in Louisiana schools that were open in the summer because of the need for children helping with the spring harvest (*11*). However, there was no extensive community-wide spread of influenza A (H2N2) in the United States until the fall of 1957, with the national level epidemic rising in September and peaking in October. Pandemic H1N1 will probably spread in a spatiotemporal pattern similar to those of previous pandemics but accelerated because of increased air travel (*12*).

Estimates of the transmissibility of pandemic H1N1 are crucial to devising effective mitigation strategies. Historically, the best characterization of influenza transmissibility has been based on the household secondary attack rate. The household secondary attack rate is the probability (sometimes expressed as a percent) that an infected person in the household will infect another person in the household during the infectious period. We used maximum likelihood methods (*13*, *14*) to estimate the illness secondary attack rate of pandemic H1N1 from reported influenza-like illness onset dates in U.S. households (fig. S1) with confirmed index cases of pandemic H1N1 (*15*). The best estimate is 27.3% (95% CI from 12.2% to 50.5%) (table S1), which is robust to uncertainty in the assumed incubation and infectious periods and source of secondary infections (*15*) (tables S1 and S2). Thus, on the basis of early spread of pandemic H1N1 in the United States, each index case has a probability of 0.273 of infecting another household member who becomes ill (table S1). This estimate places pandemic H1N1 in the higher range of transmissibility compared with other influenza viruses for which household secondary attack rates have been estimated (Fig. 1 and table S8). The estimate of the household infection secondary attack rate for the previous influenza A (H1N1) strain from the 1978–1979 epidemic, 30.6% (95% CI from 21.9 to 39.3) (*16*), was slightly higher than our estimate for pandemic H1N1. The other estimates of the household secondary attack rate for influenza A (H1N1) from 1978–1979 or before (*16*, *17*) are quite similar to our estimate.

After disappearing in 1957, influenza A (H1N1) reappeared during the 1978–1979 influenza season, cocirculated with influenza A (H3N2), and was the dominant strain in the United States (*16*). There are no estimates of the household secondary attack rate for the 1918–1919 pandemic strain of influenza A (H1N1). Another influenza virus with comparable household transmissibility to pandemic H1N1 was the avian influenza A (H5N1) virus in Indonesia, with an estimated household secondary attack rate of 29% (95% CI from 15 to 51%), that resulted in a small set of family clusters but no further spread (*14*).

The early spread of influenza A (H1N1) in 1978–1979 was predominately among children, similar to the current pattern of pandemic H1N1 (Fig. 2 and fig. S13). As the epidemic matures, we expect more spread to adults, but with children still experiencing the highest illness attack rate (Fig. 2 and table S10). From the pandemic H1N1 outbreak in the St. Francis Preparatory School in New York (fig. S2), we used maximum likelihood to estimate that the typical schoolchild infected an average of 2.4 (95% CI from 1.8 to 3.2) other schoolchildren in his or her school (table S3). This estimate is robust to uncertainty in the assumed incubation period and proportion of influenza-like illness cases positive for influenza infection (tables S3 and S4 and figs. S8 and S9). This is a very early estimate of the transmissibility of pandemic influenza in schools.

By using household studies and modeling, we estimate that 30 to 40% of influenza transmissions occur in households, about 20% in schools, and the remainder in other settings such as workplaces and the general community [see Halloran *et al.* (*18*) and table S12]. On the basis of this information and the estimated transmission parameters using maximum likelihood methods from U.S. households and the St. Francis Preparatory School (*15*), we estimated the lower bound on the R_0 to be from 1.3 to 1.7 and an upper bound as high as 2.1 (table S5). From the epidemic in Mexico (figs. S3 and S10), with use of maximum likelihood methods, we estimated the mean generation interval to be 3.2 days (95% CI from 3.0

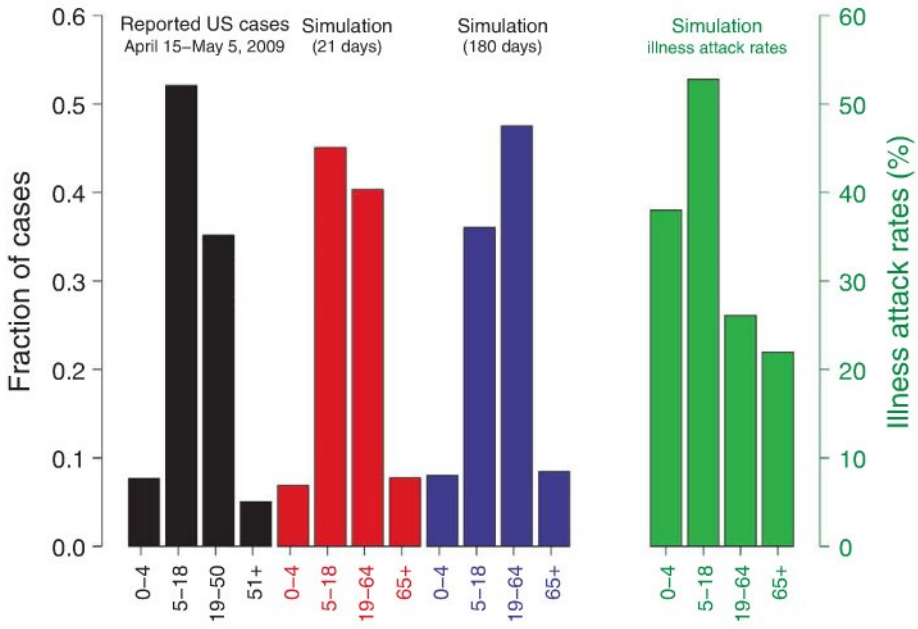

Fig. 2. Observed and simulated age-specific fraction of influenza cases and illness attack rates, with R_0 = 1.6. The black bars show the observed proportion of reported pandemic H1N1 cases by age group in the United States during the early days of the reported U.S. epidemic. The red and blue bars show the simulated proportion at different times after introduction of cases into the Los Angeles County area. The age distribution of cases at 21 days of the simulated epidemic is similar to that of the early observed epidemic. As reflected in the later epidemic, older age groups would become more involved as the infections spreads beyond schools and households. The green bars show the simulated age-specific illness attack rates by the end of an epidemic that runs to completion in the Los Angeles County area. This final age-specific attack rate pattern is similar to that observed for the 1957–1958 Asian A (H2N2) pandemic (*37*).

	Pandemic transmissibility											
	low			moderate			high					
R_0	1.3	1.4	1.5	1.6	1.7	1.8	1.9	2.0	2.1	2.2	2.3	2.4
Illness attack rate (%)	21	26	29	32	35	38	40	42	44	46	48	49
Global cases (billions)	1.4	1.7	2.0	2.2	2.4	2.6	2.7	2.9	3.0	3.1	3.2	3.3

Fig. 3. Simulated illness attack rate for the United States and projected total number of global cases for 1 year of pandemic influenza at different values of R_0. The projections were obtained by multiplying the simulated illness attack rates by the world population of 6.8 billion.

to 3.5 days) (figs. S4 and S5) and R_0 to be 2.3 (95% CI from 2.1 to 2.5), although the R_0 could be as high as 2.9 (95% CI from 2.6 to 3.2) (table S7) for that setting. We defined the generation interval as the time between illness onsets of the index case and someone he or she infects. The mean generation interval could be as low as 2.6 days (95% CI from 2.5 to 2.8 days) (figs. S6 and S7). This estimate is robust to variation in the assumed incubation and infectious periods (figs. S6 and S7). Figure 3 shows simulated final illness attack rates for the United States and the projected global number of people with influenza illness at different values of R_0.

Another previous estimate of R_0 in Mexico ranged from 1.4 to 1.6 (*19*), a lower range than our estimates from Mexico. The influenza Asian A (H2N2) pandemic of 1957–1958 and Hong Kong A (H3N2) of 1968–1969 had estimated R_0 values in the 1.5 to 1.8 range and were considered to be of moderate transmissibility, whereas the influenza A (H1N1) of 1918–1919 had an estimated R_0 in the range of 1.8 to 2.4 and was considered to be highly transmissible (*9*, *20*–*23*).

To evaluate the early transmission of pandemic H1N1 and the potential for control of the virus with pandemic vaccines, we used a previously developed simulation model (*18*, *24*) calibrated to the household (table S11), school, and community transmission given above (tables S10 and S12). Simulation results for Los Angeles County (Fig. 2 and fig. S13) reveal the characteristic pattern of early spread in schoolchildren with eventual spread of infection to other age groups. Although social distancing and the use of antiviral agents can be partially effective at slowing spread, vaccination remains the most effective means of pandemic influenza control (*24*). The primary means for early control of pandemic H1N1 has been to close schools and other social gathering places, but cost-effectiveness analysis reveals that school closure is the least cost-effective measure and that vaccination is the most cost effective for pandemic influenza control (*25*).

Currently, more than 20 manufacturers are in various stages of production for pandemic H1N1 vaccines (*26*, *27*). In the United States, vaccine could have been delivered, starting in September 2009, over several months with enough vaccine for up to 20% of the population per month (*28*). However, the start of delivery was delayed until October 2009. Early analysis of phase I and II immunogenicity data indicates that the level of protection provided should be similar to that of the seasonal influenza A (H1N1) vaccines presently in use. We assume that two doses of vaccine would be needed, with at least 3 weeks between first and second doses. However, one dose for people over 9 years old may prove to be sufficient. We assume that immunity will build over time according to the pattern shown in fig. S11. The final modeled efficacies of seasonal inactivated influenza vaccine based on human challenge studies, vaccine trials, and observational studies are given in table S9 (*29*). Estimates are given for both homologous and

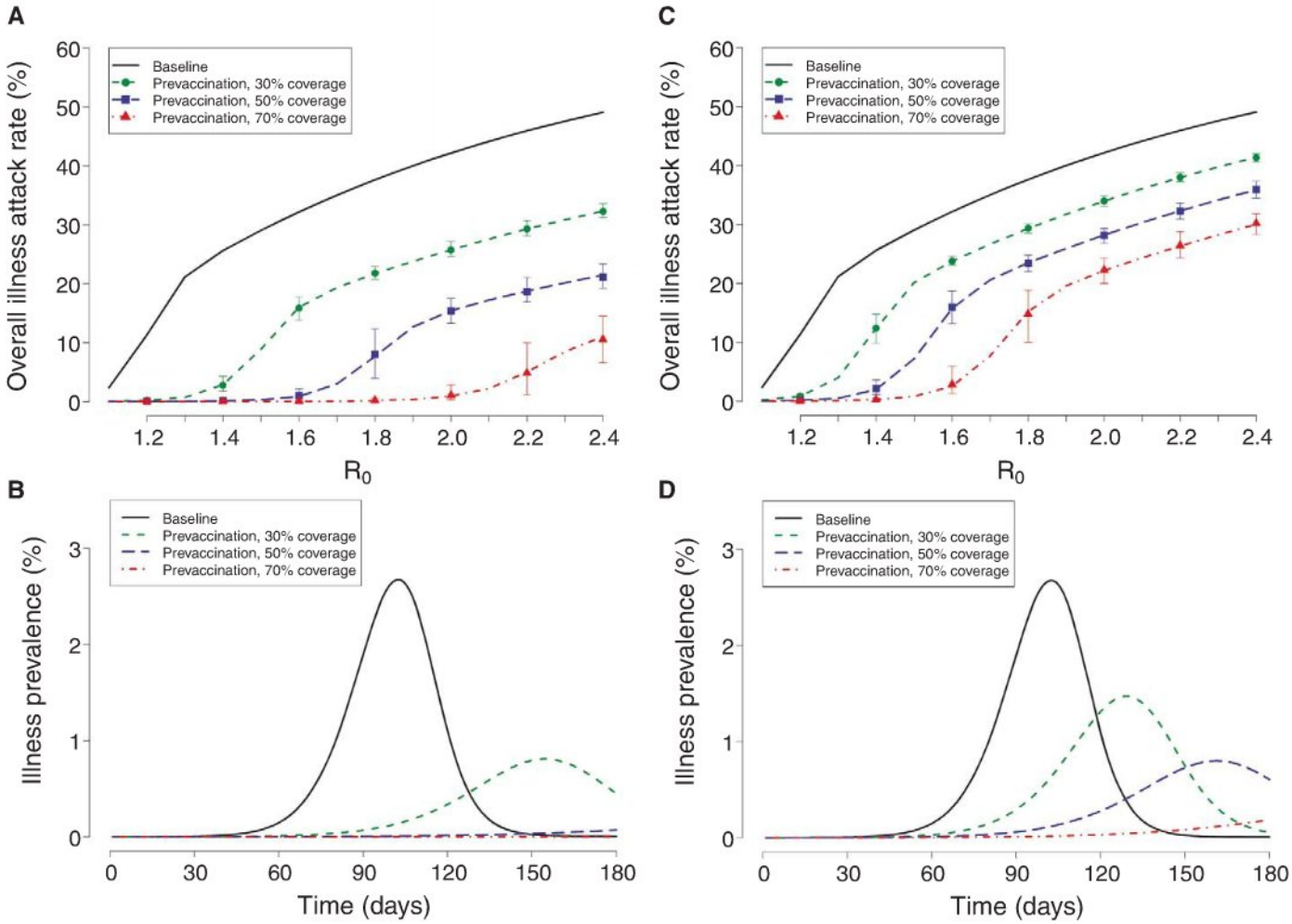

Fig. 4. Simulated effect of prevaccination with a homologously and a heterologously matched pandemic influenza vaccine at different values of R_0 and coverage for the United States. (**A**) Overall illness attack rates for homologous vaccine. Lines indicate the average illness attack rate over five simulations of Los Angeles County for each value of R_0 with the vaccine efficacies summarized in table S9. The 95% error bars indicate the empirical confidence intervals for 100 simulations where the vaccine efficacy parameters are chosen randomly within 15% of their estimated values. (**B**) Epidemic curves at $R_0 = 1.6$ with homologous vaccine. (**C**) Overall illness attack rates with a heterologous vaccine and 95% error bars indicating the empirical confidence intervals when varying the vaccine efficacy parameters. (**D**) Epidemic curves at $R_0 = 1.6$ with heterologous vaccine.

heterologous matches to the wild-type circulating virus. Because we do not know how well-matched a pandemic vaccine will be, we evaluate both scenarios.

To evaluate the effectiveness of pandemic vaccine use in the United States, we used a stochastic simulation model [section 4 of (*15*)] for both Los Angeles County and the United States, assuming different levels of vaccine match (table S9) and coverage before and during spread of the virus in the fall 2009. We assumed that the limited spread of pandemic H1N1 in the United States during the spring and summer of 2009 (*30*) will result in very limited population-level immunity in the fall 2009.

Vaccination increases population-level immunity and lowers the effective reproductive number, having two main effects: first, slowing the spread of infection and reducing the height of the epidemic peak, thus, decreasing the surge capacity needed to deal with influenza cases; second, reducing the overall illness attack rate and mortality. The effectiveness of vaccination depends heavily on the rate and timing of vaccine delivery with respect to when substantial transmission begins. We considered two possible scenarios. First, we considered universal (i.e., all age and risk groups) prevaccination before the spread of the virus in the United States. Second, we considered a phased vaccination program where vaccine is either universally delivered over time as the epidemic progresses or vaccine is delivered to children first.

With successful universal prevaccination and a homologous match with the circulating virus (i.e., homologous vaccine), 70% coverage would be sufficient to successfully mitigate epidemic spread at an R_0 as high as 2.0 (Fig. 4A). We consider an illness attack rate of 15% or less to indicate a well-mitigated epidemic. This would correspond to a relatively mild seasonal influenza epidemic. With 50% universal vaccination, we could mitigate epidemic spread at an R_0 as high as 1.8, whereas 30% coverage would not be effective. At $R_0 = 1.6$, prevaccination slows the epidemic considerably (Fig. 4B). Even at the low coverage of 30%, the epidemic peak can be moved from day 94 in the baseline scenario to day 135. If the circulating virus is heterologous to the vaccine (i.e., heterologous vaccine), 50 to 70% coverage would be effective for mitigating epidemics only at an $R_0 \leq 1.7$, although prevaccination would still slow spread considerably (Fig. 4, C and D).

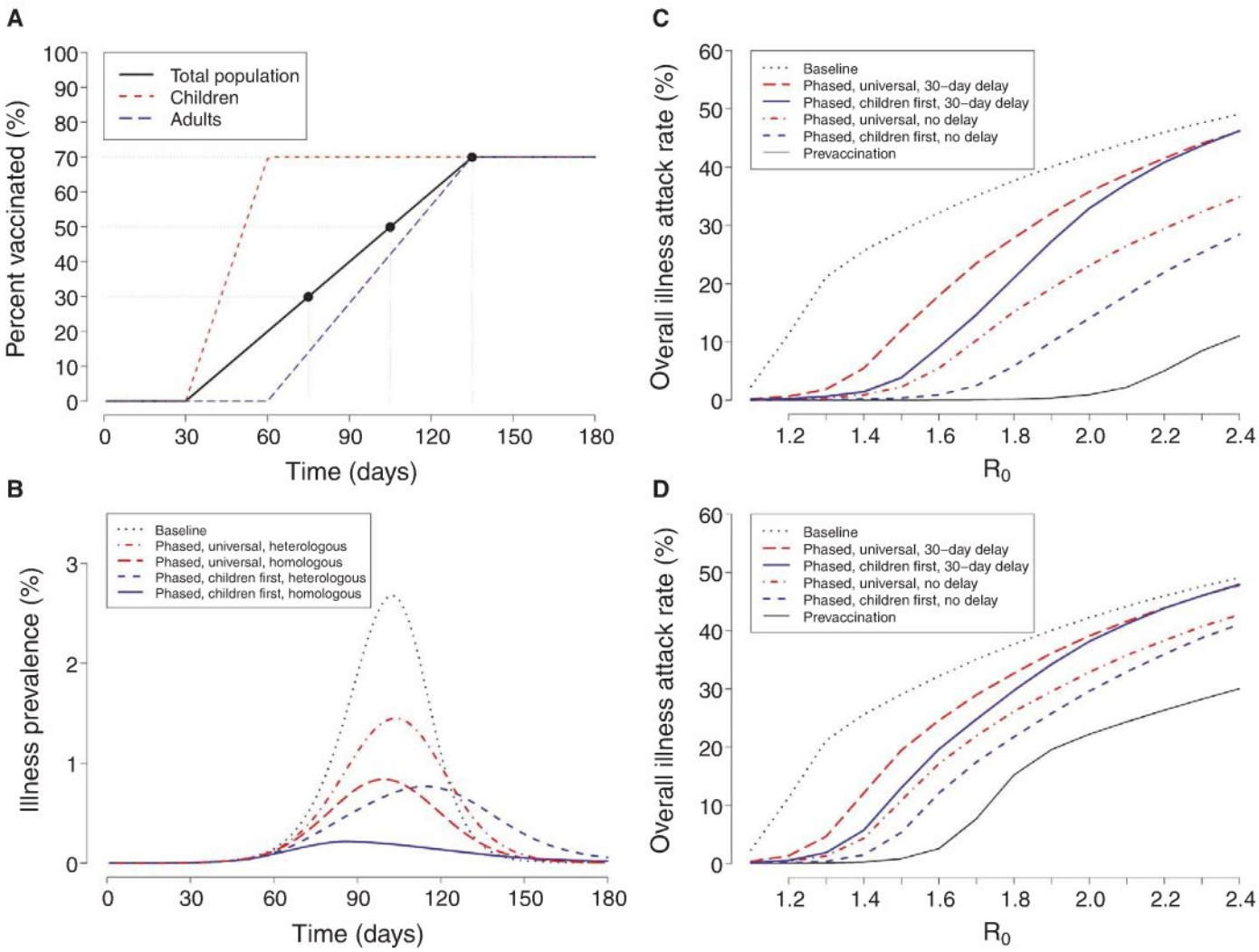

Fig. 5. Simulated effect of phased pandemic influenza vaccination for homologous and heterologous vaccines at different values of R_0 and coverage for the United States. (**A**) Vaccine coverage over time with a 30-day delay. Vaccine is delivered at a rate of 120 million doses each month or about 20% coverage per month. This is enough vaccine to give 60 million people with two doses, 3 weeks apart per month. Vaccine is delivered uniformly over the month. Day 0 is the beginning of pandemic H1N1 spread in the United States. When there is no delay in vaccine supply, vaccination would start on day 0. The dotted lines show the coverage for a strategy to vaccinate children first (red) and then adults (blue) starting when coverage reaches 70% in children. (**B**) Epidemic curves when $R_0 = 1.6$ for homologous and heterologous vaccines, delivered with a 30-day delay. Both universal and the children-first vaccination strategies are shown. (**C**) Overall illness attack rates for homologous vaccine for the universal and children-first vaccination strategies, both with and without the 30-day delay. (**D**) Overall illness attack rates for heterologous vaccine for the universal and children-first vaccination strategies, both with and without the 30-day delay.

Basta *et al.* (*31*) showed that prevaccination of 70% of schoolchildren could be effective in mitigating pandemic H1N1 in the United States for an R_0 as high as 2.0. Because of uncertainty in the eventual vaccine efficacy, we did a sensitivity analysis by varying the vaccine efficacy parameters within 15% of their estimated values (Fig. 4, A and C). This level of uncertainty does not change our conclusions about the effectiveness of vaccination.

Phased vaccination is started either at the beginning of spread or with a delay of 30 days after spread begins (Fig. 5A). We consider both phased universal vaccination and phased vaccination of children (age ≤ 18 years old) first up to 70% coverage before vaccine is delivered to adults (age > 18 years old) (Fig. 5A). Phased vaccination has a potentially large effect on reducing spread but delays the epidemic peak only slightly (Fig. 5B). Movies S1 and S2 show simulated epidemics for the entire United States for $R_0 = 1.6$, with phased universal and phased children-first vaccination, respectively, with a 30-day delay. With a 30-day delay, the phased children-first strategy would mitigate epidemic spread for an R_0 up to 1.7 (Fig. 5C). The same is true for the phased, universal, no-delay vaccination strategy. The universal strategy with a 30-day delay would be less effective. For a heterologous vaccine, phased universal vaccination with no delay and children first with a 30-day delay would be effective mitigation strategies at $R_0 \leq 1.5$ (Fig. 5D). For phased vaccination, we found that 50% final coverage could be effective only for homologous vaccine at $R_0 <$ 1.6 with children first and no delay (table S13).

All the vaccination strategies explored here with coverage of 70% have a substantial mitigating effect. Combining vaccination with other mitigation measures, such as social distancing and targeted use of antiviral agents, could be quite effective (*24*, *32*).

Our current estimates of the transmissibility of pandemic H1N1 indicate the virus is highly transmissible in schools and households, similar to the influenza A (H1N1) that caused high transmission in children during the 1978–1979 influenza season in the United States. A drifted version of that virus has cocirculated with influenza A (H3N2) and B until the present. By mid-July 2009 in the United States, 99% of all subtyped influenza A isolates were pandemic H1N1 (*33*). Similarly, by the end of May 2009, in the Southern Hemisphere during the influenza season, over 90% of reported influenza isolates are pandemic H1N1 (*34*). Pandemic H1N1 is antigenically stable with no sign of genetic drift (*35*). This implies that the vaccine match will be good and that our homologous vaccine scenarios are more likely than the heterologous vaccine scenarios. So far, in the United States and most parts of the upper Northern Hemisphere, pandemic H1N1 has caused outbreaks in close contact groups of children in schools or camps, has spread readily in households when introduced, and now appears to be spreading into the general community. Our preliminary estimate of R_0 from 1.3 to 1.7 is consistent with pandemic spread causing illness in 25% to 39% of the world's population over a 1-year period, similar to the spread of the 1957–1958 Asian influenza A (H2N2) pandemic. Given this situation, making enough pandemic H1N1 vaccine to vaccinate at least 70% of the U.S. population over time is important (Fig. 5A). Because the current pattern of pandemic spread is most likely similar to that of the Asian influenza A (H2N2) in 1957–1958, we expect substantial spread in the United States to begin in early September (around day 60 in Fig. 4B), with the epidemic peaking in October (around day 94 in Fig. 4B). In this case, children-first phased vaccination would need to start as soon as possible and no later than September to be effective in mitigating the epidemic. Should substantial epidemic spread start later in the fall, peaking in late December or early January, then a phased vaccination strategy could be effective for mitigation. The current recommendation of the U.S. Centers for Disease Control and Prevention's Advisory Committee on Immunization Practices is to concentrate early supplies of pandemic H1N1 vaccine in a number of groups (*36*). In addition to children over 6 months of age, young adults, people at high risk for complications, and health care and emergency services personnel are all included in the list. It would be prudent to cover those listed groups in addition to concentrating vaccine in children (*37*, *38*), but further work will be required to investigate the logistics of doing that with limited supplies of vaccine.

References and Notes

1. World Health Organization, "Novel influenza A (H1N1) update 59," 27 July 2009, www.who.int/csr/don/2009_07_27/en/index.html.
2. M. Chan, "World now at start of 2009 influenza pandemic: Statement to the press by WHO director-general," 11 June 2009, www.who.int/mediacentre/news/statements/2009/h1n1_pandemic_phase6_20090611/en/.
3. Centers for Disease Control and Prevention, *Morb. Mortal. Wkly. Rep.* **58**, 400 (24 April 2009), www.cdc.gov/mmwr/PDF/wk/mm5815.pdf.
4. Center for Diseases Control and Prevention, *Morb. Mortal. Wkly. Rep.* **58**, 435 (1 May 2009), www.cdc.gov/mmwr/PDF/wk/mm5816.pdf.
5. Kansas Department of Health and Environment, "Swine influenza news conference," 29 April 2009, www.dhe.state.ks.us/SwineFlu/swineflunewsconf.wmv.
6. Kansas Department of Health and Environment, "KDHE reports 2 cases of swine flu in Kansas," 25 April 2009, www.kdheks.gov/news/web_archives/2009/04252009.htm.
7. New York City Department of Health and Mental Hygiene, "St. Francis Prep update: Swine flu outbreak," 30 April 2009, www.nyc.gov/html/doh/downloads/pdf/cd/h1n1_stfrancis_survey.pdf.
8. T. Garske *et al.*, *BMJ* **339**, b2840 (2009).
9. L. A. Rvachev, I. M. Longini Jr., *Math. Biosci.* **75**, 3 (1985).
10. W. P. Glezen, R. B. Couch, H. R. Six, *Am. J. Epidemiol.* **116**, 589 (1982).
11. F. L. Dunn, D. E. Carey, A. Cohen, J. D. Martin, *Am. J. Hyg.* **70**, 351 (1959).
12. R. Grais, J. Ellis, A. Kress, G. Glass, *Health Care Manage. Sci.* **7**, 127 (2004).
13. Y. Yang, I. M. Longini Jr., M. E. Halloran, *Comput. Stat. Data Anal.* **51**, 6582 (2007).
14. Y. Yang, M. E. Halloran, J. D. Sugimoto, I. M. Longini Jr., *Emerg. Infect. Dis.* **13**, 1348 (2007).
15. Materials and methods are available as supporting material on *Science* Online.
16. I. M. Longini Jr., J. S. Koopman, A. S. Monto, J. Fox, *Am. J. Epidemiol.* **115**, 736 (1982).
17. I. M. Longini Jr., J. S. Koopman, *Biometrics* **38**, 115 (1982).
18. M. E. Halloran *et al.*, *Proc. Natl. Acad. Sci. U.S.A.* **105**, 4639 (2008).
19. C. Fraser *et al.*, *Science* **324**, 1557 (2009); published online 11 May 2009 (10.1126/science.1176062).
20. I. M. Longini Jr., *Math. Biosci. Eng.* **82**, 19 (1986).
21. G. Chowell, C. E. Ammon, N. W. Hengartner, J. M. Hyman, *Math. Biosci.* **4**, 457 (2007).
22. G. Chowell, M. Miller, C. Viboud, *Epidemiol. Infect.* **136**, 852 (2008).
23. C. Mills, J. Robins, M. Lipsitch, *Nature* **432**, 904 (2004).
24. T. C. Germann, K. Kadau, I. M. Longini Jr., C. A. Macken, *Proc. Natl. Acad. Sci. U.S.A.* **103**, 5935 (2006).
25. B. Sander *et al.*, *Value Health* **12**, 226 (2009).
26. National Institute of Allergy and Infectious Diseases, "Clinical trials of 2009 H1N1 influenza vaccines conducted by NIAID-supported vaccine treatment and evaluation units," 22 July 2009, www3.niaid.nih.gov/news/QA/vteuH1N1qa.htm.
27. World Health Organization, "Production and availability of pandemic influenza a H1N1 vaccines," 12 July 2009, www.who.int/csr/disease/swineflu/frequently_asked_questions/vaccine_preparedness/production_availability/en.
28. R. Robinson, "H1N1 vaccine products and production," Advisory Committee on Immunization Practices (ACIP) meeting, Atlanta, GA, 29 July 2009, www.cdc.gov/vaccines/recs/acip/downloads/mtg-slides-jul09-flu/05-Flu-Robinson.pdf.
29. N. E. Basta, M. E. Halloran, L. Matrajt, I. M. Longini Jr., *Am. J. Epidemiol.* **168**, 1343 (2008).
30. Centers for Disease Control and Prevention, "FluView: 2008–2009 influenza season week 20 ending May 23, 2009," www.cdc.gov/flu/weekly/weeklyarchives2008-2009/weekly20.htm.
31. N. E. Basta, D. L. Chao, M. E. Halloran, L. Matrajt, I. M. Longini Jr., *Am. J. Epidemiol.* **15**, 679 (2009).
32. I. M. Longini Jr. *et al.*, *Science* **309**, 1083 (2005); published online 3 August 2005 (10.1126/science.1115717).
33. Centers for Disease Control and Prevention, "FluView: 2008–2009 influenza season week 28 ending July 18, 2009," www.cdc.gov/flu/weekly/weeklyarchives2008-2009/weekly28.htm.
34. S. Briand, "Epidemiology and illness severity of pandemic (H1N1) 09 virus," World Health Organization Strategic Advisory Group of Experts on Immunization Extraordinary Meeting, Geneva, Switzerland, 7 July 2009, www.who.int/immunization/sage/1.Briand_epi_7th_July_2009_(rev_6July_09).pdf.
35. R. J. Garten *et al.*, *Science* **325**, 197 (2009); published online 22 May 2009 (10.1126/science.1176225).
36. Centers for Disease Control and Prevention, "Press release: CDC advisors make recommendations for use of vaccine against novel H1N1," 29 July 2009, www.cdc.gov/media/pressrel/2009/r090729b.htm.
37. I. M. Longini Jr., E. Ackerman, L. R. Elveback, *Math. Biosci.* **38**, 141 (1978).
38. M. E. Halloran, I. M. Longini Jr., *Science* **311**, 615 (2006).

39. This work was partially supported by the National Institute of General Medical Sciences MIDAS grant U01-GM070749 and the National Institute of Allergy and Infectious Diseases grant R01-AI32042.

Supporting Online Material

www.sciencemag.org/cgi/content/full/1177373/DC1
Materials and Methods
Figs. S1 to S13
Tables S1 to S14
Movies S1 and S2
References

8 June 2009; accepted 1 September 2009
Published online 10 September 2009;
10.1126/science.1177373
Include this information when citing this paper.

Hemagglutinin Receptor Binding Avidity Drives Influenza A Virus Antigenic Drift

Scott E. Hensley,[1] Suman R. Das,[1] Adam L. Bailey,[1] Loren M. Schmidt,[1] Heather D. Hickman,[1] Akila Jayaraman,[2] Karthik Viswanathan,[2] Rahul Raman,[2] Ram Sasisekharan,[2] Jack R. Bennink,[1] Jonathan W. Yewdell[1]*

Rapid antigenic evolution in the influenza A virus hemagglutinin precludes effective vaccination with existing vaccines. To understand this phenomenon, we passaged virus in mice immunized with influenza vaccine. Neutralizing antibodies selected mutants with single–amino acid hemagglutinin substitutions that increased virus binding to cell surface glycan receptors. Passaging these high-avidity binding mutants in naïve mice, but not immune mice, selected for additional hemagglutinin substitutions that decreased cellular receptor binding avidity. Analyzing a panel of monoclonal antibody hemagglutinin escape mutants revealed a positive correlation between receptor binding avidity and escape from polyclonal antibodies. We propose that in response to variation in neutralizing antibody pressure between individuals, influenza A virus evolves by adjusting receptor binding avidity via amino acid substitutions throughout the hemagglutinin globular domain, many of which simultaneously alter antigenicity.

Influenza A virus remains an important human pathogen due largely to its ability to evade antibodies specific for its attachment protein, the hemagglutinin (HA). This "antigenic drift" is due to accumulation of amino acid substitutions in HA epitopes recognized by antibodies that neutralize viral infectivity by blocking interaction of HA with sialic acid residues on host-cell membranes (*1*–*3*). The H1 subtype HA has four antigenic sites recognized by monoclonal antibodies with high neutralizing activity, designated Sa, Sb, Ca, and Cb (*4*). How can HA escape polyclonal antibodies given that the frequency of variants with simultaneous multiple point mutations is exceedingly low (*5*)? A popular model posits sequential selection by different individuals whose antibody responses focus on different individual antigenic sites (*6*, *7*).

To better understand how antigenic drift occurs in human populations, we revisited classical experiments modeling drift in outbred Swiss mice (*8*). We generated three separate infectious stocks of the mouse-adapted strain A/Puerto Rico/8/34 (H1N1) (PR8) in Madin-Darby canine kidney (MDCK) cells using reverse genetics. Each stock was serially passaged in naïve mice or mice immunized with inactivated virus. Mice were infected intranasally with virus prepared from lung homogenates.

After nine passages, HA gene sequencing revealed no detectable mutations in viruses passaged in naïve mice (Fig. 1A). By contrast, each lineage from vaccinated mice contained a predominant population with a different single–amino acid substitution: residue 158 (E to K, lineage I), 246 (E to G, lineage II), or 156 (E to K, lineage III) (E, Glu; G, Gly; K, Lys). Residue 158 is located at the interface of the Sa/Sb antigenic sites, residue 156 is in the Sb site, and residue 246 is located outside the defined epitopes (*4*) (Fig. 1B). E158K, initially detected in lineage I after passage 2, predominated by passage 3 (table S1). In lineage II, E246G abruptly emerged during passage 3. In lineage III, E158K and E156K codominated from passage 2 to 7, with E156K predominating after passage 8. None of the lineages exhibited changes in the neuraminidase (NA) gene.

We measured the mutants' ability to escape antibody responses by hemagglutination inhibition (HAI) and virus neutralization assays using immune serum pooled from 45 PR8-vaccinated mice. Each mutant escaped antibody responses in these ternary (virus, antibody, and cell) assays (Fig. 1, C and D), despite demonstrating only minor (E156K, E158K) or no (E246G) decreases in anti-HA antibody binding (Fig. 1E). More precise antigenic analysis by enzyme-linked immunosorbent assay confirmed that the amino acid substitutions had limited effects on individual monoclonal antibody binding (fig. S1). E156K modified Sb antigenicity, but had no effect on the other sites. E158K altered binding of a subset of Sa- and Sb-specific monoclonal antibodies. Notably, just 1 of 16 monoclonal antibodies tested exhibited (slightly) altered binding to E246G, consistent with the observation that the substitution resides outside defined antigenic sites (*4*).

HA mutations can decrease HAI antibody activities by increasing the viral HA binding avidity for cell surface glycan receptors (*9*–*11*). Relative to wild-type virus, such "adsorptive mutants" exhibit enhanced agglutination of erythrocytes treated with *Vibrio cholerae* neuraminidase receptor destroying enzyme (RDE) to remove terminal sialic acids, the cellular HA ligand. Notably, relative to wild-type virus, each mutant better agglutinated RDE-treated erythrocytes (Fig. 1F). Mutant-virus hemagglutination was also more resistant to competition from horse serum "nonspecific" inhibitors (fig. S2), confirming increased cellular receptor binding avidity. Mutant viruses also exhibited higher binding avidity than wild-type virus to both α2-3 and α2-6 sialylated glycans in a dose-dependent, direct glycan receptor-binding assay (fig. S3).

E156K and E158K mutants were again selected when different PR8 stocks (propagated in either eggs or MDCK cells) were passaged in PR8-immunized BALB/c or C57BL/6 mice, indicating that these are particularly adept escape mutants. Because these substitutions modify antigenicity [unlike E246G and previously described adsorptive mutants (*10*)], this suggests that polyclonal antibody escape favors substitutions that simultaneously increase cellular receptor binding and diminish antigenicity.

These findings prompted us to examine the cellular receptor binding avidities of 40 monoclonal antibody–selected HA-escape mutants (*4*). Each amino acid substitution in the panel exerts similar relatively minor effects on HA antigenicity (*4*). Surprisingly, 23 mutants exhibited altered binding to RDE-treated erythrocytes (Fig. 2A and table S2). There was a strong correlation between cellular receptor binding and polyclonal antibody HAI escape (Fig. 2B). Substitutions modifying receptor binding cover all four antigenic sites (Fig. 2, A and C). Of 18 substitutions that enhance receptor binding, 11 increased HA positive charge (Fig. 2D and table S2). Because virions possess ~900 HA monomers (*12*), increased positive charge may enhance cellular receptor binding by increasing charge attraction with negatively charged cell surfaces (*13*). Retrospective analysis supports a relation between H3 HA charge and receptor binding (*14*).

Upon further passaging of the in vivo–selected virus populations in mice vaccinated with homologous inactivated virus (e.g., E156K virus passaged in E156K-vaccinated mice), we detected minor virus populations with novel amino acid substitutions distant from the sialic acid binding site, often distant from defined neutralizing epitopes (table S3 and fig. S4). Substitutions that enhanced receptor binding (Fig. 3A) enhanced polyclonal HAI antibody escape (Fig. 3B).

Optimizing viral fitness requires balancing host cell receptor binding of input virus with release of progeny virus. Notably, passaging in vivo–selected mutants in naïve mice selected mutants (table S3) with reduced cellular receptor binding avidity (Fig. 3A). Mutations selected by passaging in naïve mice decreased polyclonal HAI antibody escape (Fig. 3B). E158K- and E246G-derived mutants were inhibited at levels similar to those exhibited by wild-type PR8, demonstrating the central role of cellular receptor binding in E158K and E246G single–point mutants escape from polyclonal antibodies (see also Fig. 1E). E156K

[1]Laboratory of Viral Diseases, National Institute of Allergy and Infectious Diseases, Bethesda, MD 20892, USA. [2]Harvard-MIT Division of Health Sciences and Technology, Koch Institute for Integrative Cancer Research and Department of Biological Engineering, Massachusetts Institute of Technology, Cambridge, MA 02139, USA.

*To whom correspondence should be addressed. E-mail: jyewdell@mail.nih.gov

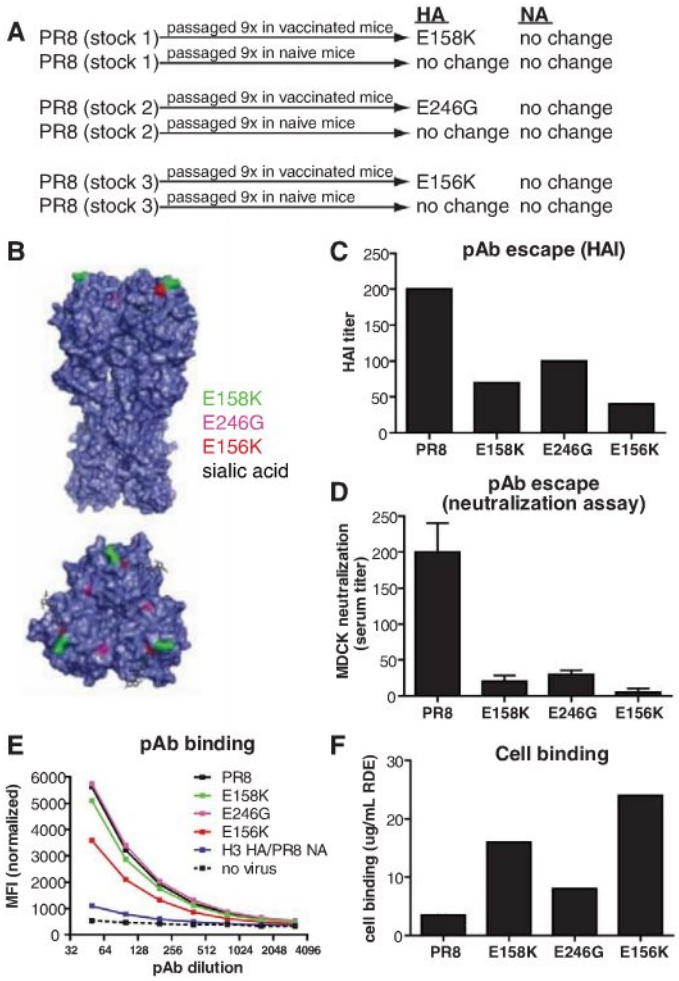

Fig. 1. In vivo influenza A virus passaging selects for mutants with altered binding avidity. (**A**) HA and NA genes were sequenced in lung homogenates from three independent PR8 stocks serially passaged in vaccinated and naïve Swiss mice. [GenBank accession numbers AF389118 (HA) and AF389120 (NA)] (**B**) Location of in vivo–selected HA amino acid substitutions in mutant viruses. (**C**) PR8 and mutant viruses were tested for escape from polyclonal antibodies to PR8 by HAI with turkey erythrocytes or (**D**) by virus neutralization assays with MDCK cells. Data are expressed as inverse dilutions of serum and are representative of three (HAI) or two (virus neutralization) experiments. Data are shown as means ± SEM. (**E**) Polyclonal antibody binding to HA was assessed by flow cytometry after addition of different dilutions of polyclonal antibody to L929 cells infected with the indicated virus followed by the addition of anti-mouse fluorescein isothiocyanate. Shown is mean fluorescence intensity (MFI) after normalizing HA expression based on the binding of a mixture of Ca monoclonal antibodies or a NA-specific monoclonal antibody (for the H3 HA/PR8 NA virus). Polyclonal antibodies bind nearly exclusively to HA, as inferred from their low binding to the H3 HA/PR8 NA–infected cells. Data are representative of three independent experiments. (**F**) Cellular receptor binding avidities were determined by hemagglutination of turkey erythrocytes pretreated with RDE. Data are expressed as the maximal amount of RDE that allowed full agglutination. Data are representative of three independent experiments.

viruses with secondary mutations acquired in naïve mice still escaped wild-type-specific polyclonal antibodies better than wild-type virus, despite a return to wild-type binding avidity, demonstrating that E156K alteration of Sb antigenicity contributes to immune escape.

Despite the absence of antibody selection, some secondary mutations selected in naïve mice modified HA antigenicity (fig. S1). A227T, located near the sialic acid–binding site, reduced binding of the Sa-specific antibody, IC5-2A7. R220G reduced binding of the Sa-specific antibody, H2-6A1. Thus, antigenic drift can be a by-product of Darwinian selection for mutations that optimize host cell receptor binding during influenza A virus transmission between immune (increased receptor binding) and naïve individuals (decreased receptor binding).

To demonstrate an independent role for cellular receptor binding avidity in polyclonal antibody–mediated evolution, we coinfected mice with wild-type PR8 and AM6, an absorptive mutant with a substitution (P186S) in the receptor binding site that does not modify antigenicity (*10*, *15*) (fig. S5A). AM6 was rapidly selected in vaccinated but not naïve mice (fig. S5B). Next, we coinfected mice with E246G virus (minor antigenic change, high receptor binding) and E246G/A227T (greater antigenic change, low receptor binding). Vaccinated mice selected E246G, whereas naïve mice selected E246G/A227T (fig. S5D), confirming the critical role of receptor binding avidity in antibody-driven viral evolution.

To extend our drift model, we passaged E156K/R220G in mice given a high vaccine dose to generate severe antibody selection pressure. This resulted in the selection of E156K/R220G/I244T (no selection occurred in naïve mice). I244T, located in the Sa/Ca interface (fig. S6A), increased cellular receptor binding (Fig. 3C), and as predicted, increased polyclonal HAI antibody escape to levels exhibited by the E156K progenitor (Fig. 3D). Thus, during these passages between naïve and immune individuals, influenza A virus

Fig. 2. Numerous HA amino acid substitutions simultaneously modulate receptor binding and escape from polyclonal antibodies. (**A**) Cellular receptor binding avidities of 40 viruses with single HA amino acid substitutions were determined with RDE-treated turkey erythrocytes. The percentages of viruses within each antigenic group with altered binding are shown. (**B**) Individual mutants were tested for their abilities to escape polyclonal antibodies to PR8 by HAI. Data are plotted as ability to escape polyclonal antibodies versus cellular receptor binding avidity. Means are represented as dots and the 95% confidence interval is represented by dashed lines. (**C**) Locations of HA amino acid substitutions that promote increased avidity are shown in yellow. (**D**) Net change in the charge of mutant viruses was determined (*n*, number of viruses in each group). Data are shown as the means ± SEM.

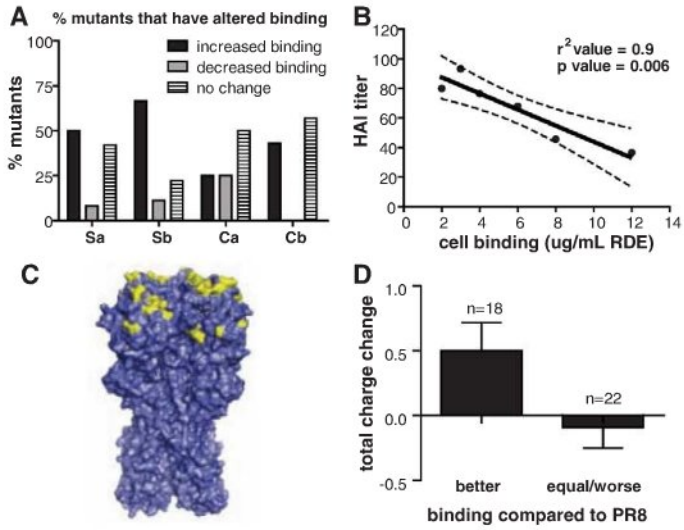

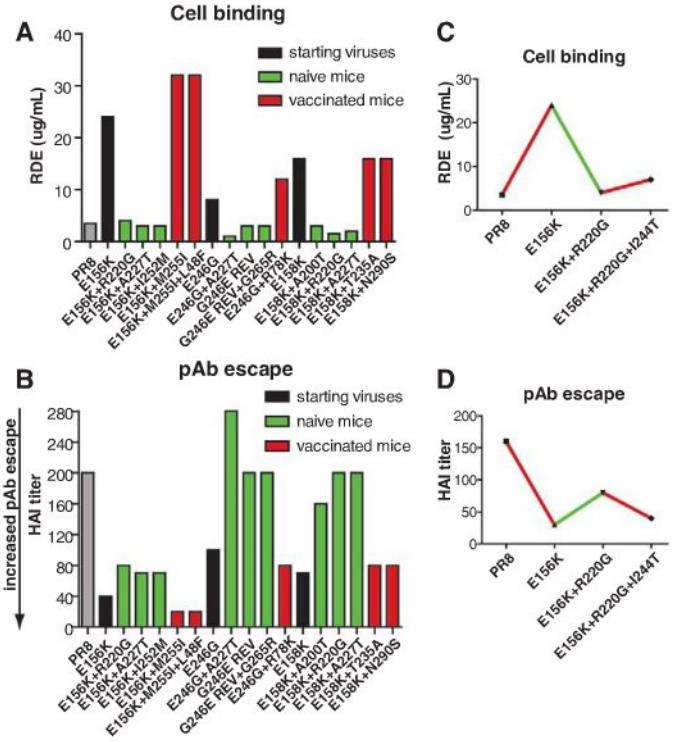

Fig. 3. Removal of polyclonal antibody selection promotes decreased receptor binding of in vivo–selected mutants. (**A**) Mutant viruses were tested for agglutination of RDE-treated turkey erythrocytes. REV denotes virus with amino acid reversion of original mutation. (**B**) Mutant viruses were tested for escape from PR8 polyclonal antibodies by HAI. Receptor binding avidities (**C**) and ability to escape PR8 polyclonal antibodies (**D**) were also determined for the virus that was isolated after further passage in heavily vaccinated mice. Abbreviations for the amino acid residues are as follows: A, Ala; E, Glu; F, Phe; G, Gly; I, Ile; K, Lys; L, Leu; M, Met; N, Asn; R, Arg; S, Ser; and T, Thr.

exhibited three cellular receptor binding avidity changes that were completely concordant with immune pressure. All of these changes were accompanied by amino acid substitutions that reduced the binding of different monoclonal antibodies (fig. S6B).

On the basis of these findings, we propose a new hypothesis for antigenic drift (fig. S7). Immune individuals select single point mutants with increased receptor binding avidity and, under optimal circumstances (for the virus), diminished antigenicity. Transmission to a nonimmune individual leads to selection of mutants with decreased receptor binding. Because binding avidity–altering substitutions exist throughout the globular domain, they frequently modify antigenicity, even when this is not a selecting factor. Repeating the cycle results in constant modulation of binding avidity along with steady alterations in antigenicity, even in the absence of antibody selection. Our model posits that cellular receptor binding alone exerts selection pressure for a substantial fraction of substitutions in defined antigenic regions and also contributes to the fixation of 30% of mutations in the globular domain outside defined antigenic regions (*16*).

The properties of recent human isolates are consistent with this model. A/Panama/2007/99, the 2003–2004 vaccine strain, did not match the circulating A/Fujian/411/02 strain by HAI assays. This difference was attributed to two amino acid substitutions (*17*). Notably, one substitution is at residue 156, which we identify as playing a critical dual role in Sb antigenicity and receptor binding avidity, while the other is at residue 155, which is immediately adjacent to the sialic acid binding site, and also located in the Sb site. During the antigenic evolution of H3N2 viruses from 1968 to 2003, a limited number of amino acids (in one case, a single N-to-K substitution increasing positive charge) dictate HAI escape from polyclonal sera (*18*).

This model complements recent work emphasizing the importance of HA receptor specificity in influenza A virus species and organ tropism (*19*). Receptor specificity and affinity are intimately related physiochemically, as demonstrated by our observation that each of the first-generation absorptive mutants (E156K, E158K, E246G) exhibits a unique avidity profile against the panel of sialylated oligosaccharides (fig. S3). Because host selection for optimal HA receptor binding avidity generates mutants with altered receptor binding specificity, this is a confounding factor in interpreting the evolutionary selection forces that generate influenza A virus isolates with altered glycan specificities.

In our model, antigenic drift is accelerated by sequential passage of influenza A virus between immune and nonimmune individuals (fig. S7), which in the human population are nearly all children. Therefore, decreasing the naïve population size by increasing pediatric influenza A virus vaccination rates will likely slow antigenic drift and temporally extend the effectiveness of influenza vaccines. Monitoring receptor binding avidity of circulating viral isolates may facilitate the accurate prediction of mutants with epidemic potential.

References and Notes

1. G. M. Air, W. G. Laver, R. G. Webster, *Contrib. Microbiol. Immunol.* **8**, 20 (1987).
2. N. J. Dimmock, *J. Gen. Virol.* **65**, 1015 (1984).
3. M. Knossow, J. J. Skehel, *Immunology* **119**, 1 (2006).
4. A. J. Caton, G. G. Brownlee, J. W. Yewdell, W. Gerhard, *Cell* **31**, 417 (1982).
5. J. W. Yewdell, R. G. Webster, W. U. Gerhard, *Nature* **279**, 246 (1979).
6. I. A. Wilson, N. J. Cox, *Annu. Rev. Immunol.* **8**, 737 (1990).
7. M. L. Wang, J. J. Skehel, D. C. Wiley, *J. Virol.* **57**, 124 (1986).
8. P. Gerber, C. G. Loosli, D. Hambre, *J. Exp. Med.* **101**, 627 (1955).
9. S. Fakekas de St Groth, *Top. Infect. Dis.* **3**, 25 (1977).
10. J. W. Yewdell, A. J. Caton, W. Gerhard, *J. Virol.* **57**, 623 (1986).
11. The term "avidity" refers to the combined strength of the multivalent interactions between viral HA and cell surface glycan receptors.
12. A. Harris *et al.*, *Proc. Natl. Acad. Sci. U.S.A.* **103**, 19123 (2006).
13. A. S. Gambaryan, M. N. Matrosovich, C. A. Bender, E. D. Kilbourne, *Virology* **247**, 223 (1998).
14. P. A. Underwood, J. J. Skehel, D. C. Wiley, *J. Virol.* **61**, 206 (1987).
15. M. N. Matrosovich *et al.*, *Virology* **233**, 224 (1997).
16. M. I. Nelson *et al.*, *PLoS Pathog.* **2**, e125 (2006).
17. H. Jin *et al.*, *Virology* **336**, 113 (2005).
18. D. J. Smith *et al.*, *Science* **305**, 371 (2004).
19. J. M. Nicholls, R. W. Chan, R. J. Russell, G. M. Air, J. S. Peiris, *Trends Microbiol.* **16**, 149 (2008).

20. We thank the staff of the National Institute of Allergy and Infectious Diseases (NIAID) Comparative Medical Branch for assistance with animal studies, G. Reynoso for technical assistance, the Consortium for Functional Glycomics for glycan standards, and S. Epstein (U.S. Food and Drug Administration) for insightful reading of the manuscript. This work was supported by Division of Intramural Research, NIAID (J.R.B. and J.W.Y.), the Singapore–Massachusetts Institute of Technology Alliance for Research and Technology (R.S.), and the National Institute of General Medical Sciences (GM 57073 and U54 GM62116) (R.S.).

Supporting Online Material

www.sciencemag.org/cgi/content/full/326/5953/734/DC1
Materials and Methods
Figs. S1 to S7
Tables S1 to S3

25 June 2009; accepted 3 September 2009
10.1126/science.1178258

Large Incubator

The CB 53 Incubator offers a 1.9-cubic-foot capacity in a compact footprint to reduce operating costs and conserve space. Hot-air chamber sterilization at 180°C makes it particularly well suited for applications in cell and tissue culture, as well as for in vitro fertilization laboratories. The Permadry condensation-free, double-pan humidification system maintains dry interior walls while the incubator operates at a relative humidity of more than 95 percent. The water level can be visually inspected, and changing the water or refilling the water pan is easy. A mixture of carbon dioxide and air is injected into the inner chamber through a cross-flow mixing valve. The mixture is distributed homogeneously because the inner chamber is under slight vacuum, which generates a Venturi effect. The need for an internal fan, which creates turbulence and complicates cleaning, is eliminated.

Binder
For information 866-885-9794
www.binderworld.com

Toxicity Reporter Assay Panel

ToxReporter is a new panel of engineered cell lines and assays that can screen compounds for toxicity early in the drug discovery process. The ToxReporter panel detects a variety of cellular responses linked to toxic stresses, including oxidative stress and antioxidant response, inflammatory response, cell cycle control, DNA damage and apoptosis, hypoxia and angiogenesis, and stress responses. The assays are flexible; researchers can test multiple compounds or multiple cell lines using a single enzyme-linked immunosorbent assay. The assays are quantitative and can be performed at multiple time points.

Millipore and CXR Biosciences
For information 800-548-7853
www.millipore.com and www.cxrbiosciences.com

LC-MS/MS System

The TSQ Vantage is a liquid chromatography–tandem mass spectrometry (LC-MS/MS) system that delivers up to 10 times more sensitivity than any other triple quadrupole instrument on the market, without a commensurate increase in noise. Breakthroughs in ionization efficiency and ion transmission have given the TSQ Vantage improved signal-to-noise performance, providing better reproducibility and precision in the quantitative analysis of small molecules, biomolecules, and peptides. A new S-Lens ion optics system makes use of novel electrostatic field technology to capture virtually every ion and transfer it into the HyperQuad quadrupole mass analyzer. The S-Lens is an advance over high-pressure, skimmer-based ion source designs because it eliminates mass discrimination and lowers the gas load on the expensive turbo-molecular pumps. This innovation keeps the ion optical path cleaner, for a longer period of time, while maintaining sensitivity.

Thermo Fisher Scientific
For information 508-742-5254
www.thermofisher.com

Liquid Chromatography System

The Flexar liquid chromatography platform incorporates a new ergonomic industrial design and delivers a wide range of pressure options to address the increasingly demanding application needs of high-pressure liquid chromatography laboratories. This multitiered platform offers solutions from semiprep to ultrahigh-pressure liquid chromatography (UHPLC). It is controlled by the new Chromera Chromatography Data System, which was built from the ground up to offer an easy approach to instrument control and chromatographic data processing. The FX-15 UHPLC system features small particle–size columns (less than 2 μm) to offer new possibilities for resolution and separations, as well as fast analysis time. The system can reduce mobile phase solvent consumption by as much as 15-fold. The Chromera software allows users to easily control instruments, rapidly visualize data, and efficiently communicate results.

PerkinElmer
For information 781-663-6900
www.perkinelmer.com

Co-Culturing Technology

Integrated Discrete Multiple Organ Co-Culture (IdMOC) is a patented technology allowing coculturing of multiple cell lines in the same culture dish as physically separated but interconnected cultures, modeling human or animals in vivo with multiple organs connected by the systemic circulation. IdMOC makes use of a "wells-in-a-well" concept, with multiple small wells inside a larger containing well. The cells are physically discrete cultures in the inner wells, with interconnection achieved by an overlying medium in the containing well, covering the inner wells. The system can be used to evaluate drug distribution, multiple organ metabolism, and toxicity, as well as other applications.

In Vitro ADMET Laboratories
For information 410-869-9037
www.invitroadmet.com

Electronically submit your new product description or product literature information! Go to **www.sciencemag.org/products/newproducts.dtl** for more information.

Newly offered instrumentation, apparatus, and laboratory materials of interest to researchers in all disciplines in academic, industrial, and governmental organizations are featured in this space. Emphasis is given to purpose, chief characteristics, and availabilty of products and materials. Endorsement by *Science* or AAAS of any products or materials mentioned is not implied. Additional information may be obtained from the manufacturer or supplier.

POSITIONS OPEN

TEXAS A&M UNIVERSITY

Texas A&M University invites qualified applicants to apply for the position of **PROFESSOR AND HEAD,** Department of Entomology in College Station, Texas. Applications will be accepted through January 15, 2010, or until a suitable candidate is selected. Position is available June 1, 2010. Specific duties and responsibilities include: (1) provide intellectual and philosophical leadership of faculty, staff, and students for integrated academic, research, and extension programs, and with expanding international activities; (2) manage and coordinate departmental human, fiscal, and physical resources; (3) serve as primary advocate for the Department to the administration in the College of Agriculture and Life Sciences and The Texas A&M University System agencies, and lead in the development of innovative joint ventures with other academic units; (4) provide leadership for statewide entomological programs of Texas; (5) represent the Department to commodity groups, state and federal agencies, other partners and collaborators; and (6) provide leadership for continued acquisition of internal and external resources. See detailed announcement at **website: http://insects.tamu.edu/departmentheadsearch/.** Submit inquiries to **e-mail: entodhsearch@ag.tamu.edu.** Applications should be submitted to **website: http://Greatjobs.tamu.edu NOV# 04537.**

ASSISTANT PROFESSOR, BIOCHEMISTRY
Dartmouth Medical School

The Department of Biochemistry at Dartmouth Medical School invites applications for a tenure-track faculty position at the Assistant Professor level. We are interested in outstanding individuals working in areas of biochemistry, molecular or cell biology relevant to the biomedical sciences. The Department consists of interactive scientists with research excellence in a variety of topics and a well-established multidisciplinary graduate program. The successful candidate is expected to establish an independent research program and to participate in graduate and medical student teaching. Candidates should have a Ph.D. or M.D. degree and relevant postdoctoral training. For more information, visit our **website: http://dms.dartmouth.edu/biochem/.**

Curriculum vitae, statements of research accomplishments and goals, and three letters of recommendation in PDF format should be sent electronically to:

E-mail: biochemsearch@dartmouth.edu
Search Committee
Department of Biochemistry
Dartmouth Medical School
7200 Vail Building
Hanover, NH 03755-3844 U.S.A.

The review of applicants will begin immediately and continue until the position is filled.

Dartmouth Medical School is an Affirmative Action/Equal Opportunity Employer and encourages applications from women and members of minority groups.

RESEARCH SCIENTIST

Research Scientist for the Henry M. Jackson Foundation for the Advancement of Military Medicine to work at Walter Reed Army Institute of Research, U.S. Military HIV Research Program, Rockville, Maryland. Lead projects to develop new methodologies to detect antibodies for the development of a prophylactic HIV-1 vaccine. Position requires a Ph.D. in microbiology or a related field plus nine years of successful and original postdoctoral research, including experience as a (Co) Principal Investigator for innovative HIV vaccine research. Send resumes to: **Recruiter, Human Resources, The Henry M. Jackson Foundation, 1401 Rockville Pike, Suite 600, Rockville, MD 20852, Job Code 204932.** Or apply online at **website: http://www.hjf.org/careers.**

POSITIONS OPEN

UNIVERSITY OF MARYLAND

OPEN FACULTY POSITION

The University of Maryland, College Park invites applications for faculty positions at the **ASSISTANT, ASSOCIATE,** and **FULL PROFESSOR** levels in the Department of Cell Biology and Molecular Genetics (**website: http://cbmg.umd.edu**), to be appointed jointly with the Center for Bioinformatics and Computational Biology (**website: http://cbcb.umd.edu**). The University has committed the resources to recruit new tenured and tenure-track faculty in order to continue building a world-class research program in genomics, bioinformatics, computer science, molecular biology, and genetics.

We seek individuals leading outstanding research programs addressing questions of broad significance in human genomics, host-pathogen genomics, and/or computational aspects of genomics and bioinformatics. Candidates will be expected to have developed, or demonstrated the potential to develop, a vigorous and externally funded research program and will teach within our undergraduate and graduate programs. All applicants are expected to have strong publications and research experience in the areas of biological science, genomics, and bioinformatics. Experience in interdisciplinary collaboration is an important asset.

Successful candidates will complement a vibrant group of researchers within the College of Chemical and Life Sciences and the Center for Bioinformatics and Computational Biology. College Park is the flagship campus of the University of Maryland System, and is located in the Washington, D.C., area adjacent to numerous government and biotechnology institutions. There are excellent opportunities for interactions with various research centers on campus and with nearby institutions, such as National Institutes of Health, The Institute for Genome Sciences, Smithsonian Institution, and Center for Advanced Research in Biotechnology.

Applicants should apply online at **website: http://www.cbmg.umd.edu/employment.** Applications should include a cover letter, curriculum vitae, and statement of research and teaching interests. Applicants at the Assistant Professor level should provide names and contact information for at least three people who will provide letters of reference. Applicants for Associate or Full Professor should provide the names of at least five references who will be contacted by the search committee at an appropriate time. For best consideration, applications should be received by December 1, 2009; however, applications may be accepted until the position is filled.

The University of Maryland is an Equal Opportunity/Affirmative Action Employer. Applications from minorities and women are encouraged.

ASSISTANT PROFESSOR, PLANT BIOLOGIST

The Department of Biology and Marine Biology at the University of North Carolina, Wilmington invites applications for a tenure-track position beginning in August 2010. Candidates with research interests in plant systematics or any area of plant metabolism at the molecular, cell, or organismal level are encouraged to apply. Candidates must have a Ph.D. and postdoctoral experience. For more information and to apply, go to **website: http://consensus.uncw.edu.** Priority consideration will be given to applications received by November 16, 2009, but applications will be accepted until the position is filled. *Equal Employment Opportunity/Affirmative Action Employer.*

POSTDOCTORAL ASSOCIATE

Stony Brook University is seeking a Postdoctoral Researcher to work on the function of the transcriptional repressor REST during neural development. Studies involve stem cells, chromatin analysis, confocal imaging, and more. For full position description or to apply online, visit **website: http://www.stonybrook.edu/jobs (Ref. #WC-R-5878-09-09-F).** *Equal Opportunity/Affirmative Action Employer.*

National Heart Lung and Blood Institute
People Science Health

Scientific Review Officer
Epidemiology/Clinical Research

The National Heart Lung and Blood Institute (NHLBI) is seeking candidates with strong backgrounds in epidemiology, translational research, or clinical trials for the position of Scientific Review Officer (Health Scientist Administrator) in the Review Branch of the Institute's Division of Extramural Research Activities. Scientific Review Officers organize and manage the comprehensive scientific and technical merit review of grant applications and contract proposals through interaction with established scientists in a variety of fields, assure the fairness and consistency of the review process, and provide guidance to applicants, reviewers, and Institute staff. The successful candidate will join a diverse and dedicated group of 18 Scientific Review Officers, who strive to provide the highest quality peer review and are instrumental in the NIH effort to reshape and improve the peer-review process. Individuals with a Ph.D. or doctoral degree equivalent are encouraged to apply. For the basic qualification requirements, please refer to the NIH guidance for Health Scientist Administrators at http://www.jobs.nih.gov/announcement-links/healthadministrator.htm

The NHLBI prides itself as an avenue fostering unique and rewarding careers. The NHLBI provides global leadership for a research, training, and education program to promote the prevention and treatment of heart, lung, and blood diseases and enhance the health of all individuals so that they can live longer and more fulfilling lives. Administrative and peer-review experience are advantageous. Academic faculty at all levels and advanced postdoctoral fellows with experience in epidemiology or clinical research are encouraged to apply. This position is open to all US citizens.

- Build a new, unique career that combines taking a leadership role in providing scientific, administrative, and logistical oversight of the peer review process with opport unities to maintain a liaison to academia and research.
- Outstanding Benefits! A Full package of Civil Service benefits is available including retirement, health and life insurance, leave and savings plan (401K equivalent).

Please apply online at http://www.USAJobs.gov

Health Scientist Administrator, Keyword Search: NHLBI-10-379255-DE
OR
Health Scientist Administrator, Keyword Search: NHLBI-10-379255-MP

How to Apply: Please view the above USAJobs website for full vacancy announcement. Please apply online at the above website. All applications must received by close of business on the announcement closing date. For additional information contact **Mariela Light, Human Resources Specialist at (301) 402-8032**.

For further information on NHLBI job opportunities, visit http://www.nhlbi.nih.gov/about/jobs/

Department of Health and Human Services
National Institutes of Health
Intramural Research Programs
NCI, NEI, NHLBI, NIAID, NIDDK, NIMH, NINDS and CIT
Bethesda, MD

Tenure Track/Tenured Positions
In Systems Biology

The NIH Intramural Research Program (IRP) is recruiting outstanding systems biologists at the tenure-track or tenured levels. These individuals will direct independent research programs on the NIH campus in Bethesda, MD and participate in a Trans-NIH Initiative in Systems Biology promoting interaction between experimentalists, theoreticians and computational investigators. Candidates will have demonstrated an ability to conduct outstanding independent biomedical research on key topics in systems biology such as computational modeling of biological processes at various scales, analysis ofglobal datasets, construction and analysis of biological networks, and 'omic' scale interrogation of biological systems. The internationally recognized NIH faculty covers a wide range of basic and clinical research topics with a growing strength, support and emphasis on systems biology and informatic approaches to biomedicine.

The NIH IRP promotes creative and innovative science unconstrained by the conventional support mechanisms demanded at academic or private research institutes. Investigators have ready access to and support from state-of-the art experimental and computational cores and facilities, and a variety of programs to recruit graduate students and post-doctoral fellows.

Candidates must have an M.D. and/or Ph.D., or equivalent doctoral degree, and an outstanding record of research accomplishment and peer-reviewed publications. Recruits will be provided a competitive salary commensurate with experience and qualifications, and will be assigned ample research space, supported positions, operating budget, and start-up funds. Appointees may be US citizens, resident aliens, or eligible foreign nationals. Review of applications will commence on Nov.1, 2009 and continue until the positions are filled. Please submit a curriculum vitae, brief (not to exceed 3 pages) statement of research interests that includes how you see your research group helping to create a world-class, integrated systems biology effort at NIH, and three letters of reference in .pdf or MS word format only (no paper applications will be accepted) to: **http://tenuretrack.nih.gov/apply/**

WORCESTER POLYTECHNIC INSTITUTE

THE CHRONICLE 2009 GREAT COLLEGES TO WORK FOR.

Life Sciences Initiative

Seven Faculty Positions

Worcester Polytechnic Institute (WPI) in Worcester, Mass., is continuing a major investment in the life sciences. In 2007 the university opened the WPI Life Sciences and Bioengineering Center (LSBC), which houses the life sciences-related graduate research programs of five academic departments and the WPI Bioengineering Institute (BEI). Since that time, WPI has recruited 12 new full-time faculty members in the life sciences and bioengineering, bringing to more than 30 the number of faculty working in interdisciplinary clusters within a strongly collaborative environment in the LSBC. As a result of this investment, graduate research and external research funding have increased considerably, with faculty awarded major funding from the NIH, NSF, DARPA, and other agencies.

In 2008-09 WPI recruited five new full-time life science and bioengineering faculty members across five departments, including a new head for the Biomedical Engineering Department. In 2009-10 we are seeking to fill seven tenure-track positions at the junior and senior levels in five departments, including a new head for the Chemistry and Biochemistry Department. The ideal candidates for these positions will have research interests and expertise that are complementary to our current research areas, and be committed to collaboration among multidisciplinary teams and to securing external funding.

Applicants for department head and senior positions will be recognized leaders in their field and have a strong record of securing extramural funding. Applicants at the assistant professor level must have postdoctoral research experience with extramural support, or strong promise to obtain funding. All applicants must hold the PhD and have a strong commitment to teaching at the undergraduate and graduate levels. To apply, and for more on the WPI Life Sciences Initiative, including detailed position descriptions, visit wpi.edu/+lsi.

Founded in 1865, WPI is one of the nation's oldest and most innovative technological universities. Its 14 academic departments offer more than 50 undergraduate and graduate degree programs, including the PhD, in science, engineering, management, and the liberal arts. WPI offers a smoke-free environment, competitive compensation, and an excellent benefits package. To enrich education through diversity, WPI is an affirmative action, equal opportunity employer. It is a member of the Colleges of Worcester Consortium.

Chemistry and Biochemistry • The Department of Chemistry and Biochemistry invites applications for a DEPARTMENT HEAD, who will also hold an endowed professorship. The new head will have a clear and creative vision for building and sustaining ambitious departmental research programs during a period of growth. This vision will include enhancing the department's role in the natural sciences. **Contact:** Applications and nominations should be sent to cbcheadsearch@wpi.edu. Further inquiries should be directed to the chair of the search committee, Professor Richard Sisson, sisson@wpi.edu, or the head of Chemistry and Biochemistry, Professor Kristen Wobbe, kwobbe@wpi.edu. The department also seeks an ASSISTANT PROFESSOR working in either biochemistry or chemistry. Contact Professor George Kaminski at faculty-searchCBC@wpi.edu.

Biology and Biotechnology • The Department of Biology and Biotechnology invites applications for a position at the ASSISTANT PROFESSOR level. Areas of particular interest include ecology and environmental biology, cell and developmental biology, and systems biology. **Contact:** Professor Eric Overström, head, Department of Biology and Biotechnology, faculty-searchBBT@wpi.edu.

Biomedical Engineering • The Department of Biomedical Engineering invites applicants for two positions, one at the ASSISTANT PROFESSOR level specializing in biosignals and bioinstrumentation and one at the ASSOCIATE or FULL PROFESSOR level specializing in regenerative medicine. **Contact:** chairs of either the Regenerative Medicine or Instrumentation Search Committees at faculty-searchBME@wpi.edu.

Mathematical Sciences • The Department of Mathematical Sciences invites applications for a position at the ASSISTANT PROFESSOR level. Applications from candidates with teaching and scholarly interest in the areas of biostatistics, computational statistics, experimental design, or Bayesian methods are especially encouraged. **Contact:** Math Search Committee, ma-chair@wpi.edu.

Physics • The Department of Physics invites applications for a position at the ASSISTANT PROFESSOR level in theoretical or experimental soft-condensed matter physics. This position will complement the university's research initiative in biophysics and regenerative biosciences. **Contact:** Professor Germano Iannacchione, head, Department of Physics, at ph-search@wpi.edu.

WPI

Weill Institute for Cell and Molecular Biology
Faculty Position in Chemistry and Chemical Biology
Cornell University, Ithaca, NY

The Weill Institute for Cell and Molecular Biology, in conjunction with the Department of Chemistry and Chemical Biology, at Cornell University is searching for a tenure-track faculty member at the level of Assistant Professor. Cornell recently established and endowed the Weill Institute **(www.icmb.cornell.edu)** as part of its New Life Science Initiative. The Institute will consist of 13 faculty (currently 7) as the core component in a $160M new research building, designed by renowned architect Richard Meier. Dr. Scott Emr relocated to Cornell in 2007 as the founding Director of the Institute. The goal of the Institute is to build a vibrant center of scientific excellence in basic biology integrated with existing outstanding programs in chemistry and chemical biology, physics, computational biology and engineering. All Institute faculty are physically located in Weill Hall, but with full appointments in academic departments, to which they contribute teaching and service.

The selected candidate for this position will be appointed in the Department of Chemistry and Chemical Biology (CCB; **www.chem.cornell.edu**) and be a member of the Institute, and must have interests and expertise consistent with both positions. Applicants are expected to have a strong background in chemistry and/or chemical biology with research that addresses fundamental questions in molecular cell biology (e.g. cell cycle, signaling, membrane traffic, cytoskeleton, etc.). Candidates exploiting specialized approaches, for example: chemical synthesis, structural biology, novel cellular probes, or high-resolution microscopy, will also be considered.

Applicants should submit a curriculum vitae (highlighting 3-5 publications with title and abstract), a research plan (2-3 pages), and a statement of teaching interests. The cover letter should indicate how the applicant fits the interests of CCB and the Institute. These materials and three letters of recommendation should be sent to: **Chemical Biology Search Committee, Department of Chemistry and Chemical Biology, Baker Laboratory, Cornell University, Ithaca, New York 14853-1301.** Review of applications will begin December 1, 2009; the closing date is January 31, 2010. However, applications from exceptional candidates will be considered after the closing date until the position is filled.

Cornell University

Cornell University is an Affirmative Action/ Equal Opportunity Employer and Educator.

Rochester, NY
RIT Rochester Institute of Technology

Organismal Biologist

The School of Biological and Medical Sciences at the Rochester Institute of Technology invites applications for a (subject to available funding) tenure-track position in organismal biology (IRC 34247). The successful candidate will teach core courses, including Comparative Animal Physiology, contribute to teaching of majors and non-majors introductory biology, and develop discipline-specific elective courses. We seek candidates with a demonstrated commitment to undergraduate teaching and research who will broaden our existing strengths in organismal and evolutionary biology. Candidates who can develop local field and laboratory research programs suitable for undergraduate and MS student participation are particularly encouraged to apply. Candidates are required to hold a Ph.D., and post-doctoral training is preferred.

The School of Biological and Medical Sciences has more than 30 full-time Faculty and more than 700 full-time students across our undergraduate majors: Biology, Biotechnology, Bioinformatics, Environmental Science, and Biomedical Sciences; and 30+ graduate students in our Masters programs in Bioinformatics and Environmental Science.

Applicants for this position should apply online at **http://apptrkr.com/129230**. Please upload your letter of interest; a vita; summaries of teaching and research interests, and a statement of your experience with and commitment to RIT's core values, honor code, and statement of diversity. Please arrange to have 3 letters of reference sent to science@rit.edu (preferred) or mailed to Dr. Robert Rothman, Department of Biological Sciences, Rochester Institute of Technology, 85 Lomb Memorial Drive, Rochester, NY 14623. Review of applications will begin on November 30, 2009 and continue until the position is filled, with a start date of late August, 2010. The Rochester Institute of Technology is an equal opportunity/ affirmative action employer. All qualified individuals with the ability to contribute in meaningful ways to the university's continuing commitment to its core values, honor code and diversity statement are encouraged to apply.

Faculty Position
Molecular Biology
Sloan-Kettering Institute

The Molecular Biology Program of the Sloan-Kettering Institute, Memorial Sloan-Kettering Cancer Center (www.ski.edu), has initiated a faculty search at the Assistant Member level (equivalent to Assistant Professor). We are interested in outstanding individuals who have demonstrated records of significant accomplishment and the potential to make substantial contributions to the biological sciences as independent investigators. Successful applicants will have research interests that move the Program into exciting new areas that complement and expand our existing strengths in the areas of maintenance of genomic integrity, regulation of the cell cycle, and regulation of gene expression. Faculty will be eligible to hold appointments in the Gerstner Sloan-Kettering Graduate School of Biomedical Sciences, the Weill Cornell Graduate School of Medical Sciences, as well as the Tri-Institutional MD/PhD Training Program.

Candidates should e-mail their application in PDF format to: **molbio@mskcc.org** by **November 16, 2009**. The application should include a CV, description of past and proposed research (3-7 pp), and copies of three representative publications. Candidates should arrange to have three signed letters of reference sent in PDF format to: **molbio@mskcc.org.** The letters should arrive by **November 16, 2009** and should be addressed to **Dr. Kenneth Marians, c/o Julie Kwan, Box 135, Memorial Sloan-Kettering Cancer Center, 1275 York Avenue, New York, New York 10065**. Inquiries may be sent to **Ms. Kwan at molbio@mskcc.org** or to **Dr. Kenneth Marians, Chair, Molecular Biology Program at kmarians@sloankettering.edu**. Memorial Sloan-Kettering Cancer Center is an Equal Opportunity Employer and smoke-free environment.

Memorial Sloan-Kettering Cancer Center

www.mskcc.org

iCeMS KYOTO UNIVERSITY WPI Research Center

Cross-Disciplinary Research Positions Available in Cell-Material Sciences

Institute for Integrated Cell-Material Sciences (iCeMS)
Kyoto University

Researcher positions are available to carry out cross-disciplinary research in cell-material sciences (for details see **www.icems.kyoto-u.ac.jp**). We are looking for highly motivated scientists at the level of research associate or research assistant professor.

Qualified candidates will be expected to 1) join a research group led by an iCeMS PI and 2) initiate research projects involving one or multiple labs of the iCeMS. Priority will be given to those who will carry out collaborative and cross-disciplinary research in conjunction with multiple PIs, but researchers with a more focused interest are also welcome to apply.

The following PIs are accepting applications, and their research information can be obtained from our website: Prof N Nakatsuji (stem cell biology), Prof S Kitagawa (coordination chemistry), Prof K Ueda (cellular biochemistry), Prof C Agladze (biophysics), Prof Y Chen (nano-biotechnology), Prof Y Harada (single molecule physiology), Prof M Hashida (biopharmaceuticals), Prof J Heuser (biophysics), Prof T Hiiragi (developmental biology), Prof H Imaori (photochemistry), Prof M Kengaku (developmental neurobiology), Prof M Kiso (glycotechnology), Prof A Kusumi (single molecule cell biophysics), Prof H Sugiyama (chemical biology), Prof M Takano (solid-state chemistry), Prof K Tanaka (teraherz optical science), and Prof M Uesugi (chemical biology).

In addition to a brief CV, interested scientists should initially send an email explaining their research interest and which lab they wish to join. The address is: **info@icems.kyoto-u.ac.jp**

PICTURE YOURSELF AS A AAAS SCIENCE & TECHNOLOGY POLICY FELLOW

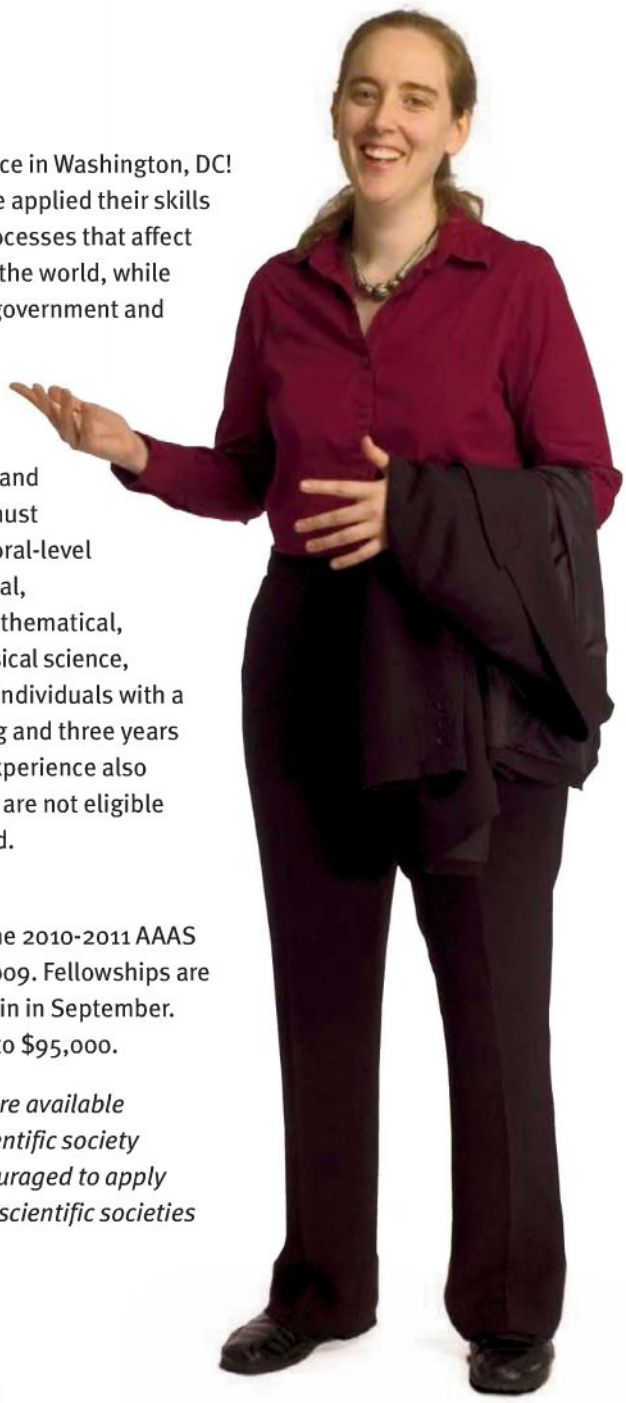

Make a Difference.
Help give science a greater voice in Washington, DC! Since 1973, AAAS Fellows have applied their skills to federal decision-making processes that affect people in the U.S. and around the world, while learning first-hand about the government and policymaking.

Join the Network.
Year-long fellowships are available in the U.S. Congress and federal agencies. Applicants must hold a PhD or equivalent doctoral-level degree in any behavioral/ social, biological, computational/ mathematical, earth, medical/health, or physical science, or any engineering discipline. Individuals with a master's degree in engineering and three years of post-degree professional experience also may apply. Federal employees are not eligible and U.S. citizenship is required.

Apply.
The application deadline for the 2010-2011 AAAS Fellowships is 15 December 2009. Fellowships are awarded in the spring and begin in September. Stipends range from $73,000 to $95,000.

Note: Additional fellowships are available through approximately 30 scientific society partners. Individuals are encouraged to apply with AAAS as well as with any scientific societies for which they qualify.

Full details at:
fellowships.aaas.org

Enhancing Public Policy, Advancing Science Careers

Kathy Kahn, PhD

Interdisciplinary Biological Sciences, University of Missouri

2004-06 AAAS Fellow at the U.S. Department of Agriculture, Biotechnology Group in the Foreign Agricultural Service

Now a program officer at the Bill and Melinda Gates Foundation, Agriculture Development Group

AAAS
ADVANCING SCIENCE, SERVING SOCIETY

University of Colorado Denver

Dean of the Graduate School

The University of Colorado Denver invites applications and nominations for the position of Dean of the Graduate School. The Graduate Dean is the chief administrative and fiscal officer of the Graduate School, as well as its principal spokesperson to academic and professional communities, students, and alumni. We are seeking an energetic and dynamic leader for the School, bringing it to greater prominence locally, nationally, and internationally.

The University of Colorado Denver was created in 2004 by consolidating the University of Colorado at Denver and the University of Colorado Health Sciences Center. The combined entity has the most extramural funding of any research university in Colorado. UC Denver awards almost 4,000 degrees each year, including more graduate degrees than any other Colorado institution. With our solid academic reputation, award-winning faculty, and renowned researchers, we offer more than 100 undergraduate and graduate degree programs in 13 colleges and schools. Undergraduate and graduate degree programs are taught on the Downtown Denver Campus, just steps from the Denver Center for Performing Arts and the LoDo District, an ideal location in one of America's most vibrant urban centers. Students and faculty have access to an array of academic, professional, community, recreational and cultural outlets. The Anschutz Medical Campus (AMC) in Aurora is home to 6 professional schools in the health sciences and extensive research and clinical care facilities. AMC is a new education, research and patient care facility and the largest academic health center between Chicago, Texas and the West Coast. The University has proudly positioned itself as one of the top urban research universities in the country.

The Graduate School Dean will provide leadership in working with the Consolidated Graduate Council. Interacting with the other School/College Deans, the Graduate Dean will develop and implement innovative and effective recruitment and retention programs for graduate students; increase recruitment, retention, and graduation of diverse graduate students; seek new sources of funding for graduate students; and help build a sense of community for graduate students and faculty that transcends academic fields. Essential to the success of the Dean also will be the assessment of graduate curricula, faculty and student performance, including research and teaching, particularly as these apply to Graduate School activities. The Dean will represent the Graduate School on various University leadership committees.

This position requires, at a minimum, a Ph.D. or equivalent degree from an accredited institution; academic qualifications and scholarly accomplishments consistent with an appointment to the rank of professor with tenure; demonstrated successful administrative experience; a strong understanding of contemporary public post-secondary education; demonstrated effective leadership in teaching, scholarship and public service; a track record of successful experience with diversity initiatives; and a record of effective interactions with multiple diverse constituencies.

The Graduate Dean will report to the Provost. Salary and benefits are commensurate with experience. A more complete job description is available on our website: **http://www.ucdenver.edu/about/WhoWeAre/Chancellor/ViceChancellors/Provost/Pages/default.aspx**

UC Denver is dedicated to ensuring a safe and secure environment for our faculty, staff, students and visitors. To assist in achieving that goal, we conduct background investigations for all prospective employees.

To apply, please go to https://www.jobsatcu.com (Job Posting Number: 808475) and attach a cover letter addressing the position requirements, current CV/resumé and the names and contact information for three professional references. Review of applications will commence on **November 12, 2009**, but applications will be accepted until finalists are identified. For additional information contact **vicky.starbuck@ucdenver.edu**

The University of Colorado Denver is committed to diversity & equality in education & employment.

NEBRASKA CENTER FOR VIROLOGY

Research Assistant Professor in virology to participate in established research program of **Dr. Charles Wood** on molecular biology and pathogenesis of HIV/AIDS. Provide management of ongoing research projects and supervise research staff in his laboratory while developing independent research associated with the Nebraska Center for Virology (**www.unl.edu/virologycenter**) through the University of Nebraska – Lincoln School of Biological Sciences. Candidates should hold PhD or equivalent with relevant postdoctoral experience in molecular virology.

Review begins **November 30, 2009**. To be considered for this position, apply at **http://employment.unl.edu** for requisition number **090625** and complete the Faculty/Academic Administrative Form, attaching required documents.

Dr. Charles Wood, Director
Nebraska Center for Virology

The University of Nebraska has an active National Science Foundation ADVANCE gender equity program, and is committed to a pluralistic campus community through Affirmative Action, Equal Opportunity, work-life balance, and dual careers.

University of Nebraska Lincoln

GRADUATE PROGRAM

The Leipzig School of Human Origins

- An International Max Planck Research School -

by

The University of Leipzig

and

The Max Planck Institute for Evolutionary Anthropology

The **Leipzig School of Human Origins** offers a unique interdisciplinary graduate program to study the evolutionary history of humans and great apes. Graduate students are accepted into one of the following areas, but are encouraged to take part in courses and seminars from all three disciplines:

Comparative and Molecular Primatology

Evolutionary and Functional Genomics, Ancient DNA, Molecular Anthropology and Genome Bioinformatics

Human Paleontology, Prehistoric Archaeology and Archaeological Science

The language of the school is English. Visit www.leipzig.de for information on living in Leipzig, Germany, in the center of Europe.

For project and application details go to www.leipzig-school.eva.mpg.de or contact us at:

e-mail: leipzig-school@eva.mpg.de
phone: ++49 (0) 341 3550-0
fax ++49 (0) 341 3550-119
Application deadline: January 31, 2010

OLD DOMINION UNIVERSITY

CHAIR
DEPARTMENT OF OCEAN, EARTH & ATMOSPHERIC SCIENCES

Old Dominion University invites applications and nominations for the position of Chair, Department of Ocean, Earth and Atmospheric Sciences (OEAS) in the College of Sciences. We seek an outstanding scholar in Oceanography, Earth and Atmospheric Science, or a related discipline, with demonstrated excellence in research, international recognition, consistent peer-reviewed research grant funding, and a strong commitment to educational programs. The successful candidate will provide leadership to further enhance the Department's excellent research and educational programs and a strong commitment to teaching and mentoring of junior faculty, post-doctoral fellows, and graduate and undergraduate students. The appointment will be at the rank of professor with tenure, with a competitive salary. The position will be available in May 2010.

The OEAS Department is nationally ranked and currently includes 22 full-time faculty, 5 research faculty, and 13 staff members. The Department has graduate and undergraduate programs of high quality, granting a Ph.D. degree in Oceanography and M.S. and B.S. degrees in Ocean and Earth Sciences. The Department receives substantial State support and is well funded by extensive peer-reviewed grants from federal agencies. An endowment of approximately $16 million provides additional support for programs within the Department. The Department of OEAS includes two research centers, the Center for Quantitative Fisheries Ecology and the Center for Coastal Physical Oceanography, and maintains a 55-foot research vessel, the R/V Slover. More information on the Department can be found at **http://sci.odu.edu/oceanography**.

Located in Norfolk, Virginia, Old Dominion University (**www.odu.edu**) is a state supported, research intensive institution enrolling more than 23,000 students, of which 6,000 are graduate students. Norfolk is a culturally rich, historic city and a major international maritime center in a metropolitan area of over 1.5 million people. Norfolk is one of the seven cities comprising Hampton Roads, located on the Chesapeake Bay, one of the world's largest estuarine systems. It is a center of research development in marine science, ship design and construction, and other areas of advanced technology.

Interested candidate should submit a curriculum vitae, a statement of research and teaching interests, and contact information for four references to **Dr. Gail Dodge, Chair of the OEAS Search Committee, Department of Physics, Old Dominion University, Norfolk, VA 23529**, or electronically to **OEASChair@odu.edu**. The review of applications will begin on **December 1, 2009**, and continue until the position is filled.

Old Dominion University is an Affirmative Action/Equal Opportunity institution and requires compliance with the Immigration Reform and Control Act of 1986.

Assistant, Associate or Senior Scientist

The Geology and Geophysics Department invites applications for two full-time tenure-track positions at the Assistant, Associate or Senior Scientist level. These positions are eligible for benefits.

The first position is in the area of metamorphic petrology (fluid-rock interaction) to pursue new research directions in fluid-rock interactions and chemical fluxes between the crust, mantle and oceans, dehydration/serpentinization processes, kinetic and thermodynamic modeling of metamorphic processes and elucidating the linkages between fluid flow, alteration deformation and the chemical fluxes across subduction zones. The candidate would bridge research between geochemists and geophysicists studying the global geochemical cycle from midocean ridges to subduction zones, and the geochemical evolution of the Earth.

The second position is in the area of isotope geochemistry. The successful candidate would apply state-of-the-art technologies of isotope geochemistry to a range of problems, including timescales of geologic processes, global geochemical cycles, mantle dynamics and evolution, biogeochemical cycles, and geochemical kinetics.

Successful candidates are expected to develop and maintain their own independent externally funded research program. Opportunities exist for teaching and advising graduate students through the MIT-WHOI Joint Program in Oceanography/Applied Ocean science and Engineering, as well as for collaborating with scientists and engineers elsewhere in the institution; the Departments of Marine Chemistry and Geochemistry, Biology, Physical Oceanography, Applied Ocean Physics and Engineering, and the Marine Policy Center.

A Ph.D. is required at the time of the appointment as well as a demonstrated record of excellence in research. The level of appointment will depend on the candidate's background and experience. Women and minority applicants are particularly encouraged to apply.

Target for applications, which should include a CV, a research statement and a list of 4 references who could submit letters of recommendation is November 30th, 2009.

Please visit **http://jobs.whoi.edu** for a detailed job description and to apply online today!

WHOI is an Affirmative Action/Equal Opportunity Employer M/F/D/V. Applications are reviewed confidentially.

Woods Hole Oceanographic Institution

POSTDOCTORAL POSITION

Hematology and Medical Oncology-
STEM CELL RESEARCH

Weill Cornell Medical College seeks a highly motivated professional PhD for a Postdoctoral position to explore the transcriptional programming and therapeutic targeting of leukemia stem cells, using the tools of high throughput analysis of chromatin and gene expression and function, and experimental therapeutics. The work will be performed under the supervision of Dr. Ari Melnick, Associate Professor and Dr. Monica Guzman, Assistant Professor, both from the Departments of Medicine and Pharmacology. The applicant would join a thriving and highly interactive research team including cancer biologists, immunologists, hematopathologists, and computational biologists.

Requirements: MD and/or PhD degree and experience in cell culturing, flow cytometry, QPCR, ChIP assays, and a basic understanding of functional genomics (microarrays, deep sequencing).

Appointments are for one year, with renewal based upon satisfactory performance and funding availability.

Excellent benefits package
(includes tuition reimbursement).

Please send cover letter and resume to:
Attn: Ari Melnick, M.D.
E-MAIL: amm2014@med.cornell.edu

WEILL CORNELL MEDICAL COLLEGE
EOE/M/F/D/V

www.med.cornell.edu/jobs

KU THE UNIVERSITY OF KANSAS

Faculty Position in Bioinformatics/Computational Biology

The Center for Bioinformatics and the Department of Molecular Biosciences at The University of Kansas invite applications for a tenure-track assistant professor position expected to begin as early as August 18, 2010. Applicants should have a clear interest in computational systems biology, genomics, protein modeling, or macromolecular interactions. The interdisciplinary Center for Bioinformatics (**www.bioinformatics.ku.edu**) complements existing strengths in the Department of Molecular Biosciences (**www.molecularbiosciences.ku.edu**), including structural biology, developmental/molecular genetics, proteomics, and computational chemistry. The Center fosters international activities in Bioinformatics and combines outstanding research and the Ph.D. program in Bioinformatics. Duties: to establish and maintain an externally funded research program, to participate in teaching, and to provide service.

Required Qualifications: Ph.D. and postdoctoral experience in a discipline related to Bioinformatics; potential for excellence in research in Bioinformatics as evidenced by publications in highly ranked journals and innovative research objectives; and commitment to teaching life sciences courses evidenced by teaching philosophy statement.

For the full position announcement and to apply online, go to: **https://jobs.ku.edu** and search for position **00001641**. Submit a CV, letter of application, statement of past and future research, statement of teaching interests and philosophy, and a list of at least three references. Initial review of applications will begin **November 30, 2009** and will continue until no longer needed. Direct inquiries to **Dr. Ilya Vakser (vakser@ku.edu)**.

EO/AA Employer. Women, minorities, and candidates who will contribute to the climate of diversity in the College, including a diversity of scholarly approaches, are encouraged to apply.

araid
FUNDACIÓN AGENCIA ARAGONESA PARA LA INVESTIGACIÓN Y EL DESARROLLO

Aragon Foundation for Research and Development
8 Research Positions

ARAID Foundation announces the opening of 8 tenure-track research positions in different fields.

Candidates are expected to fulfil the requisites of academic background as well as a significant postdoctoral experience. However, only very strong candidates with excellent leadership capabilities and an outstanding research record will be considered.

Successful applicants will have a permanent contract with the ARAID Foundation and will work along with teams from university or other research centres in Aragon in the premises of these cooperating institutions.

ARAID researchers are expected to make substantial contributions to their own areas of research and be active members of the Aragon science-technology system.

Salaries will be commensurate with the experience and potential of the candidates and will therefore be negotiated individually. The performance of the researchers will be periodically subjected to external evaluation.

The selection of applicants will take into consideration the objectives of the Aragon Government's Research and Innovation Plan, which prioritizes certain areas (see the list below). However, applications from outstanding researchers in any area of knowledge may also be considered. Candidates should submit their applications electronically through the ARAID Foundation's web page (www.araid.es) no later than **21st December, 2009**.

For Further details, please visit our web site **www.araid.es**

Priority areas:

- Biomedicine and health sciences
- Information and communication technology
- Food science and technology
- Social and cultural development
- Environment and sustainability
- Nanosciences and nanotechnology
- Technological development based on new materials and processing
- Computing atoms and molecules (CECAM) (*)

(*) To view a complete job description for this position please go to www.araid.es

Spanish National Cancer Research Centre (CNIO)

cnio
Centro Nacional de Investigaciones Oncológicas

invites applications for the position of

Director

The CNIO is one of the foremost European cancer research centres conducting basic and applied research, including a recently established clinical programme to focus on early phase clinical trials.

There are currently 36 research groups and over 500 scientists working on a wide range of topics including the molecular, genetic and cellular bases of cancer, structural biology and biocomputing, molecular pathology, molecular cytogenetics and inherited cancer syndromes. Research groups are supported by Core Units that offer a wide range of services and cutting-edge technologies.

The publication record of the CNIO in high impact factor journals over the last four years compares well with those of highly reputed research centres such as the Salk Institute, the Cold Spring Harbor Laboratory or the Netherlands Cancer Institute.

The CNIO enjoys an international atmosphere. The working language is English and about one third of its scientists, including group leaders, come from outside Spain. It has established international programmes for PhD students, postdoctoral researchers and post-resident MDs.

The CNIO receives about half of its annual budget as core funding from the Spanish government and has an autonomous administrative system with minimal bureaucracy. The Director reports directly to the Board of Directors chaired by the Deputy Minister of Science and Innovation.

The CNIO seeks:

- An outstanding scientist who is an internationally recognised leader in cancer research with an excellent track record in research and in scientific administration.
- A clear, long-term strategic vision for the Centre, that will attract top scientists and students.
- Extensive experience in establishing partnerships with academia, industry, government and private organisations, including helping with fund raising.

The CNIO offers:

- An indefinite contract with a competitive salary commensurate with his/her skills and experience and an attractive benefits package.
- The possibility to establish a research group with six fully funded positions and a generous set-up budget including all the necessary equipment and running costs for up to 3 years.

GOBIERNO DE ESPAÑA

Centro Nacional de Investigaciones Oncológicas
Melchor Fernández Almagro, 3
28029 Madrid, Spain
Tel: +34 917 328 00 | Fax: +34 912 246 980

For additional information, visit our Website
www.cnio.es/director-position

UNIVERSITY OF SASKATCHEWAN

College of Medicine
Department of Pharmacology

Tenure-Track Position
Department of Pharmacology
College of Medicine, University of Saskatchewan

Applications are invited for a tenure-track position at the rank of Assistant Professor, with salary level appropriate to qualifications, to begin **May 1, 2010**. Preference will be given to candidates with a MD degree and/or a PhD degree in Pharmacology, and expertise in neuropharmacology and appropriate postdoctoral training. In addition to joining the University of Saskatchewan's Neural Systems and Plasticity Research Group, and developing a strong, externally funded research program, the successful candidate will be expected to teach in our Physiology/Pharmacology BSc program and to contribute to the team-teaching of Medical, Dental, Pharmacy, and Graduate Students. Supervision of Graduate Students and Postdoctoral Fellows is also expected. State of the art research facilities will be available in the new Health Sciences Complex, which is currently under construction. For those candidates with clinical training and interests, a cross appointment with a clinical department is possible.

Prior to **January 31, 2010**, applicants should submit, both electronically and as signed hard copies, a curriculum vitae, a brief statement of research interests, reprints of recent publications, and the names and addresses of three referees to:

Dr. Venkat Gopalakrishnan
Professor & Head, Department of Pharmacology
Health Sciences Building, Room A120
107 Wiggins Road
SASKATOON, SK CANADA S7N 5E5
E-mails are to be directed to Executive Secretary,
Mrs. Cindy S. Wruck at cindy.s.wruck@usask.ca

All qualified candidates are encouraged to apply. However, citizens and permanent residents of Canada will be given priority. The University of Saskatchewan is committed to employment equity. Members of designated groups (women, aboriginal people, people with disabilities and visible minorities) are encouraged to self-identify on their applications.

COLUMBIA UNIVERSITY
IN THE CITY OF NEW YORK

Neuroscience Faculty Recruitment

The Department of Neuroscience at Columbia University plans to recruit new faculty in two broad areas of neuroscience: (1) the analysis of motor and cognitive processes in awake, nonhuman primates, (2) the use of molecular and cellular approaches to study neural circuitry in genetically tractable model systems. We encourage applications at all levels, from Assistant to Full Professor.

Columbia University has an exceptionally strong and broad program in the neurosciences and aims to enhance interactions between basic and clinical research, and to link the neurosciences with other scientific disciplines within the University. New faculty will be affiliated with the Department of Neuroscience and with the Doctoral Program in Neurobiology and Behavior. There are many opportunities for interaction with other scientific departments and programs at the Medical Center and Morningside Heights campuses.

Applications must be received by November 30, 2009, and should be submitted online at:

https://academicjobs.columbia.edu/applicants/Central?quickFind=52268

Columbia University takes affirmative action to ensure equal employment opportunity.

Alaska WWAMI Professor of Biomedical Sciences

Alaska's Medical School – *Alaska WWAMI* – invites applications for a senior-level Full or Associate Professor of Biomedical Sciences. We seek an established, funded investigator who demonstrates excellence in biomedical research and has experience teaching medical, graduate and/or undergraduate students. The Professor will teach 1st-year medical students at the University of Alaska Anchorage (UAA); will maintain a biomedical research program supported by NIH or comparable; and will mentor junior faculty at UAA, including INBRE program faculty whose research falls under the themes of cell and molecular basis of disease, toxicology or infectious disease.

The Professor will become a leader in Alaska's INBRE program and in COBRE development at UAA; will be the liaison for Alaska's biomedical research program with the University of Washington School of Medicine's Institute of Translational Health Sciences; and will be eligible for a UWSoM affiliate faculty appointment.

Areas of existing research emphasis include neuroscience, addictions, molecular biology, infectious diseases and environmental sciences; well-qualified candidates in other areas, especially clinical translational research, will also be considered. Must be able to work collaboratively in an interdisciplinary environment.

Competitive salary and start-up. Submit a *curriculum vitae*, a cover letter citing PCN 300625, and contact information for three professional references through www.uakjobs.com.

Quick link: **www.uakjobs.com/applicants/Central?quickFind=68629**

UAA

UAA is an Affirmative Action/Equal Opportunity Employer. Women and minorities are encouraged to apply.

THE UNIVERSITY OF TOLEDO 1872

Microbiology and Immunology Tenure-track Faculty Positions

The Department of Medical Microbiology and Immunology at the University of Toledo College of Medicine is seeking to hire a tenure-track faculty member at the level of Assistant/Associate/Full Professor. Candidates must hold a Ph.D., M.D., or equivalent degrees, be currently funded, and have at least three years of relevant postdoctoral experience (Assistant Professor) or faculty appointment (Associate or Full Professor). Successful candidates will be expected to develop/maintain an externally funded, basic and/or translational research program and contribute to teaching in our medical and graduate programs.

Applications should include: (a) CV; (b) a brief summary of research interests, past accomplishments, and future plans; and (c) names and addresses of three references. All materials should be sent electronically to: **Microbiology.Immunology@UToledo.Edu**.

Applications are continuously reviewed. For further details regarding these positions, visit our webpage at: **http://www.utoledo.edu/med/depts/micro**.

The University of Toledo is committed to diversity and equal opportunity. Applications from women and minority candidates are strongly encouraged.

UNICAMP

Job Opportunities at UNICAMP

Unicamp, the University of Campinas, is one of the leading research universities in Brazil. It offers opportunities for scholars across the world in the following fields: plant, animal and human biology, pharmacy, medicine, dentistry, speech-language therapy, physical education and sport science, chemistry, physics, materials science, mathematics, applied mathematics, statistics, computer science and engineering, geology, geography, history, philosophy, social sciences, linguistics, literature, education, economics, visual arts, music, scenic arts, cinema, multimedia art, dance, architecture, civil engineering, electrical and telecommunication engineering, food engineering, chemical engineering, agricultural engineering, mechanical engineering, control and automation engineering (mechatronics), computer technology, civil construction technology, telecommunications technology and environmental sanitation technology. Unicamp is located in Campinas, a very pleasant 1 million inhabitant city some 100km from São Paulo. Campinas is the home to several national research facilities and high tech industries. We will provide good working conditions, compatible salary and welfare, tenure track and good career development perspectives.

The applicants should be doctor degree (Ph.D.) holders with high academic achievement records, compatible with the area of expertise.

Brazil is a fast developing country.
Be part of the progress. Come work with us.

If you are interested in joining us please send a CV in English or Portuguese to **carreiras@reitoria.unicamp.br.**
If you need further information please visit our website **www.unicamp.br** or send a message to **info.carreiras@reitoria.unicamp.br.**

UNITED ARAB EMIRATES UNIVERSITY

DEAN
COLLEGE OF SCIENCE

The United Arab Emirates University is seeking an eminent scholar who is an internationally recognized and respected academic leader to serve as the Dean for the College of Science. The Dean will lead advances in academic excellence and, in particular, research development within the College.

The UAE University is the first and leading comprehensive national university in the United Arab Emirates. Established in 1976 by Sheikh Zayed bin Sultan Al Nahyan, the UAE University has grown to about 700 faculty members in ten faculties and educates over 13,000 students each year. The instructional language is English. Approximately 75% of the University students are women.

The College of Science was established in the 1977-1978 academic year, and offers degree programs in Biology, Chemistry, Geology, Mathematical Sciences and Physics. There are 126 faculty and academic staff that support more than 1100 students. The College faculty is a vibrant mixture of National and expatriate scholars, who have come together to create a climate of intellectual diversity, broad engagement and progression across departments.

UAE University is at present engaged in a process of transformation to become a research-intensive university of international standing and significance. The College of Science is committed to both basic and applied research with a special emphasis in areas of strategic importance to the UAE.

The successful candidate will possess leadership skills which include:

- The ability to develop an engaging, challenging vision for enhancement in both teaching and research.
- The ability to be a catalyst for change and to productively engage faculty in programmatic innovation.
- A commitment to firm, objective and ethical decisions.
- Strong academic and fiscal management abilities, including the willingness to delegate appropriately.
- The ability to communicate clearly and effectively with faculty, staff, students, colleagues across the institution and external constituents.
- The ability to build consensus that leads to prioritization of academic investments.

Application Procedure: The UAE University invites applications, inquiries and nominations for this key position. Letters of application or nomination should include a current curriculum vitae and the names and contact information for 3-5 referees, to be submitted in confidence electronically or via fax as indicated below. Review of materials will begin immediately and continue until the appointment is made. For full consideration, all nominations and applications should be submitted no later than **December 15, 2009** to:

Rene Dennis
Special Assistant to the Provost
UAE University
Office of the Provost
rdennis@uaeu.ac.ae
Fax submissions to +971 3-7131865
For inquiries please call +971 3-7131227

Karolinska Institutet

Invites applications for a

Professor of Cognitive Neuroscience

with a focus on cognitive aging

Thanks to a generous donation from the Jochnick Foundation, Karolinska Institutet is now establishing a chair in Cognitive Neuroscience. Increased knowledge about normal aging processes in the brain is a prerequisite for being able to detect, prevent and treat neurodegenerative diseases.

Karolinska Institutet is looking for a person who has a successful research program in cognitive function including memory and learning. The applicant should have knowledge about the substantial individual differences in how the brain ages and how cognitive abilities and functions develop through adulthood to late life. Research on training of cognitive functions to utilize the brain's potential for plasticity is a very important merit, as is research to identify early cognitive signs and biological markers in individuals who run a risk for developing neurodegenerative diseases.

Experience in combining cognitive and genetic research for a better understanding of how genes, environments and lifestyle interact in successful aging, cognitive impairment, and neurodegenerative diseases is particularly meritorious.

The successful candidate for this position has experience with many different methods, such as research in molecular biology / genetics, research at the cellular, synaptic, network, and cognitive levels. Experience with both cross-sectional and longitudinal methods is desirable.

The qualifications required for the post of Professor are both well documented internationally leading research, academic skills and the ability to build and lead a successful program of research in cognitive neuroscience at Karolinska Institutet.

In the assessment of the applicant´s merits, the required qualifications and experience carry the following weighting factors: pedagogical (1), scientific (3), and leadership, development and collaboration (2).

Contact persons Vice Dean of research, Professor Nancy Pedersen, nancy.pedersen@ki.se, +46-8-524 874 18. Union representatives: Hans Hjelmqvist (SACO), hans.jelmqvist@ki.se, +46-8-585 863 36, and Solveig Wahling (OFR), solveig.wahling@ki.se, +46-8-524 836 42.

Please send your application, marked with reference number 1164/09-221, **to reach us by no later than** 2009-12-14, to Karolinska Institutet, Registrator, SE-171 77 Stockholm.
The following documents in quadruplicate should be enclosed with your application and written in English:

- CV, qualifications and a description of future research, presented in accordance with Karolinska Institutet's qualification portfolio **http://ki.se/qualificationsportfolio**
- A selection of ten scientific papers

Please note that one copy of all documents will be kept by the college for a period of two years, in accordance with a directive from the National Archives. Published material submitted for review is exempted from this rule.

Karolinska Institutet is one of the leading medical universities in Europe. Through research and education, Karolinska Institutet contributes to improving human health. Each year, the Nobel Assembly at Karolinska Institutet awards the Nobel Prize in Physiology or Medicine.

Karolinska Institutet

CELL/MOLECULAR BIOLOGIST
FORDHAM UNIVERSITY

Individuals are invited to apply for a tenure-track position at the **ASSISTANT PROFESSOR** or the **ASSOCIATE PROFESSOR** level. An ongoing grant-supported research effort is required for consideration at the Associate Professor level. The department has an active research program with a recently launched Center for Cancer, Genetic Diseases, and Gene Regulation (CCGDGR) that provides excellent physical facilities, state-of-the-art equipment, a stimulating research environment, start-up funds and competitive salaries and benefits. Candidates with research interests compatible with our CCGDGR in areas such as stem cells, cancer, development, genetic diseases, or cellular physiology are particularly encouraged to apply. The appointee will be expected to establish and maintain an active research program and participate in teaching at the undergraduate and graduate levels.

Applicants should submit a cover letter, curriculum vitae, research statement, two reprints, and contact information for three references to: **Dr. William Thornhill, Chair, Department of Biological Sciences, Fordham University, 441 E. Fordham Road, Larkin Hall 160, Bronx, NY 10458** or by email (preferred) to **thornhill@fordham.edu** Candidates will be reviewed when their applications are received and we will continue to accept applications until the position is filled. Fordham University is an independent, Catholic university in the Jesuit tradition that welcomes applications from men and women of all backgrounds.

Fordham is an EOE.

POSITIONS OPEN

University of Nevada, Reno
Statewide • Worldwide
Department of Physiology and Cell Biology

FACULTY POSITION
Physiology and Cell Biology
University of Nevada School of Medicine

The Department of Physiology and Cell Biology at the University of Nevada School of Medicine invites applications for a tenure-track **ASSISTANT, ASSOCIATE** or **FULL PROFESSOR** position in the area of smooth muscle biology and/or vascular pathophysiology. Desirable specific subdisciplines would include: development, tissue and cell remodeling, cellular plasticity, neovascularization, cellular signaling, regulation of cellular differentiation and gene expression, epigenetics, inflammation and cytokine signaling, pathobiology, and/or bioinformatics. The candidate must have a Ph.D.-M.D. or equivalent with postdoctoral research experience. Candidates for Associate and Full Professor must have current extramural funding. Competitive salary and startup funds and research space in a new building are available. Candidates are expected to develop a strong, extramurally funded research program and to participate in the departmental teaching mission. The candidate will have leadership opportunities in a National Center for Research Resources Centers of Biomedical Research Excellence program. Information on the Department can be found at **website: http://www.medicine.nevada.edu/physio/index.html.** Interested applicants should submit curriculum vitae, statement of research interests, and three letters of recommendation to Human Resources at the University of Nevada, **website: https://www.unrsearch.com/applicants/jsp/shared/Welcome_css.jsp.**

University of Nevada is an Equal Opportunity/Affirmative Action Employer. Women and underrepresented groups are encouraged to apply.

Positions funded by federal contracts may be subject to the E-Verify process for employment eligibility verification.

POSTODOCTORAL RESEARCH SCIENTIST
Molecular Virology

A Postdoctoral Research Scientist position is available in the Department of Pathology at Children's Hospital of Pittsburgh. The candidate should have experience in virology and molecular biology, preferably with two plus years of prior postdoctoral experience; however, motivated recent Ph.D.s will be considered. Projects include: (1) effects of Epstein-Barr virus (EBV) nuclear proteins on the unfolded protein response (UPR), protein translation, and autophagy pathways in infected B-lymphocytes; (2) effects of UPR and endoplasmic reticulum stress signaling proteins on the EBV lytic program; (3) microRNAs and transcription factors involved in B cell differentiation and lymphomagenesis, in a hematopoietic stem cell model. The successful candidate will work semi-independently, with a dedicated technician. Send curriculum vitae and cover letter to: **Adam Rosendorff, M.D., e-mail: adam.rosendorff@chp.edu; telephone: 412-864-8793.**

ARBOVIROLOGIST ASSISTANT PROFESSOR
University of Florida
Florida Medical Entomology Laboratory
Institute of Food and Agricultural Sciences

The Florida Medical Entomology Laboratory invites applications from outstanding scientists with interests in arbovirology at the rank of Assistant Professor. Experience investigating arbovirus interactions with arthropods and vertebrates using molecular biology in a BSL-3 is essential. Applicants should visit **website: https://jobs.ufl.edu requisition #0803125** for information about applying. Review of applications will begin January 15, 2010, and continue until the position is filled.

The University of Florida is an Equal Opportunity Employer.

POSITIONS OPEN

LOYOLA MARYMOUNT UNIVERSITY
Frank R. Seaver College of Science and Engineering

Tenure-track Faculty Position for General Physiology and Vertebrate Biology. The Department of Biology at Loyola Marymount University (LMU) invites applications at the rank of **ASSISTANT PROFESSOR** beginning fall 2010. The campus is situated on a bluff overlooking the Ballona Wetlands. It is within a day's drive or boat ride of beaches, deserts, mountains, the California Channel Islands, and Baja California where the Department has a field station. Individuals with a Ph.D. in biology, zoology, or related fields are encouraged to apply. The candidate is expected to teach lower division courses in general biology, upper division courses in physiology, as well as courses in his or her specialty area. In addition to excellent teaching of undergraduates, the candidate is expected to establish an active research program that will include undergraduate students. Applicants should be able to teach a diverse student body. Please send letter of application, curriculum vitae, selected publications, a statement of teaching philosophy within an institution such as LMU, and a description of research projects, and arrange for three letters of recommendation to be sent to: **Dr. John Waggoner, Department of Biology, Loyola Marymount University, 1 LMU Drive MS 8220, Los Angeles, CA 90045-2659.** Review of applications will commence 1 December 2009.

Tenure-track Faculty Position for Cell Physiology/Biochemistry. The Department of Biology at Loyola Marymount University invites applications at the rank of **ASSISTANT PROFESSOR,** beginning fall 2010. Individuals with a Ph.D. in biology, biochemistry, or related field are encouraged to apply. The candidate is expected to teach lower division courses in biology, upper division courses in the biochemistry program, as well as courses in his or her specialty area. In addition to excellent teaching of undergraduates, the candidate is expected to establish an active research program that will include undergraduate students. LMU's Seaver College of Science and Engineering offers courses and conducts research in biochemistry, cell biology, molecular biology, genomics, and bioinformatics. Applicants should be able to teach a diverse student body. Interested applicants can apply online at Loyola Marymount University's **website: http://jobs.lmu.edu.** Please include a letter of interest, curriculum vitae, selected publications, a statement of teaching philosophy within an institution such as LMU, a description of research projects, and arrange for three letters of recommendation to be sent to: **Dr. Philippa Drennan, Department of Biology, Loyola Marymount University, 1 LMU Drive MS 8220, Los Angeles, CA 90045-2659.** Review of applications will commence 1 December 2009 and continue until position is filled.

Loyola Marymount, a comprehensive university in the mainstream of American Catholic higher education, seeks professionally outstanding applicants who value its mission and share its commitment to academic excellence, the education of the whole person, and the building of a just society. LMU is an Equal Opportunity Institution actively working to promote an intercultural learning community. Women and minorities are encouraged to apply.

POSTDOCTORAL POSITION

Two new positions in National Cancer Institute–supported Physical Sciences–Oncology Center to study tumor cell adhesion in the vascular microenvironment focusing on using novel technology to isolate and characterize circulating tumor cells (**Dr. David Nanus**) and study the effects of the cytoskeleton on cell force generation and metastasis (**Dr. Paraskevi Giannakakou, website: http://www.cornellpharmacology.org/faculty/labs/giannakakou**). Background in molecular cell biology required; experience in confocal microscopy and xenograft/transgenic mice desirable. Personal interview is required. Please send cover letter, curriculum vitae, and three references to **Kathleen Busa, e-mail: kab2018@med.cornell.edu.**

FELLOWSHIPS

POSITIONS OPEN

RESEARCH ASSOCIATES. Seeking two researchers for research in animal physiology core related to lung disease or the role that Na,K-ATPase plays in lung edema. Requirements: Ph.D. in biochemistry or M.D. and one year experience. Contact: **Sean Campbell, Northwestern University, Department of Medicine–Pediatric Critical Care Medicine, 240 E. Huron, McGaw M300, Chicago, IL 60611.**

BIOMOLECULAR NMR SPECTROSCOPIST
Indiana University

Indiana University has significantly expanded its nuclear magnetic resonance (NMR) capabilities with the installation of 600 and 800 MHz Varian spectrometers in the new Metabolomics and Cytomics Initiative Biomolecular NMR Laboratory in Simon Hall. We now seek to appoint a Biomolecular NMR Spectroscopist at the **ASSISTANT SCIENTIST** (research-track) level, effective April 1, 2010. Candidates must have a Ph.D. in chemistry, biochemistry, structural biology, or a related field; two years of postdoctoral experience or equivalent is desired. The successful candidate will have documented experience with the application and optimization of modern biological NMR spectroscopy to structural studies of proteins. Familiarity with partially aligned systems and nucleic acids is desirable. Experience with the operation and maintenance of high field NMR spectrometers (600 and 800 MHz) and cryogenic probe systems is required, and knowledge of hardware and Unix-based software maintenance is essential. Familiarity with Varian systems and methods of NMR data analysis through structure calculation and validation stages are also desirable but not necessary.

Applicants should submit a brief statement of interest along with curriculum vitae and should arrange for three letters of recommendation to be sent to: **Prof. James P. Reilly, Chair of Search Committee, Department of Chemistry, Indiana University, 800 E. Kirkwood Avenue, Bloomington, IN 47405. Fax: 812-856-5050; e-mail: chemchair@indiana.edu.** Applications received by December 15, 2009, will be assured of consideration. *Indiana University is an Equal Opportunity Affirmative Action Employer.*

POSTOCTORAL RESEARCH ASSOCIATE
in Microbiology

The Energy Biosciences Institute at the University of Illinois at Urbana-Champaign is seeking a Postdoctoral Researcher to work in an interdisciplinary program using microbiological and enzymological approaches for identifying novel enzymes in lignocellulose degradation that can be used to enhance biofuel production. The focus of this position is development and application of genetic tools to assist enzyme identification in *Streptomyces* and related microorganisms. The Postdoctoral Associate will construct deletion mutants of strains of *Streptomyces* so that the importance of the specific enzymes implicated in lignocellulose degradation can be established. The Postdoctoral Associate also will construct strains of *Streptomyces* to facilitate enhanced degradation of lignocellulose.

Required qualifications: Ph.D. in microbiology, molecular biology, or closely related discipline required. The applicant should be well versed in techniques of molecular biology and microbiology. Experience with genetics and physiology of *Streptomyces* is highly desired but not required. The ability to work collaboratively within a team is required.

Applicants should send electronically to **Prof. John A. Gerlt, e-mail: j-gerlt@illinois.edu** the following materials: (1) curriculum vitae, (2) a letter describing research interests and experience, and (3) names and contact information for three references. Review of completed applications will begin November 1, 2009, and continue until position is filled.

ASSOCIATE/FULL CURATOR OF INVERTEBRATE PALEONTOLOGY
ASSISTANT/ASSOCIATE/FULL CURATOR OF ARCHAEOLOGY
ASSISTANT CURATOR OF LEPIDOPTERA
Florida Museum of Natural History, University of Florida

The Florida Museum of Natural History, University of Florida, one of the country's premier museums dedicated to studying biological and cultural diversity, invites applications for three tenured or tenure-track positions. The Thompson Chair of Invertebrate Paleontology (**requisition #0803198**), to be hired at the level of Associate or Full Curator, will be expected to conduct a dynamic research program in invertebrate paleobiology and to curate and develop the museum's extensive collection of primarily Cenozoic invertebrate fossils. A substantial endowment is associated with this position. The Assistant or Associate or Full Curator of Archaeology (**requisition #0803193**) will be expected to pursue a vigorous research program and to curate and develop the museum's collection of archaeological materials from the southeastern United States, especially Florida. A modest endowment is associated with this position. The Assistant Curator of Lepidoptera (**requisition #0803201**) will be expected to develop an active research program, with a molecular component, that both benefits from and contributes to the Museum's lepidoptera collection, housed in the McGuire Center.

Successful candidates for all three positions must have a strong commitment to university education, field work, and museum-based research. Interactions with allied academic departments include supervising student research and teaching two formal courses per year. Minimum qualifications: Ph.D. and strong research and collections background. The start date is open, but may begin as early as August 2010. The salary is competitive and commensurate with experience.

To be considered, all applications must be submitted online at **website: http://jobs.ufl.edu.** The application should include cover letter, curriculum vitae, statement of research, collections and teaching experience, and goals. Reprints of no more than five publications and the names of three colleagues who might be contacted for letters of recommendation should be sent directly to the search committee chair by e-mail before the application deadline. Inquiries and nominations should be directed to the chairs of the search committees: **Dr. Steven Manchester, Chair of Invertebrate Paleontology Search Committee, e-mail: steven@flmnh.ufl.edu,** application deadline 4 January 2010; **Dr. Pamela Soltis, Chair of Archaeology Search Committee, e-mail: psoltis@flmnh.ufl.edu,** application deadline 4 December 2009; **Dr. David Reed, Chair of Lepidoptera Search Committee, e-mail: dreed@flmnh.ufl.edu,** application deadline 4 December 2009. **Florida Museum of Natural History, University of Florida, P.O. Box 117800, Gainesville, FL 32611-7800.** *The University of Florida is an Equal Opportunity/Affirmative Action Employer. The selection process will be conducted under the provisions of Florida's Government in the Sunshine and Public Records laws.*

The Department of Health Sciences in the College of Public Health at East Tennessee State University seeks applications for a tenure-track position at the **ASSISTANT PROFESSOR** level. Position available spring or fall semester 2010. The position requires teaching undergraduate lecture and laboratory courses in anatomy/physiology and upper division human anatomy. Development of a fundable research program that complements the missions of the Department and the College of Public Health is expected. Ph.D. in related field required. Application review will begin immediately. Salary will depend on qualifications and experience. Search will continue until position is filled. Please submit ETSU application, curriculum vitae, a description of research interests, and the names of three references to: **Dr. Ranjan Chakraborty, Associate Professor and Chair, Department of Health Sciences, East Tennessee State University, P.O. Box 70673, Johnson City, TN 37614-1709. E-mail: chakrabr@etsu.edu.** E-mail submission is encouraged.

POSTDOCTORAL FELLOWSHIPS

The Geophysical Laboratory, Carnegie Institution of Washington, invites applications for Postdoctoral Fellowships. The Geophysical Laboratory emphasizes interdisciplinary experimental and theoretical research in fields spanning geoscience, microbiology, chemistry, and physics. The Laboratory supports world-class facilities in high-pressure research; organic, stable isotope and biogeochemistry; mineral physics and petrology; and astrobiology.

Please see **website: http://www.gl.ciw.edu/employment/Postdoctoral_Positions** for information on the application process. Also, see **website: http://www.gl.ciw.edu/** for a listing of personnel, current research interests, major facilities, and application information.

Completed applications for Carnegie fellowships should be submitted by December 31, 2009, to: **Russell J. Hemley, Director, Attn: Danielle Appleby, Geophysical Laboratory, 5251 Broad Branch Road, N.W., Washington, DC 20015-1305, U.S.A. E-mail: dappleby@ciw.edu.** E-mail is preferred.

The Geophysical Laboratory is an Equal Opportunity Employer.

FULL-TIME FACULTY POSITION
University of Maryland School of Medicine
Department of Pathology

The Department of Pathology invites applicants with an M.D. or Ph.D. degree to apply for a full-time faculty position at the **ASSISTANT PROFESSOR** level focused on independent translational research in the area of molecular biology. The applicant should have evidence of scholarly achievement, to include a history of funded research and current research funding, and should have experience in developing and translating discoveries into novel clinical applications. The applicant will be expected to be active in the School of Medicine's teaching programs. Salary will be commensurate with experience.

The University of Maryland School of Medicine is the first public and fifth oldest medical school in the United States. On the University of Maryland, Baltimore campus, the School of Medicine serves as the foundation for a large academic health center that combines medical education, biomedical research, patient care, and community service. The School of Medicine ranks in the top tier of medical schools and is ranked sixth when compared to all public U.S. medical schools. In fiscal year 2009, external research funding exceeded $425 million.

Please forward curriculum vitae, a brief statement of research interests, funding, and teaching experience, and the names of three references to:

Sanford A. Stass, M.D.
Professor and Chairman
c/o Pati Butler
(e-mail: pabutler@som.umaryland.edu)
Department of Pathology
University of Maryland School of Medicine
10 S. Pine Street, Room 700, MSTF
Baltimore, MD 21201

The University of Maryland is an Affirmative Action/Equal Employment Opportunity/ADA Employer. Minorities and women are encouraged to apply.

POSTDOCTORAL FELLOWSHIP in molecular biology/biochemistry/immunology at the Plum Island Animal Disease Center in Orient Point, New York. The incumbent will express cytokine genes and measure the biological activity. Ph.D graduates with experience in DNA cloning/mutagenesis, protein expression, microarray analysis, and/or cell culture are encouraged to apply. Starting stipend: $57,000 for two years. Send curriculum vitae to **James Zhu, e-mail: james.zhu@ars.usda.gov.**

Federal Ministry of Education and Research

bccn

"Bernstein Award" 2010

Young Scientists Research Award in Computational Neuroscience

The German Federal Ministry of Education and Research (BMBF) has established the "National Network for Computational Neuroscience" with four high-performing "Bernstein Centers for Computational Neuroscience" as the major structural elements.

The "Bernstein Award" is equipped with up to 1.25 Mio Euros in the form of a grant over a period of five years. It will be awarded to a highly qualified young researcher, considering the candidates' verifiable research profile in the field of Computational Neuroscience and the scientific concept for a future young research group. Young researchers can apply for their own position and group. The group funded by the "Bernstein Award" will become an integral part of the National Network for Computational Neuroscience. Future announcements of the "Bernstein-Award" are in the scope of the Ministry's planning.

The grant is provided for a scientific project of a young research group headed by a postdoc regardless of nationality. The project will be conducted at a German university or research institution – within or outside the Bernstein Centers. It is a prerequisite for funding that the university or research institution concerned employs the young researcher during the funding period and supports him/her with the basic equipment in terms of laboratory space and other infrastructure. A statement made to that effect by the receiving institution must be included with the project outline to be submitted.

Deadline for applications is May 25th, 2010.

For more detailed information about the "Bernstein-Award" including application conditions please visit

http://www.nncn.de
or
http://www.gesundheitsforschung-bmbf.de/en/1834.php

POSITIONS OPEN

BCM
Baylor College of Medicine

ALICE R. MCPHERSON CHAIR IN OPHTHALMOLOGY
Retina Research Foundation
Cullen Eye Institute
Baylor College of Medicine
Houston, Texas

The Cullen Eye Institute and the Department of Ophthalmology at Baylor College of Medicine invite applications for an endowed Chair in basic retinal research. The faculty appointment will be at the level of tenured **PROFESSOR** in the Department of Ophthalmology with a joint appointment in an appropriate basic science department. The successful candidate must have the Ph.D. degree, currently hold the rank of Associate or full Professor, have active, independent, extramural funding for her/his research program, and have a record of substantial accomplishment and promise in innovative retinal research. The position provides substantial resources including an endowed Chair and multiyear research support as well as attractive startup/transition funds and customized research laboratory space in the Cullen Eye Institute. The investigator will have access to major research core facilities, an NIH pre- and postdoctoral training grant, and collaborators and possible joint appointments in biochemistry, cell biology, developmental biology, genetics, neurology, neuroscience, and physiology. Applicants with research strengths in retinal development, regeneration, information processing, or structure who use contemporary tools of molecular genetics, optical imaging, cell biology, physiology, computational and/or structural biology to study these processes are encouraged to apply. Applicants should send curriculum vitae and statement of research interests electronically to **e-mail: akoval@bcm.edu** as a single PDF addressed to: **Dan B. Jones, M.D., Professor and Chair, Department of Ophthalmology, Cullen Eye Institute, NC-205, Baylor College of Medicine, One Baylor Plaza, Houston, TX 77030.**

Baylor College of Medicine is an Equal Opportunity/Affirmative Action and Equal Access Employer.

FACULTY POSITION IN VIROLOGY
Department of Microbiology–Immunology
Northwestern University
Feinberg School of Medicine

A tenure-track position is open for a full-time faculty researcher (Ph.D., M.D.-Ph.D. or M.D.) in virology. Areas of particular interest include viral oncogenesis, pathogenesis, or immune response to viral infection.

Rank is open, and salary is negotiable. All applicants should have substantial peer-reviewed publications that demonstrate research productivity and the ability to perform cutting-edge research. Candidates for an **ASSISTANT PROFESSOR** position should have postdoctoral research experience. Persons seeking appointment as **ASSOCIATE PROFESSOR** should have substantial research productivity and a history of grant support and academic service. Candidates should have an interest in teaching graduate and medical students. Starting date is negotiable. Application materials will be reviewed as received but, to receive full consideration, should be received by January 1, 2010. Please send a complete curriculum vitae and the names and contact information of at least three references electronically to **e-mail: virologysearch@northwestern.edu.** *Northwestern University is an Affirmative Action, Equal Opportunity Employer. Women and minorities are encouraged to apply. Hiring is contingent upon eligibility to work in the United States.*

POSITIONS OPEN

FACULTY POSITION IN BIOINFORMATICS

The University of North Texas (UNT) seeks candidates for a position in bioinformatics at the rank of tenure-track **ASSISTANT PROFESSOR.** Candidates will be expected to develop an identifiable research program, obtain extramural funding, and support instructional needs at the graduate and undergraduate levels. The position is anticipated to be a joint appointment between biological sciences, computer science and engineering, or mathematics, depending upon the candidate's areas of expertise. The successful candidate will be an integral part of two UNT research cluster initiatives to build expertise in two areas: (1) Plant Signaling Mechanisms and (2) Developmental Physiology and Genetics. The new faculty member will interact with current faculty in life sciences, mathematics, and computer sciences as well as other scientists at UNT focused on modeling and computational sciences, such as those in the Center for Advanced Scientific Computing and Modeling (CASCaM). Candidates must have a Ph.D. in bioinformatics, computer science, mathematics, life sciences, or a related discipline; postdoctoral experience and evidence of scholarship in bioinformatics; and effective communication skills. Teaching experience is preferred. Preference will also be given to applicants who have expertise with systems approaches to biological questions and may include expertise in pattern recognition, statistical methods, database development, and user interfaces in the analysis and handling of large genetic and metabolite data sets. Competitive startup funds and salary are available. Applicants must apply online at **website: http://facultyjobs.unt.edu/applicants/Central?quickFind=50543.** Upload a cover letter with qualifications and research interests, curriculum vitae, two or three representative publications, teaching statement, and names/contact information of three references. Inquiries may be directed to: **Dr. Rebecca Dickstein, Bioinformatics Search Committee Chair, e-mail: beccad@unt.edu.** Applications will be reviewed beginning November 1, 2009, and continuing until the search is closed. UNT is the largest and most comprehensive university in the north Texas region with 96 bachelor's, 111 master's, and 50 doctoral degree programs. It is the fourth largest university in Texas, with over 36,000 students. UNT is located in Denton in the vibrant and rapidly expanding Dallas-Fort Worth metropolitan area with easy access to D-FW airport. For further information about the Plant Signaling Mechanisms and Developmental Physiology and Genetics research cluster initiatives, see **website: http://www.biol.unt.edu/.**

UNT is an Affirmative Action/ADA/Equal Opportunity Employer.

POSTDOCTORAL POSITIONS IN BIOCHEMICAL PLANT GENOMICS, Michigan State University, Departments of Biochemistry and Plant Biology. Michigan State University is seeking multiple postdoctoral fellows to conduct research at the interface of plant genomics, biochemistry, and computational biology in the laboratories of **D. DellaPenna** (**website: http://www.bch.msu.edu/faculty/dellapenna.htm**), **A.D. Jones** (**website: http://www.bch.msu.edu/faculty/jones.html**), and **C.R. Buell** (**website: http://buell-lab.plantbiology.msu.edu/**). The fellows will utilize metabolomic, next generation sequencing, expression profiling, bioinformatic, quantitative genetic, and/or computational biology approaches to address research questions involving metabolism of essential nutrients and pharmaceutical compounds in model, crop, and medicinal plant species. Collaborative NIH- and NSF-funded research across the DellaPenna, Jones, and Buell laboratories provides a unique opportunity for cross-training of fellows in multiple disciplines. Applicants should have a Ph.D. in biology, biochemistry, plant biology, computer science, bioinformatics, or related field and expertise in at least one of the above approaches. Send curriculum vitae, statement of research accomplishments and interests, and contact information for three references to **e-mail: dellapen@msu.edu.**

POSITIONS OPEN

OREGON HEALTH & SCIENCE UNIVERSITY

FACULTY POSITION IN NEUROSCIENCE

The Division of Neuroscience at the Oregon National Primate Research Center (ORPRC)/Oregon Health & Science University (OHSU) invites applications for a position of **ASSISTANT SCIENTIST** to develop a program in neurodegenerative diseases using nonhuman primates (NHPs). The position will include a joint appointment in the Department of Neurology at OHSU School of Medicine and faculty membership in the OHSU Neuroscience Graduate Program. Qualifications include a Ph.D. or equivalent degree, appropriate postdoctoral experience, and a strong publication record. Applicants with expertise in accessing the NHP brain via systemic and stereotaxic approaches and that focus their research efforts on the development of delivery vehicles for targeting the NHP brain are particularly encouraged to apply. Expertise in NHP cognitive behavior is also desirable. The successful candidate will be expected to establish and maintain an extramurally funded research program with international visibility.

Please send curriculum vitae, a statement of research interest and long range goals, and the names of three references no later than November 30, 2009 to:

Dr. Sergio R. Ojeda
Division of Neuroscience,
Oregon National Primate Research Center/
Oregon Health & Science University
505 N.W. 185th Avenue, Beaverton, OR 97006
Telephone: 503-690-5303
Fax: 503-690-5384
E-mail: ojedas@ohsu.edu

OHSU is an Equal Opportunity, Affirmative Action Institution.

POSTDOCTORAL ASSOCIATES

The Institute of Marine and Coastal Sciences at Rutgers, The State University of New Jersey, is seeking Postdoctoral Associates for one-year renewable appointments in the areas of biological, chemical, geological, and physical oceanography. To apply, please e-mail your resume, a statement of research interest, and the names of three references by January 15, 2010, to: **Dr. Francisco E. Werner, e-mail: postdoc2010@marine.rutgers.edu.** *Rutgers is an Equal Opportunity/Affirmative Action Employer. Employment verification required.*

MARKETPLACE

10 Ways to Improve Your Chances of Securing Research Funding

RESEARCH

APPLICATIONS

NETWORKING

HOPING

WISHING

TANTRUM

RABBIT'S FOOT

SLOTS

SELF-FINANCING

JOINING

There are many approaches to securing funding, but not all are effective. That's why the American Association for the Advancement of Science is committed to offering its members a variety of resources to help them locate the money they need—including an ongoing analysis of R&D budgets and funding, and an extensive directory of funding opportunities. Join us. Together we can make a difference. **aaas.org/plusyou**

AAAS + U = Δ

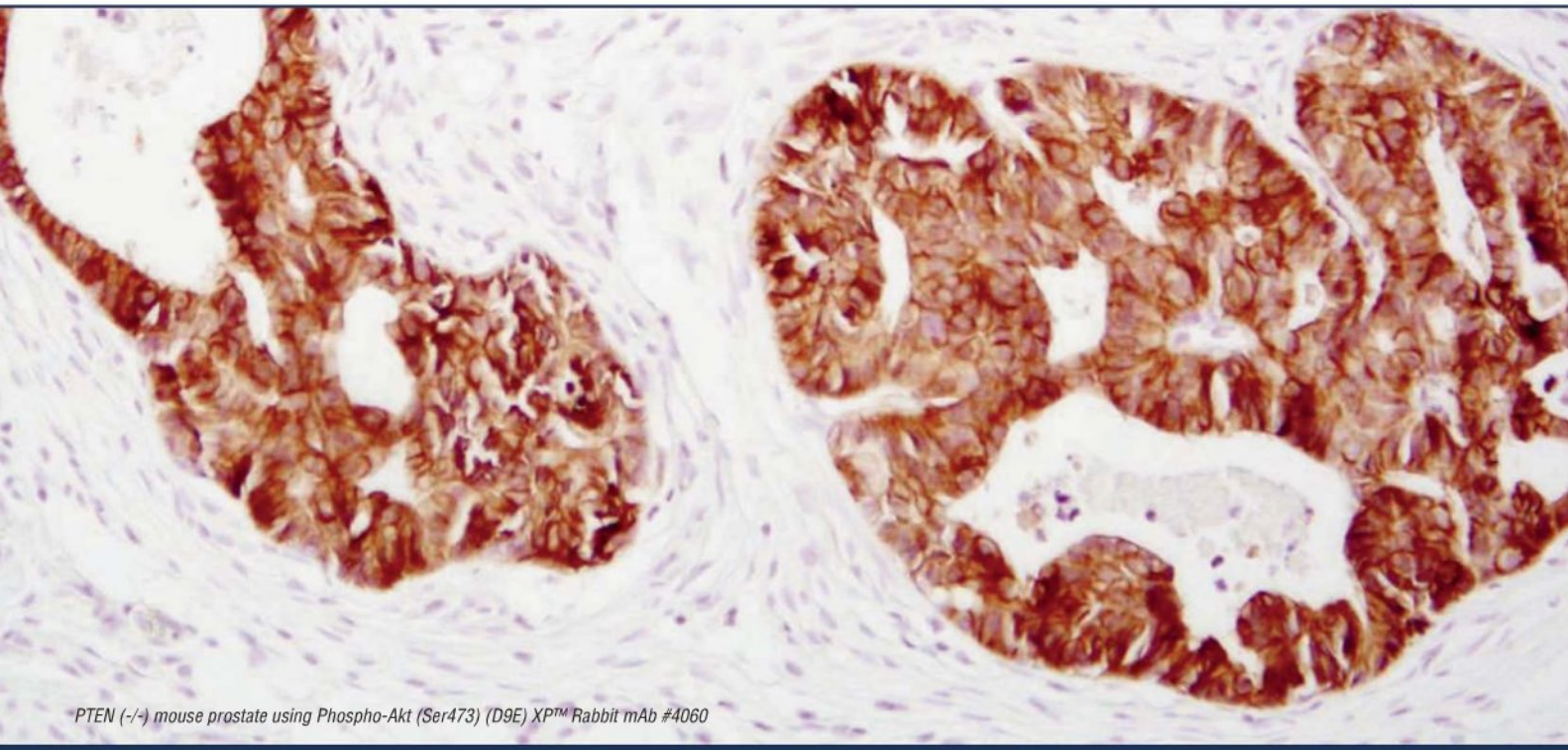

PTEN (-/-) mouse prostate using Phospho-Akt (Ser473) (D9E) XP™ Rabbit mAb #4060

Announcing XMT™ ... a proprietary eXceptional Monoclonal Technology

exclusively from Cell Signaling Technology®

XMT™ enables the development and production of XP™ monoclonal antibodies with eXceptional Performance.

This revolutionary and proprietary technology provides us with access to a broad range of antibody-producing B cells unattainable with traditional monoclonal technologies, allowing more comprehensive screening and the identification of **XP** monoclonal antibodies with:

eXceptional specificity
+ eXceptional sensitivity
+ eXceptional stability and reproducibility
= eXceptional Performance

XMT coupled with our extensive antibody validation and stringent quality control delivers **XP** monoclonal antibodies with eXceptional Performance in the widest range of applications. And as with all of our antibodies, the product will work the first and every time used.

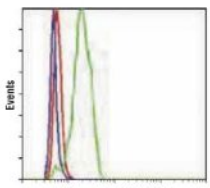

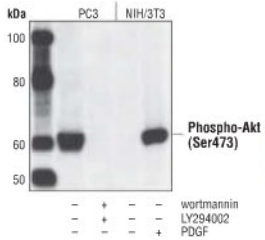

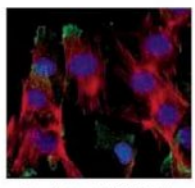
Insulin-treated C2C12 cells

◀ ***Phospho-Akt (Ser473) (D9E) XP™ Rabbit mAb #4060 demonstrates eXceptional Performance in a wide range of applications. See www.cellsignal.com for full validation details.***

for more information on XMT™ visit...

www.cellsignal.com

Cell Signaling TECHNOLOGY®

Orders (toll-free) 1-877-616-2355 | **Technical support** (toll-free) 1-877-678-8324 support@cellsignal.com | **Inquiries** info@cellsignal.com | **Environmental Commitment** eco.cellsignal.com